Off-Earth seismic

Viability and examination of use for measuring geophysical, geomechanical and structural properties of off-Earth bodies

Michael Dello-Iacovo

A thesis in fulfilment of the requirements for the degree of

Doctor of Philosophy

School of Mineral and Energy Resources Engineering

Faculty of Engineering

UNSW Sydney

Sydney, Australia

January 2022

ORIGINALITY STATEMENT

☑ I hereby declare that this submission is my own work and to the best of my knowledge it contains no materials previously published or written by another person, or substantial proportions of material which have been accepted for the award of any other degree or diploma at UNSW or any other educational institution, except where due acknowledgement is made in the thesis. Any contribution made to the research by others, with whom I have worked at UNSW or elsewhere, is explicitly acknowledged in the thesis. I also declare that the intellectual content of this thesis is the product of my own work, except to the extent that assistance from others in the project's design and conception or in style, presentation and linguistic expression is acknowledged.

COPYRIGHT STATEMENT

AUTHENTICITY STATEMENT

☑ I certify that the Library deposit digital copy is a direct equivalent of the final officially approved version of my thesis.

UNSW is supportive of candidates publishing their research results during their candidature as detailed in the UNSW Thesis Examination Procedure.

Publications can be used in the candidate's thesis in lieu of a Chapter provided:

- The candidate contributed **greater than 50%** of the content in the publication and are the "primary author", i.e. they were responsible primarily for the planning, execution and preparation of the work for publication.
- The candidate has obtained approval to include the publication in their thesis in lieu of a Chapter from their Supervisor and Postgraduate Coordinator.
- The publication is not subject to any obligations or contractual agreements with a third party that would constrain its inclusion in the thesis.

☑ The candidate has declared that **their thesis has publications - either published or submitted for publication - incorporated into it in lieu of a Chapter/s. Details of these publications are provided below.**.

Publication Details #1

Full Title:	A novel method of measuring seismic velocity in off-Earth conditions: Implications for future research
Authors:	Dello-Iacovo, M.A., Saydam, S., Anderson, R.C.
Journal or Book Name:	48th Lunar and Planetary Science Conference
Volume/Page Numbers:	
Date Accepted/Published:	
Status:	published
The Candidate's Contribution to the Work:	Primary author and performed the labwork detailed in the paper
Location of the work in the thesis and/or how the work is incorporated in the thesis:	Chapter 4 is an expanded version of this paper

Publication Details #2

Full Title:	Effect of the space environment on seismic data collection
Authors:	Dello-Iacovo, M.A., Saydam, S., Anderson, R.C.
Journal or Book Name:	Geomechanics and Geophysics for Geo-Energy and Geo-Resources
Volume/Page Numbers:	
Date Accepted/Published:	
Status:	submitted
The Candidate's Contribution to the Work:	Primary author and performed the labwork detailed in the paper
Location of the work in the thesis and/or how the work is incorporated in the thesis:	Chapter 5 is the paper with some minor modifications.

Publication Details #3

Full Title:	Determination of asteroid structure and geomechanics using penetrators and active seismics
Authors:	Dello-Iacovo, M.A., Saydam, S., Anderson, R.C.
Journal or Book Name:	Icarus
Volume/Page Numbers:	
Date Accepted/Published:	
Status:	submitted
The Candidate's Contribution to the Work:	Primary author
Location of the work in the thesis and/or how the work is incorporated in the thesis:	Chapter 7 is the paper with some minor modifications.

Candidate's Declaration

I confirm that where I have used a publication in lieu of a chapter, the listed publication(s) above meet(s) the requirements to be included in the thesis. I also declare that I have complied with the Thesis Examination Procedure.

Abstract

Space exploration and technology development present great potential to humanity through the expansion of useful infrastructure such as satellites, space stations, launch facilities and space agencies. In addition, access to scientific opportunities such as understanding the origin of our solar system may prove valuable, and resources ranging from ice to metals and rare earth elements may be utilised to great benefit. The presence of these resources has been demonstrated on the Moon, Mars, comets, and asteroids, while the concentrations remain less certain.

The risk of asteroid and comet impacts poses a great threat to life on Earth. To date, little to nothing is known about the interior of most planetary bodies. Seismic techniques are used with great success to understand the subsurface of Earth and have been proposed for expanded use in off-Earth environments, such as on the Moon, Mars, and asteroids to advance the knowledge of their interiors.

The goal of this thesis is to examine the potential use of seismic techniques to explore and understand the subsurface of off-Earth environments for the purposes of resource prospecting, mining, and asteroid/comet deflection. This thesis presents a novel and innovative methodology for measuring the seismic properties of regolith and uses it to develop an understanding of the effect of the space environment on seismic data collection, such as the differing atmospheric pressure and regolith properties. The potential use of other remote sensing and geophysical techniques to assist with seismic exploration is also reviewed in addition to mission proposals.

A novel testing system was designed for measuring the seismic properties of fine-grain, low compaction regolith, called the Seismic Apparatus for Fine-Grained Sediment (SAFGS). Seismic experiments were performed at UNSW Sydney, Australia and the Jet Propulsion Laboratory (JPL), Pasadena, the USA on two available off-Earth regolith simulants designed based on known off-Earth regolith properties; the Australian lunar Regolith Simulant (ALRS-1) and the Mojave Mars Simulant (MMS). ALRS-1 had a measured P-wave velocity of 98.6 m/s, comparable to the measured *in-situ* velocity of lunar regolith (104 m/s and 114 m/s). The P-wave velocity of the MMS regolith was measured with a possible relationship between increasing grain size and velocity being found. The MMS dust had a mean velocity of 61.3 m/s, small-grain MMS had 244.5 m/s, and medium-grain MMS had 271.2 m/s. Computational and analytical modelling methods are explored to validate and expand upon the experimental work.

Acknowledgements

Completing this thesis and my PhD program was an intensely challenging experience. I have no doubt that I would not have made it and be writing this if it were not for the help and support of countless individuals, and I would like to personally thank them here.

My primary supervisor Prof Serkan Saydam is the embodiment of kindness, patience, motivation, and support. I have not found this PhD easy, and at times I have felt despondent and ready to give up, but Serkan has always been there for me, and is more understanding and supportive than I feel I deserve. He is incredibly well connected, and many of the incredible people I have had the chance to meet over the past four years are because of him.

My co-supervisor Dr Robert Anderson went above and beyond to help organise and facilitate my trip to the Jet Propulsion Laboratory in Los Angeles, USA, and to make me feel welcome once I arrived. His knowledge of planetary science and space operations has been invaluable.

My co-supervisor Dr Simit Raval his input to the research, especially in the field of remote sensing.

Prof Andrew Dempster and the Australian Centre for Space Engineering Research for their continuous support and advice.

My parents Janine and Lou, for their support and their role in making me the person I am today.

My brother Daniel, for whom no idea is too science fiction to discuss with.

My partner Sitara Ramakrishnan, for being a constant source of inspiration and support over the past two years, and for always being there for me.

Bob and Melody Schmidt, for giving me not just a place to stay, but a home during my year in Los Angeles. They were my second family. Bob, you are missed, rest in peace.

Kanchana Gamage and Mark Whelan of UNSW, and Greg Peters of JPL, for their assistance with my laboratory work. Their insight and ingenuity were invaluable.

The School of Mineral and Resources Engineering and all the staff for their support throughout the entire program.

Dr Faham Tahmasebinia for his advice, assistance, and support during the computer modelling work. Faham went above and beyond to help create some excellent models. He was patient and generous with his time despite my lack of knowledge in the field.

A/Prof Ryan Armstrong, Ik Ling Lau, and everyone from the Graduate Research School for their support and assistance.

The UNSW UNSOMNIA program and everyone involved for giving me an opportunity to showcase some of my research and ideas and helping to make an incredible presentation.

The Jet Propulsion Laboratory for allowing me to spend a year using their facilities to undertake experiments and conduct my research. Thank you especially to Dylan Mai, Madelaine Tran, and Colin Chen for helping take hundreds of measurements.

Ram Ramakrishnan for his much needed and appreciated feedback on grammar and other minutia in my final draft.

My fellow PhD candidates, some of whom have since graduated and moved on to other great things. Thank you for the support, motivation and laughs in the office.

My friends who have helped keep me sane and motivated.

And everyone else who I may have missed, however small their role was in helping me get here. Thank you.

Contents

List of figures

List of tables

List of abbreviations

3DEC – 3D Distinct-Element Modelling

AIDA – Asteroid Impact and Deflection Assessment

ASA – Australian Space Agency

ASE – Active Seismic Experiment

ALRS-1 – Australian Lunar Regolith Simulant 1

AVO – Amplitude versus offset

BASiX – Binary Asteroid in-situ Explorer

CAI – Cerchar abrasivity index

CNSA – China National Space Administration

CONSERT – Comet Nucleus Sounding Experiment by Radio wave Transmission

DAN – Dynamic Albedo of Neutrons

DART – Double Asteroid Redirection Test

Delta-V – Change in velocity

DC – Direct current

DEM – Discrete element method

DSI – Deep Space Industries

EM – Electromagnetic

ERI – Electrical resistivity imaging

ERT – Electrical resistivity tomography

ERV – Earth return vehicle

ESA – European Space Agency

FEM – Finite element method

FLAC – Fast Lagrangian Analysis of Continua

GPR – Ground penetrating radar

GPS – Global positioning system

IP – Induced polarisation

InSAR – Interferometric synthetic aperture radar

InSight – Interior Exploration using Seismic Investigations, Geodesy and Heat Transport

ISRU – *In-situ* resource utilisation

JAXA – Japanese Aerospace Exploration Agency

JPL – Jet Propulsion Laboratory

JSC-1A – Johnson Space Centre lunar simulant

LD – Lunar distance

LEO – Low Earth orbit

LiDAR – Light detection and ranging

LPSE – Lunar Seismic Profiling Experiment

MASL – Metres above sea level

MLS-1 – Minnesota Lunar Simulant

MMS – Mojave Mars Simulant

MRS – Magnetic resonance sounding

MT – Magnetotelluric

NASA – National Aeronautics and Space Administration (of the United States of America)

NEO – Near Earth object

NPV – Net present value

NSW – New South Wales

OSIRIS-REx – Origins, Spectral Interpretation, Resource Identification, Security, Regolith Explorer

PFC – Particle Flow Code

PSE – Passive Seismic Experiment

Radar – Radio detection and ranging

REE – Rare earth elements

SASPaH – Sample Acquisition, Processing, and Handling subsystem

SEIS – Seismic Experiment for Interior Structure

SNMR – Surface nuclear magnetic resonance

SNR – Signal to noise ratio

SPB – Small planetary body

SWD – Seismic-while-drilling

TBM – Tunnel boring machine

UCS – Uniaxial Compressive Strength

USD – United States dollar

VSP – Vertical seismic profile

List of publications

Dello-Iacovo, M.A., Anderson, R.C. and Saydam, S. 2017, A novel method of measuring seismic velocity in off-Earth conditions: Implications for future research, 48th Lunar and Planetary Science Conference (The Woodlands, Texas).

Dello-Iacovo, M.A., Saydam, S. and Anderson, R.C. 2019, Measuring seismic properties of fine sediments in an off-Earth environment, Rock Dynamics Summit, Okinawa, Japan.

Dello-Iacovo, M.A., Saydam, S. and Anderson, R.C. 2021, Effect of the space environment on seismic data collection, *Geomechanics and Geophysics for Geo-Energy and Geo-Resources* In review.

Dello-Iacovo, M.A. 2021, Determination of asteroid structure and geomechanics using penetrators and active seismics, *Icarus* In review.

Dello-Iacovo, M.A. and Saydam, S. 2021, Measuring and modelling the seismic properties of off-Earth regolith simulants in off-Earth conditions, 11th Asian Rock Mechanics Symposium, Beijing, China.

1. Introduction

1.1 Background

Space exploration and technology development present an ongoing and enormous opportunity for scientific research to make novel discoveries about the Earth and the universe around us. There are numerous benefits to exploring space, such as designing technologies that utilise space such as satellite communications and observation, which are critical infrastructure for many global systems and communications today. Many innovative technologies developed for use in space are repurposed for use on Earth, known as spinoff technologies. For example, since 1976, over 2,000 technologies developed by the National Aeronautics and Space Administration (NASA) of USA have been repurposed through their spinoff program for use on Earth (NASA 2018), such as mobile phone cameras (NASA 2010) and air purifiers (NASA 2013).

Like Earth, other planetary bodies are host to a range of natural resources. Some asteroids are rich in metals such as iron, nickel, gold, and platinum group metals (Zacny et al. 2013). Ice may be abundant in some environments such as asteroids, comets, and beneath the regolith (the unconsolidated near-surface material) on Mars and the Moon, and could be used as a propellant by separating the hydrogen and oxygen through electrolysis (Lewis 1997; Sowers and Dreyer 2019). Mars and lunar regolith are expected to host gases such as oxygen and helium-3 respectively (Guerra et al. 2017; Crawford 2015), which could be used for life support or nuclear fusion.

The cost to launch payload (the cargo carried by a spacecraft) to low Earth orbit (LEO) is high, however, it has decreased significantly over time as new rocket technology has been developed. From 1970 to 2000, the cost to launch 1 kg of payload to low Earth orbit was

around 18,500 USD (Jones 2018). As of 2018, SpaceX's Falcon 9 rocket could launch 1 kg of payload for around 2,700 USD (Jones 2018). Therefore, the theoretical price of 1 kg of any material in LEO today (all else being equal) should be its price on Earth plus 2,700 USD. For example, the price of 1 kg of water on Earth is negligible, while in LEO it could be 2,700 USD. This gap presents an opportunity for a new space marketplace. If resources can be extracted from other planetary bodies for less than the cost to bring them from Earth, it could lead to a flourishing space resource prospecting and mining industry. As the cost to launch a payload to space reduces with further technological development, this may diminish the value of material in space. However, it also reduces the cost to launch missions to prospect for resources, extract/process them, and return them to Earth or Earth orbit.

There have also been proposals for decades for the Moon and Mars to host a permanent human presence, for the purposes of research, resource utilisation, and to give humanity a second home (O'Neill 1975). In addition to opening up new opportunities, this also gives humanity a long term back up in the event of a catastrophic or existential threat occurring on Earth, such as an asteroid/comet impact, super volcano, or some other natural or man-made event.

Asteroid and comet impacts are the primary known threat to life on Earth from space (Bottke et al. 2004). Despite the low frequency of major asteroid and comet impacts that threaten species extinction, smaller impacts occur frequently. In addition, given the major consequences of extinction level impact events, such as the 10 km Chicxulub asteroid believed to have resulted in dinosaur extinction (Durand-Manterola and Cordero-Tercero 2014), it is worth devoting substantial time and resources to studying asteroid detection and deflection.

It is expected that selecting the ideal method for prospecting, mining, or deflecting a planetary body will depend on its internal structure and geology (Holsapple 2004; Gritzner and Kahle 2004). Despite this fact and the potential and threat of space, relatively little is known about the structure and geology of other planetary bodies. Especially little is known about the interior of comets and small asteroids (Walker et al. 2009), with most current knowledge based on meteorite samples found on Earth. Some potential models for asteroid structure have been proposed, including monolithic, rubble piles, gravel conglomerations, solid bodies with a loose regolith exterior, and heavily fractured/porous bodies, however, none have been directly confirmed for any given small planetary body (SPB) (Walker et al. 2006; Asphaug 2014).

The seismic method of geophysical exploration is a geophysical tool that records sound waves, either with a natural or man-made source, that travel through a body to understand its interior. Seismic has been used over the past 100 years on Earth to great success to understand the planet (Harold 1926; Lehmann 1936; Hori et al. 1985; McNutt 2005; Harper et al. 2012; Dahlman and Israelson 2016). It has seen some limited use on some bodies across the Solar System such as Mars (Panning et al. 2017; Banerdt et al. 2020; Giardini et al. 2020) and the Moon (Kovach and Watkins 1973a; Nakamura 1983; Nakamura 2005; Weber et al. 2011; Knapmeyer and Weber 2015) but has not been used on asteroids or comets to date. A proposal to use seismic on an asteroid was made by Anderson (et al. 2014) but was later cancelled due to a lack of government support. Given this, this thesis aims to explore the potential for seismic to be used in off-Earth bodies to understand their interior, with a focus on its use for prospecting, mining, and deflection purposes. A combination of literature analysis and laboratory experiments has been undertaken throughout this thesis, at both

UNSW and the Jet Propulsion Laboratory (JPL), NASA, in the USA to explore the use of seismic in off-Earth environments and its potential.

There is a significant gap in the literature on research on the seismic properties of low-compaction regolith, fine-grained regolith, regolith in low atmospheric pressure, and the combination of these properties. Regolith of this nature is the primary surface material on solid planetary bodies other than Earth, which makes this a critical gap to fill to ensure the success of future seismic missions in planetary exploration. This thesis aims to fill this gap by conducting novel seismic experiments on regolith with the above properties and undertaking computer and numerical modelling.

1.2 Research aim and objectives

The main goal of the research presented in this thesis is to examine the potential for seismic geophysical exploration techniques to be used in an off-Earth context, i.e., on the Moon, Mars, asteroids, and other planetary bodies. This involves several research objectives:

- examining the effect of vacuum and other environmental effects of the space environment on the collection of seismic data;
- investigating the effect of the rock and soil media found off-Earth on seismic data collection, and their seismic properties;
- understanding the use of seismic to determine geomechanical and other rock and soil properties off-Earth;
- using computational and analytical modelling to validate and expand upon the experimental results;
- determining the effectiveness of using seismic with a limited number of sources and receivers; and

- exploring the use of other geophysical and remote sensing tools to support off-Earth geophysics.

1.4 Thesis overview

The thesis is organised into nine chapters. The main contributions are presented in Chapter 3 to Chapter 8. Chapter 1 is an introduction to the thesis and outlines the research gap and main contributions. Chapter 2 sets the motivation for this research, discussing the importance of space in terms of potential benefits and threats, and examines some ethical considerations. Chapter 3 reviews the use of seismic in space, including past off-Earth seismic missions, the fundamentals of seismic geophysics, and the potential benefits of using seismic in space. Chapter 4 outlines the design of the seismic apparatus developed for this research, which is novel and will be used to fill the gap in the understanding of seismic response to low-compaction, fine-grained regolith in low atmospheric pressure. This chapter also presents some preliminary laboratory experimental data. Chapter 5 expands upon the laboratory work to determine the effect that the off-Earth environment has on seismic data collection and results, including atmosphere, and examines the seismic properties of some off-Earth regolith simulants, further working to fill the gap in understanding of seismic properties of off-Earth regolith. Chapter 6 explores and undertakes computational and analytical modelling to validate and expand upon the experimental results of Chapter 4 and Chapter 5. Chapter 7 proposes a methodology for delivering seismic devices to off-Earth bodies using penetrator probes, which aids in filling a gap in the ability to place seismic devices on planetary bodies. Chapter 8 critically reviews the existing remote sensing technology and considers how it might be used to aid in seismic geophysics and landing site selection. It also presents a workflow for how remote sensing may be used to support geophysical work in space exploration missions, such as the techniques covered in previous chapters, further filling the gap in the ability to

place seismic devices. Chapter 9 summarises the thesis and provides conclusions and recommendations for future work. Figure 1 visualises these chapters and how they relate to each other in a flowchart.

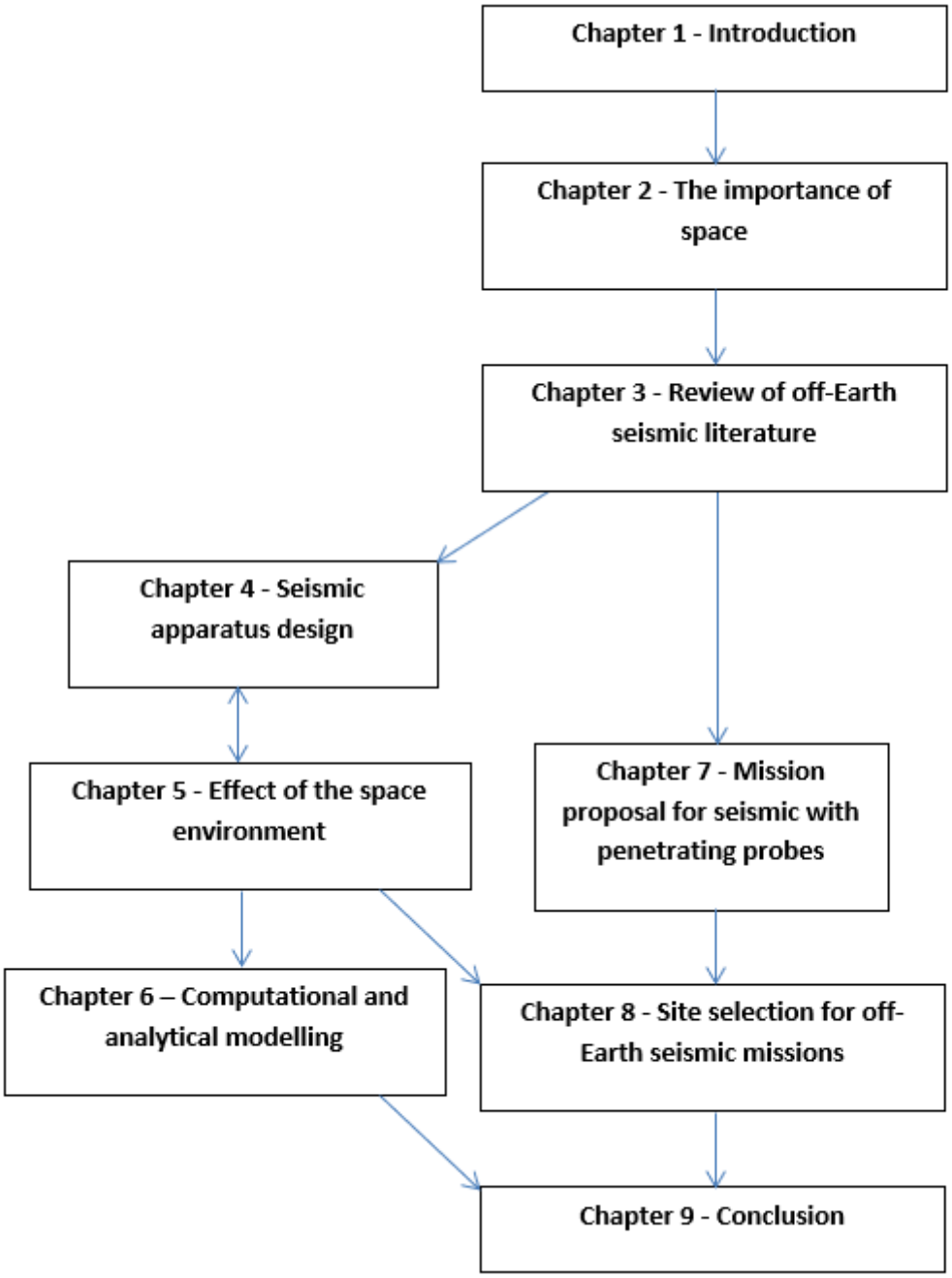

Figure 1 – Flowchart showing thesis chapters and how they relate to each other throughout the research process. Chapter 4 is an expanded version of a paper published in the 2017 Lunar and Planetary Science Conference. Chapters 5 and 7 are both papers in review with the *Geomechanics and Geophysics for Geo-Energy and Geo-Resources and Icarus* journals respectively.

2. The Motivation - The importance of space: Potential and threat

2.1 Introduction of motivation

Deep consideration of the space environment is incredibly important yet heavily neglected. To use the language of Nick Bostrom (Bostrom 2003) "*the stakes are astronomical*". Both the potential and threat that the space environment poses will be summarised here, setting the context and motivation for the rest of this thesis, which will be more specific. In addition to the economic and scientific arguments, ethical arguments for considering space will also be summarised in this chapter.

2.2 A note on ethics

Many have an intuitive sense of what it means to do good, or to be good. In this chapter, it will be argued that to consistently discuss why the potential and threat of objects from space are good and bad respectively, or why they are things we should pursue and defend against, we need to define what 'good' means, in this context. Why would it be 'bad' for future generations to not exist, such as due to a major asteroid impact, and why would it be good to prevent it? Broadly speaking, there are three main schools of ethical thought: deontology, consequentialism, and virtue ethics, though there are surely many branches within each.

Deontology is the view that ethical choices are judged by the actions themselves, not the outcome of those actions (Singer 2013). This is directly contrasted with consequentialism, in which the outcomes of an action are the primary metric used for weighing up different actions. In particular, the branch of consequentialism known as utilitarianism involves maximising good outcomes, often seen to be an increase in wellbeing and a decrease in suffering experienced by sentient minds (Singer 2013). This will be used as the framework for considering the potential and threat of space for the rest of this chapter. Finally, virtue ethics

is an examination of character, whereby a good action is the one that a person of good character would take. For more on each of these ethical frameworks can be found in Singer (2013).

Many examinations of ethics in the conventional space science literature appear to take a deontological approach (McKay 1990; Cockell and Horneck 2004; Cockell and Horneck 2006; Cockell et al. 2006; Schwartz 2013) or human-centric view (Zubrin 2011; Smith 2014) for granted. It is important not to take any given ethical approach for granted, since each will inevitably lead to a different course of action when trying to do 'the right thing' in many situations. Haynes (1990) and McKay (1990) acknowledge that important questions such as whether transforming the surface and environment of Mars would be ethically good depends on competing ethical value judgements, and that undertaking such major actions should wait for some kind of ethical consensus. Pollack and Sagan (1991) also argue for a precautionary approach in space exploration given the scale and the unpredictable consequences of actions.

Robert Zubrin, who has arguably been the leading advocate for Mars colonisation and terraforming for many years, makes human-centric utilitarian arguments, but does not appear to make them a central part of their argument. Zubrin (2011) states that "*I would say that failure to terraform Mars constitutes failure to live up to human nature and a betrayal of our responsibility as members of the community of life itself.*" Terraforming involves the transformation of a planetary body's surface and atmosphere with the goal of making it habitable by humans without the need for space suits and pressurised environments (Zubrin 2011). This concept is also referred to as ecopoiesis, which is defined as the "*fabrication of a sustainable ecosystem on a currently lifeless, sterile planet*" (Haynes 1990).

Many existing ethical examinations of space have not included any ethical consideration of non-humans. Moreover, Smith (2014) explicitly states that some or all non-human animals are not worthy of moral consideration, except through the lens of how their consideration affects humans. Yamashita and co-workers (2009) consider how non-humans might be used as tools in the process of terraforming Mars without consideration of their own interests. From the utilitarian approach at least, given that non-human animals can also experience suffering and wellbeing, they should also be worthy of ethical consideration.

More recently, researchers have begun to approach space ethics with a utilitarian outlook (Bostrom 2003; McKay 2007; Beckstead 2013; Sparrow 2015; Graves 2016). Beckstead (2013) argues that consideration of the far future is important and neglected. If not beset by some extinction event, humanity may survive indefinitely, leading to a countless number of lives in the future, potentially expanding to other planetary bodies. Actions taken today can meaningfully impact the future and the trajectory of humanity and all life, therefore considering how we affect the future and thinking about how we can maximise the good outcomes for future generations is critical.

2.3 The potential of space

The potential benefits from space include the resources that may be extracted for use, the extra space for colonisation, and the possible gains to scientific knowledge. There are many resources on planetary bodies such as the Moon, Mars, comets, and asteroids which could be utilised (Luxembourg Space Agency 2018). For example, ice is potentially abundant in some environments such as on asteroids and comets (Sunshine et al. 2006). Water (in different forms, such as ice and/or hydrated minerals) also exist in relatively high quantity on the lunar (Feldman 2001) and Mars (Byrne et al. 2009) surface. Ice can be valuable for use as rocket propellant, as it can be split into hydrogen and oxygen using electrolysis, which can be used

as fuel and oxidiser respectively (Lewis 1997; Sowers and Dreyer 2019), or it may be used for life support. Many asteroids are rich in metals (Ostro 1985; Kargel 1994; Blair 2000; Zacny et al. 2013) and other resources (Lewis 1997; Lewis 2015). The near-surface of planetary bodies, including Earth, is largely covered in regolith, a layer of unconsolidated rocky material covering bedrock created from physical, chemical or biological weathering processes (Mitchell and Soga 2005). This regolith can often contain valuable resources. in addition to ice, the lunar regolith may be a promising source of helium-3 for nuclear fusion reactors in the future (Crawford 2015), and Mars regolith may provide oxygen for use as life support (Guerra et al. 2017).

There are three main ways that space resources could be used. First is *in-situ* (*in-situ* resource utilisation; ISRU), where the resources are extracted and used on the same planetary body, for example the extraction of water ice for life support, or regolith for use in building construction. This could enable missions that are considered difficult due to resupply cost, such as manned missions to Mars.

Second is to use the material at some location between its extraction site and Earth, such as extracting water ice on the Moon or near Earth asteroids (near Earth objects - NEOs), applying relevant technology, such as electrolysis to separate the hydrogen and oxygen, and using it to refuel satellites in Earth, Mars and/or lunar orbit. Currently, no satellites besides the International Space Station are designed for refuelling. However, if refuelling was shown to be a viable option, future satellites could be launched with this capability, eliminating the need to let their orbits decay and send a replacement satellite every 20-30 years.

Third is to extract the resources and return them to Earth for use, such as platinum group metals (Blair 2000) and other valuable materials. Some processing may be performed onsite

to reduce the amount of waste material which can be transported to Earth. It is expected that this will not be feasible for less valuable bulk metals such as nickel and iron. Despite nickel-iron rich asteroids being an abundant category rich in these metals (with some asteroids being near-pure native nickel-iron), given the costs, it is not expected that returning these materials to Earth will be commercially viable for some time (Craig et al. 2014). Other materials such as platinum group metals, rare-earth elements (REE) and gold, which may be exceptionally high in concentration in some asteroids and have a higher value per kg, will likely be the first materials returned to Earth for commercial sale.

Blair (2000) estimates (with some generous assumptions) that a stony (S-type – detailed in Section 3.3.2.3) asteroid 10 m in diameter with a platinum grade of 30.7 g/ton at 500 USD/oz would be worth 690,000 USD, and that an asteroid with the same properties with a diameter of 1,000 m would be worth 690 billion USD. At the time of writing of this thesis, platinum is worth around 990 USD per ounce, bringing the same asteroids to values of 1.37 million USD and 1.37 trillion USD. These estimates do not account for the costs of extraction and return to Earth. They also do not account for the impact that returning these metals to Earth would have on the existing platinum market and therefore the price. The annual supply of platinum as of 2019 was 190 metric tons (WPIC 2019), which would be valued at around 4.8 billion USD. This makes the 1,000 m asteroid example above 200 times greater than the existing annual supply of platinum. Returning even a fraction of this would likely have a major downwards effect on the price of platinum due to massively increased supply, reducing its value.

It is expected that the first two of these options will be used initially, with the latter being less viable in the short term. A large part of the benefit of extracting resources off-Earth is that they do not need to be launched from Earth, eliminating the associated launch costs. As stated

earlier, the lowest cost to launch 1 kg of material to low-Earth orbit is currently around 2,700 USD (Jones 2018). In theory, this sets the value of 1 kg of water in low-Earth orbit at a minimum of 2,700 USD. Resources returned to Earth would be valued at their standard market value. However, there may come a time when some resources become sufficiently hard to find or extract (e.g. we are looking to deeper, more challenging and less concentrated resources on Earth in the future; Roach et al. 2016) that makes extracting them off-Earth more viable.

Craig et al. (2014) undertook an economic analysis of mining a near Earth orbit asteroid and transporting the material to Earth for use over a 100-year mission life. They concluded that such a project could not currently be considered a viable operation due to the large initial cost (1.3×10^{15} USD) compared to the net present value (NPV) of 658×10^{9} USD.

Other resource related benefits from space include collecting energy and wirelessly transmitting it to Earth (Reynolds 2015). Solar power farms could be set up on the Moon, utilising its open space, and the power they collect could be beamed back to a collection point on Earth using either a laser or microwaves (though microwaves may not be feasible due to the size of the transmitter required; Reynolds 2015). This could also be used to beam power from a satellite to an operation on a planetary body where a regular supply of sunlight may not be readily available, such as at the poles of the Moon.

When thinking about the far future, Bostrom (2003) considers the possibility of expanding humanity's presence beyond the Solar System. Given the vast number of lives that could exist over this time and space, we should put serious thought in to how we may affect them. If we think that these future individuals experiencing lives worth living is 'good' in the ethical sense,

then we should take steps today to ensure their future. Bostrom (2003) goes further and argues that delaying the spread of human life across the galaxy is an 'astronomical waste'.

To this end, this chapter discusses considerations around colonisation in space. A major long-term motivation for colonisation and consequently terraforming efforts is to give humanity or life in general a second chance. If some catastrophes were to befall Earth which caused human extinction or the extinction of all life, a colony on the Moon or Mars could survive and humanity could continue. Such events are called 'existential risk events' and are described in more detail in section 2.4.

There have been many proposals for an extended or permanent human presence on Mars and the Moon. Advocates such as Robert Zubrin and Elon Musk have been arguing for the development of a Mars colony as soon as possible. Zubrin (2011) discusses a framework for how a Mars base (and eventually Mars colony) could develop. The 'Mars Direct' plan relies heavily on ISRU, thus, reducing the amount of material that must be brought from Earth.

On day one of the plan, an Earth return vehicle (ERV – spacecraft capable of returning from Mars to Earth) is launched from Earth and arrives on Mars in approximately six months. The ERV deploys a rover capable of producing fuel via ISRU, eventually resulting in an ERV with sufficient fuel to return to Earth. Mars launch windows are once every 26 months, and so 26 months after the launch of the first ERV, two more spacecraft are launched to Mars; a second ERV and a habitat module with a human crew. After 18 months on Mars, the first human crew can return to Earth using the first ERV, which will be fully fuelled by this time. By the time they return to Earth six months later, another two spacecraft are sent to Mars, including another ERV and habitat module with astronauts. This process is repeated or can be expanded to send multiple ERVs and crews per launch window (Zubrin 2011). The main benefit of this plan is

that it eliminates the requirement to bring fuel from Earth for the return trip, which is a major limitation given the amount of additional mass it requires.

Discussions around terraforming have largely focused on Mars, given its proximity and similarities to Earth, including gravity, day/night cycle, and an existing atmosphere (~1% Earth atmospheric pressure, primarily CO_2; Zubrin 2011). By these criteria, Venus may pose another option, however, its atmosphere currently proves so hostile that probes sent to its surface rarely survive for more than a few hours (Ksanfomaliti et al. 1982), making any terraforming difficult.

Some of the technical considerations around terraforming Mars are covered by McKay et al. (1991a), Graham (2004), Marinova et al. (2005), Fogg (2011), Zubrin (2011) and Jakosky and Edwards (2018). One proposed method for terraforming includes releasing the CO_2 present at the Martian polar ice caps and in regolith using orbital mirrors, production and release of artificial halocarbon gases, and the generation of bacterial ecosystems. Zubrin (2011) estimates that this process could result in an atmospheric pressure 30% of Earth's. Uncertainties such as the amount of CO_2 in the poles and regolith strongly affect this and estimates of the time for the full terraforming process range from around 900 years (Zubrin 2011) to 100,000 years (McKay 2007), though a partially terraformed Mars may still present advantages, such as more favourable temperature ranges.

McKay (1990) argues that it would be unethical to terraform Mars if pre-existing microbial life were discovered, which seems to represent a prevailing view in the space science and terraforming community. It is noted that past discussions of the ethics of terraforming Mars rarely approach the question from a utilitarian framework, with McKay (2007) and Sparrow (2015) being two notable exceptions. However, neither considers the impacts of terraforming

on non-humans for their own sake. Some possible impacts of terraforming on non-humans arise if we consider how animals might be taken from Earth to Mars for food or populating wildlife, or if we consider proposals to use insects in the mid-late stage terraforming process (Yamashita et al. 2009). This chapter argues that we should also consider these impacts on non-humans when considering the ethics of colonisation and terraforming.

2.4 The threat of space

Another aspect of the astronomical waste argument of Bostrom (2003) is that any event which prevents humanity from realising that future would be bad. Parfit (1986) considers three scenarios to illustrate this point:

1) Peace,
2) A nuclear war that kills 99% of the world's existing population, and
3) A nuclear war that kills 100%.

Parfit (1986) further argues (and likely most people would agree) that 1) is the best outcome, and 3) is the worst. It is expected that many people would have an intuition that the difference between 1) and 2) is greater than the difference between 2) and 3) (this was tested by Schubert et al. 2019, and was found to be largely true), while Parfit (1986) argues that the difference between 2) and 3) is greatest, since human extinction would mean the loss of future human lives, which as Bostrom (2003) argues, could be astronomical in number. Therefore, we should be extra wary of existential threats, significantly more so than catastrophic threats (which may cause catastrophic damage but would not cause human extinction).

Potential existential threats include global health pandemics, super volcanoes, asteroid impacts, runaway artificial intelligence scenarios, extreme climate change and global nuclear

war to name a few. All these events could be considered catastrophic or existential threats, depending on their severity.

The threat from space objects directly is primarily due to the risk of asteroid impacts (Bottke et al. 2004), which despite their low frequency are a relatively high risk due to their large consequences (Rees 2003). Impacts from comets and asteroids (small planetary bodies; SPBs) 5 km or greater in size occur every 20 million years (Marcus et al. 2010), for example the 10 km body that impacted 66 million years ago (Renne et al. 2013). SPBs greater than 1 km in size impact every 500,000 years (Bostrom 2001), SPBs 7 m and 4 m or larger enter Earth's atmosphere approximately once per 5 and 1 years respectively (Marcus et al. 2010).

While it may be expected only the largest of these to pose existential threats, smaller SPBs may still cause catastrophic damage. For example, the Tunguska event involved an SPB with diameter 50-190 m (Lyne and Tauber 1995) air bursting (exploding from the pressure and heat) 6-12 km above the surface of Siberia in 1908, releasing 3-50 Mt of energy and flattening around 2,000 km^2 of forest (Jenniskens et al. 2019). While it remains somewhat contentious, there are reports of human deaths occurring from the Tunguska event (Jenniskens et al. 2019) and other previous impact events (Gritzner et al. 2006). Populated areas being relatively rare on Earth's surface helps mitigate the risk of loss of human life from impacts, but SPBs landing in the ocean may cause tsunamis which will impact coastal areas (Ward and Asphaug 1999).

As of at least 2006, it is likely that we have detected all near-Earth asteroids of around 1 km in diameter or larger (Huebner et al. 2009), though as of 2014 it is likely we have only detected around 10% of bodies 100 m in diameter (and an increasingly smaller proportion of smaller bodies; Harris and D'Abramo 2015; Figure 2). In addition, there is a large population of comets with long orbital periods that spend most of their life being very distant from the Sun and

hard to detect. Though unlikely, any one of these bodies could be on a collision course with Earth. There is also the problem of bodies that come from outside the Solar System, such as Oumuamua which was detected in 2017 (Trilling et al. 2018). When Oumuamua was detected, it was around 33 million km from Earth (85 times the distance from Earth to the Moon). At its average speed of 26.33 km/s, it is roughly estimated that it would been just 9 days away from impact if it had been on a collision course with Earth.

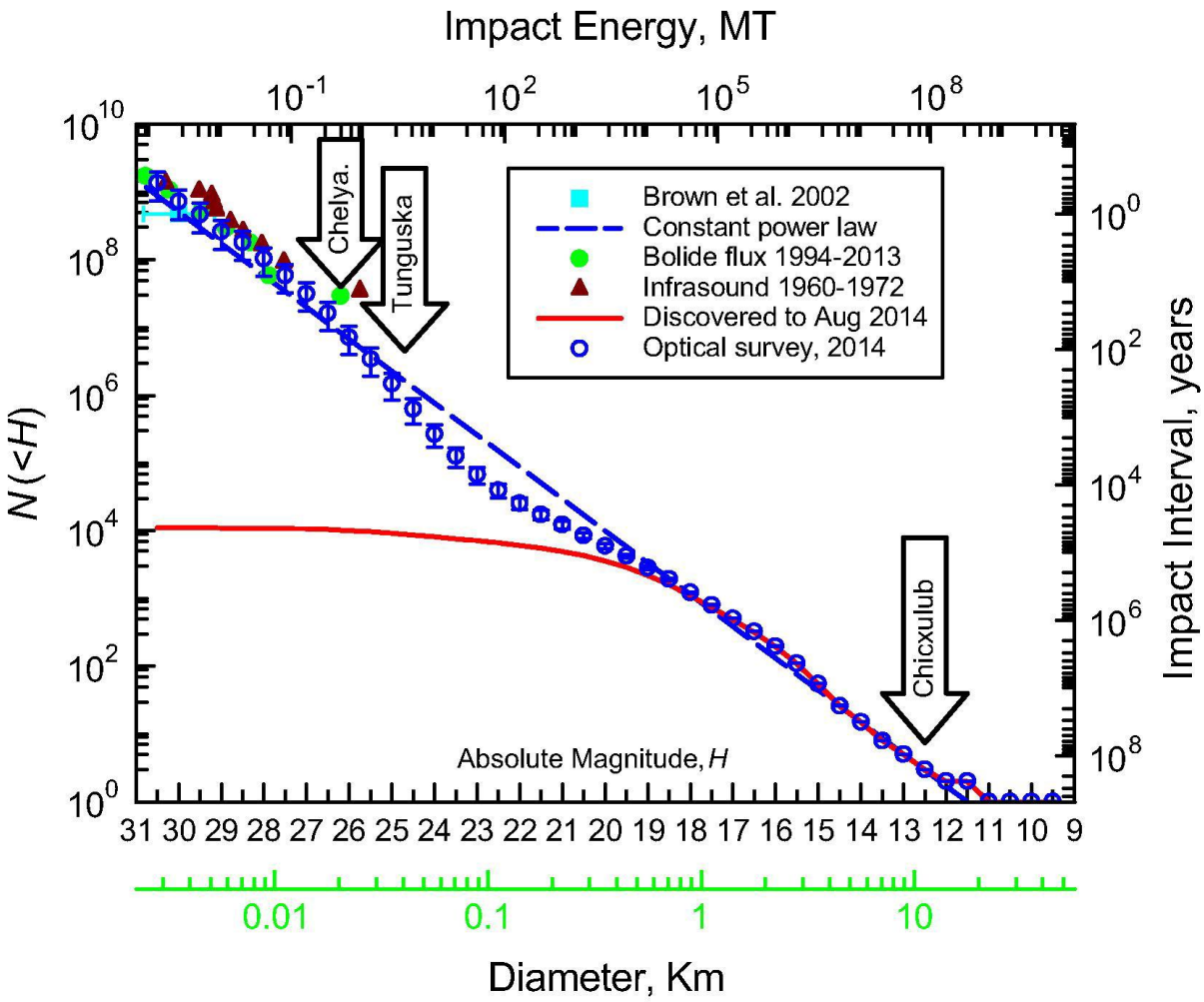

Figure 2 – The estimated number of near-Earth asteroids of a given size from various references, and the number of discovered near Earth asteroids at given sizes (Harris and D'Abramo 2015).

Accounting for loss of future lives as discussed above, Matheny (2007) has suggested that asteroid detection and deflection technology development could save a human life-year for 2.50 USD, implying a high cost-effectiveness. While this requires future lives being valued equally to present-day lives, it is worth considering as an argument for increased asteroid

detection/deflection research and development. Huebner and Bradley (2016) sought to estimate the damage from a small asteroid impact versus the cost to deflect it. If a 100 m asteroid impacted Earth and had all its energy converted to seismic energy, it might be expected to kill over 100,000 people and cause damage from uninsured losses worth 210 billion USD. Huebner and Bradley (2016) compare this with the cost of NASA's Deep Impact mission, which launched an impactor at Comet 9P/Tempel, at 330 million USD.

The deflection dilemma (Sagan and Ostro 1994) poses a counterargument to the urgency of developing deflection technology. SPB deflection technology can be used to prevent naturally occurring SPB impacts, but it could also be used to deflect an otherwise harmless SPB into an Earth-intersecting orbit, either intentionally or accidentally. Sagan and Ostro (1994) argue that asteroid deflection technology may therefore increase asteroid impact risk rather than decrease it. They also argue that, given how humanity has dealt with new weapons of mass destruction such as nuclear weapons, it may be premature to develop asteroid deflection technology. This concept is explored in more detail in Chapter 3.

2.5 Conclusion of motivation

This chapter has sought to cover some of the motivations for the work presented in this thesis and research relating to space. To return to the ethical considerations, depending on our chosen ethical framework, our goals and therefore the approach we take towards space will be different. This is a point rarely conceded in discussions about the potential and threat of space. If one takes the utilitarian approach, as is preferred by the author, our goal should be to create the most wellbeing and reduce the most suffering of sentient beings both now and in the future. How to best do this is an important but difficult question, of which this thesis plays but a small but necessary part in answering.

3. Seismic exploration in an off-Earth context: History and potential

3.1 Introduction of off-Earth seismic exploration

3.1.1 Motivation

The benefits and threats of space are many. A wide range of resources have been proposed as being possibly extracted for either return to Earth or use in space or on the planetary body itself. For example, ice may be abundant in some environments such as asteroids, in permanently shadowed craters on the Moon, and beneath the surface of Mars, and may be used as a propellant by separating the water into hydrogen and oxygen through electrolysis (Lewis 1997) or for life support (Sridhar et al. 2000). As the propellant required for travel from the Moon and some asteroids to LEO is less than the propellant required for travel from the Earth's surface to LEO (Caltech 2007; Benner 2018), it could plausibly be more efficient for satellites, space stations and other missions to refuel with hydrogen and oxygen from the lunar poles.

Several space resources companies, Planetary Resources, Deep Space Industries (DSI), and Shackleton Energy Company (these companies are no longer active) were founded with the intention of prospecting and extracting these resources. DSI proposed to use electrolysed water extracted from asteroids to refuel communications satellites in the future and extend their working life (DSI 2013). One limitation to such plans is that most satellites are not designed with refuelling in mind and will allow their orbits to decay once they run out of fuel. This presents a market opportunity; however, it also means that future satellites would have to be redesigned with refuelling capability.

Economically viable metal deposits are becoming increasingly harder to find on Earth, with many of the concentrated, near-surface deposits already being extracted (Roach et al. 2016),

leaving deeper and more challenging to extract deposits. As well as being plausibly more economically efficient, extracting metals from asteroids and returning them to Earth (Badescu 2013) may also reduce the environmental footprint of extraction. Resources returned to Earth lose the economic advantage of saving launch costs (e.g., with selling propellant in Earth orbit), and so will likely need to have a higher value to weight ratio to make them economical.

Helium-3 has a price of around 1,400 USD per gram at the time of writing and can be found in abundance in lunar regolith where it has been emplaced by solar wind (Johnson et al. 1999; Fa and Jin 2007; Fa and Jin 2010), and so extracting helium from the Moon and returning it to Earth (Taylor and Kulcinski 1999) or using it *in-situ* on the Moon (Sviatoslavsky and Jacobs 1988) has been proposed. Helium-3 is valued for its use in medicine and scientific research, and it also has the potential for use in nuclear fusion reactors in the future. Additionally, helium-3 supply has experienced a relative shortage in the past several decades (Shea and Morgan 2010). Currently, the primary source of helium-3 is the decay of tritium from nuclear weapons. As nuclear weapons are disarmed, the source of helium-3 is diminished (Zerriffi 1996).

Space-based threats largely refer to the risk of asteroids or comets (small planetary bodies – SPBs) impacting the surface of Earth (Bottke et al. 2004). SPBs greater than 5 km in diameter impact Earth once every 20 million years on average (Marcus et al. 2010), and SPBs 1 km or larger impact Earth once every 500,000 years on average (Bostrom 2001). Despite the low likelihood of a major impact event on a given year, the risk is high due to the enormous loss of life and lasting damage if one were to occur (Rees 2003). Considering present and future lives, Matheny (2007) argues that research and development in the field of asteroid detection

and deflection is incredibly important yet heavily neglected today, as reducing the likelihood of a low probability, high impact event has astronomical benefits on average.

The internal structure of an asteroid is expected to strongly control the optimum method of deflection (Holsapple 2004); however, relatively little is known about their interiors (Walker et al. 2009; Huebner et al. 2001; Greenberg and Huebner 2002). Although all NEOs greater than 1 km in diameter are reported to have been discovered (Huebner et al. 2009), other hazardous asteroids and comets might come from highly elliptical orbits, thus, being harder to detect in advance, and smaller asteroids will still cause significant local damage, despite perhaps not being civilisation ending.

Prospecting will be required to identify the location and concentration of valuable resources of other planetary bodies, and an understanding of their subsurface will be required to identify the best method for mining and extraction. Understanding the subsurface of asteroids and comets will also be critical to develop plans for their deflection in the event of an impending collision. As discussed below, geophysical methods, particularly seismic, are ideal for gaining this information.

3.1.2 Geophysical methods

A range of geophysical and remote sensing methods are available for understanding the surface and subsurface of a planetary body. These methods may be remote or requiring contact. Geophysical exploration methods include seismic, gravity, magnetics, electrical resistivity tomography, induced polarisation, magnetotellurics (MT), ground penetrating radar (GPR), surface nuclear magnetic resonance, hyperspectral imaging, and wireline logging. Table 1 compares some characteristics of these techniques. Their ability to determine the presence of water-ice and image it has been chosen as a key characteristic given the

likelihood of ice being the first resource to be extracted in space. Seismic is discussed in detail throughout the rest of this chapter, so a summary of the other geophysical methods will be given in this section.

Table 1 – A selection of geophysical methods and their ability to image the subsurface and detect the presence and quality of water/ice. Ice will likely be one of the first resources to be extracted off-Earth for use as life support and propellant, and so is prioritised in this comparison. This table was completed through a combination of the authors' experience with geophysics and a literature review.

Geophysical technique	Imaging	Presence of water/ice	Quality of water/ice	Comments
Seismic	Yes	Yes, with drilling	No	Requires surface contact
Gravity	No	No	No	
Magnetics	No	No	No	
Electrical resistivity tomography	Yes	Yes	Yes, with IP, SNMR or GPR	Requires surface contact
Induced polarisation	No	Yes	No	Requires surface contact
MT	Yes	Yes	Unsure	Unclear if this will work off-Earth as it relies on variations in Earth's magnetic field
GPR	Yes	Yes, with drilling	No	
Surface nuclear magnetic resonance	Yes	Yes	Unknown	Good for depths up to 200m
Remote sensing	No	Yes, if some surface expression	No	
Wireline logging	Yes (1 2D data point per well)	Yes	Yes	Requires drilling
Radio tomography	Yes, but low resolution	Unknown	Unknown	

The gravity method involves measuring the varying gravitational strength over an area from the ground or air and is used to infer variations in density in the subsurface which result in variations in the local gravitational field (Nabighian et al. 2005a; Hinze et al. 2013). Gravity surveys first saw success in petroleum exploration (Eckhardt 1940; LaFehr 1980), though despite still seeing some use in that field today, have been largely overshadowed by seismic (Nabighian et al. 2005a). Gravity is useful for regional geological mapping and identifying gravitational anomalies which may indicate subsurface features of interest (Carmen et al.

2011; Jallouli et al. 2005; Hinze et al. 2013). An example of a gravity survey from the Taupo Volcanic Zone in New Zealand is shown in Figure 3.

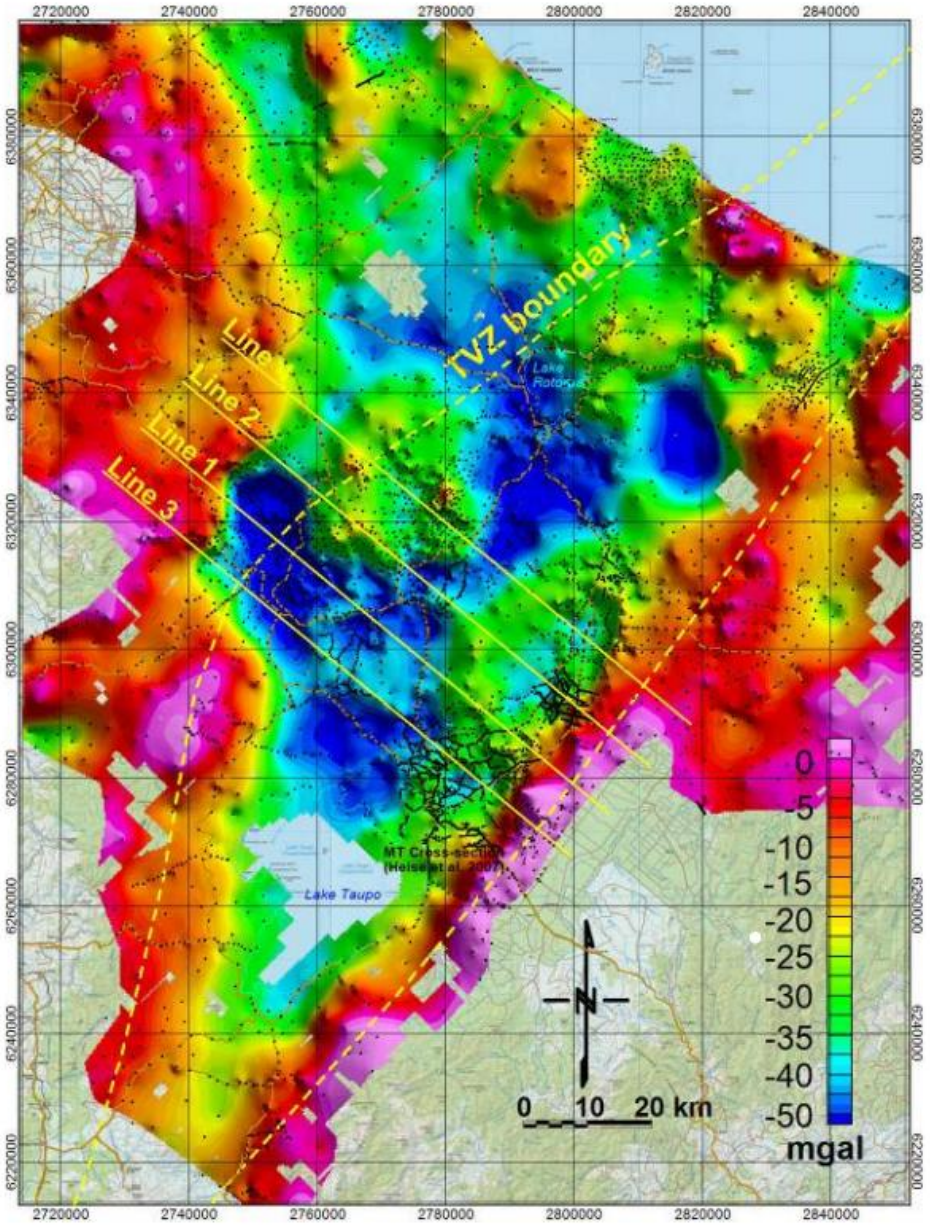

Figure 3 – Residual Bouger anomalies from a gravity survey of the Taupo Volcanic Zone, New Zealand (Soengkono 2011). The varying gravitational strength arises largely from local variations in the density of rock. Blue in this figure shows areas where the gravitational field is weaker due to less dense rock, while purple shows areas where the gravitational field is stronger due to more dense rock.

The magnetic method involves measuring the varying magnetic field over an area from the ground or from the air. This method has seen success in determining the location and concentration of low temperature (below around 580°C) iron deposits containing magnetite

and in regional geological mapping (Roux 1970; Macnae 1979; Keating 1995; Power et al. 2004; Nabighian et al. 2005b; Schetselaar et al. 2008; Barak et al. 2018). Most of the measured magnetic response is due to the Earth's magnetic field, originating from the convection of Earth's liquid iron outer core (Campbell 1997). External effects such as the interaction between Earth's magnetic field and solar wind also affect the magnetic response (Campbell 1997), and so must be removed from the data via processing (Nabighian et al. 2005b). An example of data from an airborne magnetic survey is shown in Figure 4.

The electrical resistivity tomography (ERT) method, also known as the electrical resistivity imaging (ERI) method, is a direct-current resistivity technique for imaging the subsurface using measurements of electrical resistivity made at the surface or in a borehole (Zhou 2018). ERT is commonly used for identifying and imaging near-surface features such as sinkholes and major fractures (Šumanovac and Weisser 2001; Van Schoor 2002; Zhou et al. 2002; Chambers et al. 2006; Guérin et al. 2009; Sudha et al. 2009; Valois et al. 2010; Zhu et al. 2011). Examples of raw and modelled 2D resistivity sections from an ERT survey are shown in Figure 5.

The induced polarisation (IP) technique and the similar direct current (DC) resistivity technique are imaging techniques which determine the electrical chargeability of the subsurface (Binley and Kemna 2005; Veeken et al. 2009; Gazoty et al. 2012; Sumner 2012). Like ERT, IP and DC resistivity require contact with the surface to make measurements. The measurements are strongly influenced by fluid content and type, porosity, and other rock characteristics, making it an ideal method for near-surface groundwater and hydrocarbon studies (Binley and Kemna 2005). Typically, four electrodes are used to make a measurement, with two used as a current source and sink, and two used to measure the potential difference

(Binley and Kemna 2005). An example of a resistivity pseudo-section from the IP technique is shown in Figure 6.

The magnetotelluric (MT) technique is an electromagnetic sounding technique that measures the apparent electrical resistivity distribution in the subsurface using natural variations in the Earth's geomagnetic and geoelectric field (Chave and Jones 2012). MT is commonly used in geothermal exploration (Cumming and Mackie 2010; Lee et al. 2010; Ars et al. 2019) and sees use in petroleum exploration (Xiao and Unsworth 2006; Zhang et al. 2014) and operations monitoring (coal-seam gas depressurisation; Rees et al. 2016a; hydraulic fracturing; Lanfang et al. 2012; Rees et al. 2016b), groundwater monitoring (Li et al. 2017) and deep crustal research (Mohamed et al. 2002; Hautot et al. 2006; Santos et al. 2014). An example of a MT resistivity model from the Glass Mountain Known Geothermal Area in California, USA, is shown in Figure 7.

The surface nuclear magnetic resonance (SNMR) technique, also known as the magnetic resonance sounding (MRS) technique, is used to remotely estimate subsurface water content and other aquifer properties such as porosity and hydraulic conductivity. SNMR is conducted by generating an electric current through a cable on the surface, which applies an EM field to the subsurface. The current is then ceased and the magnetic resonance (emission of EM radiation after exposure to the EM field is ceased) in the subsurface is measured through receivers at the surface (Legchenko and Valla 2002). SNMR is commonly used in near-surface groundwater studies (Lieblich et al. 1994; Legchenko et al. 2002; Hertrich et al. 2007; Parsekian et al. 2013). An example of SNMR data is shown in Figure 8.

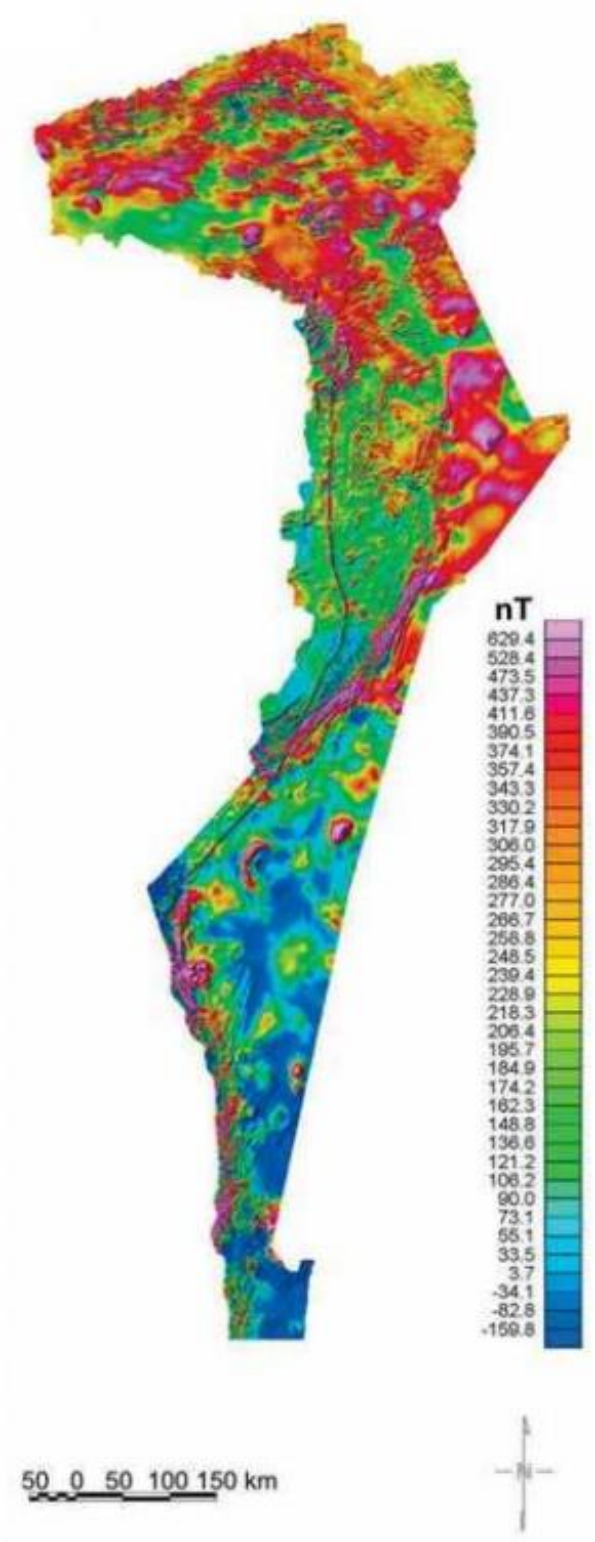

Figure 4 – Airborne magnetic survey data (residual total magnetic field intensity) from western Mozambique, with a grid resolution of 250 metres (Schetselaar et al. 2008).

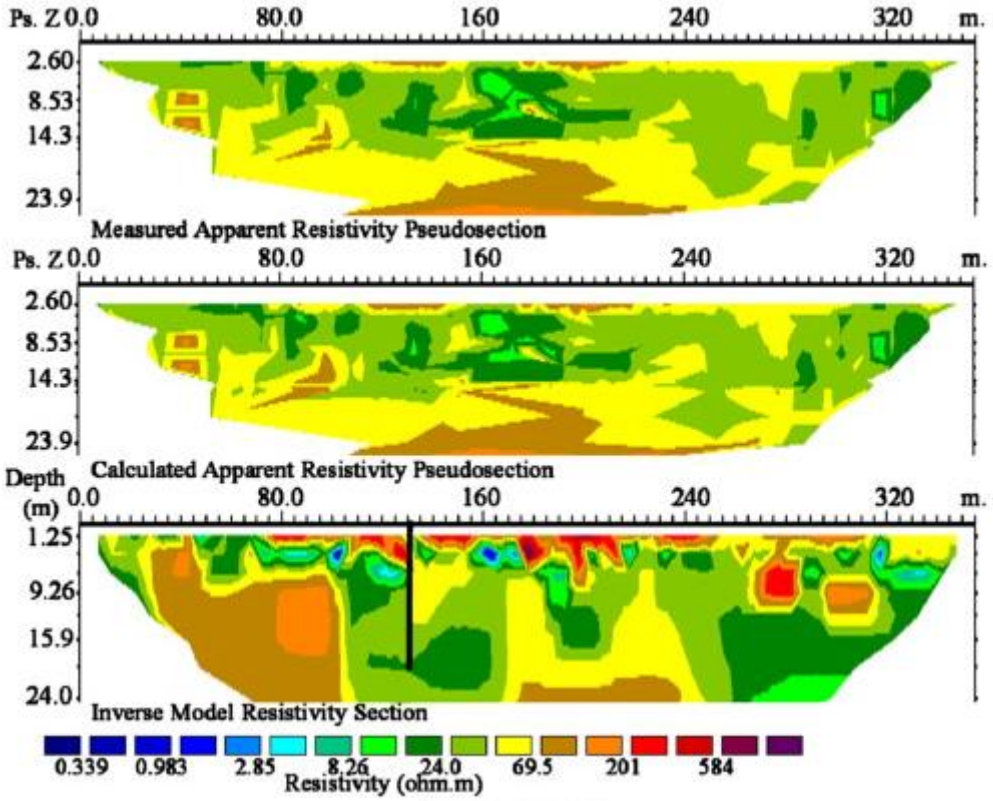

Figure 5 – Raw and modelled 2D resistivity sections from an ERT survey at Aligarh in Uttar Pradesh, India (Sudha et al. 2009). The high resistivity values near the surface of most of the profile indicates unsaturated soil.

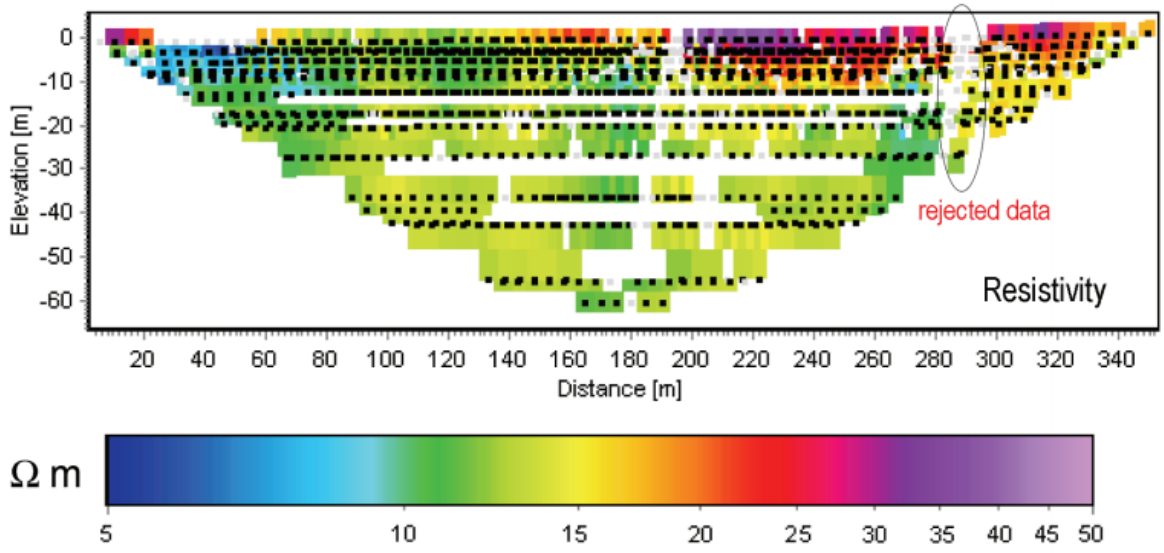

Figure 6 – A resistivity pseudo-section from data collected with the IP technique at a former landfill site at Eskelund, Denmark (Gazoty et al. 2012). The near-surface generally appears to have high resistivity, which may indicate unsaturated soil, though there are some exceptions.

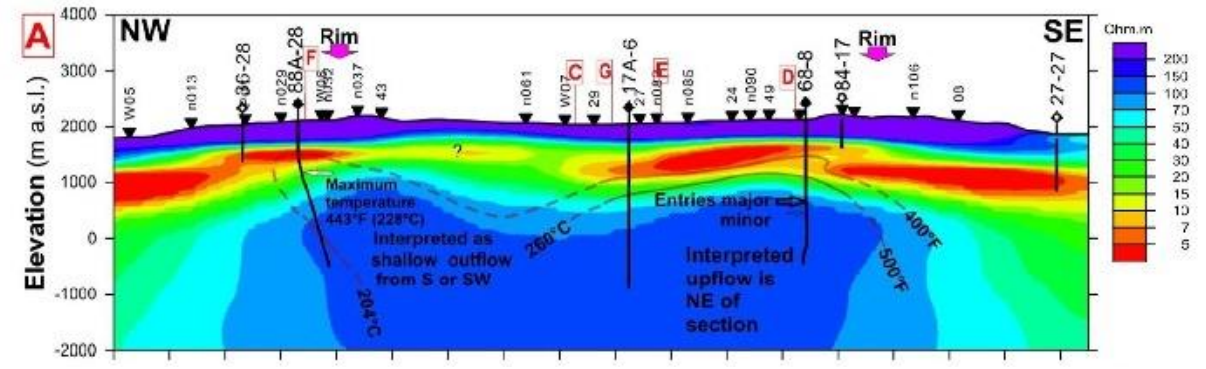

Figure 7 – 3D magnetotelluric resistivity model from the Glass Mountain Known Geothermal Area (Cumming and Mackie 2010). Elevation is shown in metres above sea level (MASL). The near-surface in this figure largely shows high resistivity which decreases with depth, though there is a large feature of moderate to high resistivity at depth.

Remote sensing techniques involve the use of EM waves to remotely determine information about the surface or subsurface of the Earth and can be either ground-based, airborne or satellite-based. Remote sensing is an umbrella term – techniques listed under this category are LiDAR (Hodgson and Bresnahan 2004), radar (Scheer and Holm 2010), radio tomography (Kofman and Safaeinili 2004), ground penetrating radar (Daniels 2005) and spectral imaging (multispectral and hyperspectral; Manolakis et al. 2016). Remote sensing techniques are discussed in more detail in Chapter 8.

Wireline logging involves the use of a range of geophysical tools attached to a device which can be lowered down a drill hole either during or after drilling. The most common wireline logging tools are a sonic log for measuring seismic velocity, a calliper for measuring drill hole diameter, and tools for measuring spontaneous potential, resistivity, natural gamma, high energy gamma, and neutron porosity (Hurst et al. 1992). Many of the other geophysical tools discussed in this section could also be placed on a wireline logging tool to grant them access to the subsurface. Wireline logging is most commonly used in petroleum exploration drilling (Mullins et al. 2004) given its ability to measure rock and reservoir properties useful for identifying hydrocarbons (Brown 2003; Tariq et al. 2017), and also sees use in groundwater

studies (Lachaal et al. 2012). An example of a continuous profile of wireline log data in shown in Figure 9.

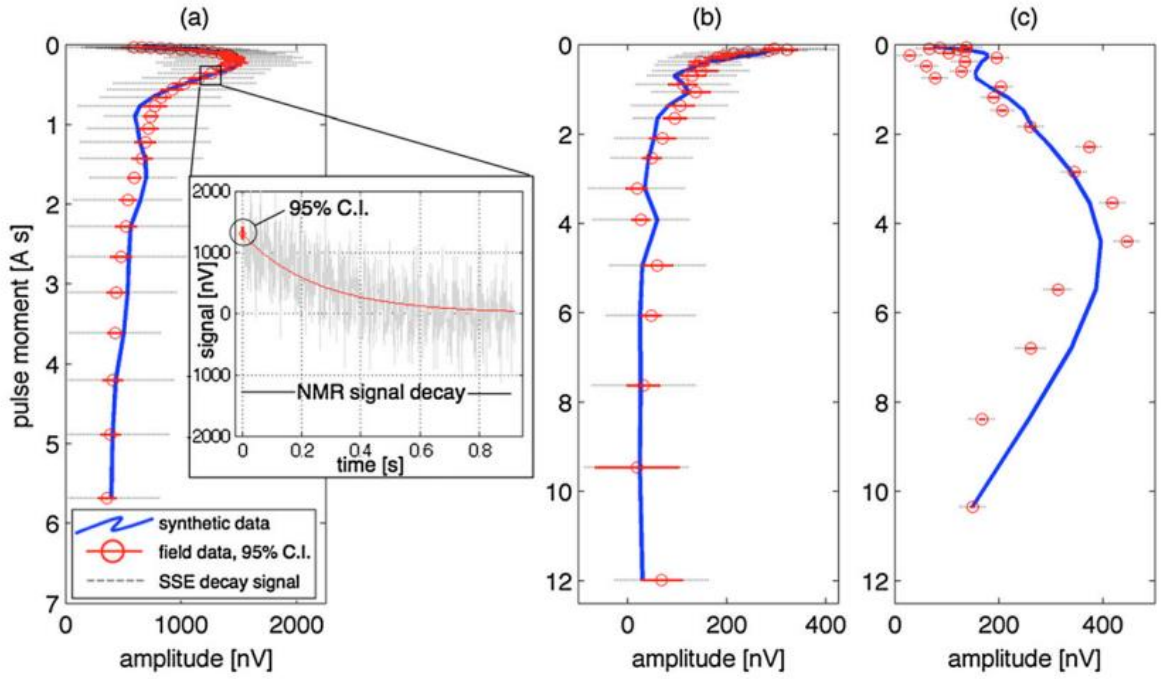

Figure 8 – Surface nuclear magnetic resonance data from three locations near Fairbanks, Alaska; Ace Lake (a), Caribou Lake (b), and Bonanza Creek (c) (Parsekian et al. 2013).

GPR imaging is similar to seismic; however, it utilises high frequency EM waves rather than mechanical waves (Daniels 2005; Jol 2009). While it has the advantage of not requiring surface contact to investigate a medium, it has limited penetration depth (especially in dry materials) and ability to infer geomechanical properties (Neal 2004; Jol 2009). It is therefore ideal for remote and shallow imaging, while seismic is preferable for deeper investigation for structural mapping and inferring geomechanical properties. GPR is commonly used in near-surface archaeology studies (Salvador and Conyers 2006; Conyers 2013), for the detection and mapping of shallow ice and water (Beres and Haeni 1991; Hinkel et al. 2001; Brandt et al. 2007; De Pascale 2008), and civil engineering (Saarenketo and Scullion 2000). GPR is also discussed in more detail in the context of remote sensing in Chapter 8.

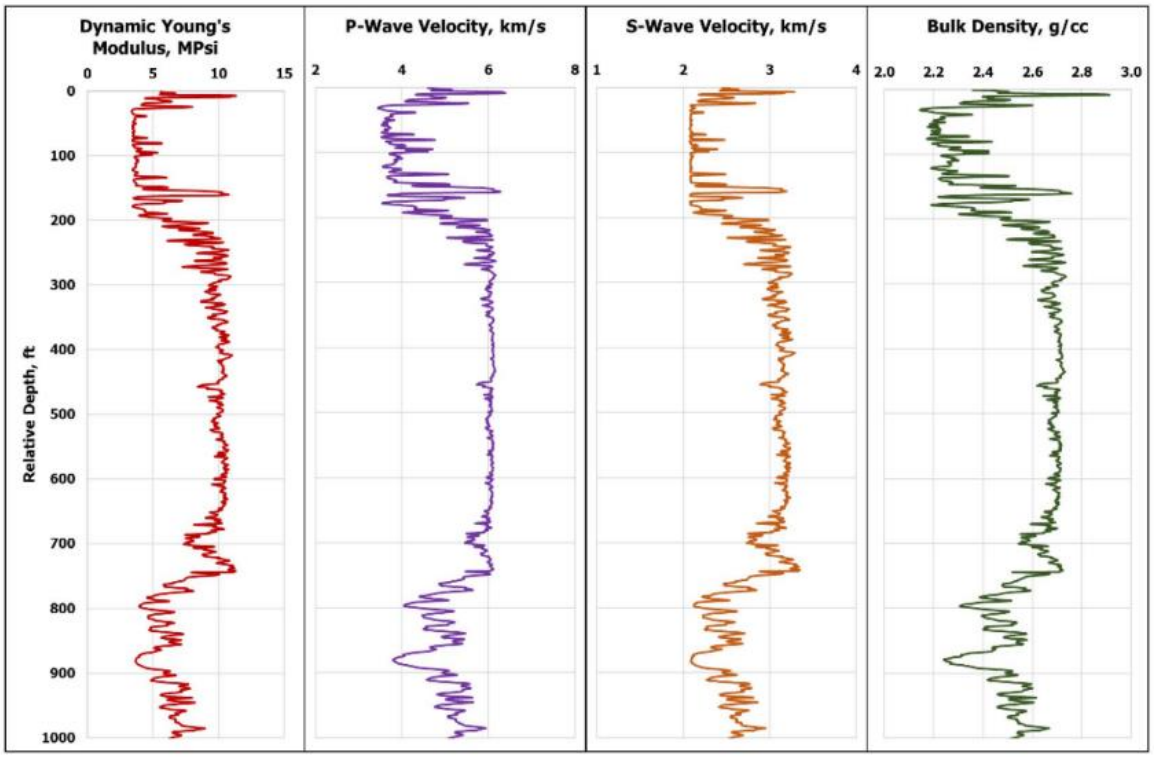

Figure 9 – A continuous log of four properties measured using wireline logging in a drill hole at a large carbonate reservoir (Tariq et al. 2017).

Non-uniqueness affects all geophysical methods, which indicates that a given geophysical measurement may result from a range of scenarios. For example, a gravity survey may indicate a region of higher gravitational strength. This may indicate a small, highly dense buried body. However, it may also indicate a large, moderately dense buried body (Figure 10). Geophysical methods should be used in combination with ground-truthing methods, such as directly observing a part of the subsurface by drilling a hole and using rock samples, or with downhole imaging.

3.2 Fundamentals of planetary seismic methods

3.2.1 Seismic method fundamentals

Seismic methods involve the measurement of a mechanical wave generated by a source, which may be either natural (passive) or artificial (active). Some examples of natural sources include earthquakes, volcanic eruptions, landslides, cave collapses, meteorite impacts and

shifting of a landscape due to thermal variation (as observed on the Moon with its day/night cycle; Duennebier and Sutton 1974). Artificial sources include explosives, kinetic impacts, and vibrational sources, the latter of which is the preferred method in modern seismic exploration. Artificial sources benefit from a known location and impulse time; however, triangulation of a natural source location may be achieved with sufficient receiver locations.

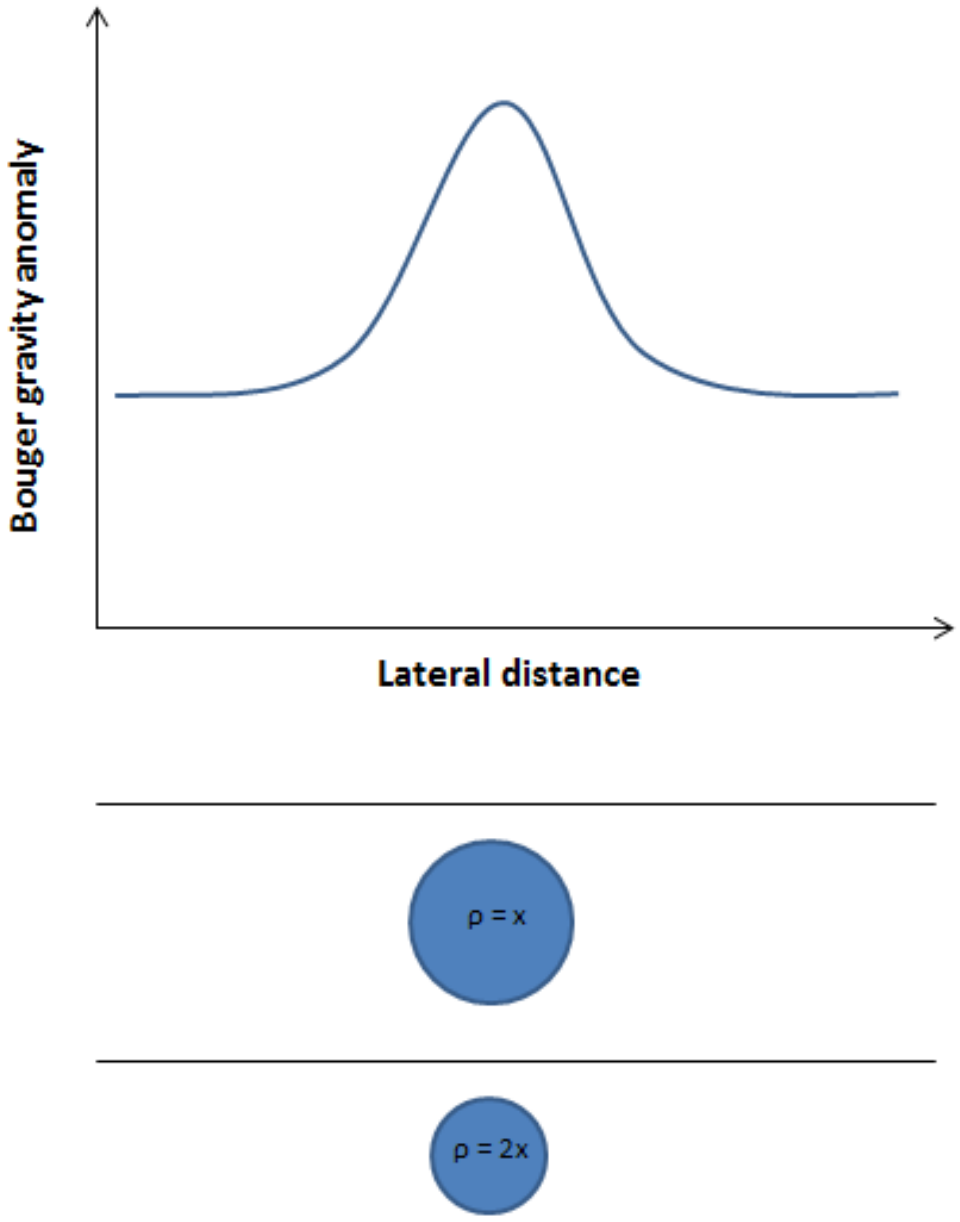

Figure 10 – An example of how two buried spheres of different sizes and densities can have the same response in a gravity survey. Sphere A is smaller and significantly denser than the surrounding rock, while sphere B is larger and moderately denser than the surrounding rock.

An impulse will produce several types of waves: compressional (P-waves), shear (S-waves), Love surface waves and Rayleigh surface waves (Ben-Maneham and Singh 2012). Different wave types will have different velocities for a given material. S-waves are slower than P-waves and do not travel through fluids or gases. Different mediums will also have different seismic velocities and acoustic impedances (the product of density and seismic velocity). Values for the seismic velocities and acoustic impedances of commonly encountered subsurface mediums are listed in Table 2.

Table 2 – Physical property values for common subsurface mediums at typical surface temperature and pressure.

Medium	**P-wave seismic velocity (m/s)**	**S-wave seismic velocity (m/s)**	**Density (g/cm3)**	**Acoustic impedance (kg/s . g/cm3)**	**References**
Saturated shale and clay	1100-2500	200-800	2.0-2.4	3.96	Bourbié (1987)
Granite	4500-6000	2500-3300	2.5-2.7	13.65	Bourbié (1987)
Air	343	N/A	0.0012	0.0004	Worland and Wilson (1999); Cavcar (2000)
Ice	3400-3800	1700-1900	0.9	3.24	Bourbié (1987)
Water	1450-1500	N/A	1.0	1.48	Bourbié (1987)
Dry sands	400-1200	100-500	1.5-1.7	1.28	Bourbié (1987)
Wet sands	1500-2000	400-600	1.9-2.1	3.5	Bourbié (1987)
Basalt	5000-6000	2800-3400	2.7-3.1	15.95	Bourbié (1987)

The primary formula used in seismic methods is:

$$V = dt \qquad (1)$$

Where V is the seismic velocity of a wave, d is the distance the wave travels, and t is the time taken for the wave to travel from point A to B. Given that different mediums have different seismic velocities, the fastest point from A to B is not always a straight line.

The sample rate refers to the rate at which the receiver records data. Understanding this is important for seismic data collection, and the sample rate will dictate the accuracy of velocity

measurements and imaging. The sample rate in seconds required for a desired accuracy of velocity measurement for a given medium velocity and travel distance is:

$$\Delta t \cong \left(\frac{L}{c_L}\right)\left(\frac{\Delta c_L}{c_L}\right) \quad (2)$$

Where L is the distance between source and receiver, c_L is the velocity of the material, and Δc_L is the desired accuracy in absolute terms (Walker et al. 2015). The result in seconds can be converted to the required frequency by dividing 1 by Δt.

The formula to calculate the acoustic impedance of a medium is:

$$Z = pV \quad (3)$$

Where Z is the acoustic impedance, p is the density and V is the seismic velocity. Upon reaching an interface between two mediums of different acoustic impedance, some of a seismic wave's energy will be reflected, and some will pass through with an angle of refraction (Figure 11). This phenomenon forms the basis for subsurface seismic imaging. A source produces a seismic wave which is reflected off various subsurface features, such as the boundary between two rock types, and the reflections are measured by an array of receivers. Through processing, this raw data is used to create 2D and 3D representations of the subsurface.

3.2.2 Challenges of seismic methods

As seismic waves propagate through a medium, they are attenuated through several mechanisms; geometrical spreading (the wave travels in a sphere from its source where the total energy is spread across the surface of the sphere), absorption (anelastic attenuation) and scattering (elastic attenuation). Attenuation reduces the amplitude of the received seismic signal, which makes it a pervasive problem for any seismic study. It is particularly problematic for the propagation of seismic waves through sediments (Purnell 1986). Physical

properties of the medium such as pore space distribution and pressure of overburden material can alter the energy which is lost to friction (Sherlock and Evans 2001). These losses of energy can be partially corrected through seismic processing; however, it puts limitations on the data quality that can be achieved with a given signal source strength. The loss of energy to friction is particularly high for samples with a low effective pressure, such as near-surface regolith and samples in a lab (Sherlock and Evans 2001).

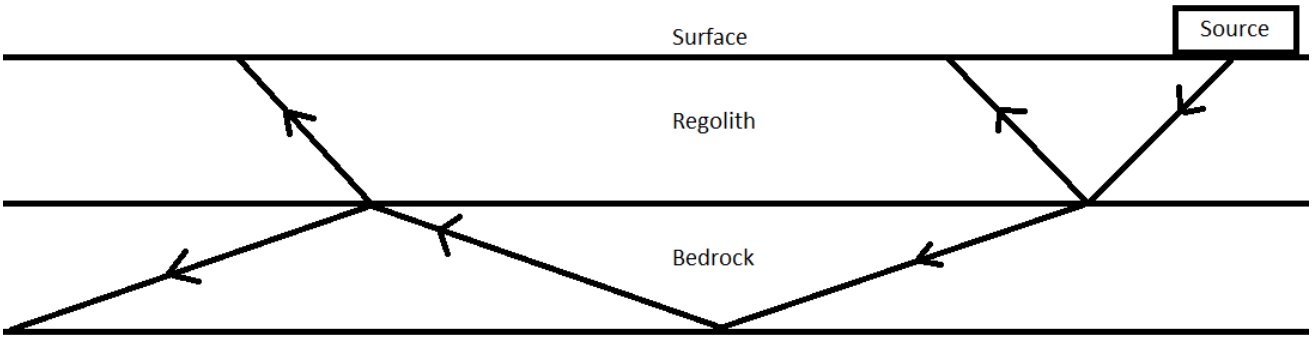

Figure 11 – An example of how a seismic wave would reflect and refract off the interface between two subsurface layers of differing acoustic impedance, such as a regolith and bedrock. While the wave front spread spherically in reality, this diagram is simplified to a single ray trace for simplicity.

3.2.3 Products of seismic methods

One of the primary end products obtained from seismic data is, as discussed about, seismic imaging. 2D and 3D representations of the subsurface can, through interpretation, reveal a significant amount of structural information. Stratigraphy and the presence of faults can be mapped over an area. For this reason, seismic imaging is commonly used in oil and gas exploration to identify possible reservoirs. Typically, seismic alone cannot confirm the presence of any resources, instead relying on a drill hole to provide confirmation and ground-truthing.

3.2.3.1 Rock/regolith type and strength from seismic data

The ratio between the P- and S-wave velocities of a rock can be used to infer rock type and Uniaxial Compressive Strength (UCS) (Butel et al. 2014). Estimating UCS from wireline logging

data is a common practice in the mining industry (McNally 1987; McNally 1990; Zhou et al. 2005; Oyler et al. 2010), and the data are used for ground control and mine design. Relationships between seismic P- and S-wave velocities and other rock properties have been developed for many terrestrial rocks and are available in the literature, however, these may not be representative for off-Earth rocks. Typically, laboratory measurements will be made on rock samples from the region of interest to update the relationships, as they often vary between locations. Such tests may not be feasible for off-Earth exploration, particularly during unmanned missions, given the equipment and set up required. However, once these tests can be performed on local samples, they will strongly increase the accuracy of rock strength estimates. The *in-situ* stress experienced by the rocks likely influences sonic velocity that is not represented by the laboratory tests, which may impact the relationship, particularly for deep tests (McNally 1990).

McNally (1990) describes a relationship between the UCS and P-wave velocity of coal samples in NSW and Queensland, Australia:

$$UCS = 250000\, e^{-0.0076t}\, MPa \qquad (4)$$

Where t is the sonic log interval transit time (slowness, inverse of velocity) measured in µs/ft. Converting this formula to use velocity in km/s as an input produces:

$$UCS = 250000\, e^{-0.076\left(\frac{0.3048}{v10^{-3}}\right)}\, MPa \qquad (5)$$

Where v is the P-wave velocity in km/s.

Other properties are known to impact the seismic velocities of rocks. For example, Han et al. (1986) propose a formula relating P-wave velocity to porosity and clay content:

$$V_p\left(\frac{km}{s}\right) = 5.59 - 6.93\phi - 2.18C \quad (6)$$

Where ϕ is the porosity and C is the clay content as percentages. They also propose a formula relating S-wave velocity to porosity and clay content:

$$V_s\left(\frac{km}{s}\right) = 3.52 - 4.91\phi - 1.89C \quad (7)$$

These relationships are both found to fit best at a confining pressure of 40 MPa and pore pressures of 1.0 MPa. Natural gamma data from wireline logging may also be used to calculate clay content from the following formula:

$$V_{shale} = \frac{\gamma - \gamma_{sandstone}}{\gamma_{shale} - \gamma_{sandstone}} \quad (8)$$

Where γ is the measured natural gamma log, $\gamma_{sandstone}$ is the predicted natural gamma log of clean sandstone and γ_{shale} is the predicted natural gamma log of shale.

Shirgiri (2012) measured the S-wave velocity and average bulk density of soils and was able to infer the shear modulus (stiffness, or ratio of shear stress to shear strain) with good correlation. Murali and co-workers (2015) showed that seismic waves travel faster through soils with a lower porosity, supporting this work. The shear modulus G_o can be calculated with the following equation:

$$G_o = V_s^2\rho \quad (9)$$

Where ρ is the soil density and V_s is the S-wave velocity (Murali et al. 2015). The shear modulus is controlled by several physical characteristics of soil; effective stress, strain, over-consolidation ratio, ratio of void to matrix, macro and micro soil structure, degree of consolidation, ageing, damping and cyclic behaviour (Lee and Santamarina 2005; Leong et al. 2009; Landon et al. 2007).

Shirgiri (2012) also found a weak inverse relationship between phase velocity (the velocity at which a single frequency component of a seismic wave propagates) and moisture content. This result is supported by Yang and co-workers (2008). It is suspected that this result arises from the fact that shear waves do not travel through water, and thus the presence of water acts to slow down the shear waves (Shirgiri 2012). However, it is unclear why this effect does not also occur due to the air present in pore spaces of dry soils, given shear waves also do not travel through gases.

3.2.3.2 2D, 3D and 4D imaging

Seismic imaging surveys involve the use of a series of seismic sources and receivers located on the surface of a region of land in a line (for 2D) or a grid (for 3D). After the collection of the data, they are processed and used to generate 2D or 3D images of the subsurface, with interfaces between features of differing acoustic impedance being revealed. This allows for the identification of stratigraphic layer, faults, folds, and other geological features. 4D seismic refers to the use of multiple measurements using the same 3D seismic grid over a period to measure any changes over time. Seismic processing is an extensive field, and readers interested in more detail are encouraged to see Zhou (2014) for a thorough overview. An example of 2D seismic data and subsequent structural interpretation is shown in Figure 12.

Vertical seismic resolution is the minimum separation of distance between two interfaces such that they can be identified as two interfaces rather than one (Sheriff and Geldhart 1995; Yilmaz 2001). A layer can be resolved in seismic data if its thickness is greater than a quarter of a wavelength, λ, which is a function of the seismic velocity, V, of the material and the frequency, f, of the seismic wave.

$$\lambda = V / f \qquad (10)$$

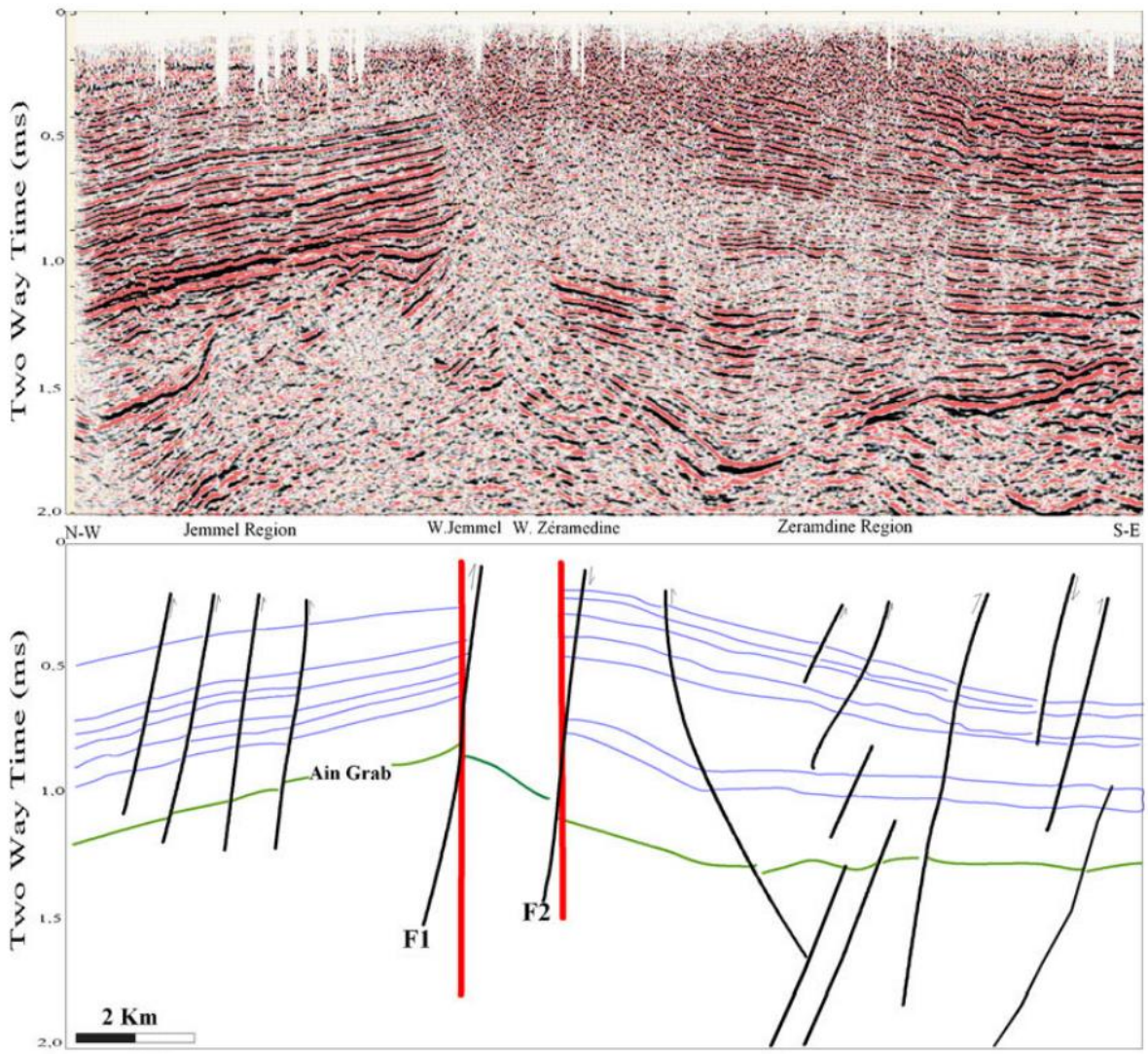

Figure 12 – A 2D seismic profile of the Zéramdine fault corridor in east-central Tunisia (top) with interpretation of faults and stratigraphy (bottom) (Lachaal et al. 2012). Y-axis is two way time, referring to the amount of time it takes a wave to travel from the surface a given depth and back. It may be used as a proxy for depth, but is not a direct representation of space.

For example, if a material has a seismic velocity 5,000 m/s and the peak frequency of the seismic source is 50 Hz, the dominant wavelength is 100 m, and therefore a layer of 25 m can be resolved. The presence of a layer below this thickness may still be detectable, however its thickness may not be determined (Sheriff and Geldart, 1995). This places constraints on the minimum source frequency that may be used to identify the thickness of layers of interest.

Any feature in the subsurface which has a lateral width of less than the Fresnel zone cannot be detected through seismic imaging (Sheriff and Geldart, 1995; Yilmaz 2001). The Fresnel zone, r, is described by:

$$r = (v/2)\sqrt{t_0/f} \qquad (11)$$

Where v is the velocity, f is the frequency, and t_0 is the time taken for a wave to travel to the depth of the feature of interest and back to a receiver directly above it, described by:

$$t_0 = 2z_0/v \qquad (12)$$

Where z_0 is the depth of the feature. A visualisation of the ability to detect subsurface features of varying lateral width is shown in Figure 13.

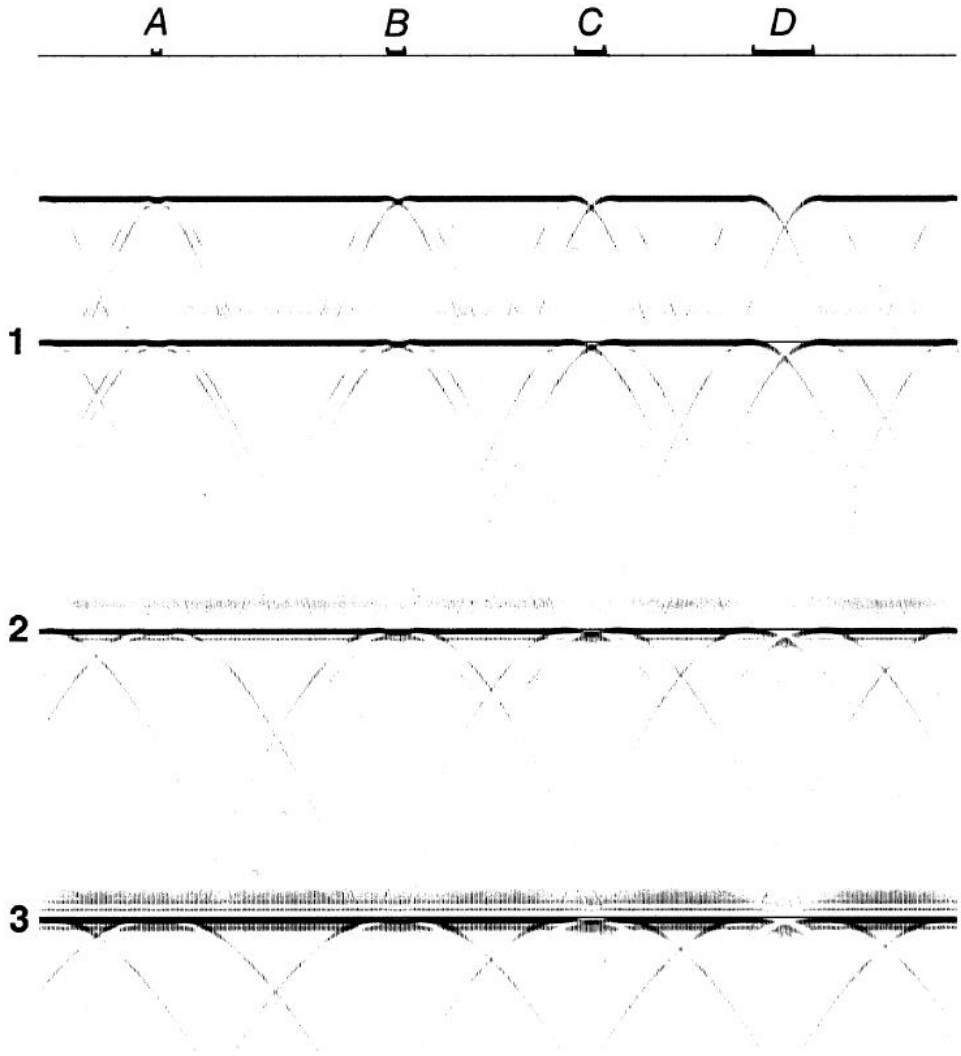

Figure 13 – Synthetic seismic traces for four reflectors at time depths of 0.5, 1, 2 and 3 seconds, each with four gaps (non-reflecting zones) of varying width, A, B, C and D, as depicted by the bars at the top. A is hardly detectable in the seismic trace at any depth due to its width being less than the Fresnel zone. B and C can be most easily inferred at shallow depths, while D can be easily inferred at all depths (Yilmaz 2001).

3.2.3.3 Seismic inversion

Seismic inversion refers to the transformation of seismic reflection data (1 to 4D imaging) from the time domain to the depth domain. This requires inputting the velocity of each rock formation to the model to determine its thickness in metres, rather than in seconds of wave travel time. This is strongly reliant on the availability of drill holes to tie features in time to depth (Veeken and Da Silva 2004) and for the use of blind wells to test the accuracy of the model. It may also include a quantitative model describing rock properties (known as quantitative interpretation). If performed successfully, seismic inversion models are exceptionally useful for understanding the subsurface geology of an area. This is typically used in oil and gas exploration to identify how reservoir properties such as porosity and fluid content vary over a region of interest (Bosch et al. 2010).

3.2.3.4 Amplitude versus offset

Amplitude versus offset (AVO) studies involve the examination of variations in received seismic wave amplitude with varying offset (distance between source and receiver). This can be used to identify variations in rock characteristics such as porosity, density, stratigraphic thickness, and fluid type/concentration (Rutherford and Williams 1989). Similar to predicting rock type and strength from wireline seismic data, this method relies on pre-developed relationships between amplitude and offset. AVO is particularly prone to the non-uniqueness problem due to just P-wave seismic energy being the primary input. AVO is best used in weakly consolidated sedimentary rocks and is less successful in strongly consolidated sedimentary rocks and igneous and metamorphic rocks (Jahn et al. 2008).

3.2.3.5 Anisotropy studies

Anisotropy refers to the seismic velocity of a medium varying depending on the direction it is travelling (may be vertical or lateral). For example, the presence of fractures in a consistent orientation could be expected to result in some anisotropy and is often indicative of the stress

history of the rocks (Schoenberg and Sayers 1995). Anisotropy may be caused in ice by strong fracture patterns or alternating clear and bubbly layers (Dewart 1968), where the P-wave velocity perpendicular to the trend of fractures is smaller than parallel to it. There are no known cases of P- or S- wave velocities varying by more than a few percent in any given direction for a naturally forming medium (Dewart 1968).

3.2.3.6 Seismic quality factor studies

The Earth (and presumably other planetary bodies) preferentially attenuates higher seismic frequencies, resulting in the loss of signal resolution as the seismic wave propagates. The measurement and prediction of the anelastic attenuation factor, or seismic quality factor (Q) is important to predict how much energy is lost to friction and heat. Q is the ratio between the energy of the seismic signal and the energy lost in each oscillation cycle. Q values of rocks in the Earth range from 10 to 1,000 (though some materials are significantly higher, e.g., aluminium with Q = 200,000; Zemanek and Rudnick 1961) and increases with increasing velocity and density. The formula for Q is:

$$Q = 2\pi E/\Delta E \qquad (13)$$

Where E is the initial energy of the seismic wave and ΔE is the energy change per cycle (Knopoff 1964). Higher Q values result in less attenuation of signal.

The rate of anelastic attenuation itself also contains information about lithological conditions, such as rock type, porosity, saturation, and pore pressure (McCann et al. 1997). Therefore, if Q can be accurately measured it can be used for compensation of loss of information and seismic attribute analysis. The geometry of a zero-offset vertical seismic profile (VSP – involving seismic sources down a drill hole and a single receiver at the surface) makes it ideal for calculating Q.

3.2.3.7 Surface wave analysis

Surface waves (Love and Rayleigh waves) are typically high amplitude relative to P- and S-waves and are therefore processed out of seismic imaging surveys as noise. However, they can also provide useful information about the shallow subsurface when sampled in a wide frequency range such as near-surface properties and lateral variations in shallow geology (Strobbia et al. 2009). Multi-channel surface wave analysis may also be used to estimate the S-wave velocity of the near-surface (Figure 14; Lin et al. 2004).

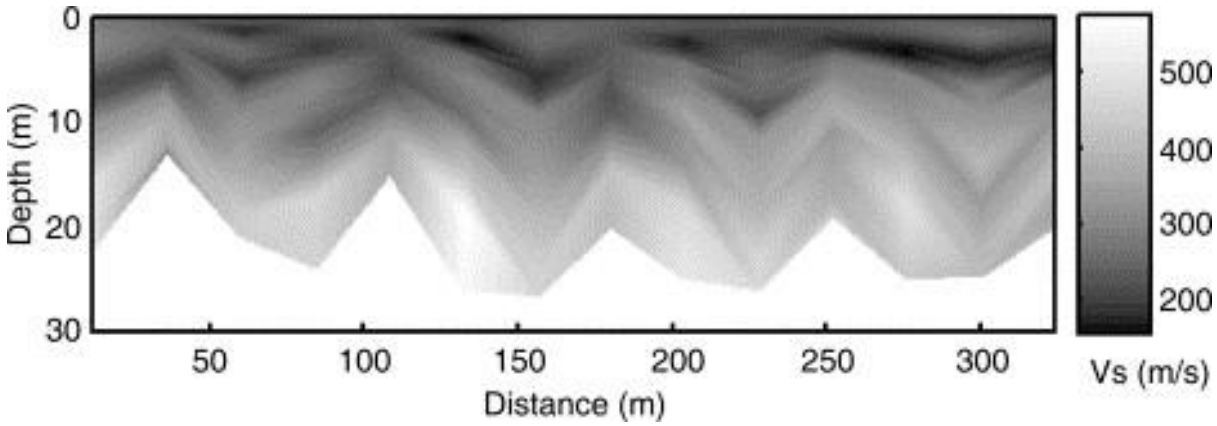

Figure 14 – 2D shear wave velocity profile from multi-channel analysis of surface waves at a site in Yuan Lin, Taiwan (Lin et al. 2004).

3.2.3.8 Passive source seismic

The above methods involve the use of active sources, typically vibrational sources in modern seismic exploration. Passive source seismic has also been used extensively to understand the subsurface of the Earth. Where passive source seismic lacks the ability to generate high-resolution data of the shallow subsurface, it makes up for in its ability to examine the deeper areas. The existence of a liquid outer core in Earth was identified by observing the S-wave shadow due to the inability of S-waves to travel through the liquid (Harold 1926), and a solid inner core was identified by examining the reflection pattern of P-waves from the interface between the inner and outer core (Lehmann 1936).

The locations, frequency and magnitude of earthquakes have also been used to make geological discoveries, including the location of plate tectonic subduction zones (Hori et al. 1985), active fault lines and volcanic events (McNutt 2005). The same seismic equipment that has been used to detect these passive sources have also detected nuclear weapons testing (Dahlman and Israelson 2016).

3.3 History of planetary seismic: Missions and learnings about off-Earth environments

This section will summarise the successful, failed, and planned missions using off-Earth seismic. Several good overviews of the use of seismic in planetary science include Lognonné (2005), and Tong and García (2015).

3.3.1 Missions

3.3.1.1 Lunar missions

The first attempt at using seismic on a planetary body other than Earth was the Ranger program starting in 1959 (Lehner et al. 1962). Three landers with seismometers all failed. Another seismometer capable of measuring seismic waves in three axes was developed for the Surveyor mission (Sutton and Latham 1964); however, it was not included in the final payload (Lognonné and Pike 2015).

The Apollo missions from the late 1960's to the early 1970's delivered several different pieces of seismic recording equipment to the Moon. The Apollo 11 mission's Passive Seismic Experiment (PSE) (Latham et al. 1969) was the first successful use of seismic on another planetary body, with the objective of recording any naturally occurring seismic events on the Moon. The device relied on solar panels for power and so was only operated during the lunar day. As low-frequency seismometers are particularly sensitive to temperature variation,

thermal control measures such as insulation were particularly important to reduce noise levels.

The Apollo 12 mission delivered another PSE station to the Moon. However, this one had a radioactive thermal generator allowing it to operate during the lunar night (Lognonné and Pike 2015). More PSE stations were delivered to the Moon during the Apollo 14, 15 and 16 missions, some of which operated and provided data for over six years.

The Apollo 14, 16 and 17 missions delivered geophone seismic receivers to the Moon for use with active seismic sources (Lognonné and Pike 2015), and a gravimeter delivered by Apollo 17 was designed to detect both gravity waves and seismic waves (Kawamura et al. 2010). The Active Seismic Experiment (ASE) of Apollo 14 and 16 each used three geophones in a 91 m line and explosive charges as sources at intervals along the line. These experiments provided information on the seismic velocity and thickness of several subsurface layers (Kovach and Watkins 1973a). The Lunar Seismic Profiling Experiment (LPSE) of Apollo 17 used four geophones in a T shape and explosive sources located up to 2.7 km from the receivers (Kovach et al. 1973a). These more distant sources allowed for the examination of deeper features than the ASE.

A series of artificial sources were utilised including impacts from spent rocket stages, and their impacts were detected by the PSE network and the LPSE (Nakamura 2015). In addition, over 1,700 events were detected which were interpreted to likely be meteorite impacts with masses between 500 g and 50 kg (Nakamura et al. 1981; Duennebier et al. 1975).

3.3.1.2 Mars missions

Viking 1 and Viking 2 carried passive seismic recorders to Mars in 1976 (Anderson et al. 1977). Viking 1's seismic device was unsuccessful. However, Viking 2 returned data which led to the

accidental discovery of wind on Mars. Due to the unexpected levels of wind noise the device was unable to confirm any seismic events. Some possible candidates for Marsquakes were identified, though they are most likely strong gusts of wind. Anderson and coworkers (1977) suggested that seismometers at least 1,000 times more sensitive than the Viking seismometers should be able to operate on Mars without being impacted by wind noise.

The position of the seismic recorder on the Viking landers (on top of the lander) was argued to be sub-optimal for noise control (Anderson et al. 1977), increasing the noise by three orders of magnitude relative to other more optimal positions. Thus, science payload positioning should be carefully considered in all seismic missions.

The Mars 96 mission was launched in 1996 and included two passive source seismic receivers (with sensitivities 100 times that of the Viking receivers) on landers and two additional passive source receivers on two penetrating probes (Lognonné et al. 1998). Unfortunately, this mission was lost shortly after launch. The network of four receivers would have been sufficient for identifying the location of seismic events and making some limited inferences on the interior of Mars.

The USSR Phobos 1 and 2 missions of 1988/1989 intended to deliver passive seismic receivers on the surface of Phobos to characterise its internal structure. However, both were lost prior to landing (Surkov 1989). Several proposals for missions to develop a network of seismic receivers on Mars have been made from 1990 to today, however did not eventuate. These are discussed by Lognonné (2005).

The InSight (Interior Exploration using Seismic Investigations, Geodesy and Heat Transport) mission (Panning et al. 2017) landed on Mars in November 2018 and is still operating. It

contains a passive source seismic receiver (Seismic Experiment for Interior Structure - SEIS) which has identified 174 seismic events (as of 30 September 2019; Giardini et al. 2020). 150 of these are small-magnitude, high-frequency events (interpreted as likely crustal source), and 24 are moderate-magnitude, low-frequency events lasting from 10-20 minutes (interpreted as likely mantle source). The main objectives of SEIS are to develop models of Mars' internal structure and to document the seismic activity of Mars (Panning et al. 2017). The Mars 2020 mission included the Perseverance Rover which contains seismic equipment and arrived at Mars in February 2021.

3.3.1.3 Small planetary bodies and other missions

Venera 13 and Venera 14 landers both delivered a seismometer and other science equipment to the surface of Venus in 1981/1982, where they transmitted data for around two hours and one hour respectively. They successfully recorded seismic data and identified two possible seismic events (Ksanfomaliti et al. 1982).

To date, seismic has not been attempted on an asteroid. NASA's BASiX (Binary Asteroid in-situ Explorer) mission (now cancelled; Anderson et al. 2014) proposed to deliver a seismic receiver to the surface of an asteroid to determine its strength and seismic properties using calibrated blasts on the body's surface. The proposed Castalia mission would, if undertaken, deliver equipment including a seismometer to the surface of the main belt comet 133P/Elst-Pizarro to map its internal structure (Snodgrass et al. 2018). Scheeres and Sánchez (2018) have proposed observing artificial craters on asteroids to infer their surface strength using cratering theory (Holsapple 1993), which is the inference of a materials' strength based on the observed crater volume and the radius, velocity and mass of an impactor.

3.3.2 Off-Earth environments

Understanding how seismic surveys on other planetary bodies will differ requires an understanding of what relevant physical features will be different. These features include, but are not limited to, gravitational strength, atmospheric pressure, temperatures (differing in both magnitude and fluctuation), electrostaticity, and rock characteristics. The medium of interest is also likely to differ on other planetary bodies. The grain size of lunar and Martian regolith has been observed to be significantly finer on average than typical Earth regolith (Papike and Simon 1982; Peters et al. 2008; Ballou et al. 1978; Christensen and Moore 1992), and the regolith grains on the Moon are highly angular (McKay et al. 1991b). The grain size of near-surface asteroid material is unknown, though is also expected to be highly fine-grained. The subsurface structure of other planetary bodies is mostly unknown. However, it is likely to differ to typical subsurface structures on Earth. Lunar regolith grains appear to be electrostatically charged due to solar radiation, causing them to be attracted to rocks, other grains, and equipment (Arrhenius et al. 1972). It is also expected that this phenomenon will be present on other airless bodies such as SPBs.

To date, the impact of gravitational strength and atmospheric pressure on seismic velocities and attenuation has not been examined. The effect of atmospheric pressure on seismic data collection is explored in this thesis in Chapter 5. It is predicted that one effect of lower gravitational strength would be for the overburden pressure to be lower, which should result in higher attenuation. Independent of tests on off-Earth bodies or Earth orbit, the effects of gravity on seismic could be examined through parabolic flights, drop tower tests, and computer modelling (this has been performed for other fields such as examining how bacteria act under reduced gravity) (Vukanti et al. 2012).

3.3.2.1 Moon

Understanding of near-surface lunar geology is largely extrapolated from relatively few landing sites. Seismic tests from one such landing site, Apollo 17 (Cooper et al. 1974), suggests that the regolith extends down to around 4 m (100 m/s P-wave velocity), under which is a layer interpreted to be rubble and broken rock to 32 m (327 m/s), followed by a layer of fractured basalt to 390 m (495 m/s). Below this is a layer of relatively less fractured basalt (960 m/s; Cooper et al. 1974), which according to more recent analysis does not have a discernible base (Nakamura 2011). It can be expected that at least the top two of these layers to be relatively similar across the surface of the Moon, due to the fragmentation from meteoroid impacts which caused them being relatively consistent across the body (Cooper et al. 1974). Grain size distributions of regolith at the lunar surface from several different sites can be seen in Figure 15.

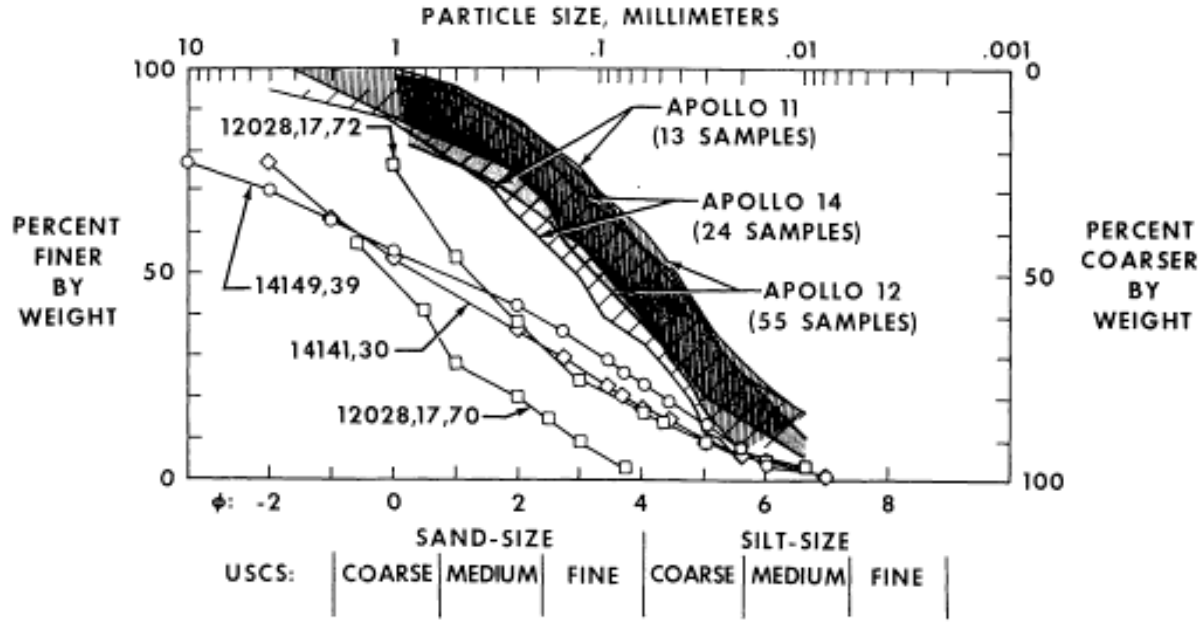

Figure 15 – Grain size distributions for lunar soil samples from the Apollo 11, 12 and 14 missions (Carrier 1973).

During the Apollo 14 and Apollo 16 missions, active source seismic experiments showed a surface layer of 8.5 m and 12.2 m thickness respectively, with P-wave velocities of 104 m/s and 114 m/s. These are interpreted to be regolith of the same consistency as the surface.

These layers lie on top of a >1 km thick layer of 299 m/s (Apollo 14) and 250 m/s (Apollo 16; Kovach and Watkins 1973a). This presents a different picture to the results of Apollo 17 and could be explained by either inconsistent surface geology over the Moon, or a lack of resolution in the Apollo 14 and Apollo 16 results to identify the rubble and fractured basalt layers.

In addition to meteorite impacts discussed above, several moonquakes were detected by the PSE network. Over 7,000 deep moonquakes were identified and are suspected to be caused by tidal effects due to their approximately 28-day cycles. However, their exact mechanism of formation remains unknown (Nakamura 2015). Around 28 shallow (maximum depth of ~300 km) moonquakes were also identified by the PSE network, making them significantly rarer, though these events were on average greater in magnitude than the deep moonquakes (Nakamura 2015). Their mechanism of formation is also unknown, though many theories exist (Shirley 1985; Frohlich and Nakamura 2006; Nakamura et al. 1974). Thermal moonquakes are common, and arise around 48 hours after sunrise, likely caused by the rapid change in temperature (from 127 C during the day to -173 C at night) on the Moon's surface (Duennebier and Sutton 1974), which results in rocks fracturing/moving at the lunar surface or the shifting of regolith (Nakamura 2015).

Lunar seismic surveys from the Apollo missions showed that seismic waves become scattered and attenuated, possibly the result of a highly fractured subsurface (Knapmeyer and Weber 2015). The depth of the fractured zone is believed to be up to 20 km (Dainty et al. 1974; Toksöz et al. 1974). Nakamura (1977) suggests that cratering is likely a significant source of the scattering through the creation of subsurface faults and fractures, and the lowered seismic velocities are noted to be like those around Earth impact craters, which result from

high porosity and fracture concentration (Weber et al. 2015). The fracturing results in moonquakes having a slower ramping up and down of seismic amplitudes than earthquakes (Nakamura 2005), which makes the exact determination of waves arrival time difficult. This uncertainty is a limitation for passive seismic data on the Moon, and with a sufficiently distant source, this effect might also be seen during active seismic lunar experiments.

3.3.2.2 Mars

The internal structure of Mars is still largely unknown, due to the lack of a network of seismic receivers. Some limited inferences on the existence and size of a core have been made using radio data (Yoder et al. 2003), and some models have been developed based on Martian meteorite samples (Okal and Anderson 1978; Spohn et al. 1998). Mars is likely to have relatively low seismic activity (Anderson et al. 1977), though it is still expected that some meteorites will impact the surface and act as seismic sources. Also, thermoelastic cooling of Mars' lithosphere is expected to result in some seismic activity (approximately 100 times that of shallow moonquake activity; Golombek et al. 1992; Phillips 1991). The wind present on Mars is likely to affect the detection of seismic events. However, it appears that the wind noise is severely reduced during the Martian night (Anderson et al. 1977).

Marsquakes appear to share the same characteristics seen on the Moon, which leads researchers to conclude that significant scattering also occurs in the subsurface of Mars (Banerdt et al. 2020). In addition, they appear to lack surface waves, though it is unclear currently whether this is the result of deep sources, scattering or something else. The degree of total seismic activity on Mars is predicted from observations by InSight (Banerdt et al. 2020). It appears to be significantly more seismically active than the Moon, though still significantly less seismically active than Earth.

The surface geology and geography of Mars is highly varied. At the site of the InSight lander in the western Elysium Planitia, a regolith of around 3-5 m thickness (possibly generated by impacts) covers ancient lava flows (Golombek et al. 2017; Golombek et al. 2018), and aeolian processes appear to dominate the regolith across the planet (Ehlmann et al. 2017).

3.3.2.3 Small planetary bodies

Small planetary bodies include asteroids and comets. Asteroids and comets exist along a spectrum; thus, there is not a clearly defined boundary between them. However, asteroids are considered to be comprised of metals and rocky material, while comets are comprised of ice, dust, and rocky material. Comets typically have more elliptical orbits than asteroids with longer orbital periods and have tails of water vapour as dust as they approach the Sun while asteroids typically do not (Tancredi 2014), though there are some notable exceptions such as asteroids P/2010 A2 (Jewitt et al. 2013a) and 3200 Phaethon (Jewitt et al. 2013b).

In the absence of any available subsurface data, several models for their interior structure of asteroids have been proposed by Walker et al. (2006) which include a solid body, solid with major factures, rubble piles and gravel conglomerations (the last two may be only loosely held together by gravity and other forces). To date, none of these possible structural types has been confirmed for any given asteroid, though it has been hypothesised that all SPBs with a diameter of around 1 km are rubble piles (Walsh 2018). Most existing knowledge of the geomechanical and geochemical properties of asteroids are from meteorite samples, which have three broad physical types, irons, stony-irons, and chondrites (Lewis 2015). These samples represent a biased subset of all asteroid material, as they are more likely to be the strongest rocks to survive the descent through the Earth's atmosphere, impact with the surface, and any subsequent weathering (Lewis 2015).

Asteroids are divided into classes based on their predicted mineralogy from remotely sensed optical data. Table 3 from Lewis (2015) shows the asteroid spectral taxonomic classes. Due to the limitations of optical data the inferred mineralogy refers to the minerals present at the surface and may not be representative of the deeper material.

Some inferences have also been made from remote sensing data, either from flybys or Earth-based observation. Mass, and therefore, densities have been estimated for some asteroids based on gravitational pull and size and range from 0.8 to 6.7 g/cm^3 (Walker et al. 2015). Compared to solid rocks on Earth (3 to 5 g/cm^3) and the average near-surface lunar density (~2.7 g/cm^3), this is a wide range. It also does not provide any information on the density distribution of an asteroid. Small asteroids likely have high average porosity (>20%) and large asteroids likely have low average porosity (<20%) (Price 2004).

Some inferences on the regolith properties of asteroids have been made using remote sensing data (Clark et al. 2002). For example, the near-surface density and porosity of 36 main-belt asteroids were estimated using radar albedo and polarisation ratio data (Magri et al. 2001). The mass and rotational speed of asteroids may also be used to provide some constraints on regolith, as a sufficiently high centripetal force should eject regolith below a certain bulk strength for low gravity bodies (Sánchez and Scheeres 2014).

The Japanese Aerospace Exploration Agency's (JAXA) Hayabusa 1 (Abe et al. 2006; Yano et al. 2006; Nakamura et al. 2011) and Hayabusa 2 missions (Watanabe et al. 2017) retrieved surface samples from asteroids 25143 Itokawa (S-type, 313 m diameter) and 162173 Ryugu (C-type, 870 m diameter), respectively. The Hayabusa 1 sample returned to Earth in 2010 (Siddiqi 2018), and the Hayabusa 2 sample returned in December 2020 (JAXA 2020). Both samples landed in Woomera, Australia, with Hayabusa 2 involving the newly founded

Australian Space Agency (ASA). The OSIRIS-REx (Origins, Spectral Interpretation, Resource Identification, Security, Regolith Explorer) mission arrived at asteroid 101955 Bennu (B-type, 525m diameter) on October 20, 2020 and underwent its sample collection operation (Enos 2020). If successful, it is expected to return samples to Earth on 24 September 2023 (NASA 2011a). These three missions represent the only asteroid sample return missions to date.

Table 3 - Asteroid taxonomic classes based on spectral data (Lewis 2015).

Class	**Description**	**Example**
C-cadre (albedo < 0.1)		
D	Extremely dark	624 Hektor
P	Extremely dark, some similarities to comets	324 Bamberga
F	Dark, denser than C	704 Interamnia
C	Dark, carbonaceous chondrite	10 Hygeia
B	Dark, altered	2 Pallas
G	Dark, altered, some polar ice	1 Ceres
T	Dark, altered, possibly dry	114 Kassandra
S-cadre (0.1<a<0.4)		
K	Rare category, like CV and CO chondrites	221 Eos
M	Metallic iron-nickel	16 Psyche
S	Siliceous/stony chondrite	3 Juno
Q	Strong FeO bands, like ordinary chondrites	1862 Apollo
Bright outliers (albedo > 0.4)		
A	Strong olivine signature	446 Aeternitas
E	Enstatite chondrite – no FeO	44 Nysa
V	Basaltic achondrite	4 Vesta
R	Rare type between A and V	349 Dembowska
Catchall group with flat spectra		
X	Bland M,E,P, etc. spectrum but poor albedo data	
Borderline cases with intermediate spectra		
Any two- or three-letter designation such as CB or MS		
U	An outlier of any of the above taxonomic groups; an unknown	

Analysis of the dust particles recovered from Itokawa suggests that LL chondrite meteorites (low iron and low metal chemical group of stony meteorites) come from stony (S-type) asteroids like Itokawa based on the strong similarities between their mineralogy and chemistry (Nakamura et al. 2011). The surface material of Itokawa at the site of spacecraft

contact was dominated by particles up to 1 cm across (Nakamura et al. 2011). Itokawa has an estimated bulk porosity of 44 ± 4% (Watanabe et al. 2019) and Ryugu has a preliminary estimated bulk porosity of over 50%, suggesting that both are rubble pile asteroids (Watanabe et al. 2019).

Preliminary data suggest that the surface of Bennu was covered with loose rubble with particles up to approximately 10 cm across (this authors' interpretation based on video footage of contact from Enos 2020), though it is not clear whether these are intact pieces of rock or loose conglomerations of smaller grains. Due to the design of the sampling device, only particles of size 2 cm or smaller are expected to be collected (NASA 2016a), and thus will not represent a representative sample of the surface material. Several boulders over 1.5 m in diameter have also been detected at the surface from OSIRIS-REx imagery (DellaGiustina et al. 2020), and the surface is observed to be generally covered with large rock pieces (Lauretta et al. 2019), which is contrast to the predictions based on earlier thermal inertia (Emery et al. 2014) and radar polarisation ratio modelling (Nolan et al. 2013), both of which suggested a smoother surface with smaller particles. This may indicate that the predictions of surface regolith grain sizes of other SPBs based on these data are also inaccurate. Based on spectroscopic data, the surface material of Bennu has been linked to CM carbonaceous chondrite meteorites (Hamilton et al. 2019).

The cratering which causes scattering and attenuation on the Moon in the upper layers is a process we also expect to see on SPBs, given the lack of atmosphere and Earth-like weathering processes. This would suggest a fine-grained, relatively porous regolith layer covering most of the surface. Weathering processes such as micrometeorite impacts, and solar wind may also contribute to this (Clark et al. 2002).

Descent imaging from the Philae lander on comet 67P/Churyumov-Gerasimenko shows that the regolith in the area is comprised of gravel (cm scale) and larger blocks (mostly 1 to 2 m) and has a depth of 0 to 50 cm for rough terrain and 1 to 2 m for smooth terrain (Mottola et al. 2015). However, accelerometer analysis from the bouncing of the lander on the surface suggests an upper soft layer thickness of around 25 cm (Biele et al. 2015). It should be noted that these inferences are not necessarily contradictory, as the upper soft layer may be a sub-layer of the regolith. While imaging resolution was at a maximum of 1 cm, grains of this size and smaller, if present, do not appear to dominate the regolith (Mottola et al. 2015). The presence of erosional features on the surface of 67P suggest an active surface (Thomas et al. 2015). Biele and co-workers (2015) suggest the possible presence of a crust layer at the surface of the comet in some areas.

NASA's Deep Impact mission imaged ejecta from comet 9P/Tempel created by an artificial impactor and indicated that the dust displaced was a mix of carbon, pyroxene and olivine (Harker et al. 2005) and water ice, with a dust to ice ratio of 1 to 5 (Sunshine et al. 2006). The porosity of 9P is inferred to be 75-88% at the impact site, which is exceptionally high, though it is not known how this compares to the rest of the body (Ernst and Schultz 2007). 9P's regolith appears to be made of particles 1 to 100 μm in diameter, as mentioned by A'Hearn (2005), which was vastly different from the estimated particle sizes on 67P's regolith. Sunshine and co-workers (2006) suggest that the smaller particles may be weakly binding to form larger particles, which could also be the source of the larger particles on 67P. This hypothesis is plausible, though more tests will need to be performed to confirm it, such as direct sample collection and analysis.

3.4 Potential future uses of planetary seismic methods

Seismic has the potential to be used for a wide range of applications in planetary science, including in prospecting and planning for off-Earth mining, construction and SPB deflection. Some of the uses including imaging the subsurface using 2D and 3D seismic surveys, inferring physical properties such as UCS and porosity, etc. These applications are discussed in detail in this section and are broken down into their respective end uses.

3.4.1 Mining

Conventional mining projects are highly sensitive to the specific characteristics of the site, which would imply that a detailed understanding of the geology of an asteroid would also be required for a mining operation to be commercially and/or technically successful (Gertsch 1993). This problem is compounded by the fact that realising you need different equipment from Earth during a mission due to the reality at the site would be catastrophic.

The physical characteristics that are required to select a mining method and its design, and also estimate resource volumes depend on a range of factors, including the target body, the desired resource (reserve), the desired end-use, and whether or not it will be a crewed mission. Prospectors targeting water-ice will be interested in the porosity, permeability, and fracture density/orientation of an asteroid, while prospectors looking to extract resources solely from the regolith will not. The properties of the rock will also impact the most efficient and effective type of processing required.

Any resources gathered may be used either at the location of extraction (*in-situ* resource utilisation – ISRU), used at another location other than Earth, or returned to Earth for use. Examples of ISRU are the creation of propellant on the surface of Mars to launch return missions to Earth (using the Sabatier process; Muscatello and Santiago-Maldonado 2012) and using lunar regolith as a building material on the Moon (such as for solar panels; Landis and

Perino 1989). Examples of using materials at a location other than Earth include mining water ice on near-Earth asteroids and using it for life support, or converting it to hydrogen and oxygen through electrolysis, and using this as a propellant to refuel satellites or space missions in Earth orbit. The delta-V between many near-Earth asteroids and low Earth orbit is less than the delta-V between the surface of Earth and low-Earth orbit, and so this may be more efficient than bringing propellant from Earth. Finally, examples of returning material to Earth for use include mining helium-3 from the surface of the Moon for use in nuclear fusion, or mining platinum group elements on asteroids for use in electronics etc.

It is necessary to examine the proposed and potential methods of mining off-Earth bodies to understand precisely what physical parameters need to be understood. The potential mining methods are explored below.

3.4.1.1 Surface mining

Many different techniques have been proposed for surface mining in off-Earth environments. Gertsch and Gertsch (2003) propose several surface mining techniques to extract gases such as hydrogen from lunar regolith, Muff and co-workers (2004) propose a bucket-wheel excavator based on a terrestrial model for use on the Moon, Mars and Phobos to collect regolith for ice and volatiles, and Bernold (2013) developed a vacuum-like machine to pull lunar regolith up a tube. The local thickness of dry regolith overburden will have a significant effect on the financial feasibility of the operation, and on the selection of mining sites. A 3D seismic imaging survey or multiple 2D lines could be used to great success to determine the thickness of regolith layers. Any buried boulders which would not be favourable to a regolith mining method could be identified and avoided. A single drill hole in the 3D grid or on a 2D line could be used to identify the depth and thickness of any resource-rich layers. This result

can be tied to the seismic data, and then the depth of the resource can be estimated across the area with some degree of confidence.

Pick cutting and pneumatic excavation may be used off-Earth (Lucas and Hagan 2014), though more testing is required. Rippability, the ease with which a regolith or rock can be excavated, may be inferred through seismic velocity and other measurements (McCann and Fenning 1995), and so seismic could, therefore, be used to estimate the technical feasibility of excavating the regolith, or identify the required form of excavation. Rock strength may also indicate the expected rate of wear of excavation equipment.

Walker and Huebner (2004) discuss a method for using a seismic receiver and an explosive source to determine the strength of the medium at the site of the explosion. High amplitude seismic waves for a given explosive source strength are correlated with high strength material, and vice versa.

Feldman (2001) identified the likely presence of water ice in lunar regolith at permanently shadowed craters in polar regions at a concentration of 1-2%. If it is the case that the icy regolith forms a layer, this may be identified through seismic imaging (Shean et al. 2007). The inclusion of both solid and liquid water in regolith has a substantial impact on P- and S-wave velocity (Carcione and Seriani 1998; Timur 1968). Ice concentrations of 1-2 % in regolith are expected to result in a measurable velocity change for a low-velocity material such as lunar regolith. Seismic velocity surveys over a polar crater region could predict the concentration of ice in the regolith, though in an unfamiliar survey environment we should expect ground-truthing (drilling or excavating to confirm geophysical data with direct observation) to be required to calibrate seismic results. Shishko and co-workers (2017a) have identified the possibility of extracting ice on Mars for use in a Mars colony, and seismic could be used to

support this, or for ice prospecting on an SPB, and Pelech and co-workers (2019) have performed a technical evaluation of some off-Earth ice mining scenarios. Casanova and co-workers (2020) have identified some water resources in the lunar polar region using play-based exploration techniques utilised by the petroleum industry.

In addition to being a valuable resource, ice also has a notable impact on the strength and rippability of regolith by acting as a cementing agent. Gertsch and co-workers (2006) examined the excavatability of the Johnson Space Centre lunar simulant (JSC-1), a lunar regolith simulant, as a function of ice concentration by mass (shown in Table 4). While Gertsch and co-workers (2006) have developed relationships between water content and the first failure specific penetration, specific energy and excavated volume, the JSC-1 sample, as with all simulants, may not be completely geomechanically representative of lunar soil, given possible differences in grain properties such as angularity. Other notable differences such as the temperature of the test samples, atmospheric pressure and gravity may result in further differences, and so *in-situ* tests will be required.

Due to the low gravity environment, anchoring, and canopies (to capture loose material ejected from the body) (Sorenson 2000) are expected to be important for mining operations on SPBs. Biele and co-workers (2015) showed how the failure to anchor a probe correctly on an SPB can be disastrous for a mission, and Craig and co-workers (2014) propose a mining system for SPBs, drilling/breaking ore on the surface and allowing it to occupy a canopy, which is later collected. Seismic may assist here by estimating regolith thickness and strength at several locations across the surface of an SPB to identify the optimum locations for anchor points.

Table 4 – Strength of the JSC-1 lunar regolith simulant at different concentrations of ice. Results from Gertsch et al. (2006). The maximum possible proportion of ice based on average near-surface lunar regolith porosities is ~19%.

Proportion of ice (as % of mass) in JSC-1	Strength
< 0.3	Easy to excavate, similar to weak coal
0.6 – 1.5	Readily excavatable, similar to shale or mudstone
~8.4	Likely can be excavated with mechanical excavators, similar to moderate-strength limestones, sandstones, and shales
~10.6	Likely can be excavated with massive excavators, similar to strong limestone or sandstone

Optical mining has also been proposed to extract volatile materials such as water from asteroids (Dreyer et al. 2016; Sercel et al. 2016), which involves directing concentrated light or heat energy to a part of the asteroids' surface, causing rock to fracture and release volatiles. These are then captured and collected by a cold trap.

3.4.1.2 Underground mining

Craig et al. (2014) propose drilling large holes through an asteroid to collect material. They suggest that the equipment could push against the walls of the drill holes to hold it in place, though this does not discount the need for initial anchoring before drilling. Knowledge of the subsurface structure and geology of SPBs before drilling is expected to be as critical as it is on Earth. The internal structure, presence of void spaces and variation of strength, porosity and other parameters throughout the body will strongly influence the feasibility and planning of drilling, and these can all be inferred through seismic surveys.

Blasting may be used in both surface and underground mining operations to break up regolith or rock and assist with mining. These blasts may not only be used as convenient sources for a network of seismic receivers to further understand the subsurface of the body, but also to monitor the structural stability of the local area over time (Worsey 1985; Hudyma et al. 2003), which may be particularly important for SPB operations. Prior to blasting, seismic anisotropy

studies may be used to identify the presence and orientation of fractures, which may assist with blast planning.

Proposals have been made to use rovers and drilling to extract ice from the shallow subsurface of Mars for use *in-situ* (Shishko et al. 2017a; Shishko et al. 2017b). A suggested purpose for this mission is as life support for a manned mission to Mars or a colony.

3.4.1.3 Biomining and other *in-situ* methods

In-situ mining methods allow resources to be extracted without the need for excavation, and is often used in terrestrial operations, such as for uranium (Sarangi and Beri 2000; Mudd 2001; Abzalov 2012; Tan et al. 2014; Skokobayev et al. 2015), copper and gold (Johnson et al. 2013; Sinclair and Thompson 2015). *In-situ* leaching has also been proposed for use in off-Earth mining. Karr and co-workers (2012) explore the use of acidic ionic liquids to dissolve metal bearing regolith from the Moon, Mars, and asteroids, either for extracting metals and water or for breaking up regolith to assist with drilling. Klas and co-workers (2015) proposed the use of biomining and biogas production to extract minerals and gases from asteroids.

Ata and co-workers (2015) examine the challenges of using biomining and *in-situ* mining in off-Earth environments. It is largely unknown how the biological and chemical processes used in biomining and *in-situ* leaching will operate in the space environment, such as with reduced gravity, differing atmospheric conditions, low water availability, high temperature fluctuations and increased radiation. Some of these factors are known to an extent, such as the impact of irradiation on bacteria (Cox and Battista 2005) and the growth conditions of bacteria in microgravity conditions (Nickerson et al. 2000; Nickerson et al. 2004).

Mineralogy and geology determine whether *in-situ* leaching is feasible, for example carbonaceous chondrite is required for biogas production on an asteroid (Klas et al. 2015).

Due to non-uniqueness, seismic methods alone would be unable to determine rock type and mineralogy, however with the assistance of drill holes and other geophysical techniques, it may be able to image the location and thickness of a rock layer or regolith containing carbonaceous chondrite.

High porosity and permeability are critical for the success of any *in-situ* leaching method. Seismic is unable to infer permeability, though it may infer porosity (Han et al. 1986) and the orientation of fractures if they have a dominant plane (Schoenberg and Sayer 1995). While direct tests would provide a more accurate result for regolith or rock porosity, this could be tied to 2D or 3D seismic imaging, allowing the porosity to be estimated across an area of interest for a given regolith or rock type.

3.4.1.4 Additional considerations

For any 2D and 3D seismic surveys, the interval between receiver locations should be as small as possible when the target layer for imaging is shallow and velocities are low (Bachrach et al. 1998). This will be especially important for imaging the near-surface regolith of other planetary bodies where we are seeing exceptionally low velocities.

Some other geophysical techniques lend themselves well to supporting seismic tests and are worth mentioning here. GPR has been used to perform low-resolution structural mapping of the lunar surface to a depth of 1,300 m (Porcello et al. 1974) and has been proposed for high resolution mapping of shallow ice layers on Mars up to depths of 3 m (Ciarletti et al. 2011).

3.4.2 Colonisation and construction

Off-Earth materials such as regolith may be used as a construction material through ISRU, which will reduce the volume of material that must be brought from Earth (Swint and Schmidt 1991; Taylor and Meek 2005; Toutanji 2005; Naeye 2008; Garnock and Bernold 2012). In

addition to the prospecting of raw materials required by a colony or base, seismic can also assist with construction surveying. Construction projects rely on an understanding of the strength and stability of the near-surface. This could be achieved through conducting UCS experimental program. Relationships between the UCS and velocity for the rock types that are expected on other planetary bodies may be developed in laboratory tests. These may then be used by wireline logging on missions to rapidly estimate the rock strength of an area in preparation for mining or construction.

The seismic velocity of near-surface regolith could also be measured and used in conjunction with a UCS/velocity relationship to estimate soil strength. UCS relationships are unique for each material, and new relationships for off-Earth regolith and rocks will likely need to be developed before this analysis can be performed.

3.4.3 SPB deflection

As discussed above in Section 3.2.3, little is known about the internal structure of SPBs, or even their near-surface characteristics. Much of the current knowledge of asteroids and comets comes from surface imagery and meteorite samples, which represent a biased population. This is a problem for deflection, because to deflect an SPB in a controlled and successful manner, it is necessary to understand its internal properties (Holsapple 2004).

Methods for deflecting SPBs which have been proposed include explosives (conventional or nuclear), kinetic impactors (Gibbings 2011), ejecting material from the body like a mass driver, altering the spin and utilising the Yarkovsky effect (Öpik 1951) to gradually alter the orbit, applying concentrated EM energy through lasers or mirrors, attaching a propulsion device, altering the reflectivity of the surface and gravity tractors. The Yarkovsky effect is a force that is applied to a rotating body in space orbiting a star. As a body is warmed by solar radiation,

it releases thermal photons. The most thermal photons are released in the direction of the star, with fewer released over time as it rotates. Depending on the direction the body is rotating in relation to its orbit, this could increase or decrease its speed; thus, altering its orbit (Öpik 1951). This effect is more easily observed in smaller bodies due to their higher surface area to mass ratio. The Yarkovsky effect is visualised in Figure 16.

These deflection techniques do not necessarily need to destroy an SPB, but rather need only to alter its velocity by 75 m/s divided by the number of days until impact for it to miss Earth (Ahrens and Harris 1994). This section does not seek to be an exhaustive list and explanation of deflection methods, but instead to consider the kinds of properties we will need to know about an SPB to deflect them, and where seismic methods may be able to assist. An extensive discussion of varying asteroid deflection methods can be found in the chapters and references therein of *Hazards due to Comets and Asteroids* (Gehrels et al. 1994) and *Mitigation of Hazardous Comets and Asteroids* (Belton et al. 2004). The above deflection techniques have been proposed and designed in lieu of internal SPB data. Therefore, acquiring these data should be a high priority.

Attempting to deflect a rubble pile asteroid using an impactor may have the effect of breaking the body up, with the individual components being harder to mitigate but still posing a threat. The strength and porosity of an SPB is expected to affect the efficiency of explosive and impactor deflection. Mitigation through these techniques may be up to 100 times less effective at deflecting SPBs with high porosity versus low porosity due to the widely varying masses of ejected volume (Holsapple 2004), and different rock types are expected to also affect the deflection (Solem and Snell 1994). Porosity and rock strength may both be inferred through seismic velocity analysis.

Nuclear standoff deflection (Ahrens and Harris 1994) involves detonating a nuclear bomb some distance from the SPB, causing the surface material to be heated and expanded, which ejects the material and applies a force. This method fundamentally relies on a sufficient volume of regolith at the surface of the asteroid (Holsapple 2004), which can be easily determined through seismic imaging. Similarly, the type of material at the near-surface will affect other deflection techniques such as EM energy concentration (Holsapple 2004). Several deflection techniques require anchoring to the surface of the SPB, and as discussed previously, seismic may be used to enhance our understanding of SPBs and plan anchoring strategies (Gritzner and Kahle 2004).

Some work has been performed to predict the extent of damage if an SPB were to impact Earth, however, these models can be improved with high quality structural data from the bodies in question to provide a more accurate picture of the expected destruction. This information may be the difference between a policy maker deciding to commit funds to deflect an SPB or ignoring it.

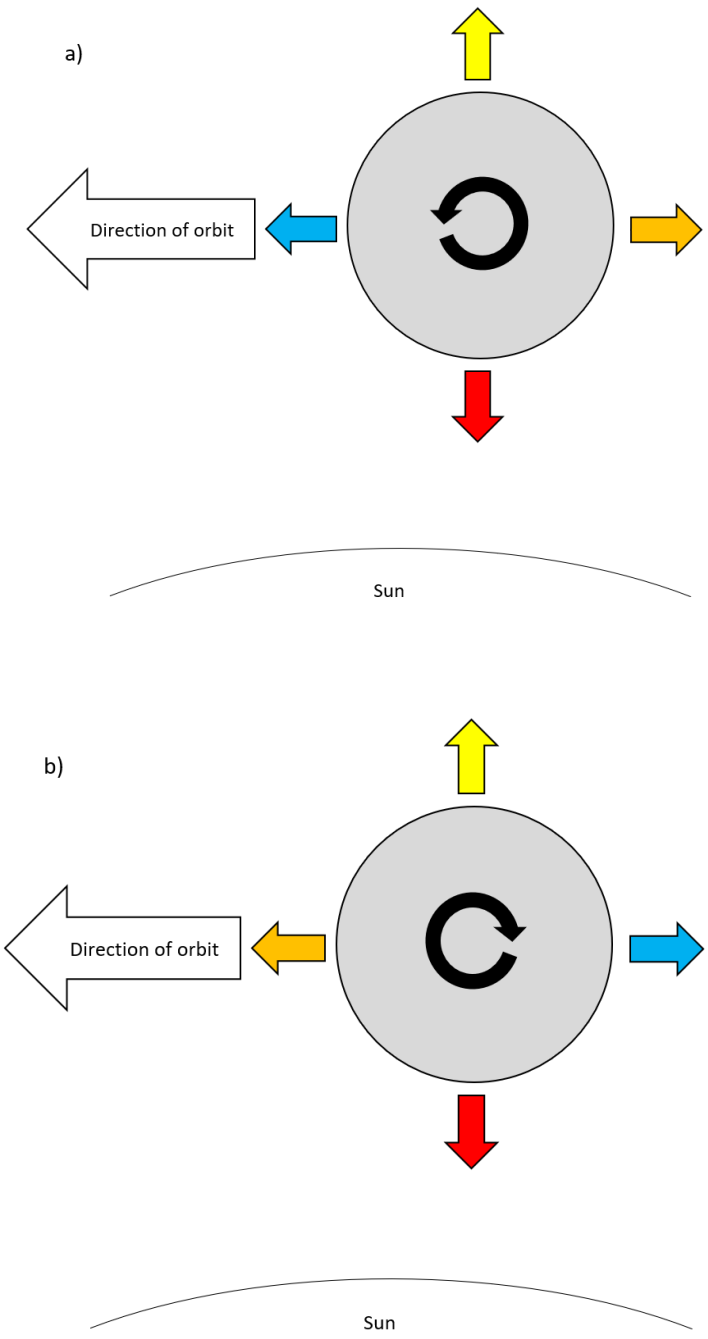

Figure 16 – Visualisation of the Yarkovsky effect on an asteroid. Coloured arrows show the thermal energy released via photons in each direction. In part a), the net thermal energy is higher in the opposite direction of the orbit, and so the effect will be to accelerate the asteroid and increase the orbit. In part b), the net thermal energy is higher in the direction of the orbit, and so the effect will be to decelerate the asteroid and decrease the orbit.

The Double Asteroid Redirection Test (DART – scheduled for launch in November 2021) will impact the natural satellite of binary system asteroid 65803 Didymos, and observations of this impact are expected to inform our understanding of its bulk internal structure (Cheng et

al. 2013). However, it is unlikely to provide finer-scale data on the structure and strength such as layering that seismic is capable of.

Walker et al. (2009) posed several key scientific questions that may be answered using seismic on asteroids: "*What is the internal structure of an asteroid? What is the material strength and cohesiveness of an asteroid's surface and interior? Is the structure homogeneous and/or isotropic? Do these structural features indicate genesis from a differentiated parent body or accretion? Is there a correlation between structure and asteroid size/type? Is there a correlation between structure and size and rotation?*" Answering the last two questions may allow inferences on internal structure of asteroids to be made from surface observations such as spectral type and size. Populating a database of structural models for asteroids based on seismic observation will allow researchers to examine any relationships between structure and spectral properties. This will enable faster generation of leads for SPB mining and faster identification of viable deflection strategies for any hazardous SPBs identified.

In addition to 3D imaging and inferring rock/regolith type and strength, seismic may also be used on SPBs to determine the normal mode frequencies, which may be used to predict the internal structure of a body with one receiver (Weber et al. 2015). Unlike the nearly spherical Earth, Moon and Mars, SPBs often have irregular shapes, making this analysis more difficult, though not impossible (Walker et al. 2015). Walker and Huebner (2004) compute the normal modes for a theoretical 1 km diameter stony SPB to examine the feasibility of this, and found that the gravitational pull of such a body would likely be too low to provide sufficient coupling to allow for the measurement of ground movement.

Phobos' bulk density estimates range from 1,530-2,200 kg/m^3 (Smith et al. 1995; Williams et al. 1988), which appears to be low for a body of its size. One possible explanation for this is

the body contained a large amount of water ice after formation (Fanale and Salvail 1990), which was lost over time (Dubinin et al. 1991), leaving significant void spaces. This process may also occur on small, undifferentiated asteroids with solar orbits more distant than where water ice is stable (Wilson et al. 1999), which would have implications for mining and deflection. Many asteroids have bulk densities of this range or lower (such as the SPB 253 Mathilde; Yeomans et al. 1997) which may support this model, although this may also result from the breakup and reassembly of asteroids, creating rubble piles. Seismic techniques can identify the presence of these void spaces in several ways, including 3D imaging, examining the scattering and attenuation of seismic waves, and observing normal mode frequencies.

3.4.3.1 Cautionary note on SPB deflection

It is important to recognise the dual-use risk of any technology which directly or indirectly aids the deflection of asteroids. Ostro and Sagan (1998) posed a new possible explanation for the Fermi paradox (why do we not see any sign of extraterrestrial civilisations in a universe with so many stars?): any species that does not develop asteroid deflection technology eventually goes extinct due to a civilisation ending SPB impact, while species that do develop asteroid deflection technology go extinct after accidentally or intentionally deflecting a large SPB into their planet. This could occur if a benign SPB with a near Earth-intersecting orbit is identified and deflected into an Earth intersecting orbit.

This so called 'deflection dilemma' raises the possibility that developing asteroid deflection technology may increase the likelihood of a large SPB impact, rather than decrease it. Sagan and Ostro (1994) argue that it is premature to develop asteroid deflection technology due to the history of 20th Century politics, which would suggest the possibility of misuse by governments, let alone by private actors. Given that the threat of nuclear weapons remains today, one can imagine that they might argue it is still too premature. A full cost-benefit

analysis of the pros and cons of developing SPB deflection technology today should be undertaken. Many workers in this field assume that developing SPB deflection technology today is a net benefit to humanity, and this may not be the case, especially when one considers the opportunity cost of what else might be done with the funding and research effort that would otherwise go towards it.

Any work that develops the understanding of SPB deflection and related fields could be considered an information hazard. A typical example of a modern information hazard would be a paper which demonstrates the ease with which one might develop and release a deadly pathogen with the aim of raising public concern. Despite the best intentions, they may simply make it easier for someone to do exactly what they are concerned about. This same issue is faced when presenting any work on the deflection of SPBs.

This should also be a concern for SPB mining, as the removal of material may have non-trivial effects on the orbit of the body through several mechanisms, including: the ejection of mass having a 'mass driver' effect and pushing the body, and changing the rotation of a body, which may alter the orbit through the Yarkovsky effect (Öpik 1951).

It may be the case that arguing for the cessation of development of asteroid deflection technology is too strange an idea for both the public and planetary defence community to accept. In this case, advocating for and developing systems that protect us from misuse of such technology (including the promotion of caution and safety for SPB mining) may be a more worthwhile pursuit.

3.4.4 Foundational science

Using radio data to examine the tidal bulge of Mars, Yoder et al. (2003) proposed that the planet likely has a liquid iron core of 1,520 to 1,840 km in radius. A series of seismic receivers

across the surface of Mars could be used to constrain the exact size in the same way that the liquid inner core of the Earth was constrained. As S-waves do not travel through liquid, an S-wave shadow where no S-waves are measured opposite the liquid core from a source on the other side of the planet. With at least three receivers to locate the source location of any natural seismic impulse, multiple source events over time may be used to confirm the existence and accurately constrain the shape of the liquid core. The reflection pattern of P-waves could also be examined to determine whether Mars has a solid inner core. It is expected that these techniques could be applied to any planetary body, as the underlying concept remains the same. In the absence of earthquakes on geologically inactive bodies, meteorite impacts could act as sources.

Nakamura (1983) used the seismic arrival times of 81 natural and artificial source events to four receiver stations to invert and estimate the seismic velocity of the upper and middle mantle. However, this work was unable to constrain the lower mantle and core, due to a lack of seismic receivers on the far side of the Moon. However, the presence of an attenuating region near the centre of the Moon, interpreted to be a core, has been proposed based on the relative lack of seismic events from the far side (Nakamura 2005), and further supported by Weber and co-workers (2011). A similar network of seismic stations on other planetary bodies should also be capable of estimating internal velocities.

The use of meteorite impacts as sources for passive seismic measurements of the Moon and Mars has been discussed (McGarr et al. 1969; Daubar et al. 2018) and remains promising. To supplement this, the use of artificial impacting sources may be considered, such as the impacts from spent rocket stages on the Moon during the Apollo missions. It has been predicted that up to 10 such natural impacts should be detected per year by a receiver on

Mars (Daubar et al. 2018), and that they could be distinguished from subsurface sources based on their seismic characteristics, though to date no confirmed meteorite impacts on Mars have been detected (Banerdt et al. 2020).

Surface (Rayleigh and Love) waves can travel around a planetary body multiple times before attenuating below detectable levels. On Earth, quakes with a magnitude of 6 or greater are required for a surface wave to travel around the body. On Mars, due to its smaller size (resulting in less geometrical spreading) and lower background noise, quakes with a magnitude of 4.5 or greater (around 40 times lower than on Earth) are required for this to occur. Multiple surface wave arrivals can, therefore, be detected for a single seismic event, which may be used to identify the source location using a single receiver location (Weber et al. 2015). However, given the lack of observation of surface waves on Mars, thus far, this may not be possible (Banerdt et al. 2020).

Seismic exploration has been proposed for several other planetary bodies, such as to Venus to develop an understanding of the planets' subsurface and structure (Stofan et al. 1993) and to the moons of Jupiter and Saturn (Kovach and Chyba 2001).

3.4.5 Penetrator probes

Penetrator probes show great promise for the delivery of science and exploration equipment to off-Earth bodies. A penetrator is a probe of up to several metres in size designed to impact and penetrate regolith or rock without damaging the equipment carried within. This can be used to easily and quickly deliver scientific tools to the subsurface of a body without the need for drilling, excavation or a soft landing, with some penetrators able to impact a surface at up to 300 m/s and survive in a range of materials including ice, penetrating up to several metres

(Smith et al. 2012; Ball et al. 2004). It has been suggested that modifications such as shock absorbers may increase survivable impact speeds to several km/s (Veldanov et al. 1999).

To date, while several penetrator probes have been launched on off-Earth missions, none appear to have survived to return data. The Mars 96 mission included penetrators, though the spacecraft failed during launch from Earth (Lognonné et al. 1998), the Deep Space 2 mission sent two penetrating probes to Mars (Smrekar et al. 1999) which were both lost upon atmospheric entry, and the Phobos 1 and 2 missions contained penetrators with seismic equipment (Surkov 1989), though neither of these missions arrived at their destination. Franqui and co-workers (2019) and Smith and co-workers (2012) have proposed emplacing seismic equipment on Europa/Ganymede and the Moon respectively using penetrators.

Multiple penetrators could be used to develop a network, with individual probes acting as either a source, receiver, or both. The imaging potential increases with the number of individual penetrators, and for optimum coverage they should ideally be arranged in a grid. Accurate targeting, onboard descent cameras, laser rangefinders and satellite imaging of the probes impact sites may be used to determine the distance between each source and receiver, allowing for seismic velocity estimates. In addition to onboard sources, natural and impacting sources may also be used, for example the Europa/Ganymede proposal includes the use of a satellite at the end of its life as an impacting source to enable a thickness estimate for the icy crust (Franqui et al. 2019). As a precedent, explosives were used as seismic sources with dozens of receivers to estimate the thickness of an ice sheet in Greenland (Harper et al. 2012), though a single receiver should be capable of measuring ice thickness on Europa (Kovach and Chyba 2001).

A single penetrator with both a source and receiver at opposite ends lengthwise may still be able to take small scale seismic measurements and infer local properties. However, there is the likelihood of the local regolith/rock being perturbed by the impact of the penetrator itself, altering the measurements. There is also the possibility of seismic waves travelling from the source to receiver through the penetrator itself, impacting the measurement. This is of particular concern for off-Earth regolith where the velocity is expected to be significantly lower than the velocity of the penetrator itself.

Accelerometers measure the rate of the probes deceleration and can provide information about the near-surface layers such as thickness and strength (Smrekar et al. 1999), supporting subsequent seismic measurements and informing operators of the depth of penetration, which is vital knowledge for accurate interpretation of seismic data.

3.4.6 Challenges and risks of off-Earth seismic methods

Off-Earth seismic are expected to experience a range of constraints, challenges, and risks. Some of these also occur during the use of seismic on Earth, and some are unique to the off-Earth environment. Some likely challenges include a lack of sources and receivers due to cost, weight, and size constraints (Walker et al. 2015) and a lack of existing data to compare with and validate the seismic data.

The creation of fractures through cratering observed on the Moon is also expected to occur on asteroids, which would reduce data quality. Observing that the data quality is similar on an asteroid may itself be a useful result, as it could indicate that the existence of a fractured subsurface. The simple calculation of the subsurface seismic velocity is not expected to be affected by this (although a fractured subsurface will likely result in a lower seismic velocity).

The calculation of UCS and other characteristics from P- and S-waves should therefore be unaffected.

SPBs have very low gravity compared to moons and planets (0.27 m/s^2 on the largest body in the main asteroid belt, Ceres, and 0.0059 m/s^2 on 433 Eros, a body 16.84 km in length, compared to Earth with 9.81 m/s^2). There is concern that this gravitational pull will not be strong enough to create sufficient contact friction (coupling) at the interface between a seismic receiver and the regolith at the asteroids' surface to allow for movement to be recorded (Walker and Huebner 2004). This may also result in seismic waves creating ground movement greater than the local gravity, which may result in the receiver being ejected from the surface (Lognonné 2005). Solutions such as releasing a hardening fluid to maintain the contact may be necessary. However, any action taken will perturb the natural *in-situ* environment, altering the measurement. While this would render short distance seismic measurements (sub-metre scale) completely invalid, it may not be a significant factor for long distance measurements, as the measured velocity would approach the true velocity of the unaltered medium.

Modern seismic imaging surveys rely on source and receiver positioning from GPS and a high-resolution digital elevation model. These may be difficult on planets and moons, and even more so on SPBs. Novel solutions may need to be developed to facilitate source and receiver positioning for accurate imaging.

Given the non-uniqueness problem, the use of drilling to support seismic data will be immensely valuable. Drilling in off-Earth environments will likely be significantly more difficult than on Earth. A large amount of equipment is needed to drill deep holes and drilling conditions are largely unknown. Unmanned missions are also unlikely to be conducive to

successful drilling missions, as everything will need to work near-perfectly. If a deep drilling mission were successful, however, it could provide important data. For example, seismic studies have identified the likely depth of near-surface geological layers on the Moon and have proposed what rock type they may be based on the limited data (Cooper et al. 1974). The drilling of a single hole in this region to examine rock chips, drill cores or downhole imaging could confirm or update the stratigraphy, allowing us to extrapolate this across the region using the seismic data.

Seismic-while-drilling (SWD) is an active source seismic method consisting of sources attached to a drill above the drill bit (such as a small explosive source) which are detonated various depth intervals (Naville et al. 2004). Receivers are placed on the surface in either a 2D or 3D array (and occasionally a single receiver at the surface to generate 1D data). In addition to convenience, SWD can provide higher quality data than typical seismic surveys. Poletto and co-workers (2015) proposed that SWD might be used on the Moon to examine stratigraphy. The same technique could be used on Mars and other planetary bodies. Pletser and co-workers (2009) have also suggested that a seismic refraction survey could be used on Mars to detect the presence of subsurface water. Data from such a survey could be combined with drilling to verify the presence of any water and identify the volume and quality of the water. These would be necessary steps before a decision is made on whether to commence mining for the resource.

Both instrument (thermal, electrical, etc.) and environmental (other sources of natural or artificial sound) noise contribute to the measured signal. With a sufficiently low signal to noise ratio (SNR), it can be difficult to identify signals. To an extent, the noise can be removed through processing. If the signal is of a known frequency, other frequencies can be removed

through bandpass filters. ‘Sweeps’ are often used, where the source changes its output frequency at a known rate over several seconds. This will be used to cross-correlate the received signal, creating a signal that would result from an instantaneous impulse source, the effect of which is to improve the SNR relative to using a real instantaneous impulse source.

Signal stacking is also commonly used to increase SNRs. This involves taking multiple repeat measurements and with the same source/receiver configuration and summing their amplitudes. The background and instrument noise should, on average, negatively interfere, while the true signal will constructively interfere. In an off-Earth environment where weaker signals are received, such as the surface of the Moon, these techniques will be critical to achieving desired SNRs. Signal stacking may also provide a solution to the presence of noise creating wind on Mars. For active seismic, measurements may be repeated and stacked using the same source-receiver configuration.

Giardini and co-workers (2020) noted the low SNR of seismic events on Mars as measured by the SEIS device on the InSight mission. Instead of identifying arrivals in the time domain, they used spectrograms and spectral envelopes to detect and investigate the events with success.

While a network of seismic receivers is needed for accurate positioning of a source, some inferences may still be made with a single receiver (such as with SEIS). For an event of sufficient magnitude, the delay between the P- and S-wave arrival can be used to predict the distance to the source, if measurements or assumptions are made of the P- and S-wave velocities of the medium the wave travels through. The direction of the source from the receiver may also be deduced using a receiver which measures displacement in three directions, allowing the direction of travel of any seismic waves to be determined. Finally, the

magnitude of the source can be predicted by using the received wave amplitude and predicting the rate of attenuation to back-calculate the original strength.

To overcome the challenge of emplacing receivers in difficult to access locations, a proposal has been made for a geostationary optical seismometer (Michel et al. 2013). This would allow for ground displacement at a location to be measured from orbit, using either an optical telescope or LiDAR/radar. This data could in theory be converted to a waveform which could be analysed in the same way as conventional seismic data. This technology is not yet proven, and will require high degrees of accuracy, though may prove promising in the future.

3.5 Conclusion of off-Earth seismic exploration

This chapter has covered the fundamentals of seismic geophysics, the history of off-Earth seismic exploration, and how seismic techniques could be utilised to further planetary science for research, prospecting, mining, and planetary protection purposes. Seismic has been utilised with great success over the past 100 years on Earth to understand the subsurface and has the potential to achieve the same in space exploration. To date, it has not yet achieved its full potential off-Earth, partly due to some challenges and limitations the space environment poses, which have also been addressed in this chapter.

Seismic has the potential to be used to infer rock and soil type, strength porosity and other geomechanical properties, produce 3D and 4D representations of subsurface features and structure, detect the presence and orientation of fractures, and determine the point of origin and source of natural seismic events.

4. Seismic Apparatus for Fine-Grained Sediment design

This chapter is an expanded version of a conference paper (reference below).

Dello-Iacovo, M.A., Anderson, R.C. and Saydam, S. 2017, A novel method of measuring seismic velocity in off-Earth conditions: Implications for future research, 48th Lunar and Planetary Science Conference (The Woodlands, Texas).

4.1 Introduction of seismic apparatus design

Knowledge of the strength of regolith and subsurface structure on non-Earth planetary bodies such as the Moon, Mars and asteroids is expected to be critically important for planning future exploration, mining, colonisation, and asteroid deflection missions. For example, the structural/composition type of an asteroid is likely to control the effectiveness of various deflection methods (Gibbings 2011; Holsapple 2004) and understanding the strength and composition of regolith is needed for the selection of *in-situ* anchoring devices (Gritzner and Kahle 2004) and extraction techniques. One proposed method for determining the strength of the regolith and the internal composition on these bodies is to place seismic sensors on its surface. However, interpreting the data from these sensors may be difficult, given the challenges outlined in Section 3.3.2.1, such as the presence of a highly fractured subsurface resulting in scattering and attenuation of seismic waves (Knapmeyer and Weber 2015).

To date, little is known about the geomechanical properties of the regoliths of these airless planetary bodies, especially asteroids (Walker et al. 2009). On Earth, relationships exist between seismic properties and the strength of consolidated and unconsolidated materials found (Butel et al. 2014). To understand the geomechanical properties of airless bodies, there needs to be an understanding of how seismic sensors work when placed on these bodies. Chapter 4 and Chapter 5 will contribute to this knowledge gap by examining the impact of off-Earth regoliths and atmospheric conditions on seismic data collection. While also important to understand, the effect of gravitational strength on seismic data collection is out of the

scope of this research given the costs of utilising a parabolic jet to undertake the necessary experiments.

Limited work has been performed to test seismic sensors on Earth for use on other planetary bodies (Banerdt et al. 1993). However, according to the knowledge of the author, no data have been published for testing seismic sensors in simulated near-vacuum, weightless conditions as expected on asteroids.

This chapter outlines a novel methodology for measuring the seismic velocity of low compaction, fine grained regolith on airless bodies using piezoelectric transducers and presents some preliminary results from measurements of the seismic velocity of the Australian Lunar Regolith Simulant (ALRS-1). The approach is to set up a 'seismic in a box' experiment (Sherlock and Evans 2001; Buddensiek 2009) which can be used to measure the P- and S-wave seismic velocity of soils and regolith. This methodology is used in Chapter 5 to take more measurements, including of the Mojave Mars Simulant (MMS). The apparatus designed in this chapter has been called the Seismic Apparatus for Fine-Grained Sediment (SAFGS).

4.2 Piezoelectric transducers

Piezoelectric transducers were chosen as the seismic sources and receivers for the experiments in this thesis over geophones (commonly used in terrestrial seismic exploration) due to their higher source/receiver frequency. The frequencies measured by geophones typically range from 1 to 100 Hz, while the frequencies measured by piezoelectric transducers range from several kHz to several MHz. As demonstrated below, this is an advantage for experiments where the distance between the source and receiver is small, as it significantly increased the accuracy of velocity measurements.

Piezoelectricity is the property of some materials (such as crystals and ceramics) to generate an electric charge in response to changes in stress. This electric charge may be measured by attaching an electrode, allowing a piezoelectric material to act as a sensor for changes in stress, such as that caused by seismic waves (Valle-Molina and Stokoe 2012). An electric current may also be applied to a piezoelectric material to generate internal stress, which in turn causes the material to vibrate, producing a seismic wave. Piezoelectric transducers have been used extensively in laboratory-based seismic experiments due to their small size and ease of use (Valle-Molina and Stokoe 2012).

Piezoelectric transducers can be used to generate and measure both P- and S-waves. P-waves are generated and measured using piezoelectric disks, while S-waves are generated and measured using bender elements (Valle-Molina and Stokoe 2012). A diagram depicting piezoelectric transducers is shown in Figure 17.

Figure 18 depicts a single seismic trace. This is a recording of amplitude over time from one seismic receiver. Seismic velocity of a material is determined by measuring the distance between the source and receiver and dividing it by the time it takes for a wave to pass through the material (delay time). A higher signal frequency makes identifying the time of the first wave arrival easier and more accurate, thus improving the accuracy of the delay time component. Accurately identifying the time of the first wave arrival is critically important in seismic studies (Boschetti et al. 1996). This is due to the shorter time between the peaks and troughs of the event, and the existence of background noise before the first arrival.

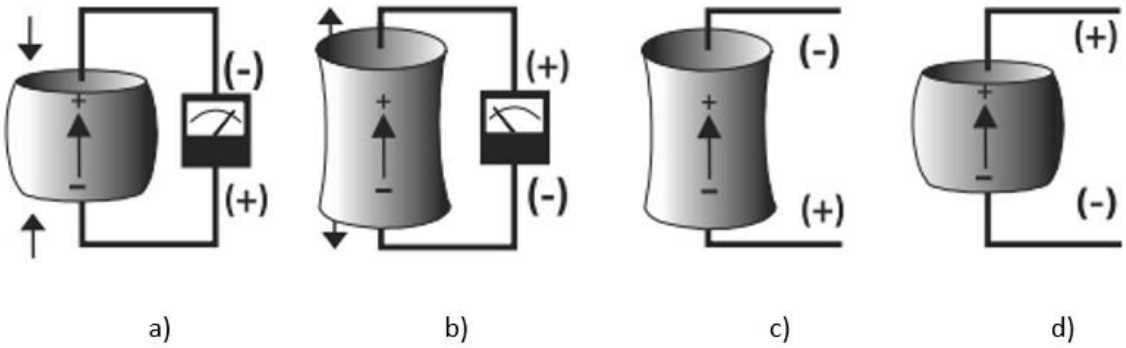

Figure 17 – a) and b) show the reaction of a piezoelectric transducer element to applied external stress. As the element contracts and expands, it produces a current, which may be measured. c) and d) show the reaction of a piezoelectric transducer element to applied current. In response to the current, the element contracts and expands, acting as a seismic wave source (Moheimani and Fleming 2006).

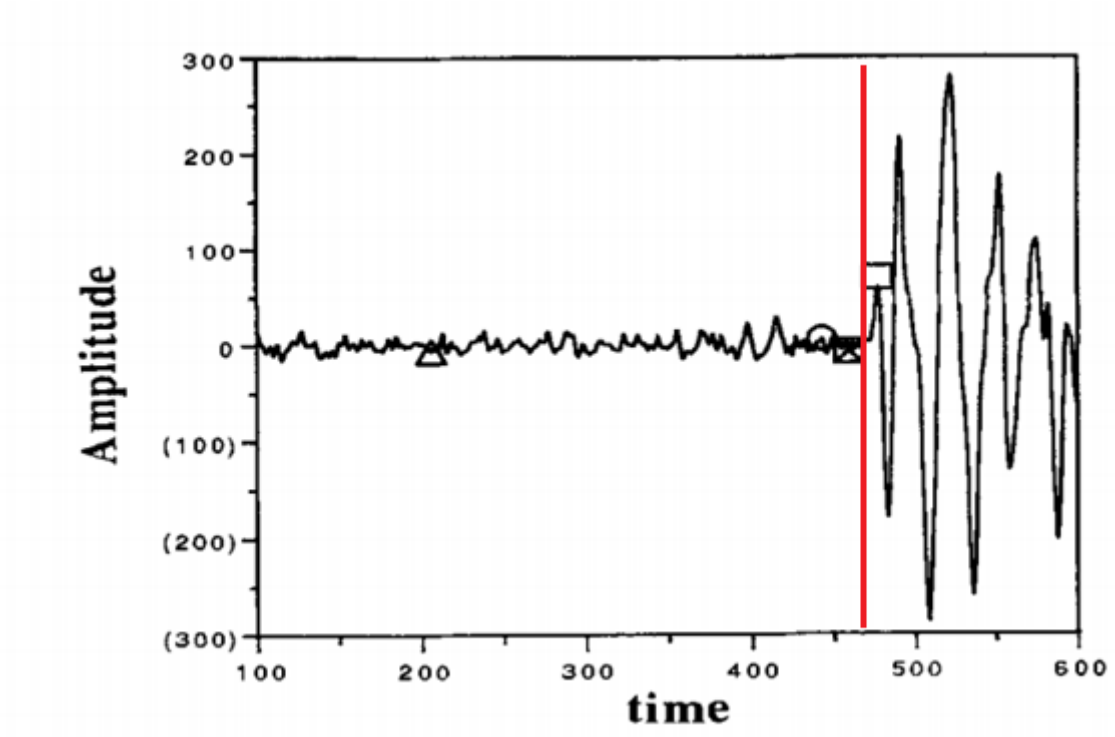

Figure 18 – A recording over time of amplitude from a single seismic receiver, called a seismic trace. The first arrival of the seismic event being recorded, also called the first break, is marked with the red line. Prior to this, a level of background noise can be observed (Boschetti et al. 1996).

In large seismic surveys where the source and receiver are often over one kilometre apart, the uncertainty in the delay time measurement is relatively small compared to the delay time. However, in the laboratory experiment designed in this chapter the distance between the source and receiver and therefore the delay time will be negligible (sub-10 cm). Therefore,

reducing the uncertainty in the delay time measurement by increasing the source frequency is critical. Piezoelectric transducers were thus chosen over geophones for these experiments.

4.3 ALRS-1 regolith simulant

For this research, two planetary regolith simulants were chosen for testing: the Mojave Mars Simulant (MMS) and the Australian Lunar Regolith Simulant (ALRS-1). Both materials have been designed based on observed regolith properties of samples taken from and examined on the Moon and Mars.

The ALRS-1 (Figure 19) was created by Garnock and Bernold (2012) at UNSW based on the geochemistry and geomechanics of lunar regolith from the lunar mare area identified from the Apollo landers. The material was created using basaltic soils from northern Sydney, NSW, Australia, and was prepared by sieving to achieve a particle size distribution comparable to lunar regolith (Figure 20). The grain size distribution of true lunar regolith within the lower 15% is unknown as wet separation tests were not allowed (L. Bernold 2020, Pers. Comms. 16 May). Therefore, the geomechanical accuracy of the lunar regolith simulants in the lower 15% will remain unknown unless wet separation tests are performed on true lunar regolith.

While the geochemistry of ALRS-1 has been measured and is comparable to the lunar regolith (Bonanno and Bernold 2015), the geomechanical and seismic properties remain untested. Comparing these properties of the simulant with that of the *in-situ* lunar regolith is critical to ensure that previous experiments performed using the material (Bonanno and Bernold 2015) can be accurately applied to the lunar environment, and to open the way for future experiments.

The ALRS-1 appears to have formed some aggregates of regolith, as seen in Figure 19. These are relatively weak and can be broken up with moderate pressure. It is hypothesised that

these formed as the result of moisture in the air. These aggregates were not used in the experiments, as they are not believed to be representative of the *in-situ* lunar regolith.

The MMS (Figure 21) was created for testing of flight hardware for the sampling system (Sample Acquisition, Processing, and Handling subsystem - SASPaH) on the Mars Science Laboratory rover (Peters et al. 2008). Basaltic boulders were crushed to submicron particle size simulating the particle size distribution of regolith on Mars. Four different particle-size samples of MMS have been developed: dust, fine, medium, and coarse size sand. In this thesis, the MMS dust, small-grain, and medium-grain sand samples were used.

The highly fine-grained nature of the ALRS-1 meant that it imposed a potential health hazard (Figure 21). Thus, dust masks and fume hoods were utilised while handling and testing the regolith. Dust masks were also used during handling of the MMS samples due to its fine grain size (Figure 22).

In this chapter, tests are performed using only the ALRS-1 sample. In Chapter 5, tests are performed using both the ALRS-1 and MMS samples.

Figure 19 – Photo of the Australian Lunar Regolith Simulant (ALRS-1) developed by Garnock and Bernold (2012).

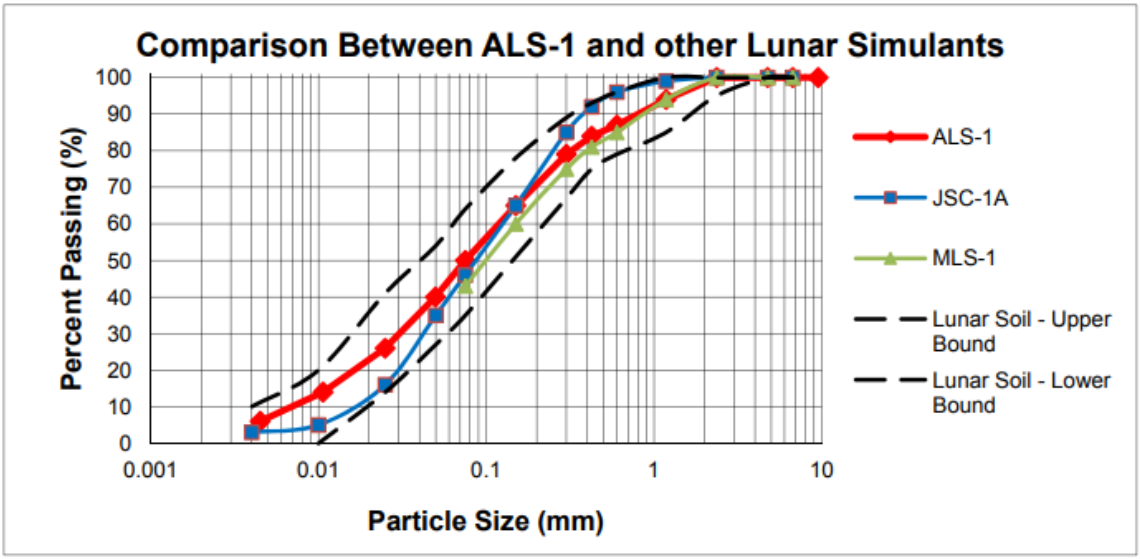

Figure 20 – Comparison of grain size distributions of lunar regolith samples from the Apollo 11, 12 and 14 missions with the ALRS-1, the Johnson Space Centre Lunar simulant (JSC-1A), and the Minnesota Lunar Simulant (MLS-1) (Garnock and Bernold 2012).

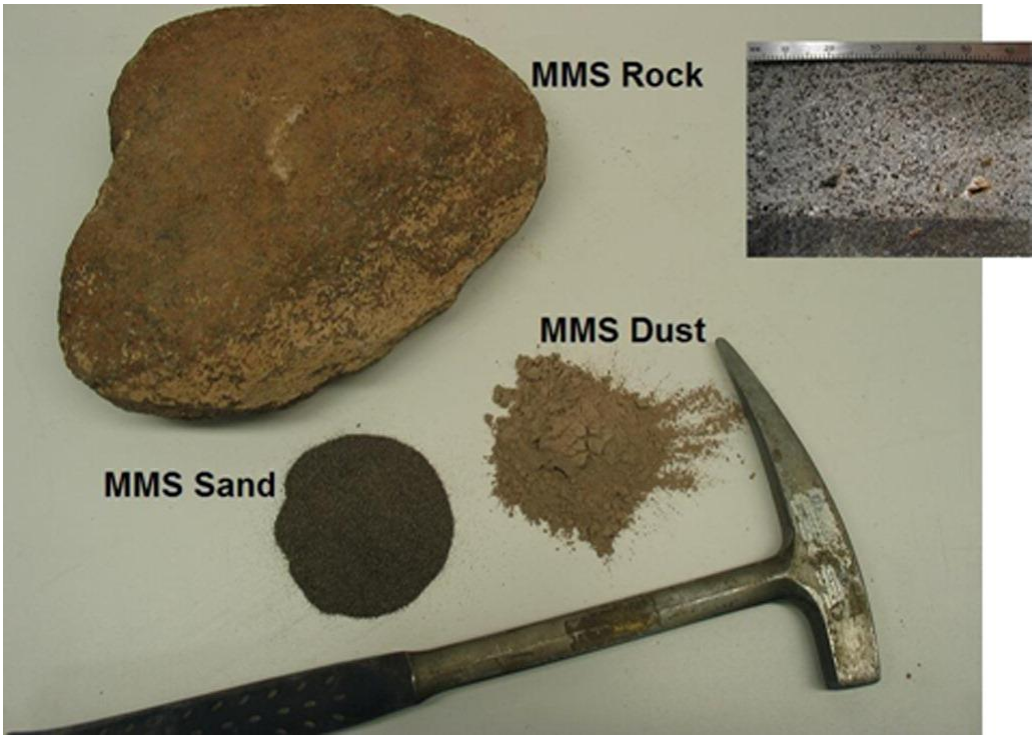

Figure 21 – Photo of the Mojave Mars Simulant (MMS) developed by Peters et al. (2008). Image from Peters et al. (2008).

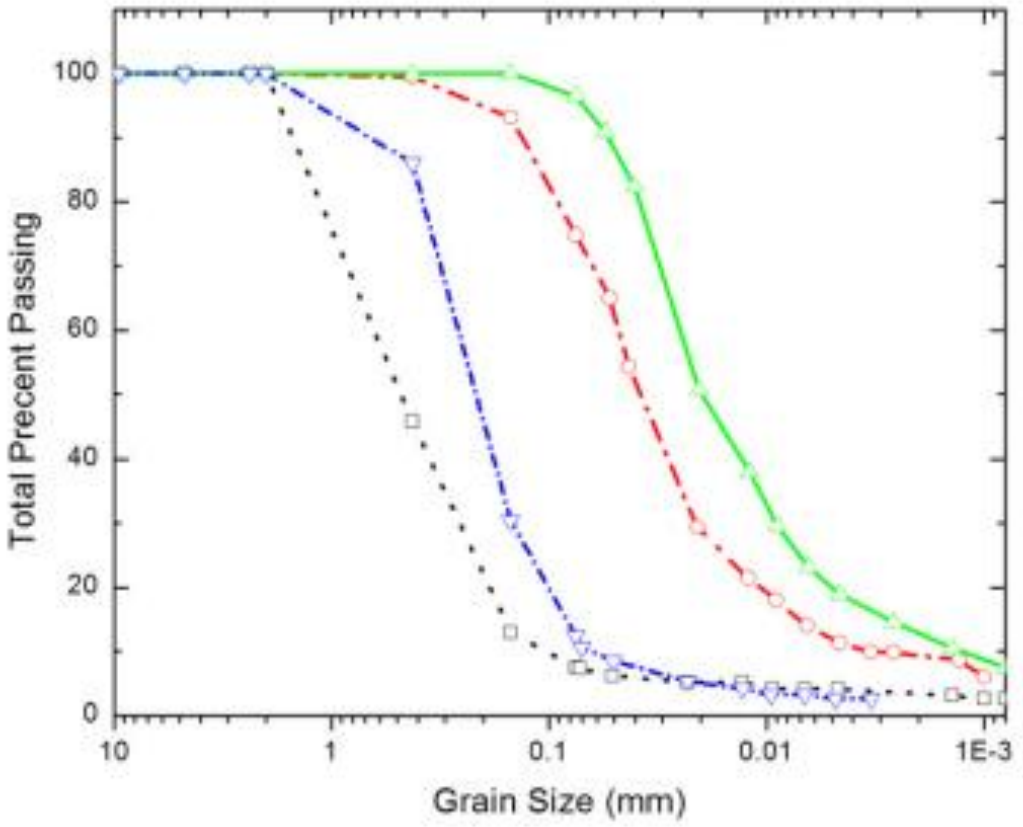

Figure 22 – Comparison of grain size distributions of MMS dust 1 and 2 (triangles and circles respectively), MMS sand (inverted triangles), and JSC Mars-1 (squares) (Peters et al. 2008).

4.4 Apparatus design

Small scale, 'seismic in a box' testing of regolith is relatively uncovered in the literature. Buddensiek (2009) and Sherlock and Evans (2001) used small, high frequency seismic receivers in a relatively confined sandbox to measure seismic velocities. However, these studies focus primarily on imaging small scale versions of regional geological features reconstructed with varying layers of sand; they did not focus on measuring seismic velocity. The experiments in these studies were undertaken by covering the regolith in water to provide a medium for the seismic waves to travel through. Seismic waves experience strong attenuation when travelling through unconsolidated sand due largely to friction between individual grains and uneven pore space distribution, which has been a major issue for imaging sandbox models with seismic (Purnell 1986). The water was included in these studies to combat this (Sherlock and Evans 2001; Buddensiek 2009). This approach will not be taken in this study for several reasons; to preserve the integrity and accuracy of a limited sample, and to better recreate the true lunar environment.

A container for the ALRS-1 to fill during testing was designed with several factors in mind. It should be sufficiently large such that two piezoelectric transducers can fit in with some room to spare. It should be small and light enough to be portable. It should be made of a sturdy material and have the ability to be sealed and bolted down so that it can be used in 'zero gravity' experiments (such as a parabolic jet or a drop chamber) without risk of the regolith escaping and entering the air and presenting a health hazard. For these reasons, stainless steel was used.

Stainless steel has a high seismic velocity (5740 m/s) (Olympus 2020) compared to the velocity of *in-situ* lunar regolith (104-114 m/s) (Kovach and Watkins 1973). The container should, therefore, be sufficiently large in all dimensions that seismic waves travelling through the low

velocity regolith arrive before any waves that travel from the source to receiver via an indirect route, such as along the frame of the container. If a seismic wave travelling along any route other than directly from the source to the receiver arrives first, the first wave arrival will not be the seismic wave path that is intended to be measured. A simple way to achieve this is to ensure that the source-receiver distance is always smaller than the distance from both the source and receiver to the frame of the container. Given the aim of measuring the seismic velocity over distances of up to 5 cm, the distance from the source and receiver to the containers' frame should always be at least 5 cm. Assuming they are located in the middle of the box and surrounded by regolith, this requires a box of at least 10 cm in every direction. Dimensions of 200 x 300 x 300 mm were chosen to allow for extra space, and the walls of the container were made 1.2 mm thick. The container also has a free-floating lid with a Perspex window and six latches to hold it closed for work in dynamic environments and has two carry handles for portability.

Two identical boxes were made, and holes were drilled in the sides of one to allow the cables connecting the transducers to the recording system to pass through the wall for use in 'zero gravity' experiments. The holes could then be sealed with the cables in them. While the 'zero gravity' experiments were ultimately not undertaken as part of this thesis, the same apparatus could be used for such experiments in the future. Some preliminary schematic drawings of the boxes can be seen in Figure 23.

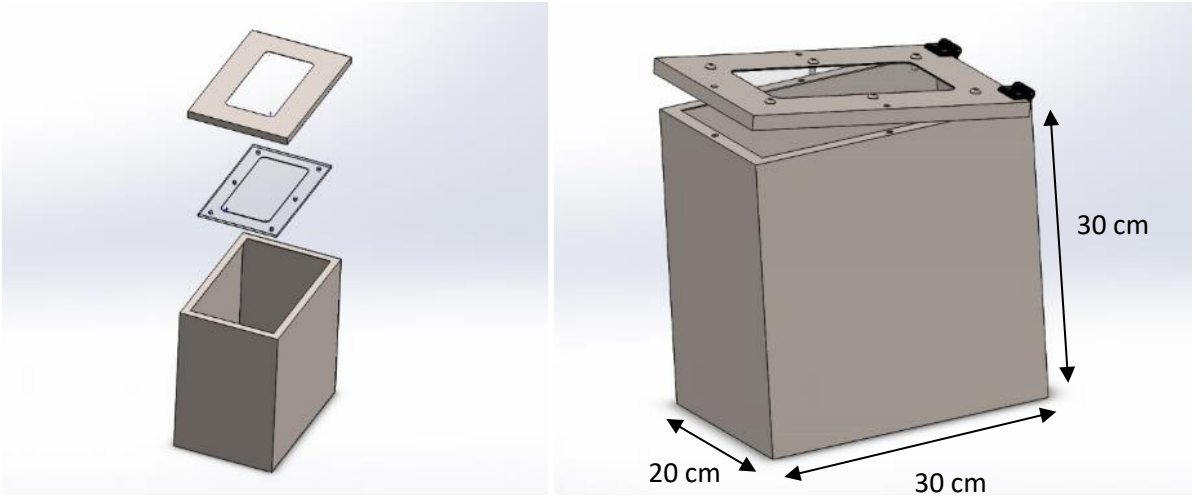

Figure 23 – Preliminary schematic drawings of the boxes designed to contain the regolith during testing.

4.5 Methodology

The Pundit PL-200 system was used to collect seismic data, which has interchangeable piezoelectric transducer sources and receivers of different frequencies. The source and receiver used for the preliminary tests were rated at 54 kHz. The full set-up of the recording system and container is displayed in Figure 24. The tests were undertaken at the UNSW Sydney Mineral and Energy Resources Engineering lab.

The container is filled with loose ALRS-1 (no compaction applied) to approximately 5-10 cm high, and the source and receiver are placed inside and buried under the regolith. The distance between the closest edges of the source and receiver is measured, and the Pundit is used to determine the delay time of a 54 kHz seismic wave transmitted through the regolith, using the first arrival of the received seismic wave. The recordable delay time ranges from 0.1 – 7930 µs, with a resolution of 0.1 µs (for < 793 µs) and 1 µs (for > 793 µs).

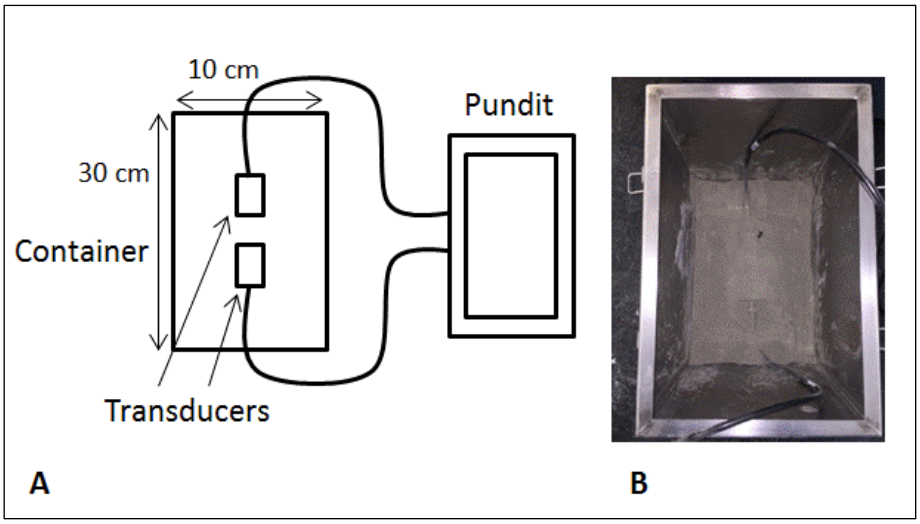

Figure 24 – a), sketch of experimental set-up, and b), image of piezoelectric transducers buried in ALRS-1.

4.6 Results

Velocity measurements were made by measuring the separation distance of the source and receiver and using the range of delay times read by the Pundit for that distance. To get a good estimate of the delay time, 23 measurements were taken at a range of separation distances from 0.5 cm to 3.5 cm. The measured velocities ranged from 38.6 m/s to 286.7 m/s with an average of 98.6 m/s. The source-receiver distance versus delay time is displayed in Figure 25, and the source-receiver distance versus velocity is displayed in Figure 26. An example of a seismic wave as measured by the Pundit PL-200 system and its interpreted first arrival time is shown in Figure 27.

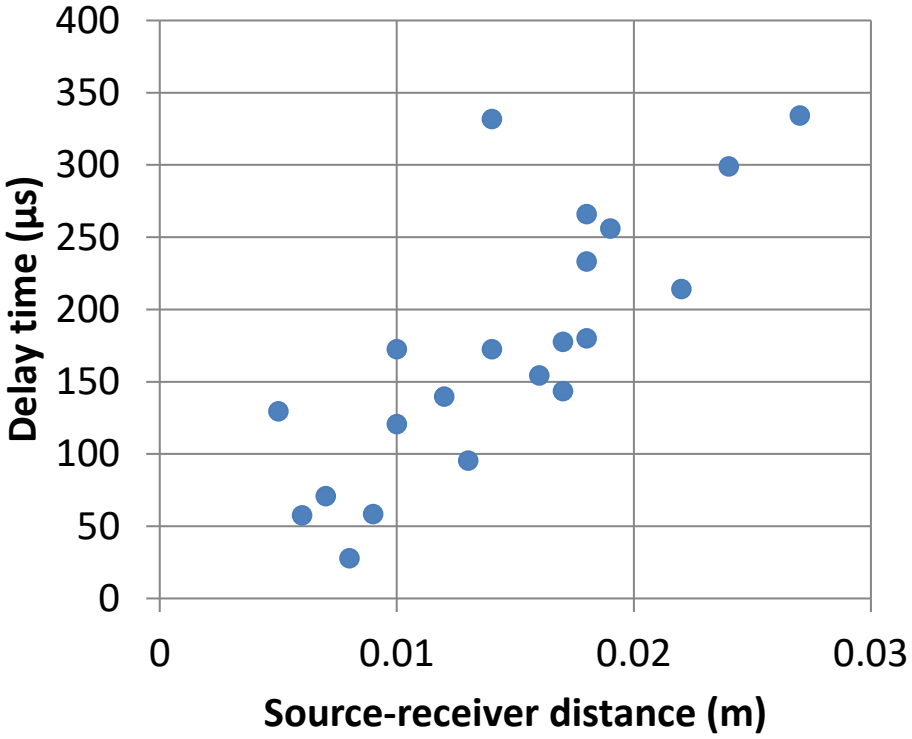

Figure 25 – The delay time of each measurement of the ALRS-1 vs the source-receiver distance.

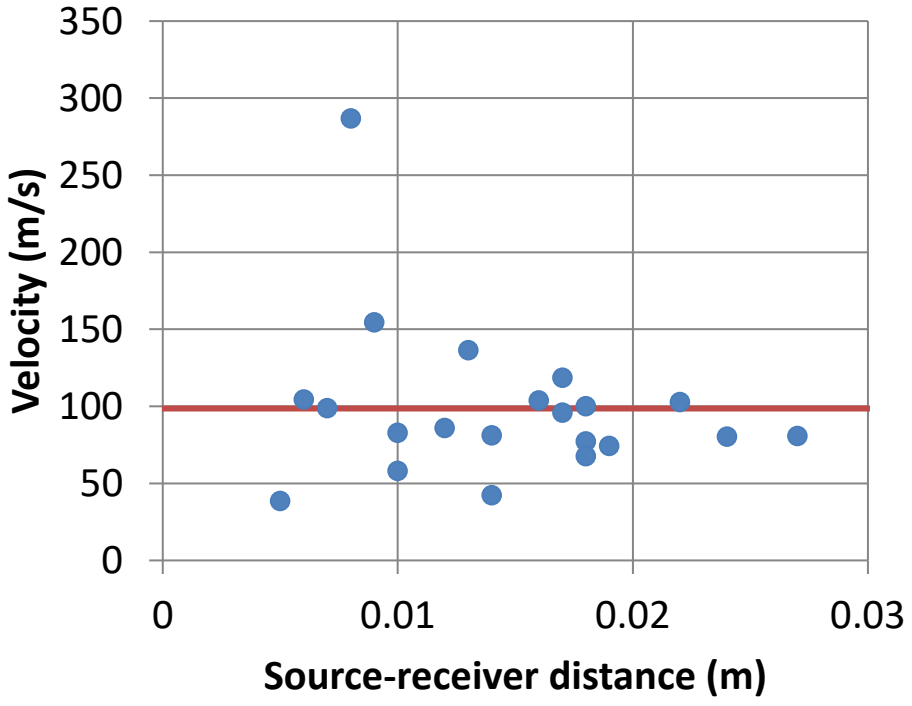

Figure 26 – The P-wave seismic velocity of each measurement of the ALRS-1 vs the source-receiver distance.

Figure 27 – An example of a seismic wave as measured by the Pundit PL-200 system and its interpreted first arrival time of 255.9 µs.

4.7 Discussion

The average measured velocity for ALRS-1 is compared to the *in-situ* measurements of lunar regolith during the Apollo 14 and Apollo 16 missions, which are 104 m/s and 114 m/s respectively (Kovach and Watkins 1973). While preliminary, this is an encouraging result for the geomechanical and seismic accuracy of the ALRS-1. Further refinement of this methodology will improve the accuracy of this measurement. Some differences in regolith velocity between laboratory and *in-situ* conditions are expected, due to the differences in measurement environment in the laboratory and the Moon. Chapter 5 will further explore the impact of off-Earth environments on seismic data collection.

The delay time and velocity of the measurements were plotted against source-receiver distance to quality check for any unforeseen relationships that might indicate some error in the methodology. It is expected that there should be a linear relationship between delay time and source-receiver distance, and that there should be no relationship between velocity and

source-receiver distance. This appears to be the case for both, however in Figure 26 a potential reduction in the scatter of the velocity with increasing source-receiver distance can be observed. This could be interpreted as any uncertainty in the measurements being relatively smaller with increased distance or could potentially be an unforeseen phenomenon. This is explored further in Chapter 5.

Two outliers are observed in the results. The first, at 0.014 m separation and a delay time of 331.8 µs, is most visible in Figure 25. This corresponds to a velocity of 42.19 m/s in Figure 26. The second, at 0.008 m separation and a delay time of 27.9 µs, is most visible in Figure 26. This corresponds to a velocity of 286.7 m/s. It is not clear why these outliers exist. One possible explanation is measurement uncertainty. Another is the possibility that these are real results caused by a local but major variation in soil properties such as grain packing that may vary between measurements.

4.8 Conclusion of seismic apparatus design

This chapter has presented a novel methodology for measuring the seismic properties of fine-grain regolith in a low compaction environment which will be useful for testing seismic equipment for use in space exploration. Preliminary results using the ALRS-1 were presented and discussed. The measured velocity of the ALRS-1 is close to the *in-situ* measured velocity of regolith on the Moon. This indicates that the ALRS-1 and the lab environment is likely a good representation of the lunar regolith and environment, which is encouraging for the accuracy of this methodology. Chapter 5 will expand upon this work by using a vacuum chamber and examining other regolith simulants.

5. Effect of the space environment on seismic data collection

This chapter is a submitted journal paper with minor modifications (reference below).

Dello-Iacovo, M.A., Saydam, S. and Anderson, R.C. 2021, Effect of the space environment on seismic data collection, *Geomechanics and Geophysics for Geo-Energy and Geo-Resources* In review.

5.1 Introduction

Off-Earth bodies such as asteroids and comets offer great potential for off-Earth mining. These small planetary bodies (SPBs) are host to numerous resources that might be utilized in space (Sanchez and McInnes 2012), such as metals and ice (Badescu 2013). There is also the possibility of SPBs impacting the surface of Earth, which could cause substantial damage and loss of life (Bottke et al. 2004). Other planetary bodies such as the Moon and Mars may also offer resources and locations for future landing attempts (Casanova et al. 2020; Dallas et al. 2020; Pelech et al. 2019). Creating and developing methods for the rapid determination of structural and geomechanical properties on these planetary bodies is crucial. For example, SPBs of different structural types may react differently to different types of deflection efforts (such as kinetic impactor vs explosive; Gibbings and Vasile 2011). Developing an understanding of the rock/structural type of these bodies will also aid in the selection of mining methods in the future, or indeed determining whether mining is feasible.

Active source seismic exploration is a terrestrial tool that has been widely used over the past hundred years in a range of geophysical contexts, including but not limited to resource exploration, groundwater mapping, archaeology, and the detection of buried objects such as pipes and power cables. It is proposed that seismic exploration (such as placing sources and receivers on the surface of a body) could be a useful technique on SPBs, the Moon and Mars to understand their subsurface properties, including their structure and geomechanical properties.

The active source seismic method has been overlooked in recent planetary exploration missions due to insufficient testing under planetary conditions. For example, the impact gravity and atmospheric pressure have on wave propagation in regolith is poorly understood. In this chapter, a new method of measuring P- and S-wave seismic velocity in fine-grained, weakly compacted regoliths (such as the Mojave Mars Simulant - MMS) is explored, using active source piezoelectric transducers under regular and Martian atmospheric pressure conditions. MMS is a planetary regolith simulant which has been noted for its similar geomechanical properties to Mars regolith. Several mixtures of this simulant were used to carry out tests aimed at understanding the response of seismic waves in Mars conditions (such as particle size, packing, etc.) along with results collected from the Australian Lunar Regolith Simulant (ALRS-1) in Chapter 4. The Mars environment differs from Earth in several ways. The gravitational pull at the surface is around 38% that of Earth's, the atmospheric pressure is ~1% of Earth's, and the temperature on Mars varies from around -125 °C to 30 °C. The atmospheric pressure was considered during the experiments covered in this Chapter with a vacuum chamber. Accounting for the gravitational strength and temperature fluctuations, while useful to understand, was deemed out of scope for this research. To simulate Mars gravity, a parabolic jet could be used. However, this is an expensive endeavour and was not available.

The objective of this Chapter is to understand the effect that atmospheric pressure has on the propagation of seismic waves. This information will be critical knowledge for future planning for off-Earth seismic planetary missions.

5.2 Seismic and geomechanics

Seismic involves the use of mechanical sound waves that travel through some medium, typically soil, water, or rock. Sound waves can be generated either by passive (such as

meteorite impacts and earthquakes) or active (such as electronic vibrating or explosive) sources. The advantage of using active seismic sources is that you can choose your source locations and impulse times. Measuring the delay time between source impulse and received signal together with the distance can allow for the estimation of the seismic velocity of the medium the waves travelled through. Incorporating an array of source and receiver locations can be used to generate 2D, 3D or 4D imagery of the subsurface.

To date, the number of off-Earth seismic missions are relatively few; current seismic missions include the InSight lander (Panning et al. 2017) presently on the surface of Mars and the Mars 2020 rover (Williford et al. 2018), which arrived at Mars in February 2021. In the 1970's several seismic experiments were performed on the lunar surface (Knapmeyer and Weber 2015), generating seismic velocity estimates and some low-resolution imagery of the subsurface. The Viking 1 and 2 missions to Mars both included seismic receivers, though they were unable to identify any seismic events due to the unexpected interference of wind (Goins and Lazarewicz 1979).

The attenuation of seismic waves is an ongoing difficulty in seismic studies, particularly with wave propagation in sediments (Purnell 1986). Attenuation and source/receiving power are the primary factors determining the maximum distance at which a seismic signal can be measured. A range of factors, including the uneven distribution of pore spaces and friction between grains, contribute to seismic wave attenuation (Sherlock and Evans 2001). Low pressure of overburden soil and rock increases the amount of energy lost to friction. Grain shape and sorting are strong contributing factors to the seismic velocity within unconsolidated sediments (Sherlock and Evans 2001); density, grain size, permeability, and porosity appear to have little to no effect (Talwani et al. 1973; Bell and Shirley 1980), with

mineralogy playing a minor role. The process of deposition of sediment grains can itself result in vertical sorting which may create internal reflections and also produce inaccurate velocity measurements. Poorly sorted sediment will produce this effect even more strongly.

Velocity dispersion is another phenomenon of seismic waves with different frequencies travelling at different velocities. This concept is not well understood (Sherlock and Evans 2001); however, it was proposed that the first arrival of a seismic wave is typically the lowest frequency (Liu and Nur 1996). The part of the waveform of most interest in is the first arrival of the wave. For an ideal measurement, the first arrival will be the first time at which the amplitude increases. However, there will always be some noise present, and therefore, the first arrival should be the point at which a consistent signal is first visible above the noise. It should also be considered that the first arrival is not always the wave ray that travelled the shortest distance. An indirect ray moving through along a higher velocity medium may arrive before a direct ray travelling through a lower velocity medium. For example, sediments, in general, tend to have a lower velocity than solids. The apparatus used in this study consists of sediment surrounded by a metal box and air, all of which have differing velocities. To ensure that the first arrival measured is the direct ray, the distance between the source and receiver should never be greater than half of the shortest distance from the source/receiver to the box or the surface of the regolith. Typically, the P-waves travel faster and have a lower amplitude than S-waves, allowing a user to discern between the two.

5.3 Methodology

The primary seismic properties of interest in this experiment are P-wave velocity and attenuation. Tests performed at Earth's atmospheric pressure were performed in a steel box, while tests were performed at a range of reduced atmospheric pressures in a vacuum chamber.

The test setup used in the experiments covered in this chapter was discussed in Chapter 4). Piezoelectric transducers are ideal seismic sources/receivers for small scale seismic tests of sediment (Buddensiek 2009). Transducers of varying frequency are attached to a Pundit PL-200 recording system. One transducer acts as a source while the other acts as a receiver. The ALRS-1 tests were performed at UNSW in Sydney, New South Wales, Australia at the School of Mineral and Energy Resources Engineering's Geomechanics Laboratory; while the MMS tests were performed at the Jet Propulsion Laboratory (JPL), Pasadena, California, USA in the Planetary Soils Laboratory.

5.3.1 Recording system

The recording system measures the travel time of a seismic wave between the source and the receiver. The distance between the closest point of the source and receiver is manually measured to calculate the seismic velocity. The following P-wave piezoelectric transducers were used in these experiments; 24 kHz (P-24), 54 kHz (P-54), 150 kHz (P-150) and 250 kHz (P-250).

5.3.2 Earth atmosphere tests

Tests in regular atmospheric conditions were conducted in open containers filled with a regolith simulant (as discussed in Chapter 4). The containers are partially filled, then the transducers are placed on top of the regolith. The distance between them is measured, then more regolith is added to cover the transducers to a depth of several centimetres. The transducers are placed near the centre of the box to avoid the walls or air above interfering with the seismic wave measurement.

The regolith for these experiments was either uncompacted or compacted using a flat tool. There was no easily achievable means of producing a consistent level of compaction between

tests, and so the degree of compaction in the compacted tests may not be uniform. Efforts were made for the compaction to be as consistent as possible by hand.

5.3.3 Reduced atmosphere tests

Tests performed in a 30.48 cm by 45.72 cm vacuum chamber (Figure 27) from Laco Technologies with a vacuum rating of 0.1 Torr and an approximate volume of 33.364 litres (part number: LVC1218-1121-VC). This allowed for the measurement of varying atmospheric pressures. Pressure was measured in inches of mercury (in. Hg) relative to the typical atmospheric pressure at sea-level. With the pump and chamber, pressures of around -29 in. Hg can be achieved. This is ~3% of Earth's atmospheric pressure. While Mars' atmospheric pressure is ~1% of Earth's (~ -29.77 in. Hg; Hess et al. 1979), this was deemed close enough to provide insight on the effect of Mars-like atmospheric pressure on seismic data.

Using the same methodology as the Earth atmosphere tests, the transducers are buried in the regolith. They are connected to the recording system via feedthrough ports on the lid of the chamber. The lid is sealed, and the pump is activated to reduce the atmospheric pressure. The pump is stopped at various pressures, measurements are made, then the pump is activated again. This process is repeated until the minimum atmospheric pressure attainable is reached. When pumping is stopped, the pressure is observed for some time to ensure that no more air is leaking from the pore spaces of the regolith. There is no way to ensure with certainty that all the air has left the pore spaces before taking a measurement unless mechanical mixing of the regolith is undertaken, which would risk perturbing the sample too much from its ideal state.

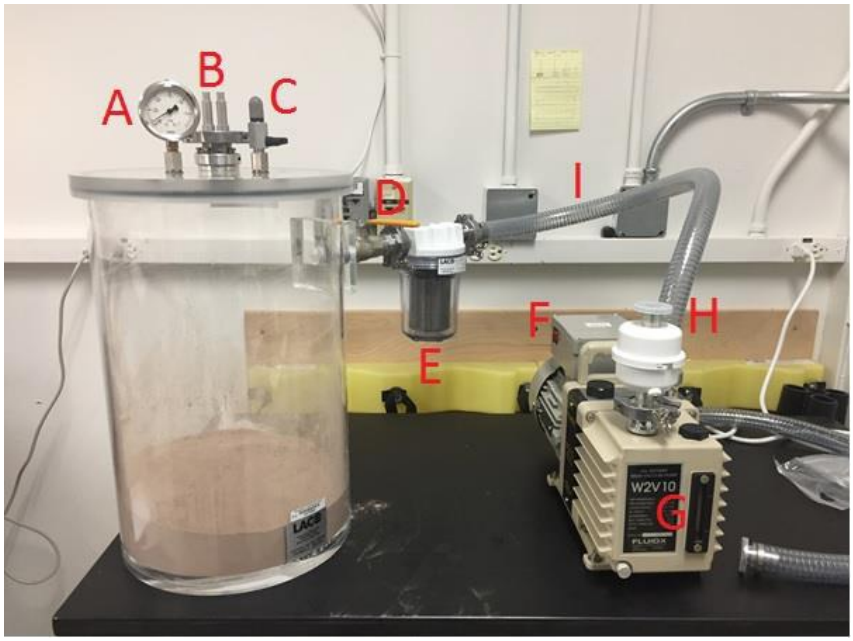

Figure 27 – Chamber and pump prior to connecting the recording system. A, pressure gauge, B, BNC feedthrough connection (mirrored on the inside of the lid), C, pressure release valve, D, main access point to the chamber, E, filter, F, pump power switch, G, oil level, H, filter, I, pipe. The chamber is 30.48 cm wide, and 45.72 cm tall.

5.4 Results

The measured seismic velocity of the ALRS-1 using the P-54 kHz transducers in regular atmospheric conditions and with no compaction are shown in Figure 28. The mean velocity of these measurements is 98.6 m/s. The measured seismic velocity of the MMS dust is shown in Figures 29, 30, 31 and 33. Figures 29-31 show the velocity using P-24, P-54 and P-150 kHz transducers in regular atmospheric conditions and with no compaction. The mean velocities for these measurements are 83.1 m/s, 61.3 m/s and 72.6 m/s respectively. Figures 32-33 show velocity measurements with the P-54 kHz transducers using the vacuum chamber. Figure 32 shows the results of measurements without regolith in the chamber, aimed at measuring the velocity of the air. Figure 33 shows a total of five runs; the P-wave velocity of the MMS dust with a source-receiver separation distance of 0.6 cm with no compaction (1 run), 0.8 cm with no compaction (1 run) and heavy compaction (2 runs), and 1.5 cm with heavy compaction (1 run).

Some measurements from these tests did not have seismic arrivals visible above background noise levels. No signal could be detected from ALRS-1 at greater than 2.7 cm source-receiver separation, and no signal could be detected from the MMS dust at greater than 2.3 cm source-receiver separation. No signal could be detected from the MMS dust at near-Mars atmosphere at greater than 0.6 cm source-receiver separation without compaction, and 1.5 cm with compaction.

The results of the experiments on the small-grain MMS are shown in Figures 34-37. They show the velocity of individual measurements in regular atmospheric conditions with the P-24, P-54, P-150 kHz and 250 kHz sources respectively. For P-24, the mean velocity of the no compaction results is 223.1 m/s, and the mean velocity of the compaction results is 218.3 m/s. For P-54, the mean velocity of the no compaction results is 244.5 m/s, and the mean velocity of the compaction results is 200.5 m/s. For P-150, the mean velocity of the no compaction results is 276.4 m/s, and the mean velocity of the compaction results is 159.0 m/s. For P-250, the mean velocity of the no compaction results is 247.3 m/s, and the mean velocity of the compaction results is 201.2 m/s.

The results of the experiments on the medium-grain MMS are shown in Figures 38-41. They show the velocity of individual measurements in regular atmospheric conditions with the P-24, P-54, P-150 kHz and 250 kHz sources respectively. For P-24, the mean velocity of the no compaction results is 269.3 m/s, and the mean velocity of the compaction results is 417.1 m/s. For P-54, the mean velocity of the no compaction results is 271.2 m/s, and the mean velocity of the compaction results is 258.1 m/s. For P-150, the mean velocity of the no compaction results is 249.7 m/s, and the mean velocity of the compaction results is 266.6

m/s. For P-250, the mean velocity of the no compaction results is 252.7 m/s, and the mean velocity of the compaction results is 302.1 m/s.

5.5 Discussion

The two available measurements of *in-situ* P-wave velocity of lunar regolith simulant are 104 m/s and 114 m/s (Kovach and Watkins 1973b). These are similar to the measured P-wave velocity of the ALRS-1 of 98.6 m/s. This seems to imply that the seismic properties of the simulant are accurate, however it cannot be ruled out that this may be a coincidence. No *in-situ* measurements of Martian regolith velocity are available to compare to the MMS measurements, however once they become available, comparing them to the MMS measurements will be of interest.

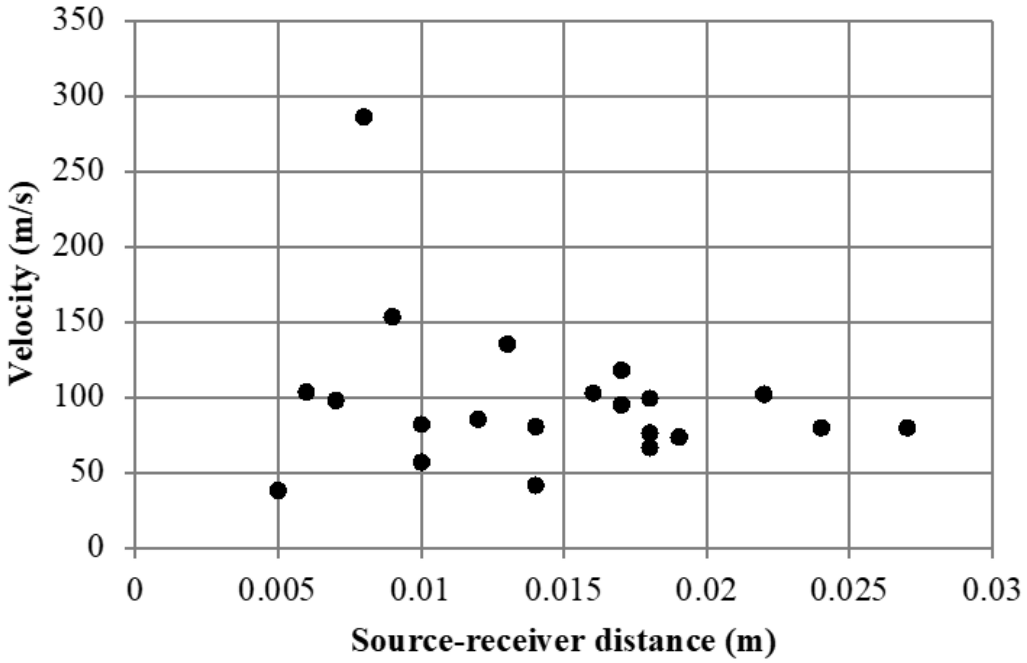

Figure 28 – Source-receiver distance vs velocity of ALRS-1 using P-54. Of 23 measurements, 2 had no signal. Mean velocity of 98.6 m/s.

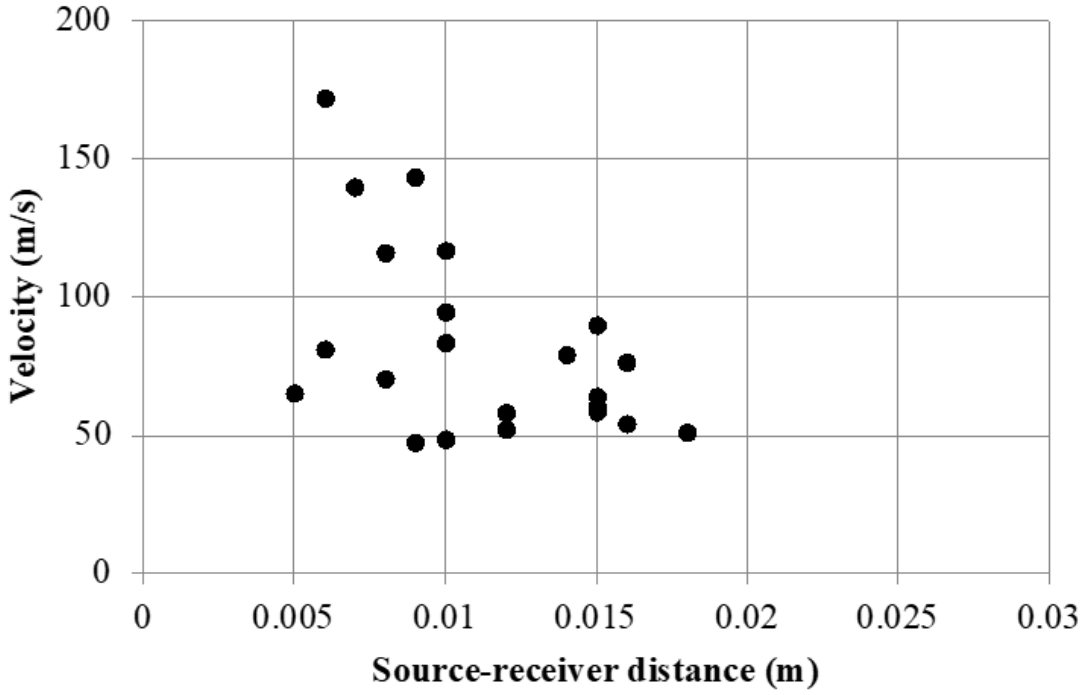

Figure 29 – Source-receiver distance vs velocity of MMS dust using P-24. Of 22 measurements, all had signal. Mean velocity of 83.1 m/s.

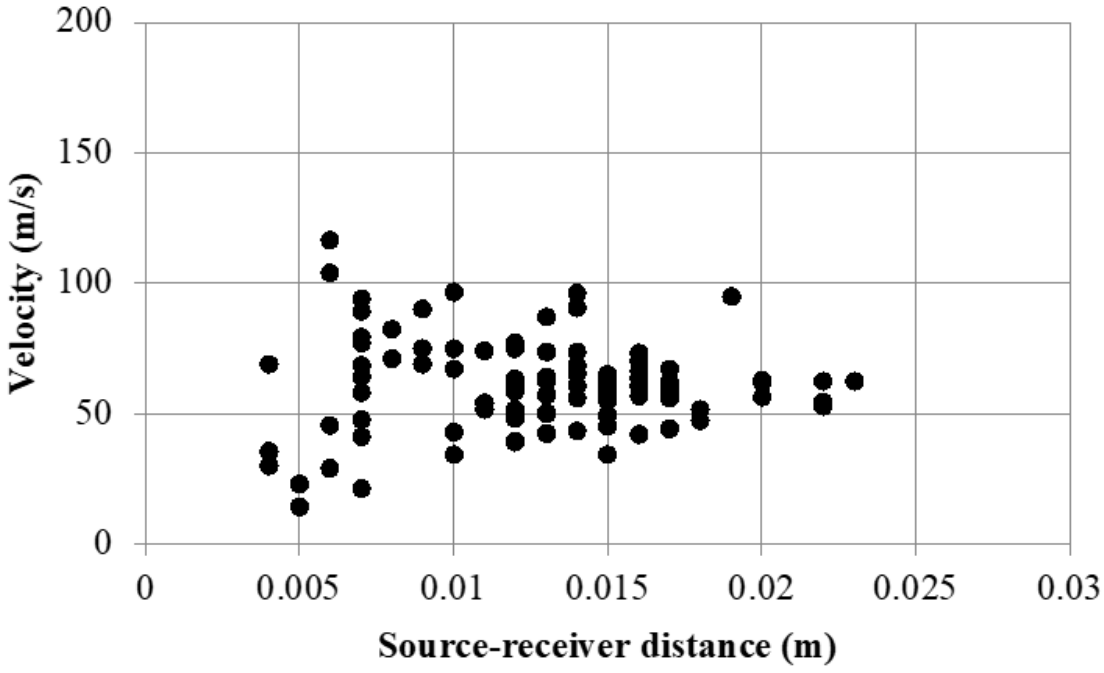

Figure 30 – Source-receiver distance vs velocity of MMS dust using P-54. Of 93 measurements, all had signal. Mean velocity of 61.3 m/s.

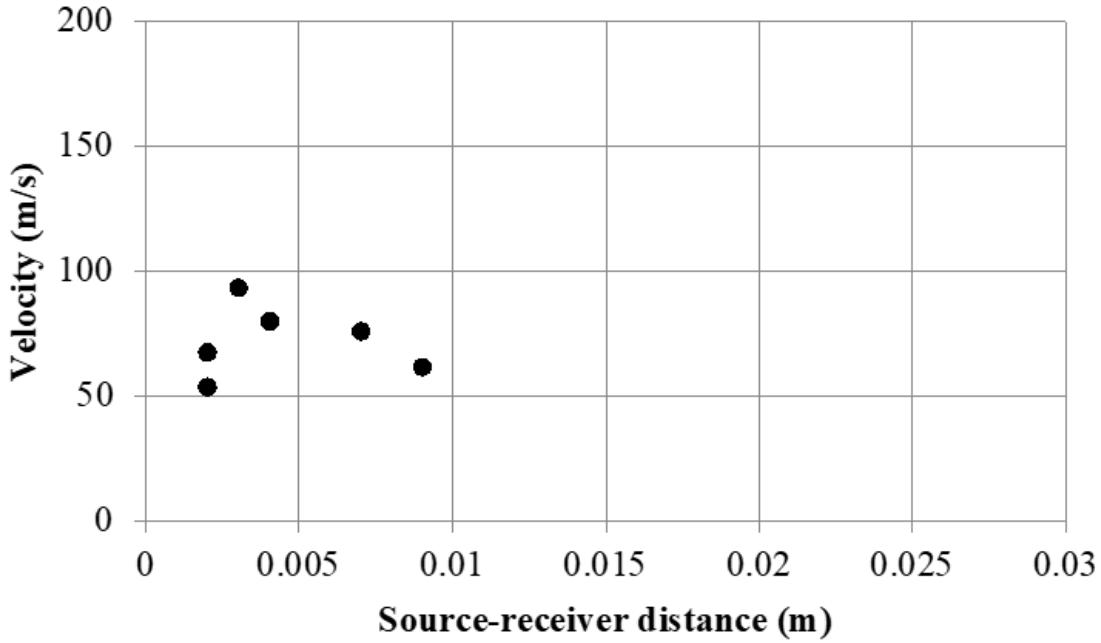

Figure 31 – Source-receiver distance vs velocity of MMS dust using P-150. Of 9 measurements, 3 had no signal. Mean velocity of 72.6 m/s.

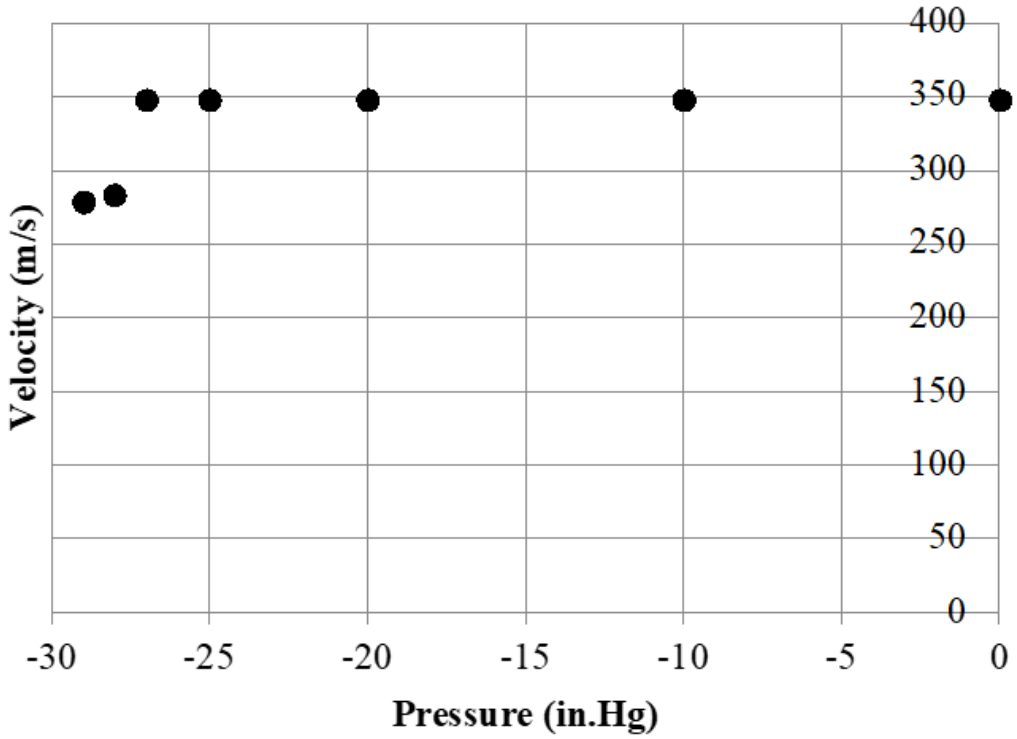

Figure 32 – Chamber pressure vs velocity of air using P-54.

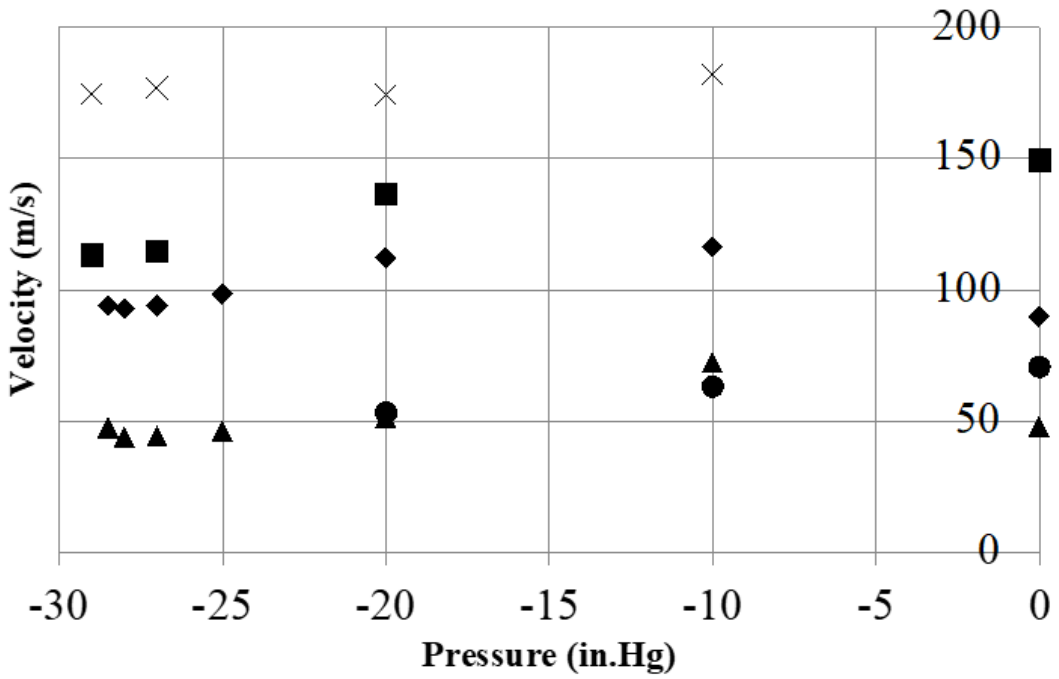

Figure 33 – Chamber pressure vs velocity of MMS dust using P-54 for five different runs. Triangle is 0.6 cm separation with no compaction, circle is 0.8 cm separation with no compaction, the diamond and square are 0.8 cm separation with compaction, and the cross is at 1.5 cm separation with compaction.

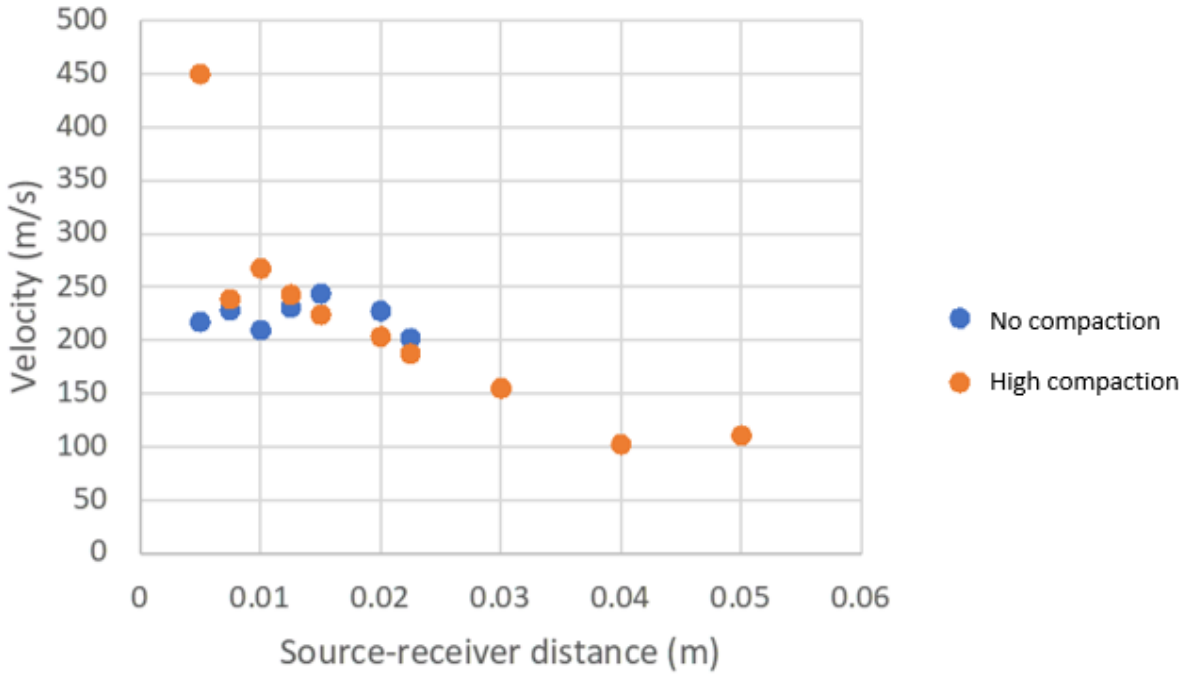

Figure 34 – Source-receiver distance vs velocity of small-grain MMS using P-24. No compaction tests are shown as blue, and high compaction tests are shown as orange.

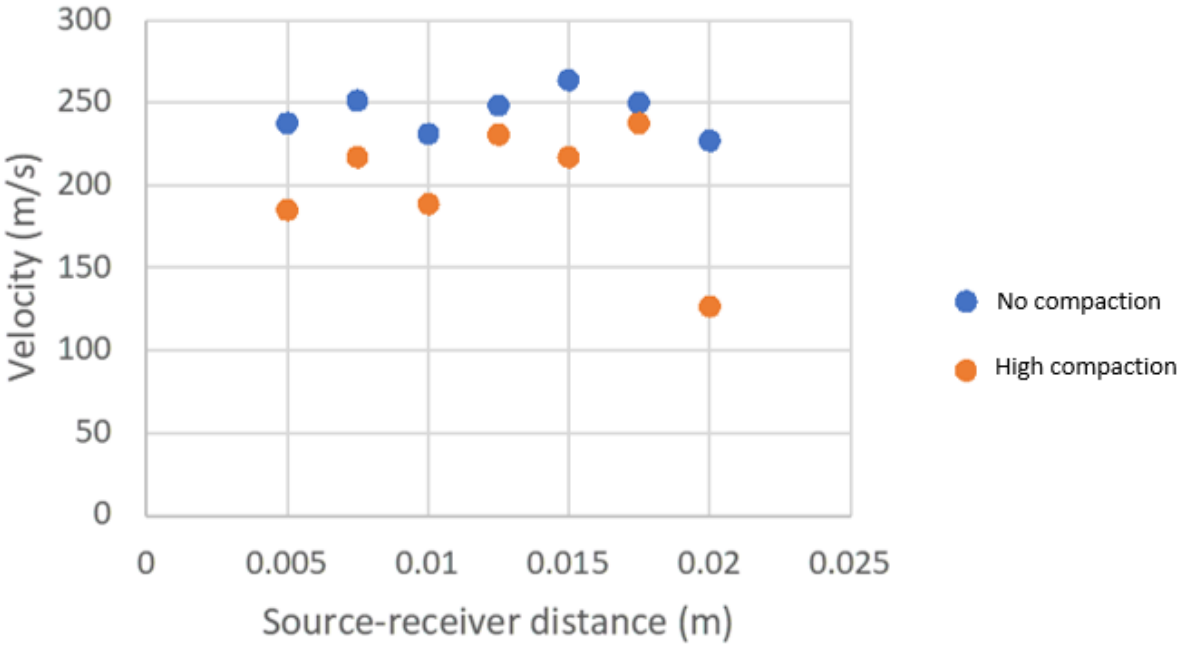

Figure 35 – Source-receiver distance vs velocity of small-grain MMS using P-54. No compaction tests are shown as blue, and high compaction tests are shown as orange.

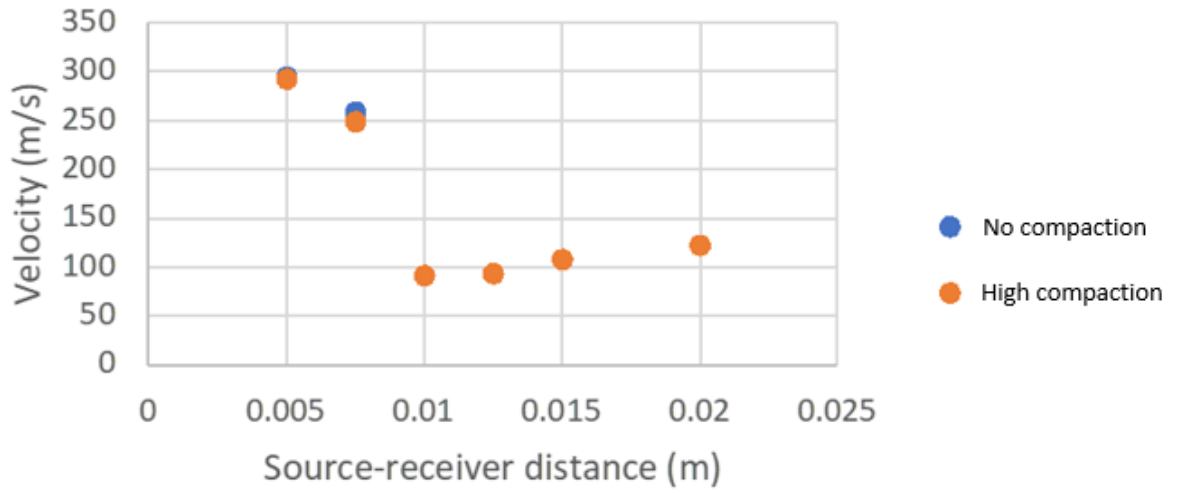

Figure 36 – Source-receiver distance vs velocity of small-grain MMS using P-150. No compaction tests are shown as blue, and high compaction tests are shown as orange.

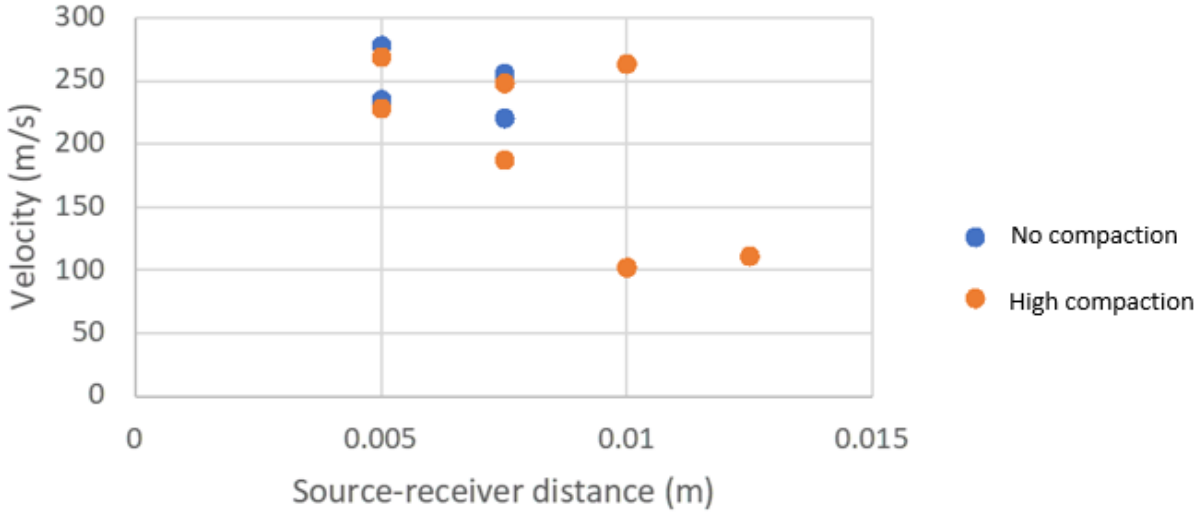

Figure 37 – Source-receiver distance vs velocity of small-grain MMS using P-250. No compaction tests are shown as blue, and high compaction tests are shown as orange.

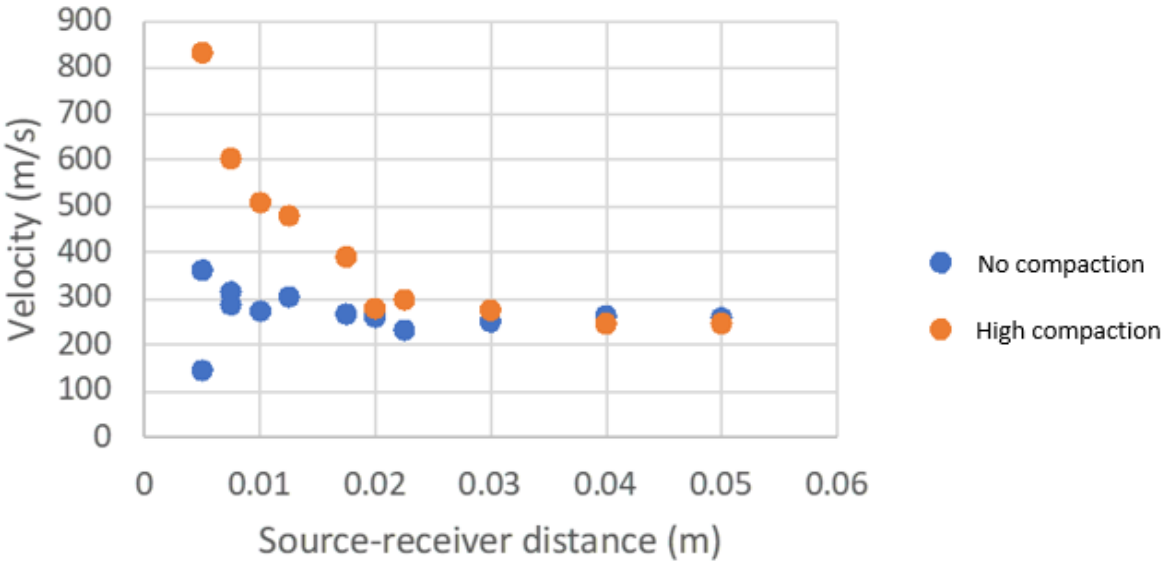

Figure 38 – Source-receiver distance vs velocity of medium-grain MMS using P-24. No compaction tests are shown as blue, and high compaction tests are shown as orange.

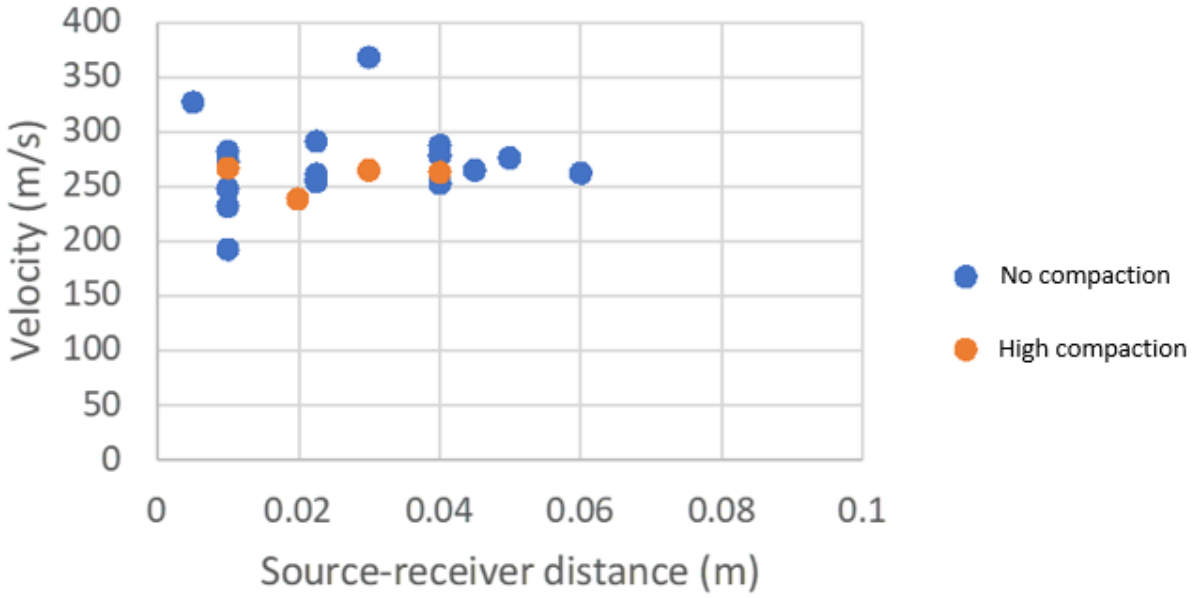

Figure 39 – Source-receiver distance vs velocity of medium-grain MMS using P-54. No compaction tests are shown as blue, and high compaction tests are shown as orange.

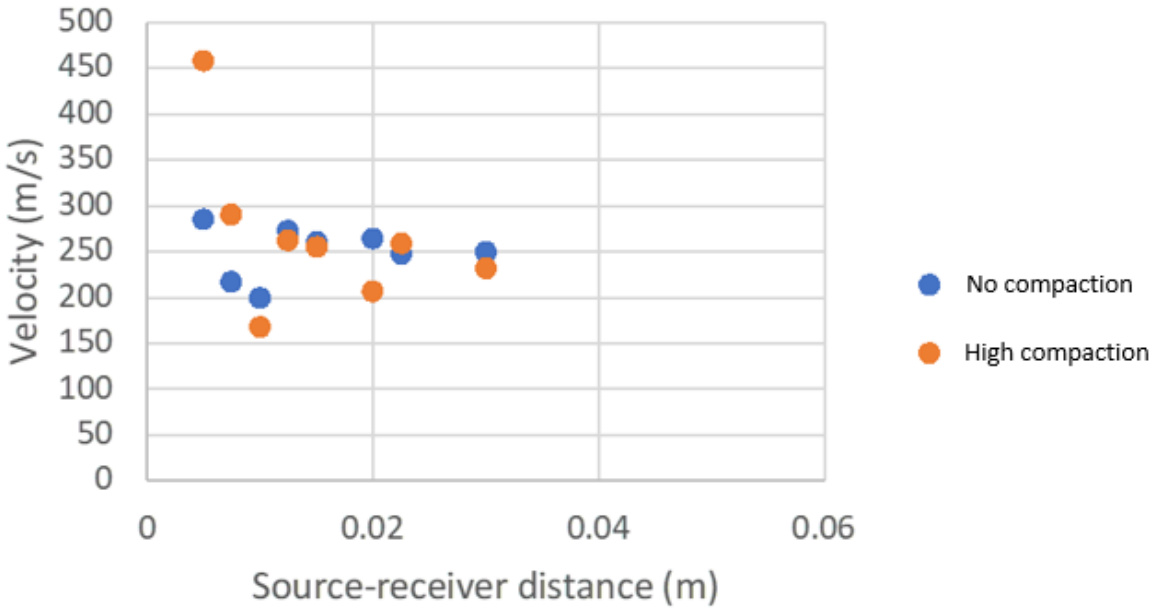

Figure 40 – Source-receiver distance vs velocity of medium-grain MMS using P-150. No compaction tests are shown as blue, and high compaction tests are shown as orange.

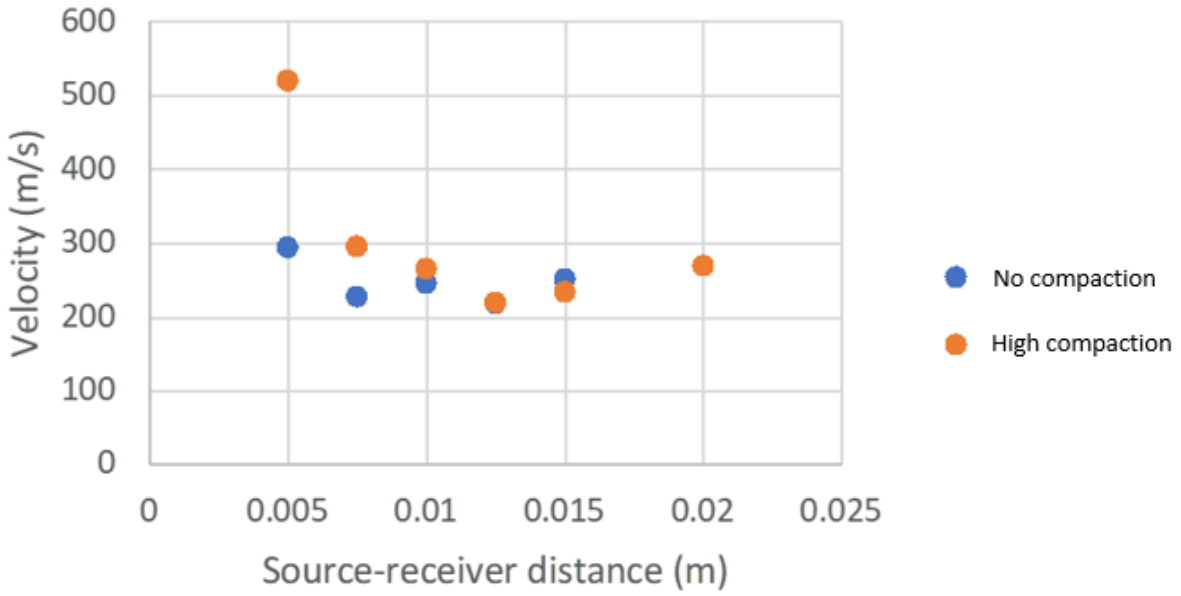

Figure 41 – Source-receiver distance vs velocity of medium-grain MMS using P-250. No compaction tests are shown as blue, and high compaction tests are shown as orange.

Previous studies have stated that grain size does not appear to influence the velocity of sediments (Talwani et al. 1973; Bell and Shirley 1980), however, the ALRS-1 and MMS dust both have velocities that are uncommonly low compared to terrestrial sediments. Given that the most common factor between the simulants appears to be their small grain size, this leads us to consider the possibility of such a relationship. Comparing the mean velocities from the no compaction P-54 results of all four samples (98.6 m/s for ALRS-1, 61.3 m/s for MMS dust, 244.5 m/s for small-grain MMS, and 271.2 m/s for medium-grain MMS), a trend of larger grain sizes leading to higher seismic velocities can be observed.

As discussed in Chapter 4, the scatter in individual measurements is lower at greater separation between source and receiver. This trend appears consistent with the latest data from the MMS small/medium-grain. This effect appears to be the result of the non-reproducibility of the experiment. At greater measurement distances the local/small scale variation between the regolith at time of measurement for a given regolith type is averaged out. On a centimetre scale, the velocity of the regolith likely varies from its bulk average.

Velocity dispersion may explain the difference in velocity of the MMS dust and small/medium-grain MMS when measured by different frequency transducers. The mean velocities of the P-24, P-54 and P150 for the MMS dust were 83.1 m/s, 61.3 m/s and 72.6 m/s respectively. The mean velocities of the P-24, P-54, P-150 and P-250 for the small-grain MMS (no compaction) were 223.1 m/s, 244.5 m/s, 276.4 m/s and 247.3 m/s respectively. The mean velocities of the P-24, P-54, P-150 and P-250 for the medium-grain MMS (no compaction) were 269.3 m/s, 271.2 m/s, 249.7 m/s and 252.7 m/s. Contrary to expectation, the velocity does not consistently increase or decrease with increasing frequency. If the inherent error in the measurement process were greater than the effect of any velocity dispersion, this could provide an explanation.

The P-wave velocity of air was measured in the vacuum chamber as a calibration test. However, as the pump reduced the atmospheric pressure, an exciting result was produced. At regular atmospheric pressure, the measured velocity of the air was 348 m/s, similar to its known mean velocity of 343 m/s. The velocity remained consistent around this point, and then rapidly dropped to 283.3 m/s at -28 in. Hg (~6.7% of mean sea level atmospheric pressure).

It was assumed that the seismic velocity of air would approach zero as the atmospheric pressure approaches vacuum (-30 in. Hg), which appears to be supported by these measurements. However, it was also assumed that the relationship between atmospheric pressure and seismic velocity would be approximately linear, which does not appear to be supported by these measurements.

In Figure 33, the measured P-wave velocity of the MMS dust decreases slightly with decreasing atmospheric pressure. In particular, the effect seems strongest as the minimum

pressure attainable by the chamber/pump (~ -29 in. Hg) is approached. If the experiment in this study is solely measuring the velocity of the regolith grains, it should be expected that the seismic velocity remains the same as the atmospheric pressure is reduced. The fact that the velocity of the MMS dust as a function of atmospheric pressure follows a similar trend to the velocity of the air suggests that the experiment may be measuring some combination of the regolith and the air in the pore spaces.

The velocity of air at regular pressure appears to be several times higher than the MMS dust and is somewhat higher than the velocity of the small and medium-grain MMS. Therefore, the seismic wave may be partially or completely travelling through the air between the grains. This may increase the total measured velocity of the sample up to the velocity of air (343 m/s). A diagram depicting a possible scenario of this taking place is shown in Figure 42.

Maintaining good contact (coupling) between the measured medium and the source/receiver is critical for producing a strong seismic signal, however this is not a trivial task (Jefferson et al. 1998). Receivers placed in loose surface regolith in the field have been observed to result in weak signals. As the regoliths investigated in this study are highly fine grained it should be expected that coupling will be an issue. It is possible that the air itself is providing some coupling between the transducers and the regolith, in cases where the coupling between the transducers and the regolith directly is weak. This would imply that approaching Martian atmospheric pressure also reduces some of the coupling.

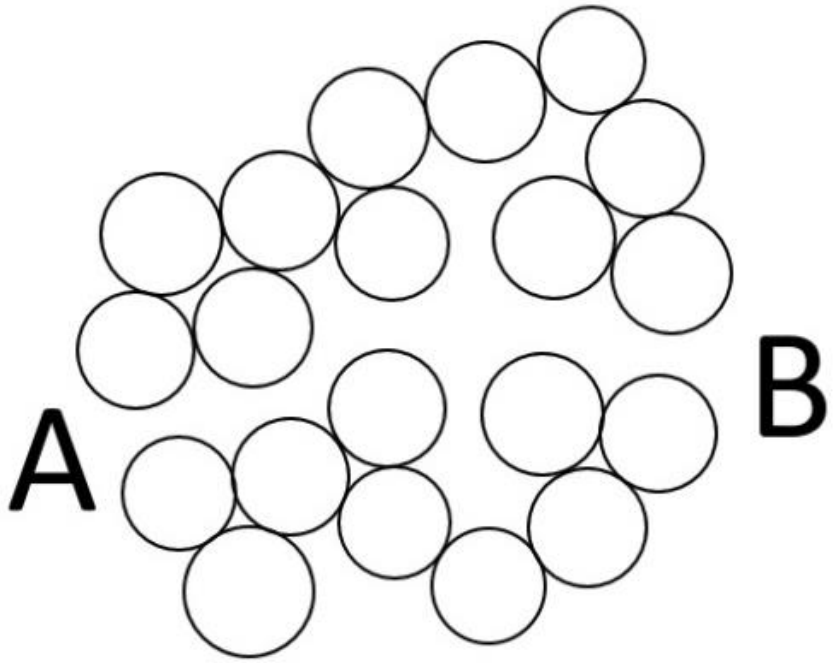

Figure 42 – A possible scenario showing how the measured velocity of sediment might be higher than the velocity of the grains themselves. For a sample with a lower velocity than air velocity, the fastest path for a seismic wave to travel from A to B may be via the air pathway (permeability). If this were scaled up to a typical measurement of regolith velocity, the measured velocity could approach the air velocity.

Given the short maximum distance that a seismic signal can be identified over the background noise, it can be inferred that the degree of seismic wave attenuation in the ALRS-1 and MMS dust, small and medium-grain samples is substantial. As the air in the chamber is pumped out, approaching Mars atmospheric pressure, there also appears to be a notable effect on signal attenuation. Quantifying the influence of grain size, compaction, source power and source frequency on signal attenuation in future experiments will be enlightening. If the coupling is affected by atmospheric pressure, this may explain some of the attenuation.

It is unclear whether the primary issue with resolving the signal is that the signal has completely attenuated, or that the signal to noise ratio is simply too low. It may be worthwhile examining whether generating multiple waveforms for the same measurement and summing

their amplitude can resolve some of the issues with signal strength. Noise filtering processes may also aid in resolving the signal.

Using the results from the small and medium-grain MMS samples (Figures 34 – 41), one can examine the difference in velocity between uncompacted and strongly compacted scenarios. The data are mostly inconsistent. The expected effect of compacting any sediment should be that the seismic velocity increases, due to the increased density. This does not appear to be obvious for these data. This could potentially be explained if the experiments were partially measuring the seismic velocity of the air between the grains as well as the grains, as discussed above. Compacting the sediment would squeeze out some of the air, removing the higher velocity medium.

Earlier in this chapter, it was discussed that the larger grain sediments have a higher measured seismic velocity. Assuming perfectly spherical and uniform grains, grain size should not directly affect porosity. However, given that grains are not spherical or uniform, a side effect of the increasing grain size may be to reduce the porosity, reducing the amount of air between the grains and therefore the velocity. While the porosity of ALRS-1 and MMS have not been directly measured, Peters and co-workers (2008) measured the particle size distributions of the MMS dust and sand. From this, it can be observed that the sand has a more homogeneous grain size distribution, which implies it likely has a higher porosity (Latham et al. 2002).

The literature strongly suggests that grain size and porosity do not control velocity (Talwani et al. 1973; Bell and Shirley 1980; Sherlock and Evans 2001). It is proposed that, in this case, the grain size distribution is controlling velocity indirectly by controlling porosity. This effect is perhaps not seen in existing literature as it relies on the velocity of the grains themselves to be lower than the velocity of the air in the pore spaces. As these off-Earth regolith simulants

have unusually low velocity, this may explain why this effect can be observed. While the conclusion cannot be definitively made now, a future study which looks at the porosity of these regoliths at different grain sizes and compaction states could shine further light on this hypothesis.

A major limitation of geophysics, including seismic, is the non-uniqueness problem. The same geophysical response may result from multiple different subsurface scenarios. Geophysics is best used in combination with some ground-truthing, which requires drilling, digging or otherwise physically observing a part of the subsurface and comparing it to the survey results from that location. For example, the detection of a subsurface layer through seismic does not inform definitively what the layer is. Drilling a hole and retrieving a core sample, or using downhole imaging, can reveal the layer's composition. Using this information, it can then be inferred that the entirety of the layer is of a similar nature, with some exceptions.

Drilling on other planetary bodies is believed to be difficult, due to the large volume of equipment required, lack of access to direct human assistance, unknown drilling conditions etc. However, drilling a single hole on the Moon, Mars or a SPB could provide immensely valuable information to complement any seismic studies. Seismic-while-drilling (SWD) technology involves the use of downhole seismic sources being activated during the drilling process, which are measured by surface receivers (Naville et al. 2004). SWD has been proposed for use on the Moon to investigate subsurface rocks (Poletto et al. 2015) and could potentially be used on Mars as well. In combination with more 2D and 3D seismic surveys, this could generate a wealth of knowledge about the near-surface interior of planetary bodies.

To use an example, a proposal for detecting subsurface water on Mars through a manned seismic refraction survey has been made (Pletser et al. 2009). Combining this with ground-truthing will enable the mission to determine whether any identified subsurface layers detected through seismic are ice, allowing the survey to then map its thickness and depth over the area.

5.6 Conclusions

This chapter used the seismic apparatus explained in Chapter 4 to examine the seismic velocity of different off-Earth regolith simulants, expanding upon it with the inclusion of the vacuum chamber. Measurements of ALRS-1 and MMS were used, with three distinct grain sizes used for the latter (dust, fine-grained and medium-grained. The conclusions that can be made from these experiments include:

- Reducing the air pressure in a vacuum chamber appears to reduce the velocity of the sediment. This could be explained if the experiment is partially measuring the velocity of the air, given that the regoliths being measured have a lower seismic velocity than air.
- Contrary to the existing literature, grain size appears affect seismic velocity, with larger grain sizes producing higher velocities. The larger grain size samples appear to have a less heterogeneous grain size distribution, which should reduce porosity. If the air velocity is affecting the measurement, this may explain the result, as there would be less air in the regolith.
- It was expected that increased compaction in samples should lead to increased seismic velocity due to the increased density. However, this does not appear to be obvious. This may be explained by the same phenomenon measuring air velocity.

- Seismic waves of different frequencies appear to be travelling at different velocities, which is consistent with the velocity dispersion theory. However, there does not seem to be a linear effect, and therefore the difference could be explained by a measurement error or some other factor.
- While gravity and other variables have not yet been tested, it is expected that small scale seismic tests such as the one presented here will be capable of producing usable data in planetary exploration. However, attenuation of the signal remains a major problem, and this is made worse by the apparent attenuating effects of small-grain size and vacuum. These issues may be resolvable through increased source strength or signal processing techniques.

6. Computer and analytical modelling of laboratory results for validation and extrapolation

6.1 Introduction

Chapters 4 and 5 developed the methodology of the Seismic Apparatus for Fine-Grained Sediment to measure the seismic velocity of regolith, and presented results using the ALRS-1 and MMS regolith simulants. This chapter will explore the use of computer and analytical modelling methods to validate the results of the laboratory experiments using known inputs of regolith grain properties. The regolith grain properties include the grain size distribution and the grain physical properties to fully describe the material such as particle density, normal stiffness, shear stiffness, range of particle friction coefficient, normal strength of parallel bonds, shear strength of parallel bonds, normal stiffness of parallel bonds, shear stiffness of parallel bonds, viscous damping ratio of normal direction, and viscous damping ratio of shear direction (Feng et al. 2017). The ultimate output is the travel time of the seismic P-wave, which is then used to determine the P-wave velocity of the regolith.

The purpose of this work is to use the modelling techniques to expand on the laboratory results by varying the known parameters outside of the ranges seen in the laboratory. For example, examining how a varying internal friction angle influences seismic waves. This would be a valuable tool for future seismic missions looking to validate their results or predict the results in advance. Possible grain properties of the target material in a planetary seismic mission could be input to determine the required seismic source strength to achieve a received signal of a desired strength for a given source-receiver separation distance. This would also be useful for terrestrial seismic missions, and could see use in resources exploration, environmental monitoring, and civil engineering.

Computational and analytical modelling methods were both explored. The modelling software package used for the computational modelling analysis was Abaqus (version 6.11-1), a finite element modelling tool. The analytical modelling method involved generating relationships between grain properties and P-wave seismic velocity to predict the velocity from grain size distributions. The grain size distributions of terrestrial sands were then used to predict their seismic velocity using the relationships developed from the experimental results.

6.1.1 Introduction of numerical modelling methods

The finite element method (FEM), or continuous model, is a modelling method that solves a problem by subdividing a system into smaller parts called finite elements. FEM is used to understand and quantify physical phenomena, such as structural analysis, heat transfer, mass transport, electromagnetic potential and fluid flow.

FEM has seen some use in seismic modelling since the 1960's (De Basabe and Sen 2009; Padovani et al. 1994), to analyse the seismic response of soil/retaining walls (Cai and Bathurst 1995) and to analyse the seismic response to vertical loading (Chatterjee et al. 2015).

The discrete element method (DEM), or discontinuous model, is a modelling method that solves a problem through the use of a large number of small particles. DEM is commonly used for engineering problems relating to granular materials, such as rock, soil and powder mechanics.

DEM has been used to simulate seismic results in several contexts, including seismic monitoring of hydraulic fracturing (Nabipour et al. 2011) and landslides (Feng et al. 2017), though it is still a relatively new and underexplored field. Nabipour and co-workers (2011) were able to model the propagation of a seismic wave in 2D and observe the effect on the

seismic wave velocity of the inclusion of a fracture at various stages in its development using Particle Flow Code (PFC). Feng and co-workers (2017) used PFC in combination with Fast Lagrangian Analysis of Continua (FLAC) (Itasca 2011) to simulate the process of a landslide and model the seismic response to that event. This result was compared to data from the Xiaolin landslide in 2009 and a good fit between this and the model was observed (Feng et al. 2017). Previous studies have simulated and analysed the evolution of landslides using discrete element method codes (Tommasi et al. 2008; Lo et al. 2011; Chang et al. 2012; Tang et al. 2009; Liu and Koyi 2013). However Feng et al.'s (2017) work is the first study to examine the seismic response.

The DEM has also been used to simulate the response of buildings to seismic events (Sincraian 2001; El Shamy and Zamani 2012; Calió et al. 2012; Lemos 2019; Mordanova and de Felice 2020; Mendes et al. 2020). However, they did not simulate the propagation of a seismic wave through a medium with the intention of determining its velocity.

General advantages of FEM over DEM include the ability to accurately represent complex geometry, capture local effects, easy representation of the full model, and the inclusion of dissimilar material properties (Budynas and Nisbett 2011). For large-scale seismic modelling FEM has the advantages of being able to easily accommodate surface topography and discontinuities in the subsurface (De Basabe and Sen 2009).

General advantages of DEM over FEM include the ability to better simulate a range of granular and rock mechanics situation and allowing for a more detailed analysis of powder flows. However, DEM is heavily restricted by computing power and related constraints such as the number of particles being simulated and the duration of the simulation. This limitation

becomes more prevalent as the size of the particles decreases, or as the area and length of time being simulated increases.

One FEM package (Abaqus) and two DEM packages (3DEC and PFC – Particle Flow Code) were examined for use in this modelling. However, only Abaqus had the capability of being able to produce the data required to estimate P-wave velocity over the volume of the simulant, and therefore Abaqus was selected to undertake the modelling.

6.2 Regolith simulant modelling properties

6.2.1 Grain size distribution

During testing of the DEM packages (3DEC and PFC), it was determined that the grain size distribution of the regolith could not be input in the way they are typically described (i.e., in Figure 20 and Figure 22). The standard is for grain size to be displayed as the percent of mass that passes through a sieve of a given size. For use in DEM packages which rely on generating individual particles, the necessary input is the number of particles that exist of each discrete size. Therefore, the grain size distributions need to be converted to estimates of the number of particles at each grain size for a discrete number of sizes. As a simplified example of the required input: in every 1,000 grains, 500 grains are 1 mm in radius, 150 grains are 2 mm in radius, and 350 grains are 3 mm in radius. Converting from a grain size distribution to this format is not trivial, and no methodology for doing so could be found in the literature. While it was ultimately not necessary, as FEM packages such as Abaqus do not require this input, the work done to produce a conversion workflow is still considered to be a contribution to modelling the seismic properties of regolith and is included in this chapter. An example of this workflow is carried out and the final result is provided for the ALRS-1 sample.

An estimate of mean grain size could be performed in three ways, by number of particles, by volume of particles, or by weight of particles. The grain size distributions from Garnock and Bernold (2012) and Peters and co-workers (2008) have been performed using weight of particles. This means that the discrete data points will need to be taken and converted to the number of particles at a given grain size to input them to the model. The range for each inputted grain size will need to be used. It will be assumed that the grains in that range have the size of the middle point of that range.

For example, it can be seen from the ALRS-1 grain size distribution that around 7% of particles by weight are smaller than ~0.0045 mm. Given the lack of a lower bound for grain size, it will be assumed that the average grain size in this range is 0.00225 mm, giving a radius of ~0.001 (first entry in Table 5). Around 6% of particles by weight are between 0.0045 mm and 0.011 mm. If it is accepted that the average grain size of the particles is the halfway point between these (0.00775mm, or radius of 0.0039 mm, second entry in Table 5), this needs to be converted to the number of particles within that range relative to the number of particles within every other range. Assuming that the weight per unit volume is the same for each grain size and the grains are perfectly spherical, this can be estimated.

The formula for the volume of a sphere is:

$$V = \frac{4}{3}\pi r^3 \qquad (14)$$

Where r is the radius of the sphere. The volume of the average grain within each grain size range is calculated with equation 14. The ratio of the number of grains of a given size relative to the other grain sizes is given by:

$$R_1 = \left(\frac{V_s}{V_1}\right) p_1 \quad (15)$$

Where R_1 is the ratio, for the one given grain size, V_1 is the volume of the one given grain size, V_s is the sum volume of all given grain sizes, and p_1 is the proportion of grains of the one given grain size passing. This is then converted to the proportion of all grains that are grains of one given size using:

$$TP_1 = \frac{R_1}{R_s} \quad (16)$$

Where TP_1 is the total proportion for one given grain size, and R_s is the sum of the ratio of all given grain sizes as calculated with Equation 15.

For ALRS-1, these results are shown in Table 5, and the final output of the number of grains at each grain size in a sample of 1,000,000 grains is shown in Figure 43.

This analysis reveals that the dominant grain size by number of grains is significantly smaller than the dominant grain size by percent of weight. While this is an intuitive result, the exponential degree to which the smaller grains dominate the larger grains by number of grains is a surprising result. It is, therefore, argued here that grain size distributions in general should also be shown as a proportion of grains at a given size in addition to the proportion of grains at a given weight, as having both may be more informative.

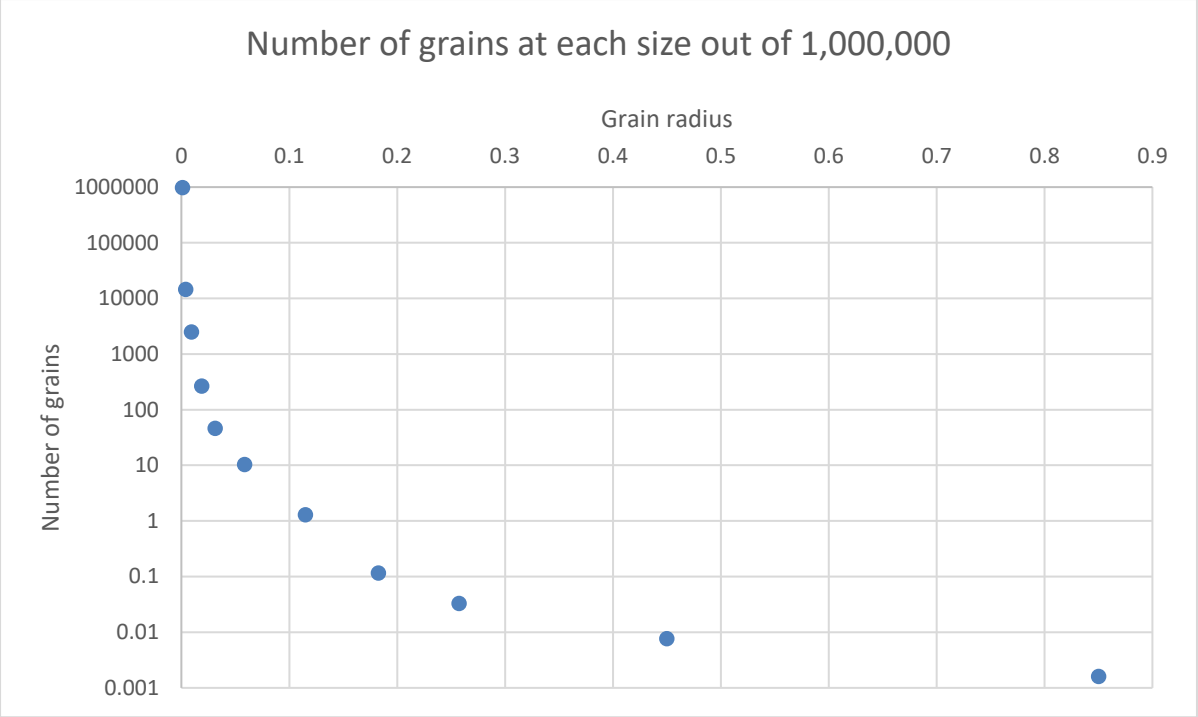

Figure 43 – The number of ALRS-1 grains at each grain radius size for a sample of 1,000,000 grains.

Table 5 – The inputs and outputs of the grain size calculations for ALRS-1.

Average radius (mm)	**Proportion of grains this size by weight (p_1)**	**Volume of one average grain of this size (mm^3)**	**Proportion of total volume being grains this size**	**# of grains this size out of 1,000,000 grains**
0.001	0.07	4.18879E-09	0.982716174	982716.1741
0.0039	0.06	2.43727E-07	0.014476587	14476.58731
0.0093	0.14	3.31523E-06	0.002483321	2483.32123
0.019	0.13	2.87309E-05	0.00026608	266.0802338
0.0313	0.1	0.000127832	4.60023E-05	46.00234799
0.0588	0.15	0.0008494	1.03848E-05	10.3847898
0.115	0.14	0.006370626	1.2923E-06	1.292303673
0.1825	0.05	0.025461103	1.15481E-07	0.115481246
0.2575	0.04	0.071518815	3.28896E-08	0.032889582
0.45	0.05	0.381703507	7.70305E-09	0.007703047
0.85	0.07	2.572440785	1.60019E-09	0.001600189

6.2.2 Other regolith properties

Six regolith properties were required to model the regolith with Abaqus; internal friction angle, elastic modulus, Poisson ratio, cohesion value, Young's modulus and grain density. Some of these properties were not available from the original sources describing the ALRS-1 and the MMS. To fill the gaps, an exhaustive literature review was required to find the properties of regoliths which were deemed sufficiently similar, i.e. fine grained basaltic regolith.

The regolith properties of ALRS-1, MMS dust and MMS small/medium-grained sand used in the Abaqus modelling are shown in Table 6-8. These properties are input to Abaqus to determine the viability of FEM to model seismic velocity of regolith. The MMS small-grained sand and MMS medium-grained sand are merged into one sample for the purpose of modelling, as their grain size distribution as depicted in Peters (et al. 2008) was merged into one. The MMS small/medium-grained sand is therefore treated as one sample.

It is noted that only the regolith properties are being examined in this work. The environmental properties which may affect the seismic properties of these samples in their *in-situ* environments on the Moon and Mars, such as atmospheric pressure, gravitational strength etc. are not being considered. Typical Earth conditions are assumed throughout this work to ensure a consistent comparison between the different samples, and to ensure that only the effect of the physical properties of the grains are being compared.

Table 6 – Grain properties used to model the ALRS-1. a is from Tuncer and Lohnes (1977), b is from Bowles (1996), c is from StructX (2021), d is from Philpotts and Ague (2009), and e is from Heiken et al. (1991).

Internal friction angle (°)[a]	42
Elastic modulus (MPa)[b]	14
Poisson ratio[c]	0.325
Cohesion value (kPa)[e]	0.525
Young's modulus (kPa)[b]	12.5
Grain density (g/cm^3)[d]	2.9

Table 7 – Grain properties used to model the MMS dust. a is from Peters et al. (2008), b is from Bowles (1996), c is from StructX (2021), d is from Philpotts and Ague (2009).

Internal friction angle (°)[a]	31
Elastic modulus (MPa)[b]	14
Poisson ratio[c]	0.325
Cohesion value (kPa)[a]	0.38
Young's modulus (kPa)[b]	12.5
Grain density (g/cm^3)[d]	2.9

Table 8 – Grain properties used to model the MMS small/medium-grained sand. a is from Peters et al. (2008), b is from Bowles (1996), c is from StructX (2021), and d is from Philpotts and Ague (2009).

Internal friction angle (°)[a]	38
Elastic modulus (MPa)[b]	14
Poisson ratio[c]	0.325
Cohesion value (kPa)[a]	0.81
Young's modulus (kPa)[b]	12.5
Grain density (g/cm^3)[d]	2.9

6.3 Abaqus model design

The process for 3D FEM numerical modelling is described by Tahmasebinia (2008):

1) Selection of element type
2) Selection of mechanical behavior of material
3) Assign sections
4) Defining proper step
5) Connection between elements
6) Specify boundary and initial conditions
7) Subdivide the sections
8) Assign the job
9) Evaluate the results

The Abaqus model was designed to match the setup used for the laboratory experiments. The dimensions of the model are 20 cm x 30 cm x 30 cm (to replicate the dimensions of the laboratory set up). Figure 44 shows the 3D mesh used to setup the model. Due to the limitations of the software used, therefore a seismic source with a given frequency could not

be used, therefore, the source of the seismic wave was approximated with a single impulse originating from the centre of the volume. This location was selected as opposed to the edge of the volume to recreate the location of the source in the physical experiments.

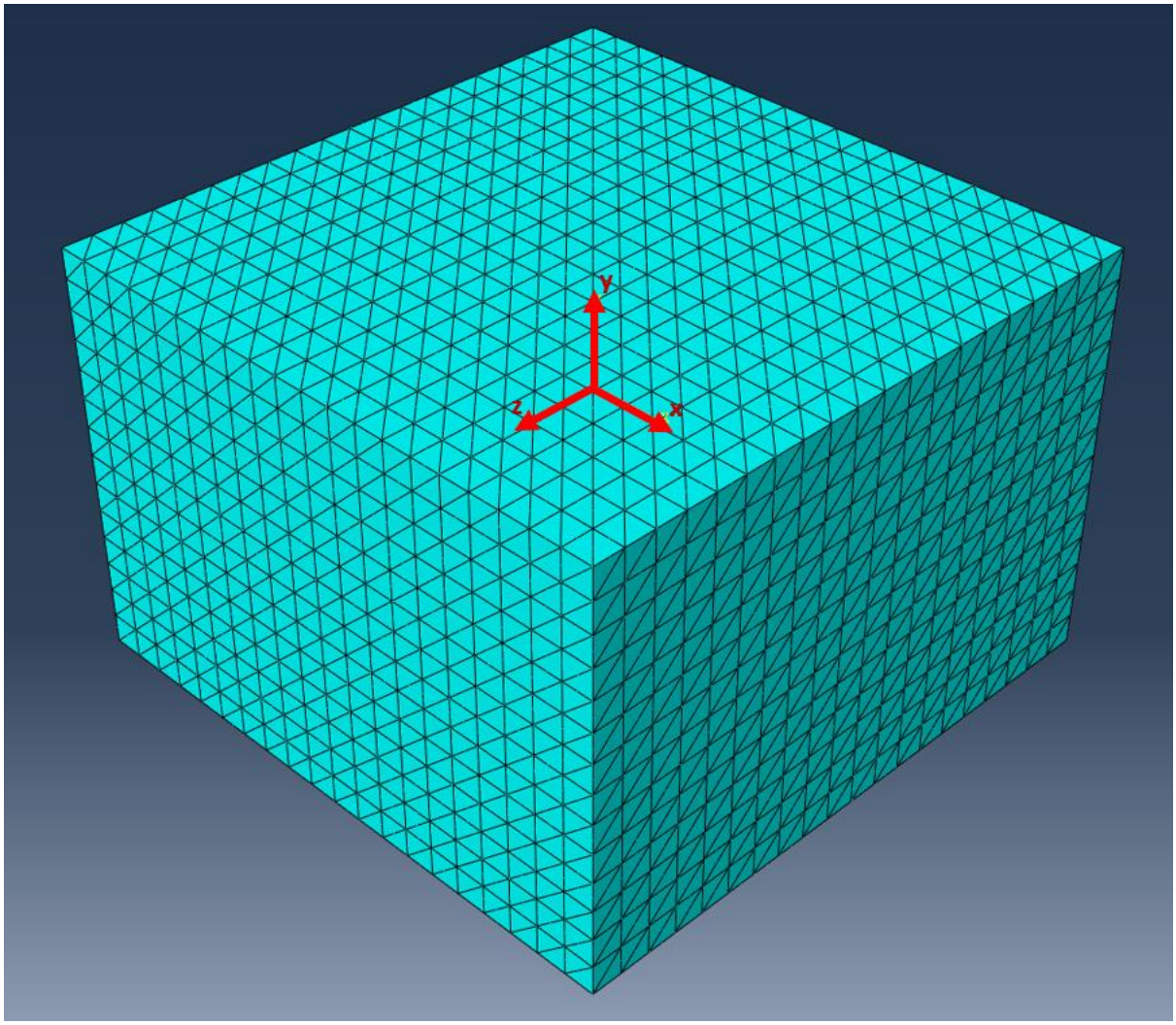

Figure 44 – The 3D mesh used to set up the Abaqus model. The model dimensions are 20 cm x 30 cm x 30 cm.

6.4 Abaqus model results

The Abaqus model outputs a 3D mesh of instantaneous seismic velocities in the Y-axis direction following a seismic loading event. Figure 45 shows the instantaneous seismic velocities with a seismic loading at the surface, while Figure 46 shows the instantaneous seismic velocities with a seismic loading at the centre of mass of the model. Positive values refer to the local velocity of the mesh being upwards, while negative values refer to the local

velocity of the mesh being downwards. This velocity is the instantaneous velocity of the particle at that location, not the velocity of the seismic wave front.

To calculate the velocity of the seismic wave propagation through the medium, the instantaneous velocity over the volume can be examined at different time intervals to observe how quickly it travels through the medium. Using this delay time with the known distance given the dimensions of the volume (20 cm x 30 cm x 30 cm) allows the calculation of velocity. For this purpose, the volume is sliced in half after computation to allow the propagation of the wave on the interior to be examined. Using the ALRS-1 properties shown in Table 6, six time intervals at a separation of 0.005 seconds each are shown in Figures 47-52 after a seismic loading event. 0.005 seconds was chosen as it is the smallest possible time interval in Abaqus, and is therefore ideal for giving the most accurate velocity estimate.

It is important to note that the time shown is computational time. This is not necessarily the same as real time. Therefore, this analysis should be seen as relative and not necessarily absolute. This still allows for the velocity of the samples to be compared to other samples but does not necessarily correspond to the real velocity.

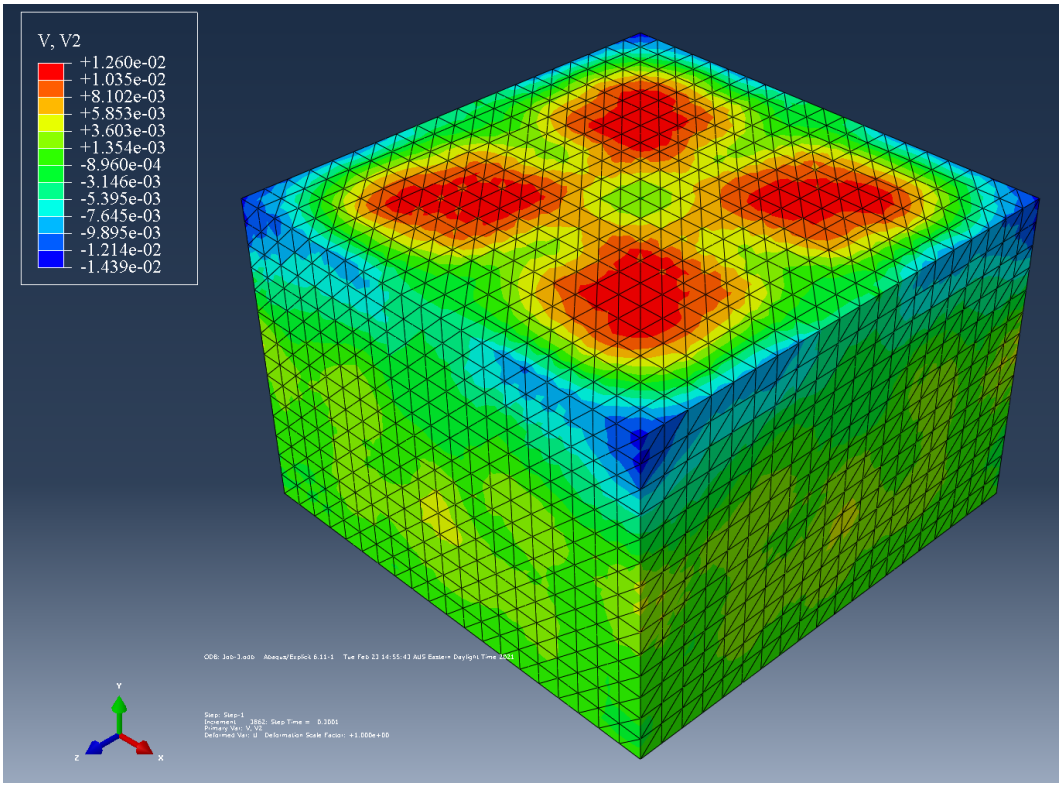

Figure 45 – Instantaneous P-wave seismic velocities in the Y-axis direction over the Abaqus ALRS-1 model with seismic loading at the surface. Positive values refer to the local velocity of the mesh being upwards, while negative values refer to the local velocity of the mesh being downwards.

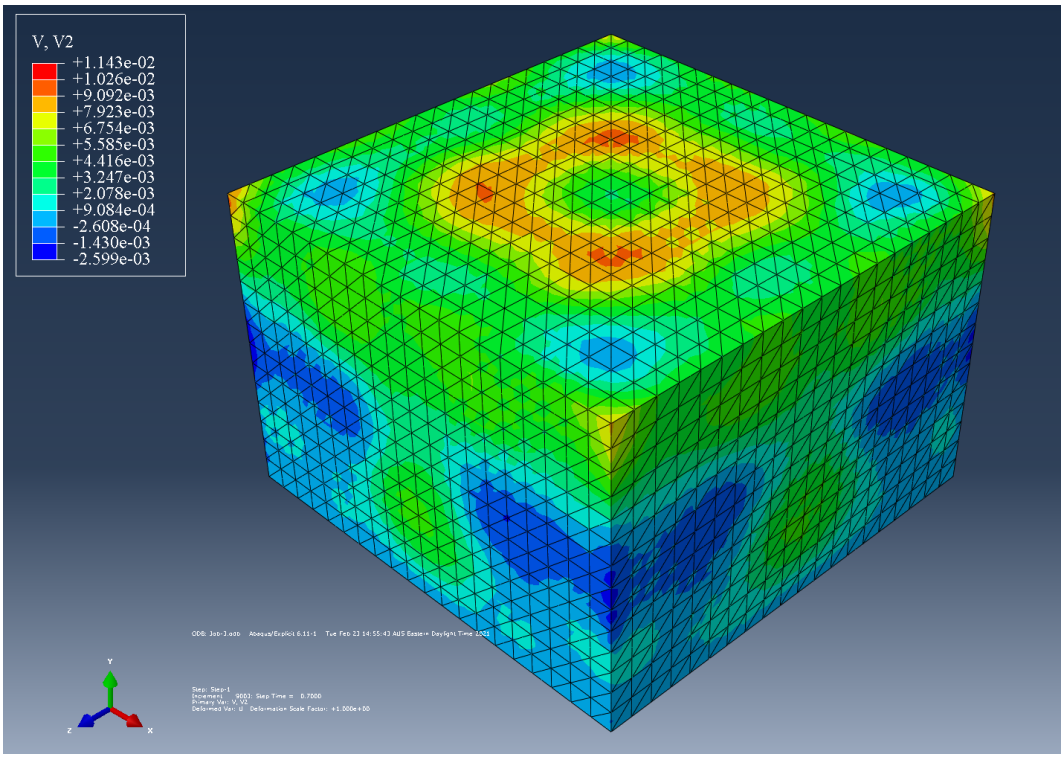

Figure 46 – Instantaneous P-wave seismic velocities in the Y-axis direction over the Abaqus ALRS-1 model with seismic loading at the centre of mass. Positive values refer to the local velocity of the mesh being upwards, while negative values refer to the local velocity of the mesh being downwards.

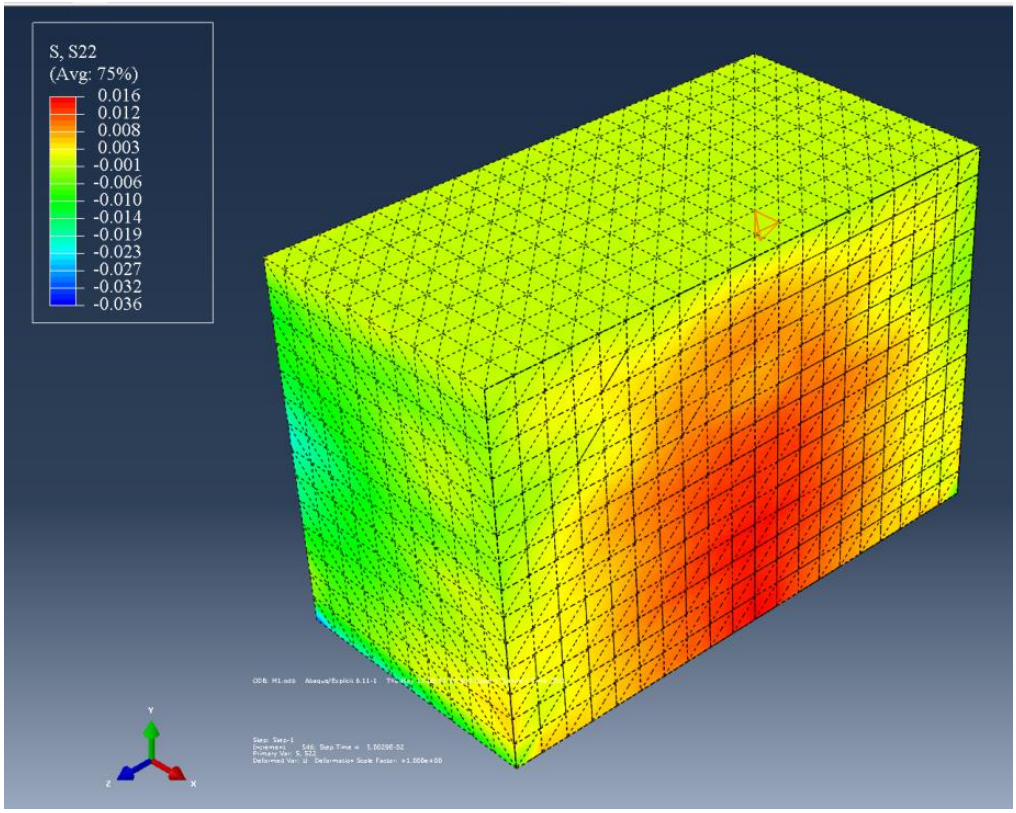

Figure 47 – Instantaneous velocity over the volume of the ALRS-1 sample at T1 (0.005 seconds after seismic loading at the centre of mass). Half of the volume is not displayed to show the internal velocity.

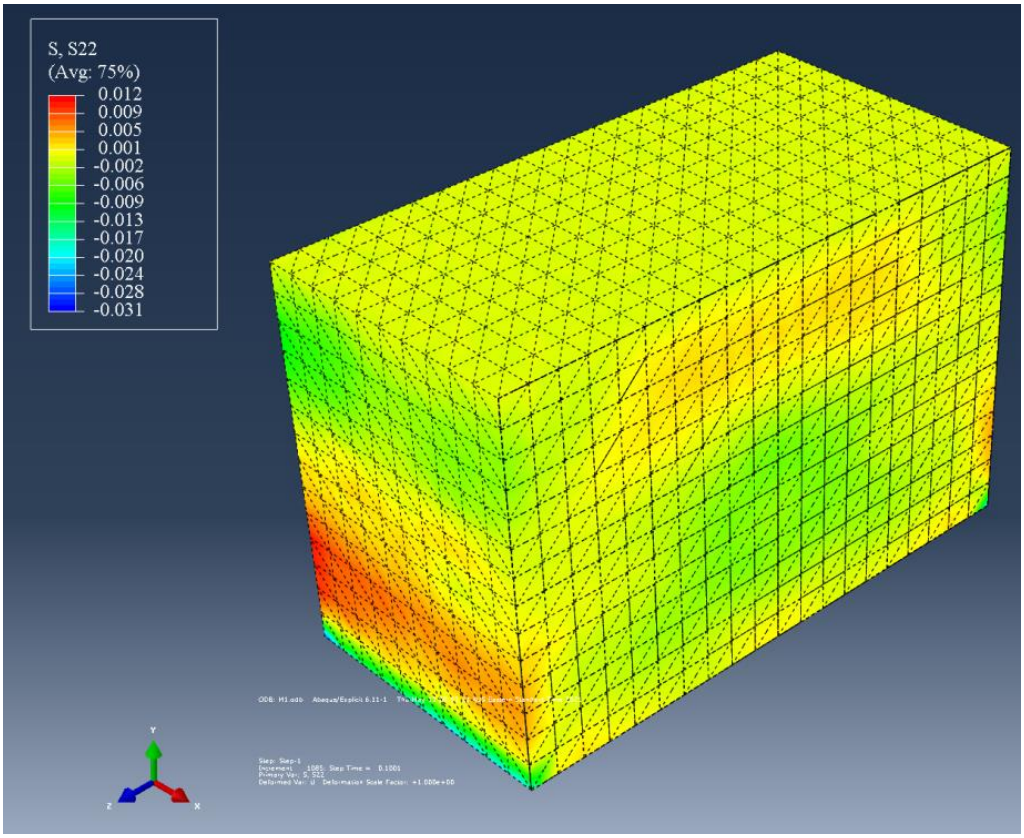

Figure 48 – Instantaneous velocity over the volume of the ALRS-1 sample at T2 (0.01 seconds after seismic loading at the centre of mass). Half of the volume is not displayed to show the internal velocity.

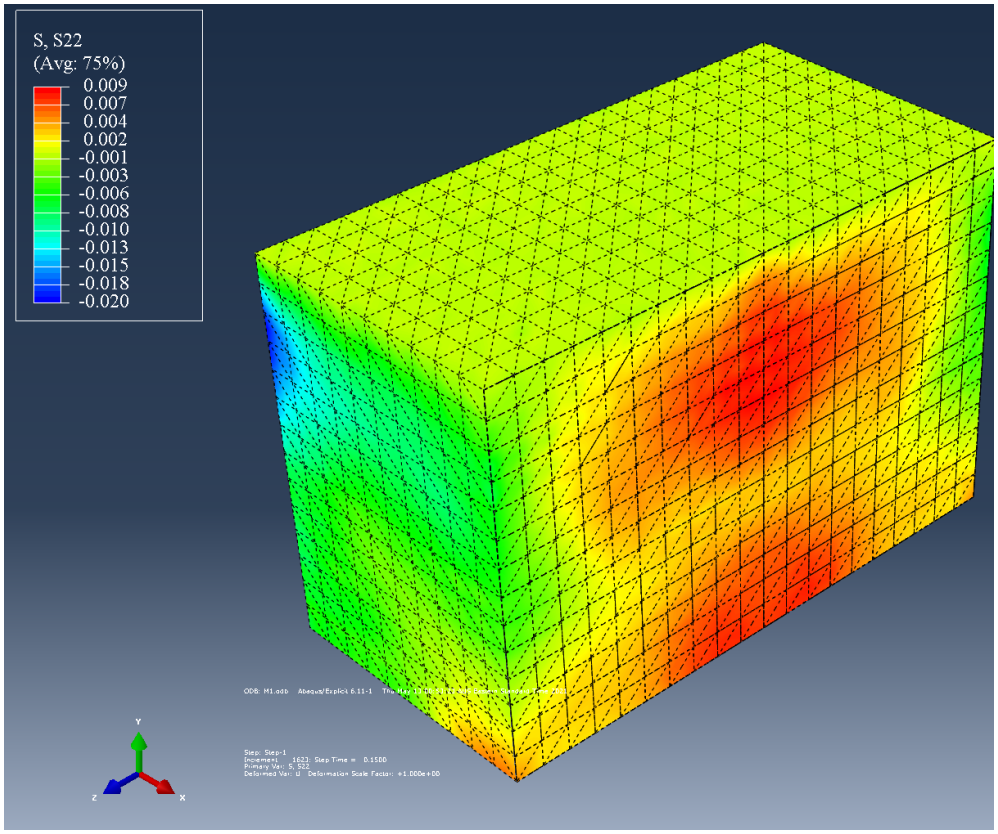

Figure 49 – Instantaneous velocity over the volume of the ALRS-1 sample at T3 (0.015 seconds after seismic loading at the centre of mass). Half of the volume is not displayed to show the internal velocity.

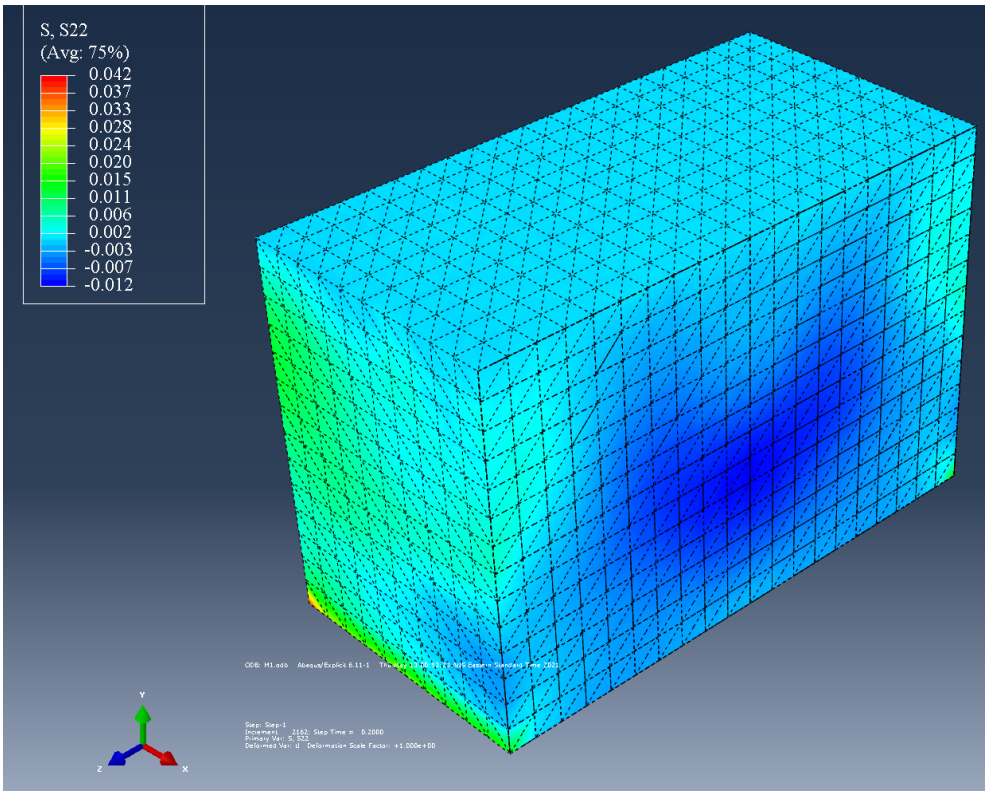

Figure 50 – Instantaneous velocity over the volume of the ALRS-1 sample at T4 (0.02 seconds after seismic loading at the centre of mass). Half of the volume is not displayed to show the internal velocity.

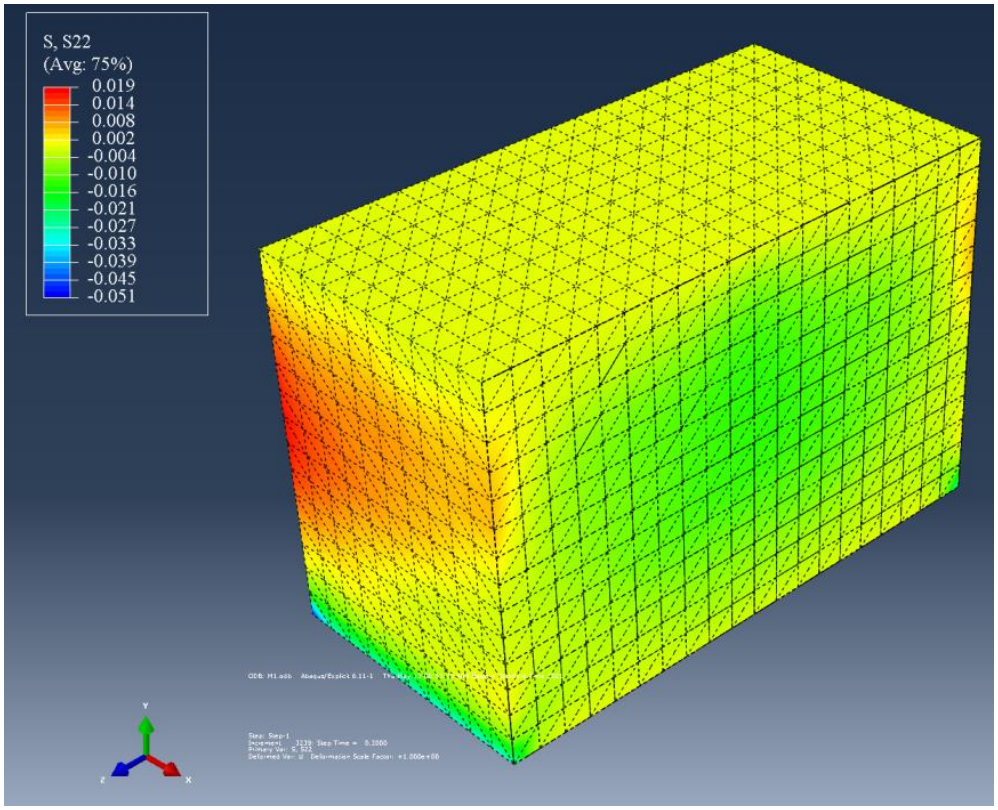

Figure 51 – Instantaneous velocity over the volume of the ALRS-1 sample at T5 (0.025 seconds after seismic loading at the centre of mass). Half of the volume is not displayed to show the internal velocity.

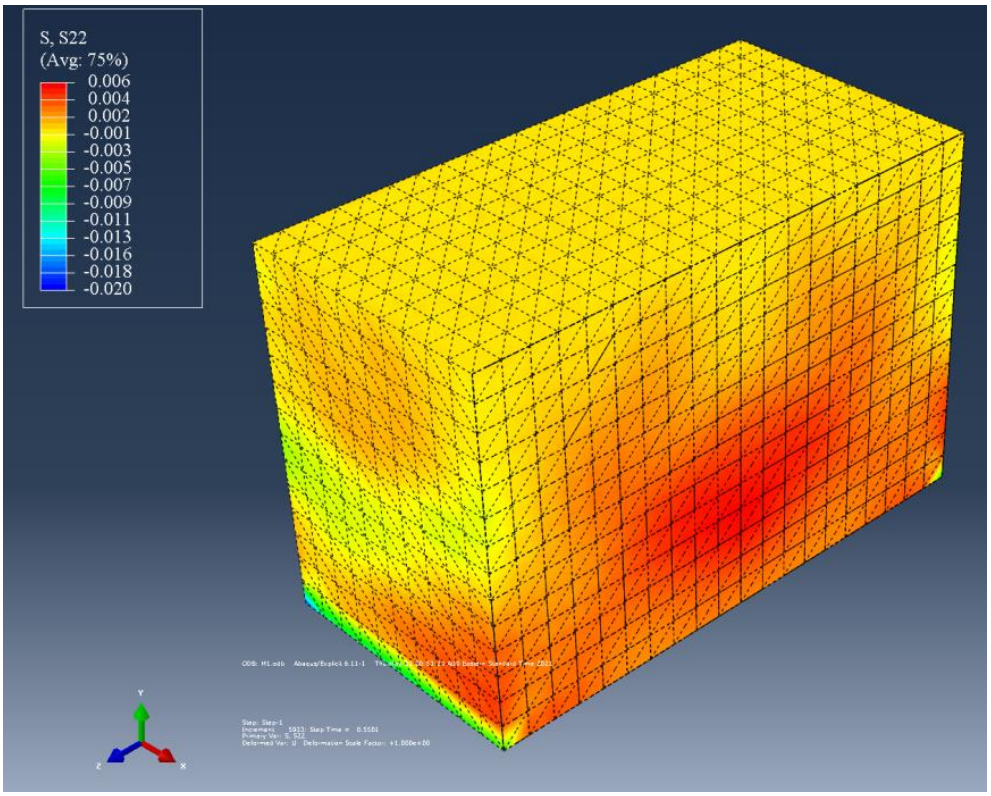

Figure 52 – Instantaneous velocity over the volume of the ALRS-1 sample at T6 (0.03 seconds after seismic loading at the centre of mass). Half of the volume is not displayed to show the internal velocity.

6.5 Abaqus model discussion

The intention of modelling the volume for the ALRS-1 sample at time intervals as in Figure 47-52 was to determine the P-wave seismic velocity for comparison with the other samples. Using the time intervals, it is not possible to identify a single wave front which can be followed between different time intervals. This implies that the wave front is travelling more than 15 cm (half of the 30 cm width of the volume) every 0.005 seconds. This gives a lower bound to the velocity of 60 m/s. This is not inconsistent with the measured velocity of the ALRS-1 sample (98.6 m/s).

If the initial tests of the ALRS-1, MMS dust and MMS small/medium-grained sand samples were successful, the next step would have been to generate synthetic samples by varying the regolith properties in a controlled way for input to the Abaqus model to determine how each property affects seismic velocity. Given that this may be useful for future researchers, this work is carried out in this section. The properties of six more samples are shown in Table 9-14. They are each given the grain properties of the MMS small/medium-grained sand as a starting point and have one parameter changed. Given that there are 6 grain properties used (internal friction angle, elastic modulus, Poisson ratio, cohesion value, Young's modulus and grain density), there are 6 synthetic samples listed. Each parameter that has been altered has been reduced by around 20-40%. The amount each is altered by is arbitrary, but with the goal of changing it enough to observe any change in the velocity while remaining a realistic sample that might exist in nature.

Table 9 – Grain properties used to model artificial sample 1.

Internal friction angle (°)	30
Elastic modulus (MPa)	14
Poisson ratio	0.325
Cohesion value (kPa)	0.81
Young's modulus (kPa)	12.5
Grain density (g/cm^3)	2.9

Table 10 - Grain properties used to model artificial sample 2.

Internal friction angle (°)	38
Elastic modulus (MPa)	10
Poisson ratio	0.325
Cohesion value (kPa)	0.81
Young's modulus (kPa)	12.5
Grain density (g/cm^3)	2.9

Table 11 - Grain properties used to model artificial sample 3.

Internal friction angle (°)	38
Elastic modulus (MPa)	14
Poisson ratio	0.25
Cohesion value (kPa)	0.81
Young's modulus (kPa)	12.5
Grain density (g/cm^3)	2.9

Table 12 - Grain properties used to model artificial sample 4.

Internal friction angle (°)	38
Elastic modulus (MPa)	14
Poisson ratio	0.325
Cohesion value (kPa)	0.5
Young's modulus (kPa)	12.5
Grain density (g/cm^3)	2.9

Table 13 - Grain properties used to model artificial sample 5.

Internal friction angle (°)	38
Elastic modulus (MPa)	14
Poisson ratio	0.325
Cohesion value (kPa)	0.81
Young's modulus (kPa)	8
Grain density (g/cm^3)	2.9

Table 14 - Grain properties used to model artificial sample 6.

Internal friction angle (°)	38
Elastic modulus (MPa)	14
Poisson ratio	0.325
Cohesion value (kPa)	0.81
Young's modulus (kPa)	12.5
Grain density (g/cm^3)	2.4

Due to the time interval limitation with the Abaqus model, analytical modelling is also performed in Section 6.6 as an alternative to computational modelling. Equations which relate seismic velocity to regolith grain properties in low atmospheric pressures to perform the analytical modelling are lacking in the literature. Talwani et al. (1973) perform laboratory experiments to examine the possibility of a relationship between seismic velocity and grain properties, however, they suggest that only confining pressure appears to have any strong impact on P- and S-wave velocity of regolith.

6.6 Analytical modelling

This section will discuss the use of analytical modelling to relate the regolith and source properties to the seismic wave travel time of samples using equations from the literature.

Sherlock and Evans (2001) note that grain shape and sorting contribute strongly to the frame rigidity and therefore seismic velocity of unconsolidated sediments such as sands. However, they do not provide a correlation to relate these properties.

Wyllie et al. (1956), Talwani et al. (1973) and Bell and Shirley (1980) suggest that density, grain size, permeability and porosity appear to have little to no impact on the P- or S- wave seismic velocity, with mineralogy playing a minor role. Talwani et al. (1973) notes that cycling confining pressure from low to high and back to its original low will result in the measured P-wave velocity also returning to its original low, despite a reduction in porosity, suggesting that pressure is the dominant factor in determining P-wave velocity in unconsolidated sediments. Talwani et al. (1973) show from experimental results (Figure 53) that the P-wave velocity of a silica sand is ~1,000 m/s at a pressure of 0.001 kilobars (atmospheric pressure) regardless of grain size. Grain size appears to impact the seismic velocity of the samples at higher confining

pressures, with the coarse-grained sample having a higher velocity than the fine-grained sample, and the sample which combines both has an even higher velocity.

Figure 54 shows the relationship between P-wave and S-wave velocities and confining pressure of a powdered basalt from Talwani et al. (1973), which is more representative of the ALRS-1 sample than the sands in Figure 53. This sample has a P-wave velocity of ~800 m/s at a pressure of 0.001 kilobars. This result is lower than the sand samples, possibly as the result of a differing grain size and mineralogy, though is still significantly greater than the ALRS-1 P-wave velocity of 98.6 m/s. This difference in velocity seems too great to be reconciled by a differing mineralogy between the two basalts, and so is suggested to be the result of differing grain size, given the highly fine-grained nature of ALRS-1. It should be noted that no grain size distribution is provided for the basalt sample by Talwani et al. (1973) to make this comparison.

Wichtmann and Triantafyllidis (2009) suggest that while the P-wave velocity of a regolith at atmospheric pressure is not controlled by the mean grain size (d_{50}, the sieve size at which 50% of the regolith passes through), it does seem to be strongly inversely correlated with the coefficient of uniformity, a measure of the variety in particle sizes in regolith. The coefficient of uniformity is:

$$C_u = d_{60}/d_{10} \qquad (17)$$

Where d_{60} is the sieve size through which 60% of the regolith (by weight) passes, and d_{10} is the sieve size through which 10% of the regolith passes through. Higher values of C_u indicate higher variety in grain size. Wichtmann and Triantafyllidis (2009) proposed a relationship between C_u and P-wave velocity that has been tested in samples up to C_u values of 16.

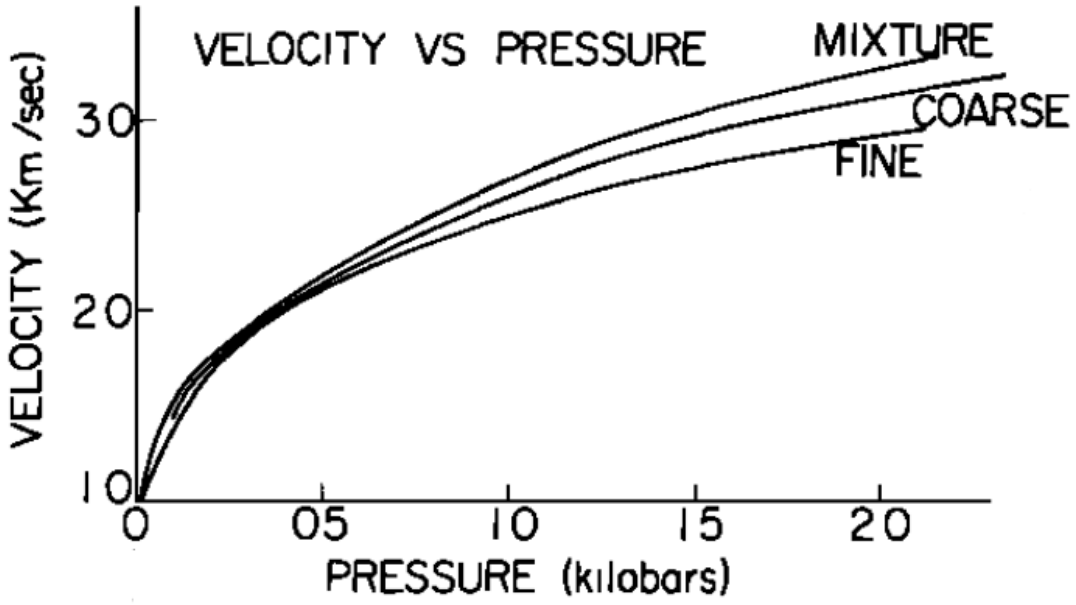

Figure 53 – P-wave velocity vs confining pressure of three sands – fined-grained, coarse-grained and a mixture (Talwani et al. 1973).

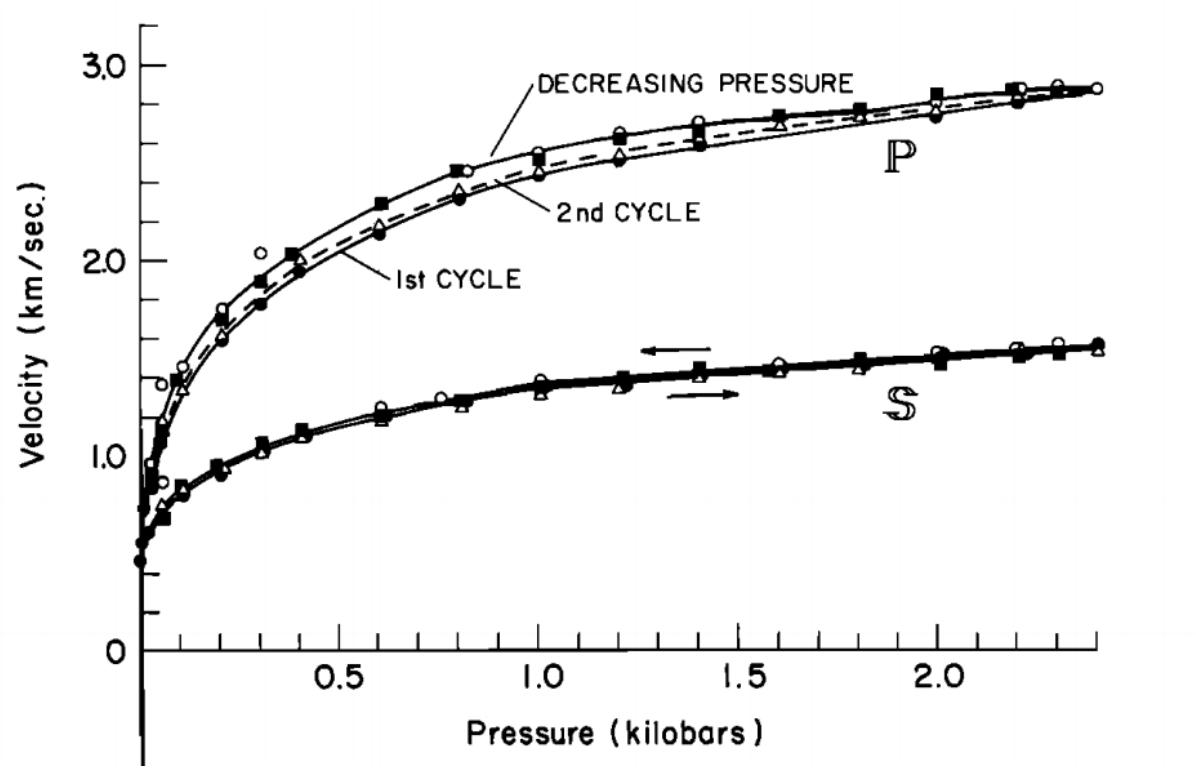

Figure 54 – P-wave and S-wave velocity vs confining pressure of a powdered basalt (Talwani et al. 1973).

The coefficient of curvature (C_c) is also used to describe grain size distributions and is a measure of how poorly graded a soil is. C_c is defined as:

$$C_c = \frac{(d_{30})^2}{d_{10}\, d_{60}} \qquad (18)$$

Where d_{30} is the sieve size through which 30% of the regolith (by weight) passes, d_{10} is the sieve size through which 10% of the regolith passes through, and d_{60} is the sieve size through which 60% of the regolith passes through. C_u and C_c are typically considered together. A C_c value of 1 to 3 indicates a well graded soil if C_u is greater than 6 for a sand. A poorly graded soil is expected to have a higher porosity than a similar soil which is well graded. While there is no literature suggesting a correlation between C_c and P-wave velocity of a regolith, it will also be examined here.

To explore the possibility of a relationship between P-wave velocity and d_{50}, C_u or C_c of a regolith, relationships for each will be plotted from the ALRS-1, MMS dust and MMS sand regolith samples examined in this thesis. Table 15 shows the d_{50}, C_u, C_c and mean P-wave velocities for each regolith. d_{50} and C_u values for each sample are determined from their grain size distributions in Figures 20 and 22.

Table 15 – d_{50}, C_u and P-wave velocity values for the regolith samples.

Regolith	$\boldsymbol{d_{50}}$ **(mm)**	$\boldsymbol{C_u}$ $\boldsymbol{(d_{60}/d_{10})}$	$\boldsymbol{C_c}$ $\boldsymbol{(\frac{(d_{30})^2}{d_{10}\, d_{60}})}$	**P-wave velocity (m/s)**
ALRS-1	0.075	17.14	1.07	98.6
MMS dust	0.03	10	3.21	61.3
MMS sand	0.2	3.846	1.19	257.85

Figures 55 plots the relationship between d_{50} and P-wave velocity, Figure 56 plots the relationship between C_u and P-wave velocity, and Figure 57 plots the relationship between

C_c and P-wave velocity for the ALRS-1, MMS dust and MMS sand, and creates a relationship for each.

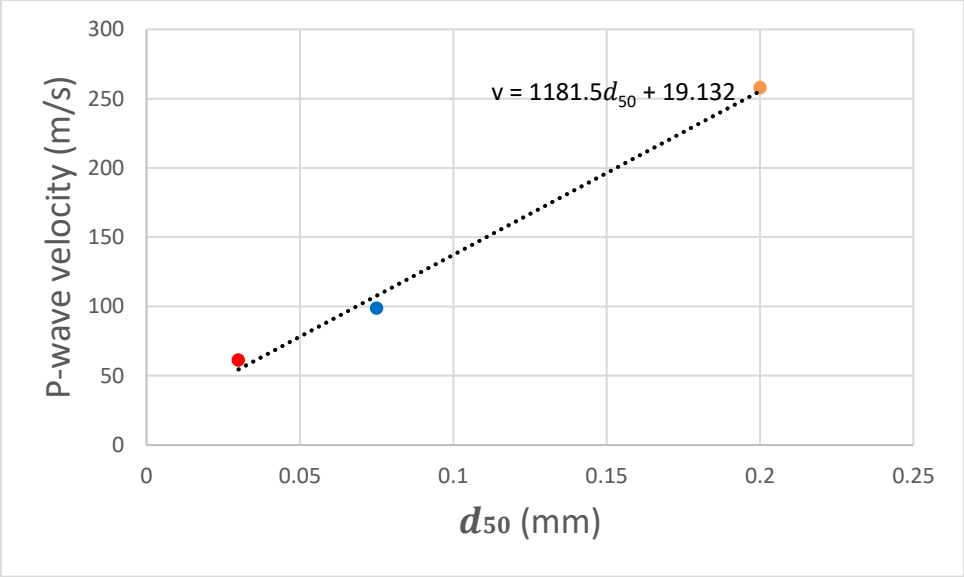

Figure 55 – Comparison of P-wave velocity and mean grain size (d_{50}) of regolith simulant samples ALRS-1 (blue), MMS dust (red), and MMS sand (green).

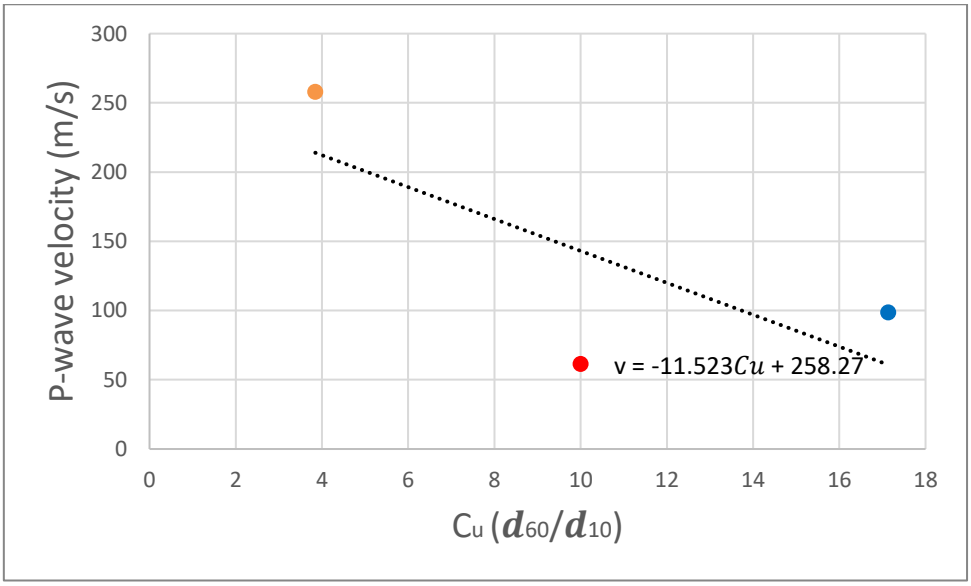

Figure 56 - Comparison of P-wave velocity and coefficient of uniformity (C_u) of regolith simulant samples ALRS-1 (blue), MMS dust (red), and MMS sand (green).

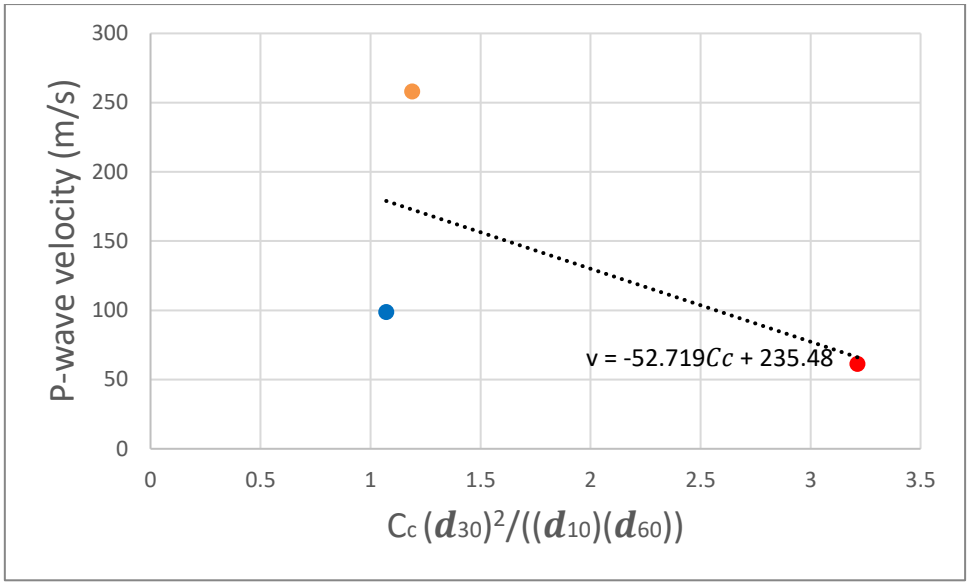

Figure 57 - Comparison of P-wave velocity and coefficient of curvature (C_c) of regolith simulant samples ALRS-1 (blue), MMS dust (red), and MMS sand (green).

Eberhart-Phillips et al. (1989) use a multivariate analysis of laboratory measurements from 64 samples to describe the following equation for the P-wave velocity (V_p) of sandstone.

$$\boldsymbol{V_p = 5.77 - 6.94\emptyset - 1.73\sqrt{C} + 0.446(P_e - e^{-16.7P_c})} \qquad (19)$$

Where $\emptyset$ is the porosity, P_e is the effective pressure and C is the clay content. However, this relationship is designed for consolidated rock rather than unconsolidated regolith. No similar relationships to relate the seismic velocity of unconsolidated regolith to other grain properties can be found in the literature. This constitutes a significant gap which could be filled by performing a comprehensive series of laboratory tests of regolith, of which Chapters 4 and 5 of this thesis represent the first stage.

6.6 Analytical model discussion

d_{50} appears to have a good, linear relationship with P-wave velocity, with velocity consistently increasing with increasing d_{50}. From this plot, it might be suggested that increased mean grain size corresponds with increased P-wave velocity. The equation for this relationship is v = 1181.5d_{50} + 19.132.

C_u appears to have a less consistently linear relationship with P-wave velocity than d_{50}, but velocity does appear to decrease with increasing C_u. The equation for this relationship is v = -11.523Cu + 258.27. As an increasing C_u value results in increasing porosity (as a more uniform regolith implies more porosity), a decreasing velocity with increasing C_u is expected.

C_c appears to have the weakest relationship with P-wave velocity. The equation for this relationship is v = -52.719Cc + 235.48.

It is proposed as a result of the relationship between d_{50} and velocity that P-wave velocity does have a direct correlation with grain size at very low confining pressures (such as Earth atmospheric pressure and in vacuum), and that this hasn't been observed to date given the lack of experimental work performed on unsaturated highly fine-grained regoliths.

If the inverse relationship between C_u and velocity is consistent in other samples, this implies that P-wave velocity is higher for regoliths with less variety in grain size (i.e., more homogenous). In other words, the more well sorted a regolith is, the higher its velocity is expected to be.

To further expand on the comparisons of d_{50}, C_u and C_c with P-wave seismic velocity, a useful exercise would be to include other regoliths from the literature. As discussed previously, seismic velocity measurements of dry regolith at atmospheric pressure are sparse in the literature. No P-wave velocity measurements with full grain size distributions from which to determine the d_{50}, C_u and C_c values could be found in the literature. A potentially useful exercise in lieu of these data would be to take the grain size distribution of regolith from the literature and predict what its dry, atmospheric pressure P-wave velocity would be using the

relationships developed here from the off-Earth simulants and determine whether the predicted velocity is realistic.

The grain size distribution of several offshore sand sediment samples from the "El Puntal" Spit, Santander, in Spain, are determined by Medina (et al. 1994) and are shown in Figure 58. This distribution is used in combination with the relationships between P-wave velocity and d_{50}, C_u and C_c to generate three predictions of the P-wave velocity of the sediment as shown in Table 16.

The predicted P-wave velocity of the 120 m, 330 m and 660 m samples from d_{50} are 279.06 m/s, 279.06 m/s and 255.43 m/s respectively. The predicted P-wave velocity of the 120 m, 330 m and 660 m samples from C_u are 244.71 m/s, 240.99 m/s and 239.07 m/s respectively. The predicted P-wave velocity of the 120 m, 330 m and 660 m samples from C_c are 173.46 m/s, 180.56 m/s and 164.31 m/s, respectively.

The predicted velocities from d_{50} and C_u are relatively consistent, compared to the predicted velocities from C_c. Zimmer (et al. 2007) show the P-wave velocity of a number of dry sands at 0.1 MPa (approximately atmospheric pressure) as ranging from around 300-550 m/s. The predicted velocities of the offshore sand samples from the "El Puntal" Spit from d_{50} and C_u are just below the lower end of this range, while the predicted velocities from C_c are significantly lower. This is an encouraging result for the viability of using d_{50} and C_u to predict seismic velocity, as it suggests that the predicted velocities are not completely unrealistic.

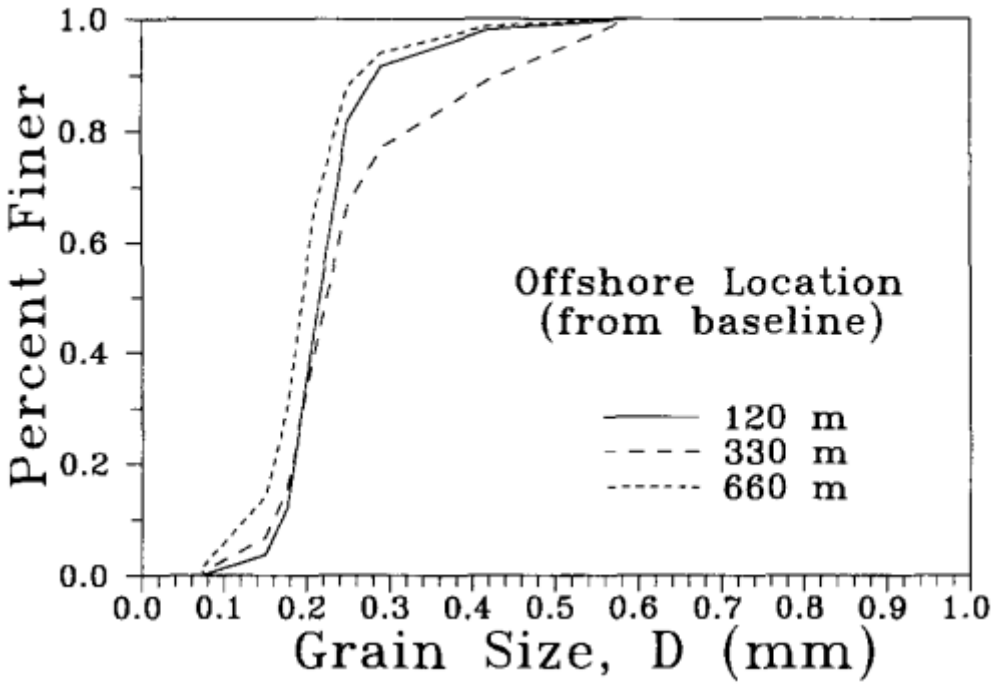

Figure 58 – Grain size distributions of sediment taken from different offshore locations at the "El Puntal" Spit, Santander, Spain (Medina et al. 1994).

Table 16 – d_{50}, C_u and P-wave velocity values for the sediment samples from Figure 58.

Regolith	d_{50} **(mm)**	C_u (d_{60}/d_{10})	C_c $(\frac{(d_{30})^2}{d_{10}\,d_{60}})$	**P-wave velocity from** d_{50} **(m/s)**	**P-wave velocity from** C_u **(m/s)**	**P-wave velocity from** C_c **(m/s)**
120 m	0.22	1.18	1.18	279.06	244.71	173.46
330 m	0.22	1.5	10.4	279.06	240.99	180.56
660 m	0.2	1.67	1.35	255.43	239.07	164.31

This analysis is severely limited by the lack of available dry regolith samples with both grain size distributions and P-wave velocity measurements at atmospheric pressure. However, this work has shown that there is a potential relationship between mean grain size and the uniformness of the grain size distribution of a regolith and the P-wave velocity. Future work to measure the grain size distribution and P-wave velocity of dry regoliths at atmospheric pressure will further determine the accuracy of this relationship and refine the equations developed here.

The analysis in this section only considers d_{50}, C_u and C_c independently. As C_u and C_c are often considered together in practice, future work with more available data points should also consider all three parameters together, rather than just separately.

6.7 Conclusion

This chapter explored the use of computational and analytical modelling in an attempt to verify the experimental results of Chapters 4 and 5 of this thesis. Computational modelling of the laboratory setup was successfully performed using Abaqus. However, due to computational limitations of the software, the upper bound of the P-wave velocity that can be determined using this methodology was too low to determine the velocity of the regolith in the model, which provides a minimum possible velocity. Encouragingly, this minimum velocity of 60 m/s is lower than the measured velocity of ALRS-1. The modelling, therefore, is consistent with the experimental data.

Analytical modelling was explored as an alternative to the computational modelling. A lack of correlations between seismic velocity and grain properties of unconsolidated regolith in low confining pressure made analytical modelling of the laboratory experiments impossible. Relationships between the velocity of a regolith and three key descriptors of grain size distribution, d_{50}, C_u and C_c were developed from the experimental work performed in this thesis on the off-Earth regoliths. The relationships between velocity and d_{50} and C_u were determined to be realistic, while the relationship between velocity and C_c was less encouraging. These relationships are the first of their kind for dry, low confining pressure regoliths. This work supports the hypothesis proposed in Chapter 5 that P-wave velocity is directly correlated with grain size, which is in contrast with existing literature.

Future work to measure the P-wave velocity of dry regoliths at atmospheric pressure with known grain size distributions is expected to be a useful addition to this work to improve the accuracy of the relationships developed here.

7. Determination of asteroid structure and geomechanics using penetrators and active seismic

This chapter is a submitted journal paper with minor modifications (reference below).

Dello-Iacovo, M.A. 2021, Determination of asteroid structure and geomechanics using penetrators and active seismics, *Icarus* In review.

7.1 Introduction

7.1.1 Asteroid impact risk

In recent years humanity has become aware of the potential threat from asteroid impacts (Bottke et al. 2004), primarily from Near-Earth Objects (NEOs). Opinion remains divided over whether any human has been killed in an asteroid impact in recent history (Jenniskens et al. 2019; Gritzner et al. 2006). However, the probability of a major impact is fairly well understood, and it can be argued that the likelihood of being killed by an asteroid is comparable to the likelihood of being killed by some other event, for example an airline crash (Rees 2003). This is because when a catastrophic asteroid impact does occur, it may result in an enormous number of deaths. There is also a small but non-zero chance on a year by year basis of an asteroid or comet impact large enough to wipe out all of humanity (Matheny 2007).

Although all NEOs greater than 10 km in diameter (i.e. the size of the Chicxulub asteroid assumed to have killed the dinosaurs; Durand-Manterola and Cordero-Tercero 2014) are believed to have been discovered (Harris and D'Abramo 2015), other hazardous asteroids and comets might come from highly elliptical orbits or outside the Solar System, thus being harder to detect in advance.

7.1.2 Asteroid structure

Existing knowledge of the internal structure of asteroids comes from meteorite samples found on Earth. A variety of structural models have been proposed for asteroid structures,

including monolithic, rubble piles, gravel conglomerations, solid bodies with a loose regolith exterior and heavily fractured/porous bodies (Walker et al. 2006).

In addition, inferences about internal structure have been made from visual observations and hyperspectral imagery of the surface and limited direct measurements. It is expected to be highly challenging to drill deep holes (i.e., to a depth of multiple metres) on asteroids and retrieve core samples or use downhole logging tools due to equipment limitations, so proving a structural model is difficult. The Philae lander of the Rosetta mission to comet 67P Churyumov-Gerasimenko featured a smaller drill for soil sampling (Finzi et al. 2007), however, due to a failed landing, this did not return any usable data (Boehnhardt et al. 2017). The Asteroid Impact and Deflection Mission (AIDA – joint NASA and ESA mission) scheduled to launch in November 2021 will be targeting the asteroid called 65803 Didymos (Naidu et al. 2016) and is expected to provide useful information on the internal structure of an asteroid (Cheng et al. 2013; Cheng et al. 2018), though is expected to come at a significant financial cost. The NASA component was budgeted at 313.9 million USD (Planetary Society 2020) while ESA's component is expected to cost 151.5 million USD for design, manufacture and testing alone (Clark 2020). Ideally, a cheaper methodology should be designed to map the internal asteroid structure.

Geophysical techniques such as seismic, ground-penetrating radar (GPR), and radio tomography are used to map the internal structure of Earth, and all may provide useful techniques for mapping asteroids and comets (Herique et al. 2018).

Walker et al. (2009) suggested that there may be a correlation between asteroid structure and size/type. Unfortunately, there is not currently enough information to correlate the asteroid structures and size/type. Once a database of structural models for different asteroid

types has been constructed, it should be possible to determine whether there is any link between spectral type and structural type. This dataset will be invaluable for rapid target selection for asteroid mining and rapid determination of appropriate asteroid deflection techniques, especially for those asteroids discovered shortly before fly-by or impact.

7.1.3 Asteroid mining and deflection

In addition to the lifesaving potential of investing in asteroid detection and deflection research, understanding asteroids also has applications for off-Earth resource extraction and colonisation. Due to the high costs expected to be associated with asteroid mining missions, characterising the available resource is critical to prioritise and select targets. For example, ice is a potentially valuable resource to extract because it can be converted to propellant through electrolysation for use in space (Lewis 1997), saving the cost of transporting fuel from the Earth's surface. Therefore, understanding the concentration and distribution of the ice deposit in an asteroid is critical for prospecting and later for mining. Further, extraordinarily little is known about asteroid interiors, including their geomechanical and structural characteristics (Walker et al. 2009). These factors influence the selection of mining methods and related systems design, and thus, should be known before planning and undertaking a mining mission.

Improving the understanding of asteroids generally may also assist in determining whether an asteroid is potentially hazardous and how much damage it is likely to cause (Gritzner and Kahle 2004). Understanding which asteroids are hazardous could result in significant cost savings by ensuring that multi-billion-dollar deflection efforts are not made for asteroids that would pose no threat as they would break up in the atmosphere (Ostro and Giorgini 2004).

Asteroid deflection via explosives, impactors or other means has been proposed to protect Earth from any impending asteroid or comet impact. It is unclear how asteroids of different structural composition will react to deflection attempts and what the ideal method of deflection would be. For example, a rubble pile might break up after being hit by a kinetic impactor (such as a direct impact from a satellite to impart momentum) and still pose a threat to Earth, demanding a more sophisticated technique such as a smart cloud of smaller impactors (Gibbings 2011). Deflection techniques such as impactors and explosives are expected to have a reduced efficiency of as much as two orders of magnitude when targeting highly porous bodies (Holsapple 2004). Understanding the presence and strength of regolith can assist with planning anchoring techniques for deflection and mining devices in the low gravity environment (Gritzner and Kahle 2004).

Finally, due to the lack of structural understanding of asteroids and comets, much foundational research and modelling work on asteroid deflection may be based on assumptions that are incorrect. Testing and updating these models with data should be a priority.

7.1.4 Mission proposal

The objective of this chapter is to propose and describe a mission to place seismic sources, receivers, and other scientific tools on the surface of a NEO asteroid using penetrators. Penetrators can emplace a scientific payload under the surface of an asteroid, allowing for the collection of *in-situ* data about the interior. This mission concept can also be useful as a technology demonstration for future space exploration missions to generate a database and search for correlations between the surface and subsurface features. The intersection, data collection and interpretation of NEO 99942 Apophis during its 2029 fly-by is considered as a case study.

The proposed mission concept is as follows. A target NEO passing close to Earth with acceptably low delta-V (relative velocity between Earth and the NEO) will be selected prior to its fly-by. A mothership carrying a series of penetrators will be placed in an orbit that will near-intersect with the path of the NEO. The orbit will be designed to minimise the relative velocity between the mothership and the NEO at the time of impact. Just before the asteroid reaches the mothership, the spacecraft will slow down to a relative velocity of within 300 m/s for impact and bring the spacecraft to an intersection path. The penetrators will be deployed in a line where they will intersect the NEO. The mothership itself may either alter its orbit to end of life in Earth's atmosphere, or also be impacted into another body for planetary protection.

7.2 Geophysics

As previously mentioned, the primary geophysical techniques that have been proposed or are already in use for probing asteroids are GPR, radio tomography, gravity, magnetics, and seismic. Gravity and magnetics are useful for determining bulk properties of asteroids, however, they are not capable of providing detailed subsurface imaging, and so are not discussed in this chapter. GPR and radio tomography are useful in that they do not require surface contact, however, they have limited penetration and resolution respectively (Annan and Cosway 1992; Kofman and Safaeinili 2004). Therefore, the primary geophysical tool to examine the interior of asteroids in this chapter is seismic.

Asteroid densities can be determined from meteorite samples, direct sample return (the Hayabusa 1 and Hayabusa 2 missions) (Abe et al. 2006; Yano et al. 2006; Watanabe et al. 2017), or bulk density, which is inferred from the deflection of another body due to the gravitational strength of the asteroid and volume estimates. Estimated asteroid densities range from 0.8 to 6.7 g/cm^3, suggesting that many asteroids are rubble piles or highly fractured and porous (Walker et al. 2015). The problem with using bulk density to understand

an asteroid is that it does not account for potential largescale variations, such as an ultra-low-density regolith with a high-density core, or two separate bodies which coalesced.

Other than these samples and measurements, understanding of the composition of asteroids is generally based on remote sensing data which gives information only about the surface, however, the interior may be vastly different. To date, no seismic information has been directly measured on an asteroid, although the proposed BASiX mission would have been the first if it had not been cancelled due to budget changes (Anderson et al. 2014).

7.3 Background of seismic

Seismic geophysics involves the generation of sound waves which propagate through a body of rock at a velocity which varies depending on the rock characteristics. When sound waves reach an interface between two materials of different acoustic impedance (the product of density and seismic velocity), a portion of the wave energy is transmitted through the material and the other part is reflected, eventually reaching the surface where the vibrations can be measured using seismic receivers.

With a network of multiple receivers and source locations, a significant amount of information can be derived, including the location, depth, size and shape of subsurface features, the seismic velocity of the rock, from which rock strength can be estimated, the presence of porosity or voids, density, and the type of rock.

For asteroid deflection and mining, the goals of using seismic geophysics are to determine whether it is a rubble pile or a monolithic rock, and to estimate physical parameters such as unconfined compressive strength (UCS), rippability (the ease with which a material can be excavated) and porosity, which can all be directly inferred from seismic velocity.

The P-wave (compressional wave) and S-wave (shear wave) speeds are required to describe an elastic body, and can give the two elastic constants, Young's modulus and Poisson's ratio (Walker et al. 2015). The P-wave has a higher velocity than and arrives before the S-wave. If the source and receiver locations are known, the average seismic wave velocity can be determined from the distance between the locations and the travel time.

7.3.1 Source types

Seismic sources that can be used to generate waves include explosives, impactors (impulsive sources) and vibrators. Vibrators are commonly used in terrestrial seismic exploration (Bagaini et al. 2010), and typically involve a plate which contacts the ground and vibrates at a range of frequencies over a period of time known as a 'sweep' (for an example see Figure 59). The returning sound waves are cross-correlated with the known input sweep to generate a signal expected to result from a single impulsive source.

7.3.2 Designing a source

T The typical vibrating source can create signals with a bandwidth from about 5-100 Hz. Broadening the bandwidth by adding both low and high frequencies can enhance the resolution of seismic reflectors. Increasing the amount of low-frequency energy improves the ability to perform accurate seismic modelling and enables imaging of deep targets as low frequencies are attenuated less and propagate deeper than high frequencies. However, high frequencies have higher resolving power, which is why a spread of frequencies is desirable. Some small vibrating sources, such as that described by Haines (2006), can output frequencies of up to 1,000 Hz. However, with such a source, a received signal at a distance of 0.5 m has lost most data above 300 Hz, and at 12 m, most data above 100 Hz is lost.

Vibrational sources provide a degree of control of frequency spectra, and therefore resolution and imaging potential, that is not possible with explosive and impacting sources. Further, the vibrational source can be used multiple times and with customisable sweeps. Impulsive sources impart higher energy than vibrational sources and are ideal for maximising resolution (Bagaini et al. 2010), however vibrators can supply power over a long period to generate the same energy (Figure 60). These concepts are advantageous for a volume and mass constrained space exploration mission, and therefore vibrational sources are recommended for a mass constrained planetary science mission.

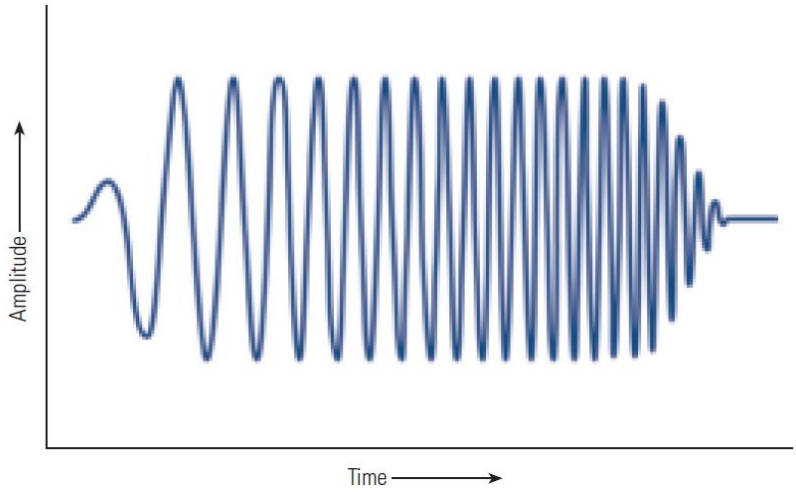

Figure 59 – A seismic sweep signal with increasing frequency over time, called an upsweep (Bagaini et al. 2010).

7.3.3 Resolving power

An understanding of the frequency of the waves and the speed at which the waves travel through a medium can be used to estimate the wavelength, which in turn allows the estimation of the smallest feature detectable and resolvable. This is an important concept to consider when planning an asteroid mission as it allows us to estimate whether features could be detected with typical seismic frequencies.

The resolution achievable through seismic waves in the vertical direction is equal to one-quarter of the wavelength. This is also the minimum distance between two boundaries such that they can be distinguished as separate features (Sheriff and Geldart 1995). The achievable resolution R is given by:

$$R = \frac{1}{4}\lambda = \frac{1}{4}\frac{V}{f} \qquad (20)$$

Where λ is the wavelength, V is the seismic velocity and f is the frequency of the seismic wave. Note that this estimation of resolution is a theoretical limit, as other factors such as receiver sampling rate, background/signal noise and preferential attenuation of higher frequencies will also impact the resolution.

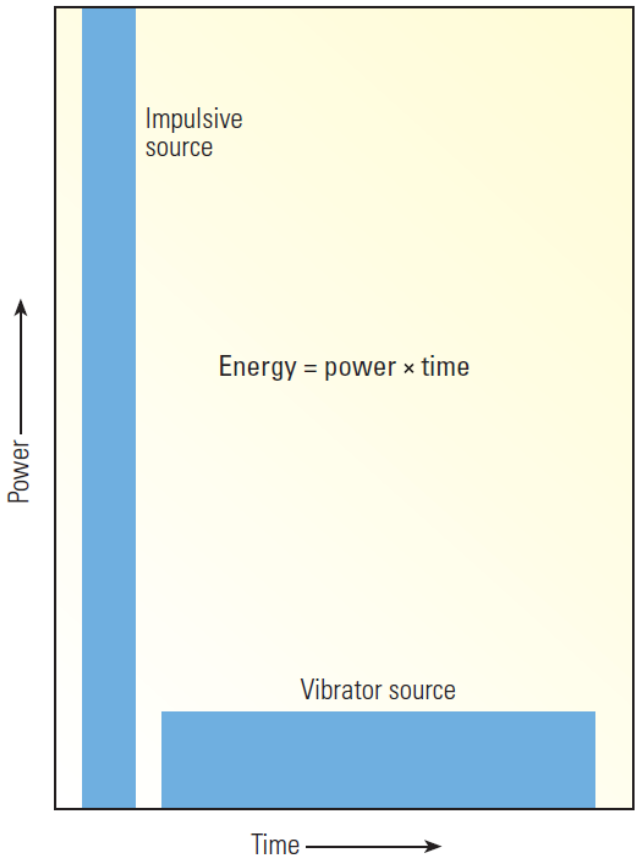

Figure 60 – The source energy of impulsive and vibrational sources. Impulsive sources have a large power input over a short period of time, and vibrating sources have the opposite, with both having the same total energy (Bagaini et al. 2010).

To estimate the resolution attainable through seismic, frequencies of 5, 50, and 100 Hz are applied to the velocities of various materials we might expect to see something similar to in asteroids in Table 17. Based on this analysis, it can be expected to resolve small features and layers in unconsolidated, low-velocity materials (around 0.5 m thick with 100 Hz), but not in more consolidated, high-velocity materials (around 15 m with 100 Hz). In practical terms, this might mean that one can map the thickness of unconsolidated, near-surface layers, but not the presence of any small or thin high-density features which could be high value, metal-rich zones.

Table 17 – Estimates of the minimum size of feature (in metres) detectable by a seismic wave with a given frequency in a given medium (Knapmeyer & Weber (2015)[a]; Press (1966)[b]).

	5 Hz	**50 Hz**	**100 Hz**
Lunar regolith (100 m/s)[a]	5	0.5	0.25
Brecciated lunar material (250 m/s)[a]	12.5	1.3	0.63
Basalt (5900 m/s)[b]	295	29.5	14.75

7.3.4 Challenges and risks with performing seismic on asteroids

It must be acknowledged that extraterrestrial seismic will suffer from significant constraints compared to terrestrial seismic, including, but not limited to: fewer sources and receivers due to cost, weight, and size constraints (Walker et al. 2015), a low gravitational pull of the host body, and an unknown environment together with the inability to easily calibrate data and test models with drill holes.

Seismic surveys performed on the Moon have revealed that received waves are scattered and lose all coherent character, likely due to significant fracturing in the near-surface (Knapmeyer and Weber 2015). It is expected that relatively small seismic sources on asteroids will produce sufficient signal for detection across the whole asteroid (Walker et al. 2015), though seismic

sources and receivers specifically for this mission are discussed in more detail in Section 7.5.3. However, if asteroids have similar subsurface characteristics as the Moon, as seems likely from imaging of asteroids such as Ryugu and Bennu (Otto et al. 2021; Lauretta et al. 2019), the received waves may also be similar, reducing imaging quality. Such a result could still be useful, as it reveals that the interior of the asteroid is heavily fractured or disjointed, and it will not impact the determination of velocity and therefore UCS and other characteristics. If the degree of wave scattering is sufficiently high, it may be difficult to identify wave information beyond the first arrival, which will make the determination of S-wave velocity and imaging difficult.

The first arrival may also be difficult to interpret given the slow onset of seismic wave events seen on the Moon, making the exact determination of P-wave arrival time and therefore P-wave velocity difficult. This will increase the uncertainty for the velocity and all subsequent inferences made using it. Despite this limitation, the active seismic data collected on the Moon was still used to identify the depth and velocity of subsurface layers (Kovach and Watkins 1973).

Seismic sources and receivers require 'coupling', or frictional contact, with the ground. There is a concern that the gravity on an asteroid will be too low for frictional forces to be strong enough to measure ground motion (Walker and Huebner 2004). This problem may be overcome by the size of the penetrator and the depth at which it is buried, though further modelling and testing will be required to prove this. Additionally, other solutions such as a fluid to be released and hardened in the regolith around the receiver, have been proposed to improve coupling (Walker and Huebner 2004).

Combined with a digital elevation model, accurate locations of sources and receivers are required for high-resolution subsurface imaging (or at least locations relative to each other). It is, therefore, preferable to target a NEO that has previously had its surface mapped to facilitate this.

7.4 Penetrators

While never successfully used on bodies other than Earth, penetrators have been proposed for several planetary science missions (Smrekar et al. 1999; Smith et al. 2012). Penetrators are designed to impact the surface of a planetary body to perform science that requires or is benefited by direct access to the subsurface. This removes the requirement for the probe to be soft-landed, which reduces the number of technical and financial constraints.

The proposed Lunar Net mission (Figure 61; Smith et al. 2012) was designed to survive impacts of up to 300 m/s in a range of materials including ice. It massed 13 kg and contained a full suite of science equipment. The penetrators would be buried 2 to 5 m into the lunar regolith after impact and have battery power for around 1 year. The depth of penetration for such probes is expected to be largely controlled by the surface materials, with ice content being a primary factor (Smrekar et al. 1999). Accelerometers can be used to estimate the depth a probe penetrates the regolith, its hardness, and the presence of layering (Smrekar et al. 1999).

It is suggested that 300 m/s may be the upper limit for penetrator survivability on impact (Ball et al. 2004), though a shock absorber component on the nose of the penetrator may significantly increase the feasible impact speed up to several km/s (Veldanov et al. 1999).

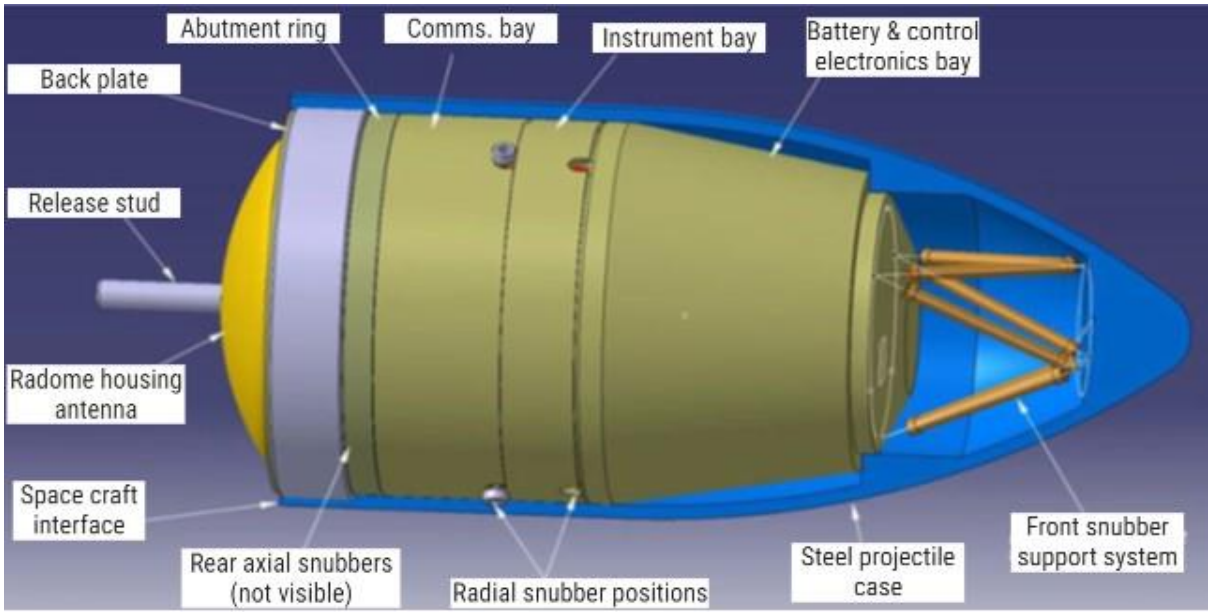

Figure 61 – The Lunar Net penetrator design. From Smith et al. (2012).

7.5. Equipment

7.5.1 Mothership

The penetrators will be kept in a mothership at the appropriate orbit until shortly before the NEO approaches Earth. The mothership will provide power, communications and may be used as a communications relay after the penetrators are deployed. Shortly before the NEO fly-by, the mothership will thrust to bring the relative velocity of the NEO to the spacecraft to 300 m/s for impact. The penetrators will then be ejected with a low-velocity spring to place them, noses facing forwards, in a line perpendicular to the path of the NEO.

After deploying the penetrators there are two options for the mothership. Either its orbit can be adjusted to intersect Earth's atmosphere and burn up, or it can be impacted into some other body. It is critical that the mothership does not collide with the NEO due to the risk of deflection, breakup and destroying the penetrators. Therefore, further work on mission operation design should be performed to eliminate this risk.

7.5.2 Penetrator

The penetrator model described above is based on the Lunar Net model due to its simple and robust design. While the science payload for this mission is different from that of the Lunar Net mission, the same mass of 13 kg is used for mission design.

Two or more penetrators should be used to increase the chance that at least one survives and can provide data, and so that the network can be used to measure seismic velocity and structure. However, at least five are recommended if mass and volume constraints allow. As the number of seismic sources and receivers increases, the imaging potential improves.

Using the probes as a seismic source/receiver network requires that the distance between the probes is known and that the onboard clocks are synchronised. The distance between the probes can be preset by positioning them at a known distance to each other just before the collision, which assumes a relatively flat surface on the scale of the penetrator. A more accurate positioning might be possible using another probe ahead of the asteroid with photometry, which can serve the dual purpose of relaying data to Earth if necessary. Given concerns about signal strength for data transmission a relay satellite may be necessary. If the asteroid has already had its surface mapped to some extent, a descent camera on each penetrator could provide accurate pinpointing of the impact location, as was suggested for the Lunar Net penetrators (Smith et al. 2012).

A key risk for the survivability of the penetrator is that the asteroid exterior will be monolithic, rather than covered in regolith as the probe would be unlikely to survive such an impact. It is expected that regolith is present on the surface of all asteroids greater than 200 m in diameter (Whiteley et al. 2000), and so by selecting a sufficiently large target, this risk can be mitigated.

A shock absorber should be included to increase the maximum achievable penetration velocity.

The science equipment onboard the penetrator will continue to take measurements and transmit data back to Earth for as long as possible. Battery life should be sufficient for an extended period of operation of around a year. Communications between the penetrator and Earth will be sent via the communications bay in the probe. This will be complicated by the slow rate of rotation of many asteroids, and so there may be a substantial length of time where the penetrator is in a dead zone. Attaining sufficient signal strength at greater distances from Earth is a concern that needs to be addressed, however, is beyond the scope of this thesis.

7.5.3 Seismic receiver and source

It is proposed that a variant of the Lunar Net seismic receiver (Smith et al. 2012) is used for the asteroid penetrators, after being fine-tuned to the more demanding requirements of receiving seismic signals on an asteroid. The receiver is suggested to have 3 components, meaning that they can measure ground movement in three dimensions. The seismic receiver in the Lunar Net penetrator proposal has a mass of 0.3 kg, a volume of 200 cm^3, a power requirement of 0.053 to 0.112 W, energy of 500 W h, and total data volume of ~5 Mbits (720 bps). The noise levels of the receiver are lowest in the 0.1 to 10 Hz range, and higher at frequencies lower and higher than this (Smith et al. 2012).

Multiple receivers could be mounted on each penetrator to stack the signals and improve signal to noise ratio. This will assist with reducing instrument noise but is unlikely to be beneficial for other sources of noise given they would be mounted on the same rigid body and be susceptible to the same external noise sources.

A vibrational source will be present in each probe so each can be used as a source, a receiver, or both. The small electromagnetic vibrating source described by Haines (Haines 2006) is still too large for a conventional penetrator (20.5 cm across), though it was developed with a small budget (~1,000 USD) and could be made smaller and more powerful with further development. As discussed in Section 7.3.4, relatively small sources are expected to be sufficient for detection across an asteroid, but further testing and modelling is required to demonstrate what signal can be received for given input energies and frequencies.

The Haines (2006) vibrating source is capable of producing sweeps with frequencies of 5 to 650 Hz, and is stated to have sufficient energy for recording data in terrestrial settings at distances of up to 20 m. While this could still be used to produce useful data if the penetrators are emplaced within this distance, it is not far enough to transmit a seismic wave that can be detected across most asteroids. A source will have to be developed to be smaller and more powerful than the Haines (2006) source, or other source options such as explosive and kinetic impacts will have to be considered.

The source and receiver will be entirely enclosed within the penetrator and will rely on sound waves being transmitted through the probe itself. The effects of this on the received signal will have to be tested in a known environment on Earth.

Panning and Kedar (2019) examined the feasibility of transmitting seismic waves through a rover to avoid externally placing seismic equipment. The transmission of waves appears to be effective for wave frequencies that are below the resonant frequency of the rover. The Curiosity Rover has a resonant frequency of around 3.5 Hz. The penetrator will be significantly smaller than the Curiosity Rover, and so would be expected to have a greater resonant frequency. 3.5 Hz therefore represents a lower bound for the maximum effective frequency

with seismic wave transmission through the penetrator. Testing on the penetrator itself should be performed to determine its resonant frequency and therefore upper bound for source frequency.

Given that the partially or completely buried nature of the penetrator as compared with a rover, it is possible that it will act like a buried geophone. The additional coupling between the sides of the penetrator and the regolith/rock may be enough such that the resonant frequency will not affect the seismic wave transmission.

7.5.4 Accelerometer

An accelerometer measures the rate at which the penetrator slows after it enters the regolith. The design will be based on the Lunar Net model (Smith et al. 2012) and will be used to estimate the rock/regolith strength and the presence of any layering.

The necessary accelerometer sampling rate required for a given spatial resolution and impact speed can be determined using the following equation:

$$S = \frac{v}{R} \qquad (21)$$

Where S is the minimum required sample rate in Hz, v is the impact velocity in m/s and R is the desired resolution in m.

7.5.5 Tiltmeter

A tiltmeter will be included based on the model in the proposed Lunar Net mission (Smith et al. 2012), which would be used to orientate and calibrate the receivers. The impact of a substantially lower gravity on an asteroid compared to the Moon on the tiltmeter will be tested.

7.5.6 Descent camera

This mission will use a descent camera on each penetrator, which will be used for determining the landing location based on any pre-existing imagery of the NEOs surface. The model of the camera used is based on that described in Smith et al. (Smith et al. 2012).

7.5.7 Neutron logging device

The Dynamic Albedo of Neutrons (DAN) experiment on the 2009 Mars Science Laboratory mission (the Curiosity rover) was used to determine the presence and distribution of water in the Martian subsurface to a depth of around 0.5-1 m (Litvak et al. 2008), and is ideal for use on an asteroid. The device is similar to a neutron log used in downhole terrestrial logging.

7.5.8 Launch vehicle

While a discussion of the launch vehicle and final thrust system hardware required for this mission is beyond the scope of this proposal, a medium-lift launch vehicle such as the Falcon 9 is likely required.

7.6 Target selection and intersection

To intersect the target NEO, the mothership will be put into orbit around Earth at an orbital radius matching the closest flyby distance of the NEO. The mothership will deploy the penetrator probes in a way such that the asteroid will pass through their location, causing them to impact the NEO. A schematic of this intersection method is shown in Figure 62.

Using the Jet Propulsion Laboratory (JPL) NEO online database (Benner 2016), NEO asteroids have a delta-V ranging from 3.82 – 26.79 km/s, and so the mothership and penetrators will have to substantially reduce their relative speed (increase relative to Earth) to bring it to within 0.3 km/s of the NEO.

Satellites in orbit around Earth already have some delta-V which can assist in achieving the rendezvous speed. To utilise this velocity, the instantaneous direction of satellite movement

should be close to the path of the NEO at the time of fly-by. To calculate the speed of a satellite at a given orbital distance around Earth, the following equation is used.

$$V = \sqrt{\frac{Gm_e}{r}} \qquad (22)$$

Where m_e is the mass of the Earth and r is the radius of the orbit from the centre of the Earth. For example, a satellite at an orbit of 200 km above the Earth's surface, or 6580 km from the centre, has a velocity of 7.79 km/s. A full range of satellite velocities vs radius from Earth's surface to one lunar distance (LD; 384,000 km) is available in Figure 63.

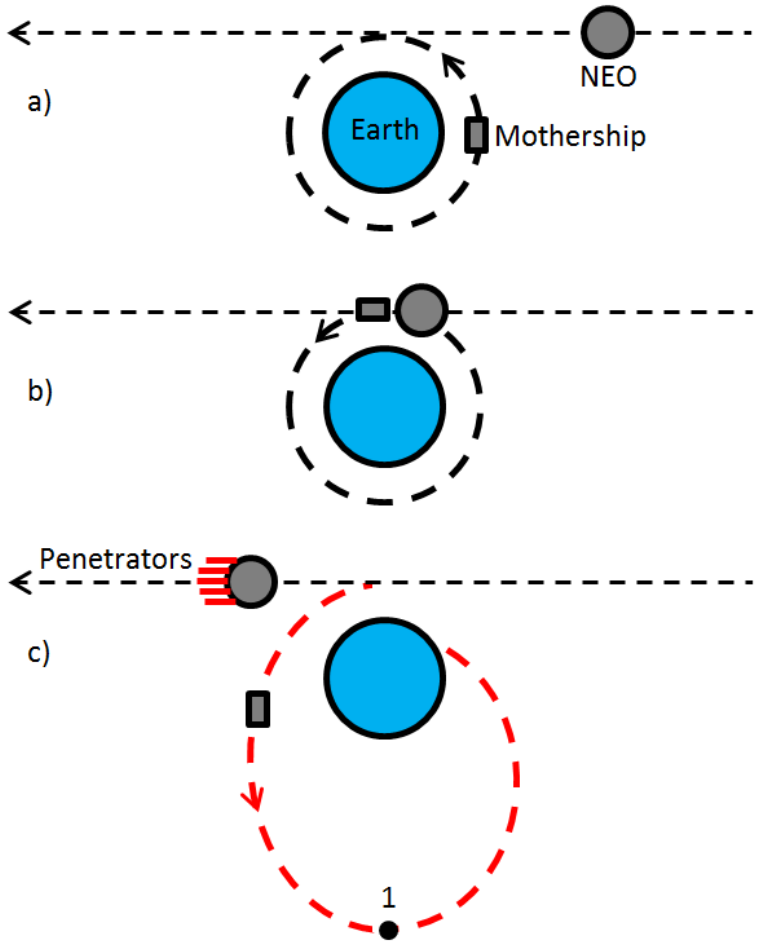

Figure 62 – Schematic of NEO intersection (not drawn to scale). a) The mothership is orbiting Earth such that it will near intersect the NEO, b) The mothership burns shortly before the NEO approach to reduce delta-V and intersect, c) Penetrators detach from the mothership and intersect NEO. Mothership deorbits by burning again at apoapsis (1) to reduce its speed and intersect Earth.

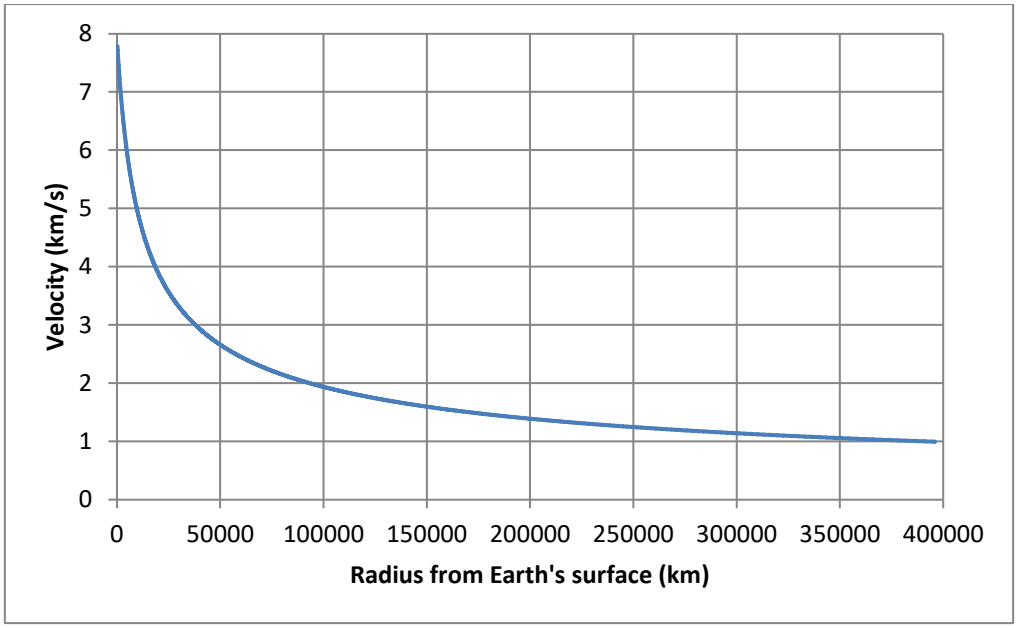

Figure 63 – Instantaneous velocity of satellites in Earth orbit at given radii.

From the JPL NEO database, the average delta-V of NEOs is 7.89 km/s. For a satellite, this speed corresponds to an orbital distance of under 200 km. The lowest delta-V for a NEO is 2018 AV2 with 3.758 km/s, which corresponds to a satellite orbital distance of 20,925 km (0.054 LD). For NEOs with a nearest approach to Earth of more than their corresponding satellite orbital distance (calculated from the NEOs delta-V) a combination of initial orbital velocity and additional thrust velocity will be required to reduce the difference in relative velocity between the NEO and the penetrator to within 300 m/s for a successful penetration.

The NEO 99942 Apophis is used as a case study to demonstrate the feasibility of such an intersection. Apophis has a diameter of 300 m (Shuvalov et al. 2017) and a delta-V of 5.685 km/s (https://echo.jpl.nasa.gov/~lance/delta_v/delta_v.rendezvous.html). In 2029 Apophis will approach Earth at the closest distance of ~0.1 Lunar distance (34,000 – 39,000 km; Shuvalov et al. 2017).

A satellite with an orbit of 38,440 km from Earth's surface will have a velocity of 2.98 km/s. If it is assumed that a penetrator can withstand an impact 0.3 km/s (potentially significantly

higher with a shock absorber), it will require an extra 4.14 km/s of thrust shortly before the impact. The mothership will take care of altering the orbit as estimates of the path of the NEO approach change. The Apophis fly-by of 2029 represents a tremendous opportunity for potentially cheap science and improved understanding of asteroid interior structure, and will be used as a case study.

Several variations to this mission can also be designed. One alternative design is to expand the target selection to include NEO asteroids passing further from Earth, which reduces the orbital speed of a satellite but also increases the chances of finding a NEO asteroid of appropriate size with low delta-V. Additionally, non-Earth crossing asteroids could also be targeted using the same probe design.

There is substantial uncertainty in the trajectory of NEOs ahead of time (Chodas et al. 2005), which will be reduced as more observations are made closer to the fly-by. The mothership will take care of altering the orbit as estimates of the path of the NEO approach change.

The Apophis fly-by of 2029 represents a tremendous opportunity for potentially cheap science and improved understanding of asteroid interior structure, as NEO approaches such as this only occur approximately once every 1,300 years (Chodas et al. 2005).

Several variations to this mission can also be designed. One alternative design is to expand the target selection to include NEO asteroids passing further from Earth, which reduces the orbital speed of a satellite but also increases the chances of finding a NEO asteroid of appropriate size with low delta-V. Additionally, non-Earth crossing asteroids could also be targeted using the same probe design.

7.7. Discussion

7.7.1 Interpretation of seismic data

As discussed in Section 7.3, having two or more probes on the surface of the asteroid with known separation distances will allow the P- and S-wave velocities of the near-surface material to be determined. These waves can be distinguished from each other by their wave character as determined by the 3-component receivers. This allows Young's modulus and Poisson's ratio to be determined, from which the material can be described. Also, with enough source and receiver locations, the presence and thickness of large-scale layering can be determined, as well as the seismic velocity of each layer. An example of this analysis performed on the Moon is discussed by Walker and Huebner (2004).

The UCS can also be estimated from seismic velocities (Butel et al. 2014) and can then be compared to estimates of rock/regolith strength from the accelerometer data. The rippability of the regolith and underlying rock or rubble can also be estimated using seismic velocity. However, rippability also depends on other parameters such as the type of rock or regolith, the degree of weathering, and the presence, spacing, size and type of joints and fractures (MacGregor et al. 1994).

As discussed in Section 7.3.4, wave scattering from a heavily fractured near-surface (as present on the lunar surface; Knapmeyer and Weber 2015) may be sufficiently great that it becomes difficult to determine any wave information beyond the first arrival (P-wave). This may result in the S-wave velocity being difficult or impossible to accurately determine even with processing. In this event, rock and regolith strength could still be estimated from P-wave velocity. However, it's predictive power becomes substantially diminished without the S-wave velocity.

Scattering may also result in imaging using reflected P-waves becoming increasingly difficult. However, basic imaging of subsurface features would still be plausibly expected given the success of determining the depth of regolith layers from first P-wave arrival on the Moon (Kovach and Watkins 1973).

If the data quality is sufficiently high, it could be used to determine whether the asteroid is monolithic, heavily fractured, or a rubble pile. As evidenced on the Moon, seismic data travelling through a heavily fractured medium is expected to undergo extreme scattering and attenuation, which can be determined from the received seismic signal (Knapmeyer and Weber 2015).

7.7.2 Interpretation of accelerometer data

Relationships have been developed between the accelerometer data and the geomechanical properties of the material being penetrated, such as material hardness. This relationship depends on several conditions, including the mass, shape, and size of the penetrator and the mechanical properties of the regolith.

The accelerometer data is first linked to the depth of penetration, and can then be related to the penetrability index, or hardness, using the methodology described by Lorenz et al. (2000). The use of this methodology will require calibration to the final probe design, which may be complicated by the presence of a shock absorber.

7.7.3 Interpretation of neutron log data

The neutron log will determine the presence and distribution of ice in the subsurface of the regolith at a maximum range of around 1 m around the penetrator (Litvak et al. 2008). The presence of water ice may suggest that the asteroid is prospective for mining, however, it could also suggest a high rippability, which will make the resources on the asteroid more

difficult to extract. The rippability of regolith will increase significantly with increasing ice concentration (Gertsch et al. 2006).

7.7.4 Momentum transfer of penetrators

Chesley and Spahr (2004) describe a simplified relation for the change in velocity required to move an asteroid fly-by path by 1 Earth radius.

$$\Delta v = \frac{0.035\ m\ s^{-1}}{T} \qquad (23)$$

Where T is the number of years into the future the asteroid fly-by occurs after the change in velocity is applied. While the true values show significant deviation from this relationship (around one order of magnitude in both directions), it can be used to provide a range of how much a NEO might be expected to shift path as the result of penetrators colliding with it, and whether there should be any cause for concern.

By calculating the change in velocity imparted on an asteroid due to the penetrators, it can be determined how much its path is likely to shift for future fly-bys. To do this, the mass and velocity of the penetrators are used to determine their momentum, then that momentum shift is applied to the asteroid to determine its change in velocity, assuming a 100% efficient transfer of momentum.

For a mission using five penetrators, the total impacting mass is expected to be approximately 65 kg. The equation for the momentum of a body is:

$$p = m\ v \qquad (24)$$

Where m is the mass of the body and v is its velocity. Therefore, the total momentum of the penetrators impacting at 300 m/s is 19,500 kg.m/s. Using Apophis' mass of 20 billion kg

(Shuvalov et al. 2017), the change in velocity of Apophis as a result of this momentum transfer is 9.75 * 10^{-7} m/s.

Using Equation 23, the delta-V required to move the fly-by path an asteroid by 1 Earth radius in 100 years is 0.00035 m/s. The delta-V of Apophis as a result of the proposed mission is 0.028% of 0.00035 m/s, and so the corresponding change in fly-by path 100 years after the mission is 17.75 km. After accounting for the spread of data from the relation in Equation 23, a range of possible path shifts of 1.775-177.5 km might be expected. Therefore, for a moderately sized asteroid and mission payload of this mass, there should be no concerns for inadvertently moving their path into an Earth intersecting orbit soon. As discussed in Section 7.1.3, highly porous asteroids are expected to be harder to deflect with kinetic impacts by up to two orders of magnitude in terms of energy required, and so inadvertently moving a porous asteroid into (or out of) a hazardous path is significantly more difficult.

This analysis does not consider the possibility of breaking up the asteroid through impact, and so a more detailed study should be undertaken before a mission of this nature is launched. As noted, however, such an analysis is still likely to be incomplete until the internal asteroid structure can be inferred.

7.8 Conclusions

This mission will provide useful information about one asteroid, but there is no guarantee that all asteroids will have a similar internal structure, even within the same asteroid class. Furthermore, it is unlikely that an asteroid that provides the opportunity characterise it in this way will be an asteroid that becomes a risk for collisions or is feasible to mine. Therefore, an attempt should be made to link easily acquired surface characteristics, such as their spectral signature and surface features, to the internal structure and characteristics, if such a link

exists. This would require multiple missions of this type to be carried out. If such a relationship can be discerned, it will be invaluable to planning deflection missions if a hazardous asteroid is discovered shortly before Earth collision, for example if an asteroid comes from a highly elliptical orbit, and for selecting targets for mining missions or further prospecting.

Understanding the structural and geomechanical properties of asteroids is critical for planning deflection, prospecting, and mining missions, but is currently an undeveloped field. Seismic is expected to be ideal for determining this information, and so a mission plan was designed and discussed in this chapter to undertake seismic exploration on a NEO. This mission plan includes a novel method of intersecting NEOs with penetrators to emplace vibrating seismic sources and receivers below the asteroid's surface. These tools, together with an accelerometer present on each probe, will be used to estimate UCS, rippability, porosity, and the presence, shape, and size of layering and other internal structures. A neutron logger will be used to measure the distribution of ice, which has implications for geomechanics and resource prospectivity.

This mission was discussed in the context of the 2029 fly-by of NEO Apophis. It is suggested that this fly-by presents a remarkable opportunity for potentially cheap science, which this design proposes to take advantage of. The probability of this mission inadvertently moving a moderately sized, otherwise harmless asteroid into an Earth-crossing path through momentum transfer is found to be exceedingly low.

Several additional experiments should be performed to confirm the validity of this mission and to calibrate relationships, such as the penetrability index, to the final probe design and the predicted asteroid properties. Further work is also required to develop an ideal launch vehicle and delivery system for the mission.

8. Use of remote sensing for seismic mission landing site selection

8.1 Introduction of remote sensing and landing site selection

The determination of landing site location is a critical part of any surface-landing space mission. The ideal landing site is a combination of area of scientific interest, ease of landing and access, and propellant constraints. Landing site committees and workshops are used by NASA and other space agencies for space exploration missions to determine an ideal landing location based on a variety of characteristics (Hinners 1972; Hinners 1973; Wilhelms 1986; Golombek et al. 2012; Golombek et al. 2016), including engineering and safety constraints (the relationship between the equipment technical capabilities and the local environment) and the potential for scientific payoff from that location. The concentration of dust and rocks, and the degree of slope at the surface impacts landing capability (Golombek et al. 2012). Landing site committees therefore use a dust index to determine an ideal location (Golombek et al. 2012; Golombek et al. 2016).

It is suggested that a remote sensing methodology might be devised to preselected sites on planetary bodies to undertake further and more detailed geophysical surveys such as seismic. This might involve using hyperspectral imagery to select an area with interesting chemical composition. For example, if regolith was determined to have a different spectral signature to solid rock, this might be used to dictate where a penetrator should land for survivability. Since hyperspectral imagery only targets the top 30 cm of a body, this assumes strong correlation between surface composition and subsurface features.

Remote sensing techniques might also be used to gain information about the body up to a depth of several metres. This will be especially useful for the exploration of asteroids and

comets, since little is currently known about their interiors (Walker et al. 2009; Huebner et al. 2001; Greenberg and Huebner 2002), as discussed in more detail in Chapter 3.

Regolith properties, particularly the size of grains, strongly influences the mechanical strength and temperature of near-surface layers (Gundlach and Blum 2013). If the average grain size of the regolith can be determined using remote sensing, ideal landing sites on asteroids or comets could potentially be selected prior to descent. For example, it might be beneficial to determine the presence/thickness of regolith layers for a penetrating probe mission as it can identify locations where the probe will be most likely to survive impact.

The underlying basement can be inferred by the characteristics of the overlying regolith, and the regolith is often largely formed from the underlying rock (Bhattacharya et al. 2015), implying that remote sensing can be used to scout for deeper targets of interest to be mapped with geophysics.

The Asteroid Impact and Deflection Assessment (AIDA) mission will use thermal infrared and spectral signature to infer regolith properties of the asteroid 65803 Didymos. The mission will contain a light detection and ranging (LiDAR) instrument, a hyperspectral imager, and a radio device (Michel et al. 2018).

This chapter seeks to examine the potential use of remote sensing to select landing sites for further exploration on planetary bodies and for other practices. The advantages and disadvantages of each method for generating useful data from a satellite or probe will be discussed.

8.2 LiDAR

LiDAR is a topographic mapping tool where an airborne or satellite mounted laser light is used to measure the distance between the tool and the ground by recording the time delay

between its output and input (Hodgson and Bresnahan 2004). The laser is typically fired in a sweep, where it scans back and forth perpendicular to the movement of the of carrier, creating a corridor or swath of 3D topography. LiDAR has been used for range finding, station keeping, atmospheric studies, and to create digital elevation maps of other planetary bodies in spaceflight, such as for the Moon (Smith et al. 1997; Smith et al. 2009) and Mars (Zuber et al. 1992). It could also be utilised to assist with landing site selection for a seismic mission, given the importance of local topography for landing site feasibility. See Figure 64 for lunar topographical data collected using LiDAR.

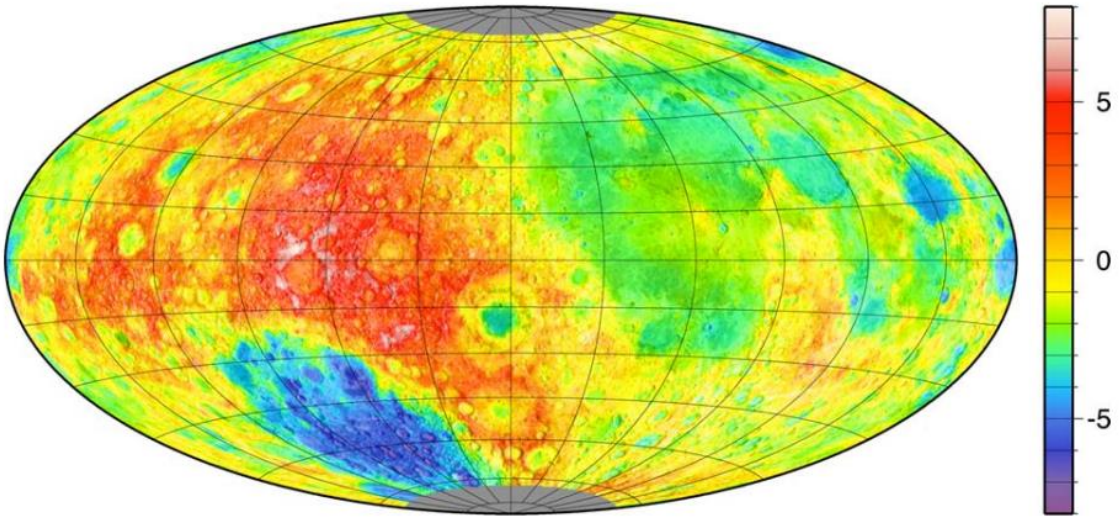

Figure 64 – Lunar topography as measured by the Clementine LiDAR device. Data were not recorded at the poles. Spatial accuracy is 100 m, and the topographical scale is in kilometres (Smith et al. 1997).

With sufficient spatial resolution, LiDAR can map the small-scale texture of the surface, such as individual regolith grains. Many LiDAR tools available today, such as the Lunar Reconnaissance Orbiter LiDAR with 10 cm surface resolution (Smith et al. 2009) do not have the required resolution to detect individual grains in typical off-Earth environments (such as the sub-millimetre grains of the lunar regolith; Papike and Simon 1982; Peters et al. 2008; Ballou et al. 1978; Christensen and Moore 1992). It should be noted that LiDAR technology,

and in particular LiDAR spatial resolution, is rapidly developing, and so the desired resolutions may be available in the near future.

The intensity of the returned signal can also be useful data. For example, the physical characteristics and the orientation of the plane of the surface might be inferred. The intensity of the returned LiDAR signal is used in terrestrial LiDAR studies to improve detection of features beneath forest canopies such as extent of flooding (Lang and McCarty 2009), and has potential for use in identifying differing surface characteristics such as mineralogy and regolith properties. Similar uses may be found for LiDAR signal strength in off-Earth studies, such as determining ice content in the near-surface regolith, however relationships between the signal strength and the phenomena being observed will need to be developed and calibrated prior to this, due to the difficulty of calibrating the measurements with surface samples at the location of interest.

An advantage of LiDAR over some other remote sensing techniques is that it does not require a natural source of light. For example, multispectral/hyperspectral imagery relies on natural light to be reflected off the surface. This may not be available at some locations, such as in permanently shadowed craters at the lunar poles. LiDAR is an active source remote sensing and can gain data from these permanently shadowed locations.

Unless a LiDAR tool becomes available with sufficient spatial resolution to detect individual regolith grains, the primary use of LiDAR for landing site selection is likely to be as a first pass tool to create an accurate 3D topography map and possibly to infer local mineralogy, especially in permanently shadowed locations where multispectral/hyperspectral imagery is not available. Multiple passes over areas of interest are recommended to reduce uncertainty.

As a drawback, LiDAR cannot gather any data on anything beneath the surface due to its low penetration and design.

8.3 Radar

Radar functions in a similar manner to LiDAR, with the key difference being that it uses radio waves instead of a laser (Scheer and Holm 2010). Typically, the radar antenna will function as both a transmitter and a receiver in a radar tool. Interferometric synthetic aperture radar (InSAR) involves the use of radar mounted on a plane or spacecraft to create 3D topographic images of a surface (Sharafzadeh et al. 2018). Radar has also been proposed for use of asteroids (Herique et al. 2018), given its potential for mapping the surface and subsurface and gain insight on their poorly understood interiors.

Many of the same considerations for LiDAR can be considered for radar, such as being able to use the intensity of the returned signal to gather more information about the surface. It also shares the limitation of LiDAR in that it cannot provide any information about anything below the surface, unlike some other geophysical and remote sensing tools. The role that it would fill in a mission to gather data for landing site location is also expected to be similar to the role of LiDAR. Other uses include surface subsidence monitoring over time using multiple passes to generate a 4D map of an area (Morgan et al. 2013; Figure 65).

8.4 Radio tomography

Radio tomography involves the use of low-frequency electromagnetic waves transmitted from an aeroplane or spacecraft (Kofman and Safaeinili 2004). The transmitted waves can penetrate typical subsurface materials, such as regolith, rock, and ice, to depths of up to several kilometres. These waves are reflected off features in the subsurface and received by the aeroplane or spacecraft in a manner similar to seismic (this is known as radio reflection

tomography). The primary material property investigated with this method is the electrical permittivity, a measure of how a material interacts with electromagnetic fields.

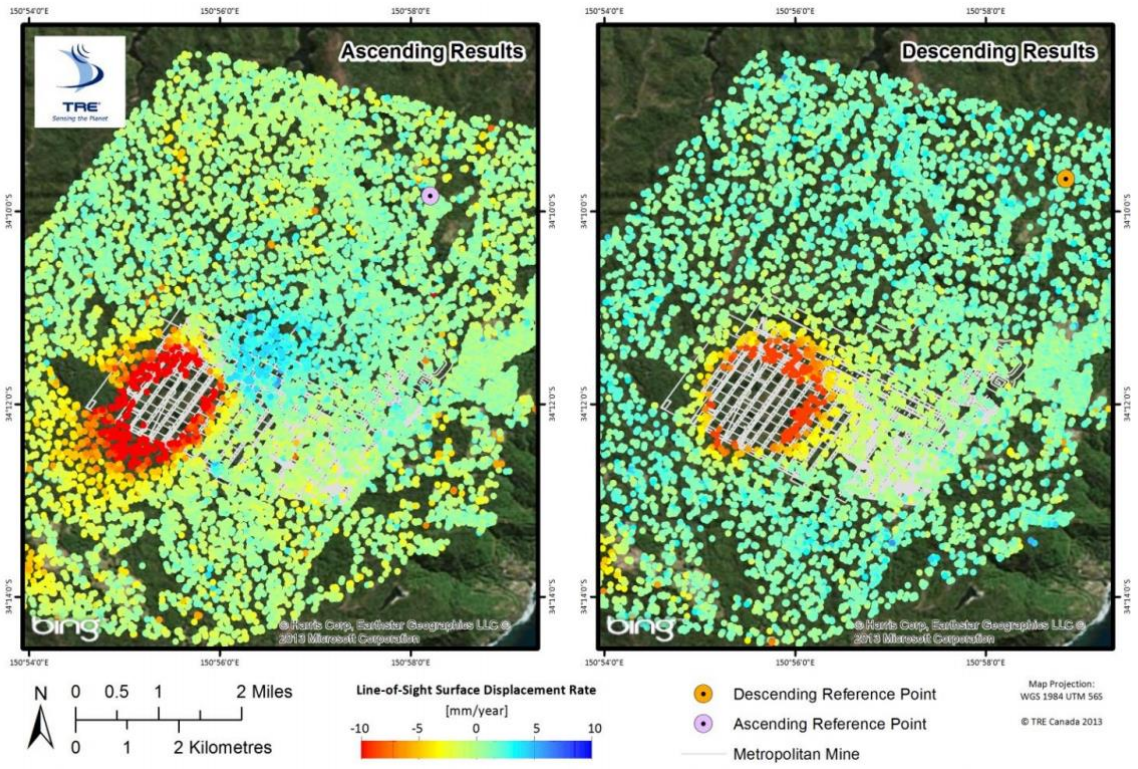

Figure 65 – Measured surface displacement at an active mine site in New South Wales, Australia, from satellite InSAR data, in millimetres per year (Morgan et al. 2013).

Plane-mounted radio reflection tomography has been used to measure the thickness of ice layers in glaciers on Earth (Gudmandsen et al. 1975) and in mineral exploration to infer the presence of metal deposits (Zhou et al. 1998; Figure 66). It has been suggested that radio tomography could be used to detect the presence and thickness of ice layers in the subsurface of other planetary bodies such as Mars and Europa (Kofman and Safaeinili 2004).

Radio transmission tomography is similar to radio reflection tomography; however, it relies on a receiver being located opposite the body being investigated from the source. This may be ideal for mapping small planetary bodies such as comets and asteroids. With enough passes, radio reflection and transmission tomography can build up a detailed 3D tomographic image of the subsurface (Kofman and Safaeinili 2004). This image could then be used to

identify major subsurface features. Source frequencies of 1-20 MHz are recommended for use on an asteroid to allow for sufficient penetration (Kofman and Safaeinili 2004).

The Mars Advanced Radar for Subsurface and Ionospheric Sounding (MARSIS) mission arrived at Mars in 2003 and was designed to investigate the subsurface up to a depth of 5 km to detect the presence of liquid water and map the subsurface geology using radio tomography (Picardi et al. 2004). It was able to provide evidence of subsurface geological features, such as buried basins (Watters et al. 2006).

The Comet Nucleus Sounding Experiment by Radio wave Transmission (CONSERT; Kofman et al. 1998) was placed on the ESA's Rosetta mission, which arrived at comet 67P/Churyumov-Gerasimenko in 2014 and used the radio transmission approach. The primary goal of CONSERT was to determine the dielectric and attenuation properties of 67P, and to estimate the extent of heterogeneity of the body. Radio tomography has also been proposed for use on asteroids (Su et al. 2016; Pursiainen and Kaasalainen 2013; Pursiainen and Kaasalainen 2014). Radar tomography is included in the proposed Castalia mission to the main belt comet 133P/Elst-Pizarro and would be used to map ice in its subsurface (Snodgrass et al. 2018).

Due to the relatively low resolution of radio tomography, it is not expected to directly assist in the selection of suitable landing sites for a seismic mission. However, it may assist with identifying locations of interest that might benefit from a seismic mission to achieve higher resolution of the subsurface.

8.5 Ground penetrating radar

Ground penetrating radar (GPR) functions similarly to radio reflection tomography in that a source is used to transmit electromagnetic waves which penetrate the subsurface, are reflected by features (such as changes in rock type), and are recorded by a receiver, either on

the surface or on a plane or spacecraft (Daniels 2005; Jol 2009). GPR typically uses much higher frequencies than radio tomography (in the microwave band, 3 to 30 GHz), which results in higher resolution but lower penetration depth. Penetration depth is especially limited in dry materials (Jol 2009).

GPR is ideal for near-surface archaeological investigations (Salvador and Conyers 2006; Conyers 2013), for the detection and mapping of shallow ice and water (Beres and Haeni 1991; Hinkel et al. 2001; Brandt et al. 2007; De Pascale 2008), and for civil engineering (Saarenketo and Scullion 2000). An example of a 2D GPR profile used for subsurface ice detection is shown in Figure 67.

GPR has seen some use in space missions. It was used to create a low-resolution structural map of the lunar subsurface up to 1,300 m (Porcello et al. 1974). During the Chang'E 3 and Chang'E 4 missions to the Moon, undertaken by the China National Space Administration (CNSA), rover mounted GPR was used to image the shallow subsurface lunar structure. The GPR on the Chang'E 3 rover allowed for detection of subsurface structure up to a depth of around 10 m (Ip et al. 2014; Fa et al. 2015). The GPR on the Chang'E 4 rover allowed for the imaging of several distinct geological layers (Li et al. 2020; Figure 68). GPR has also been proposed for use in Mars exploration to map subsurface structure and detect ice (Leuschen et al. 2003).

GPR will likely serve a similar role to that of radio tomography, except with a higher resolution and lower penetration depth. It will be useful to identify areas of interest for a seismic mission but will not be especially useful at directly assisting with optimal landing site selection.

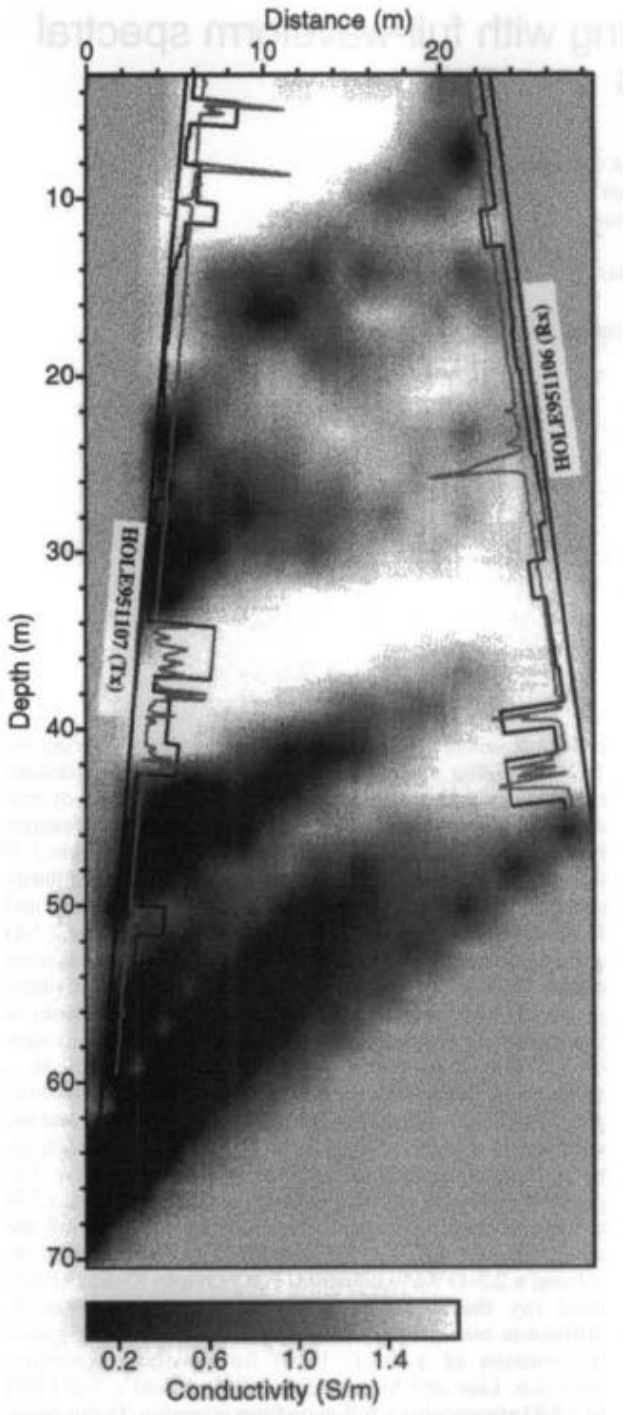

Figure 66 – Radio tomography conductivity data taken at Mt Isa with the source suspended down one drill hole, and the receiver suspended down the other. Copper grade (dark curve) and magnetic susceptibility (light curve) from other measurements are superimposed for both drill holes (Zhou et al. 1998).

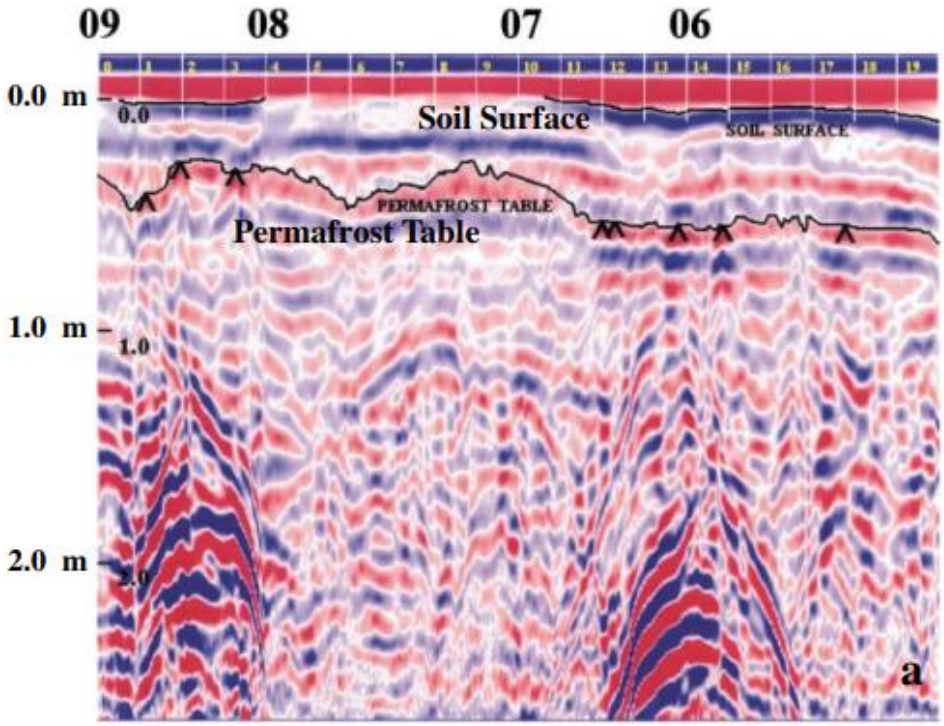

Figure 67 – A 2D GPR profile 20 metres long and 2.5 metres deep used to interpret the depth of permafrost at Barrow, Alaska (Hinkel et al. 2001).

8.6 Spectral imaging

Spectral imaging is a type of imaging that collects multiple bands of electromagnetic wave frequencies for analysis, rather than just visible light. The relative amplitudes of these frequency bands are analysed to gain information about the surface materials (Manolakis et al. 2016). Spectral imaging devices can be handheld but are often mounted to airplanes and spacecraft to map the surface of the Earth or some other planetary body. In a manner similar to LiDAR and radar, spectral imaging is used to build up a 2D image of the spectral signature of the surface over an area. Multispectral imaging captures light in three to fifteen spectral bands, while hyperspectral imaging captures a full spectrum of the magnitude of each frequency of light.

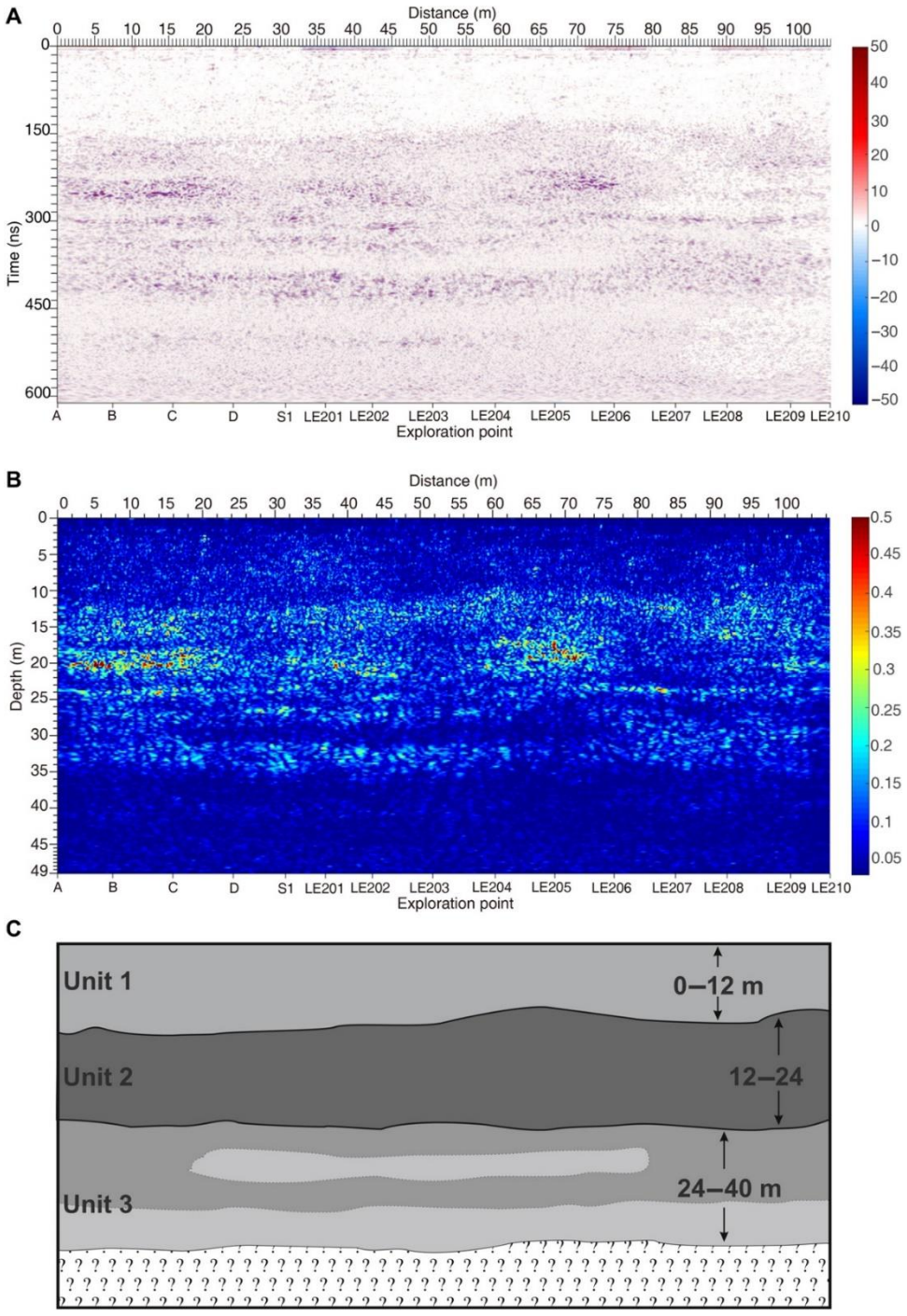

Figure 68 – GPR data from the Chang'E 4 Lunar mission. A) shows the GPR data after processing, B) shows a tomographic reconstruction of the data, and C) shows an interpretation of the data with three distinct geological layers (Li et al. 2020).

The measured spectral signature may be compared to a library of known spectral signatures of materials as measured in a laboratory to infer the material that is present at the surface. Lau and co-workers (2003) used a combination of soil samples and airborne surveys to

examine the hyperspectral signature over a region in South Australia to develop an understanding of the distribution of materials present in the regolith. Hörig and co-workers (2001) used hyperspectral imagery to detect the presence of near-surface hydrocarbons in a region. Kruse and co-workers (1990) used a 63-channel imaging spectrometer to map mineral concentrations in Nevada, USA, and Sabins (1999) also used spectral imagery for mineral exploration in Nevada (Figure 69). Remote sensing spectral imaging may also be used for environmental monitoring and military operations (Gat et al. 1996).

A major limitation of spectral imaging is that the surface regolith is not always representative of the underlying regolith and rock, and so care should be taken in inferring subsurface features from the surface data. Hyperspectral imagery typically collects data from a depth of up to 30 cm (Manolakis et al. 2016).

There is evidence that grain size plays a role in the reflectance of the surface (Bras and Erard 2003), which indicates that hyperspectral imagery could be used to estimate the grain size distribution and presence of regolith at the surface. Spectral imagery has also been used in space exploration to determine the extent of weathering of the surface on planetary bodies (Clark et al. 2002). Areas with a lower extent of weathering may represent fresh outcrop, which could represent an ideal landing site for some landing methods (such as conventional landers), or unideal for others (such as penetrating probes). Singer and Roush (1985) identified a possible relationship between the spectral data and the surface temperature of asteroids and Johnson and Fanale (1973) identified a potential relationship between spectral data and the surface grain size of asteroids, though it remains to be seen if these relationships can be successfully applied across the surface of a single body to generate a map, rather than just producing a bulk estimate of the grain size and temperature of the body.

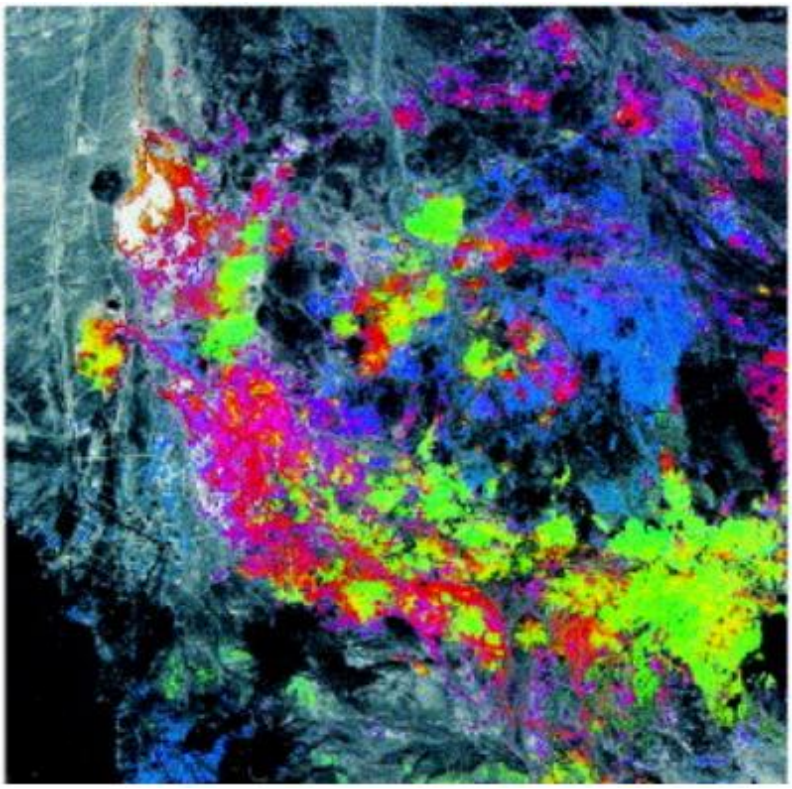

Figure 69 – Composite colour image of mineral abundance as inferred from satellite-based spectral imaging from a site in Nevada, USA. Illite = red, alunte = green, kaolinite = blue (Sabins 1999).

Spectral imaging data may be used to identify locations of interest on off-Earth bodies which might benefit from a method of investigation with a deeper penetration depth, such as radio tomography, GPR or seismic. Telescope based spectral imaging could also be used to identify asteroids or comets with a bulk surface expression of interest, such as having a particular ice or mineral concentration.

8.7 Thermal inertia

Thermal inertia is the inverse of the speed at which a body approaches the temperature of its surroundings. Thermal inertia has been estimated across the surface of Mars from orbit at 5° resolution by the Mars Global Surveyor Thermal Emission Spectrometer (Putzig and Mellon 2007).

Gundlach and Blum (2013) developed a methodology to estimate the average grain size of regolith at the surface of a body using thermal inertia. They performed this analysis for several

asteroids and Moons across the Solar System and found that there is some correlation between asteroid size and mean surface grain size, with larger asteroids having finer grain sizes. It may be possible to use this workflow in reverse to give a rough estimate of the mean grain size of an asteroid based on its size. While this study had one grain size estimate for each planetary body, it may be possible for this methodology to be used with a greater spatial resolution to assist with landing site selection. In lieu of this, the methodology may still be useful to identify asteroids with a sufficiently small average grain size to suggest that they may be ideal targets for a penetrating probe.

8.8 Proposal for a remote sensing mission to select a landing site for a seismic mission

This section will outline a proposal for how remote sensing tools could be used to select a landing site on an off-Earth body for a seismic mission, with examples given for a conventional lander and a penetrating probe. To enable multiple locations on a given planetary body to be examined in one mission the remote sensing equipment should be mounted to a space probe which will make multiple orbits around the body.

First, a target body of interest will be identified, for example the Moon, Mars, an asteroid or comet. Any existing remote sensing, geophysical or surface data from previous missions will be examined alongside Earth-based data such as telescope observations. Once the locations of interest are identified, a space probe with a suite of remote sensing equipment may be sent to the target body to investigate the locations of interest.

The space probe should be equipped with LiDAR, radar, radio tomography, GPR, hyperspectral imaging and temperature sensors to determine thermal inertia. The radio tomography and GPR will be used to image the subsurface and identify any features of interest that may benefit from further investigation with seismic, which would allow for

higher resolution imaging and the inference of geomechanical properties. The hyperspectral imagery will achieve a similar goal, but for the surface material. The composition of the near-surface may be inferred which may result in identifying a feature of interest that seismic could investigate further. LiDAR and radar will be used to generate a high-resolution topographical map which may be used to select an ideal landing location within the area of interest. With sufficient spatial resolution the presence and concentration of boulders and rubble may be identified. Finally, thermal inertia measurements and inferences from hyperspectral imagery may assist in determining the average grain size of regolith at the surface, allowing for predictions on the stability of the surface and the degree of dust to determine whether the location meets engineering and safety requirements. This process is visualised as a workflow in Figure 70.

A mission as outlined in this proposal is not likely to be necessary for a seismic mission to the Moon or Mars as there are already geophysical and remote sensing datasets available across all or much of their surface. Rather than sending a new mission, these existing data may be analysed for the same purpose of landing site selection.

8.9 Conclusion of remote sensing and landing site selection

There are a wide range of remote sensing techniques that could be used for understanding the surface and subsurface of other planetary bodies without requiring surface contact. While these methods lack either the penetration depth or the vertical resolution of seismic (or both), they can still be used to gather valuable information and assist with the selection of landing sites for seismic missions. They can assist with identifying regions of scientific interest and determining whether a landing site meets the safety and engineering constraints of the mission and lander.

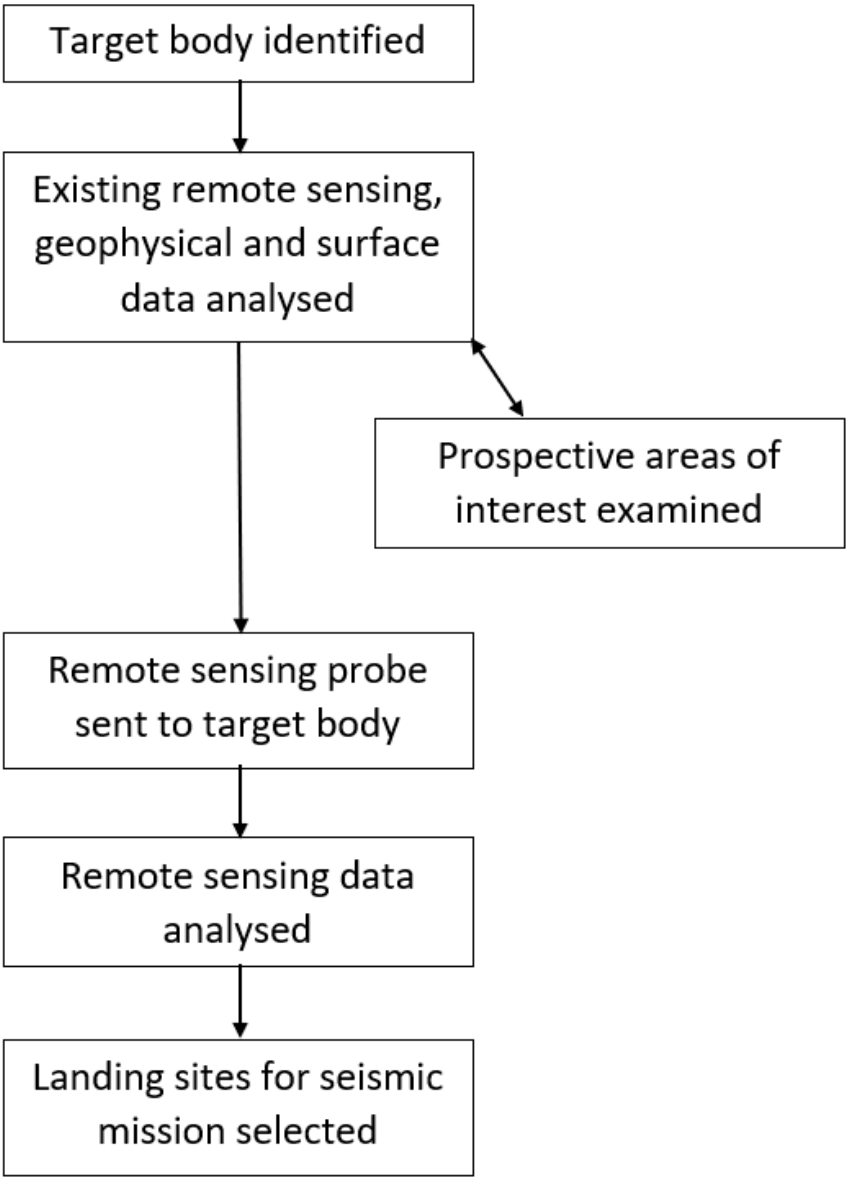

Figure 70 – Flowchart of how remote sensing data could be used to support the selection of landing site for a seismic mission as outlined in Section 8.8.

Radio tomography, ground penetrating and spectral imagery all have the potential to identify points of interest on a planetary body for a seismic mission to investigate further. Spectral imagery has the additional advantage of potentially being useful for determining the feasibility of landing, or the ideal landing method at a given location. LiDAR and radar techniques are ideal for developing a 3D topographic map to further assist with landing site

selection, and thermal inertia techniques may assist with selecting a planetary body of interest.

A proposal for a remote sensing mission to select a landing site for a seismic mission in the form of a lander or a penetrating probe has been outlined and will strongly assist in enabling the seismic mission to achieve the maximum value.

9. Conclusions and recommendations

9.1 Conclusions

In this thesis, the seismic techniques have been described, and the relevant literature on the use of seismic in Earth and space exploration was reviewed. Laboratory tests were performed at both UNSW in Sydney, New South Wales (NSW), Australia and the Jet Propulsion Laboratory (JPL) Caltech/NASA in Pasadena, California, USA to explore how seismic might be used in an off-Earth environment, and what the effects of the space environment are on seismic data collection. A new apparatus was developed for these experiments called the Seismic Apparatus for Fine-Grained Sediment (SAFGS), and regolith simulants based on lunar (ALRS-1) and Mars (MMS) regolith properties were used. The impact of the smaller grain size of these regolith simulants compared to Earth regolith, and the impact of a reduced atmospheric pressure were both assessed. Computational and analytical modelling were explored to validate and expand upon the laboratory results.

Based on the literature review and the results from the laboratory and modelling work, this chapter summarises the major findings of this thesis, and makes recommendations for further research that would expand on this work.

9.2 Major outcomes

- Seismic has been used on Earth to produce a wide range of outputs useful to resource prospecting and exploration, mining and environmental applications, including inferring rock and soil type, strength porosity and other geomechanical properties, producing 3D and 4D representations of subsurface features and structure, detecting the presence and orientation of fractures, and determining the point of origin and source of natural seismic events. Terrestrial mining operations often use drilling for sampling and exploration; however, a drilling program is expensive. It will likely be

infeasible in the near future for use on other planetary bodies such as the Moon. There is, therefore, a great potential to use seismic on other planetary bodies to understand their interior cheaply and easily. This thesis provides a critical review of seismic techniques and their usefulness and opens a new opportunity to investigate the potential of seismic in space seismic applications.

- Seismic techniques have seen some limited use on Mars and the Moon; however, they have not been used on asteroids or comets to date. There is an opportunity to learn more about the interior of planetary bodies, particularly small planetary bodies given the complete lack of knowledge of their internal structure and geomechanics. Understanding the genesis and history of planetary bodies, determining whether off-Earth mining is feasible for a given body/location, selecting an ideal mining method, and determining how to deflect an asteroid that threatens Earth all require a detailed understanding of the internal structure and geomechanics of the body, and seismic provides an ideal technique to determine this. Therefore, this thesis presents and reviews the ways in which seismic could be used to gain useful insights into the interior of planetary bodies.
- A novel method for measuring the seismic properties of uncompressed fine-grained regolith called the seismic apparatus for fine-grained sediment (SAFGS) was developed and tested with several off-Earth regolith simulants based on lunar (ALRS-1) and Mars (MMS) properties. Such a method is completely innovative for the seismic industry and other end-users, and will provide a solution for space mission designers to test their equipment in simulated off-Earth environments. The ALRS-1 simulant was measured to have an average P-wave velocity of 98.6 m/s, which is comparable to the existing *in-situ* measurements of near-surface lunar regolith on the Moon of 104 m/s

and 114 m/s during the Apollo 14 and Apollo 16 missions, respectively (Kovach and Watkins 1973). The P-wave velocity of the MMS regolith was measured with three different mean grain sizes, and a possible relationship was found between increasing grain size and increasing velocity, with the MMS dust having a mean velocity of 61.3 m/s, small-grain MMS having 244.5 m/s, and medium-grain MMS having 271.2 m/s. These results will be valuable for comparisons for any *in-situ* measurements of near-surface Mars regolith in the future.

- As the air pressure approaches Mars atmospheric pressure, the measured P-wave velocity of the MMS regolith simulant decreases. This has led to the preliminary conclusion that the measured velocity of low velocity dry regoliths such as those found off-Earth is partly controlled by the gas in the pore spaces. This contradicts the current understanding based on regoliths found on Earth, where the gas in the pore spaces appear to have no effect. It is expected that this is the result of the regolith simulants having P-wave velocities lower than air, which is rare for a sediment. More research and tests need to be performed to verify this hypothesis. However, if it is confirmed, it may revolutionise the field of soil mechanics and seismic investigation of soils, as it will show that much existing literature is based on an incorrect assumption about the relationship of grain properties and the seismic velocity of soil.
- Increased compaction of the regolith samples was not found to have a strong effect on P-wave velocity, which is in contrast with what would be expected based on the literature. This is likely due to the result of compaction reducing the pore space, removing the gas, and thus, reducing the velocity. This is a ground-breaking discovery and is one of the key contributions of this thesis, as it may identify a major gap in existing soil mechanics literature that has simply not been discovered to date due to

insufficient work with low velocity regoliths. Future tests with low velocity regolith in differing conditions such as low atmospheric pressure and high compaction will aid in confirming or disproving this hypothesis.

- Computational finite element and analytical modelling works were explored to validate and expand upon the laboratory measurements of P-wave velocity of regolith. The computational modelling with Abaqus was successfully performed but could only determine a lower bound for the velocity of the regolith due to technical limitations of the software. Conventional analytical modelling could provide limited outcomes due to a lack of existing relationships between seismic velocity and grain properties for dry, unconsolidated regolith in low confining pressure in the literature. Relationships between seismic velocity and the grain size distribution parameters d_{50}, C_u and C_c were developed from the experimental results presented in this thesis. Of these, d_{50} and C_u are promising. This work supports the hypothesis that increasing mean grain size affects P-wave seismic velocity, which is in contrast with existing literature, and would represent a major discovery if confirmed by future work.
- The possibility of using penetrating probes to emplace seismic equipment on off-Earth bodies was explored and is a promising way to overcome some of the challenges of using seismic off-Earth. A mission was proposed to deliver seismic equipment to an asteroid using penetrating probes, which would allow for seismic equipment to be rapidly emplaced on an off-Earth body. Rapid emplacement is particularly important in the event of an asteroid or comet on a collision course with Earth, as it will allow for rapid determination of the best method of deflection.
- The use of other geophysical and remote sensing tools to support a seismic mission and assist in identifying points of interest and landing sites was explored, including

LiDAR, radar, radio tomography, ground penetrating radar, spectral imagery and thermal inertia measurement. Radio tomography, ground penetrating radar and spectral imagery are expected to be useful for identifying areas of interest for a seismic mission to follow up on, and LiDAR, radar and thermal inertia are expected to be useful for identifying optimum landing sites based on technical requirements such as presence of regolith, with spectral imagery and ground penetrating radar being useful for this to a lesser extent.

9.3 Recommendations for further research

- The experiments performed as part of this thesis were all performed in a laboratory environment. Efforts were made to recreate a natural and realistic environment; however, further field tests on Earth may be useful to validate and improve upon the existing results. Directly emplacing the piezoelectric transducers used in this thesis into the ground and measuring the seismic velocity of terrestrial environments will be useful.
- The effect of varying gravity on seismic data collection is largely unquantified and was outside the scope of this thesis to examine. This could be examined via computer modelling, or via experiments in a drop chamber or on a parabolic jet, where effective weightlessness is achieved for short periods of time. The facilities to perform the latter option were not available, and therefore, could not be performed. It would be useful to identify the role of gravity on the seismic velocity and data quality in the same way that the role of atmospheric pressure was explored in this thesis.
- Further experiments should be designed to explore the hypothesis presented by this thesis that the measured P-wave velocity of low velocity sediments is partially controlled by the gas present in pore spaces. This might include saturating the pore

spaces with gases other than air with varying velocities, controlling and varying the pore space, and performing more tests in a vacuum chamber with varying atmospheric pressure.

- Future work to measure the P-wave velocity of dry regoliths at atmospheric pressure with known grain size distributions is expected to improve the accuracy of the relationships developed in Chapter 6. Currently, this work is limited by a lack of existing samples of this nature in the literature with P-wave velocity and grain size distribution measurements.

References

A'Hearn. M.F., Belton, M.J.S., Delamere, W.A., Kissel, J., Klaasen, K.P., McFadden, L.A., Meech, K.J., Melosh, H.J., Schultz, P.H., Sunshine, J.M., Thomas, P.C., Veverka, J., Yeomans, D.K., Baca, M.W., Busko, I., Crockett, C.J., Collins, S.M., Desnoyer, M., Eberhardy, C.A., Ernst, C.M., Farnham, T.L., Feaga, L., Groussin, O., Hampton, D., Ipatov, S.I., Li, J-Y., Lindler, D., Lisse, C.M., Mastrodemos, N., Owen Jr., W.M., Richardson, J.E., Wellnitz, D.D. and White, R.L. 2005, Deep Impact: Excavating comet Tempel 1, *Science* 310: 258-264.

Abe, S., Mukai, T., Hirata, N., Barnouin-Jha, O.S., Cheng, A.F., Demura, H., Gaskell, R.W., Hashimoto, T., Hiraoka, K., Honda, T., Kubota, T., Matsuoka, M., Mizuno, T., Nakamura, R., Scheeres, D.J. and Yoshikawa, M. 2006, Mass and local topography measurements of Itokawa by Hayabusa, *Science* 312: 1344-1347.

Abzalov, M.Z. 2012, Sandstone-hosted uranium deposits amenable for exploitation by *in situ* leaching technologies, *Applied Earth Science* 121: 55-64.

Ahrens, T.J. and Harris, A.W. 1994, Deflection and fragmentation of NEAs, in: T. Gehrels, M.S. Matthews, and A.M. Schumann, (Eds.), Hazards due to Comets and Asteroids, Vol. 24, University of Arizona Press, pp. 897-928.

Anderson, D.L., Miller, W.F., Latham, G.V., Nakamura, Y., Toksöz, M.N., Dainty, A.M., Duennebier, F.K., Lazarewicz, A.R., Kovach, R.L. and Knight, T.C. 1977, Seismology on Mars, *Journal of Geophysical Research*, 82: 4524-4546.

Anderson, R.C., Scheeres, D., Chelsey S. and the BASiX Team 2014, Binary asteroid in-situ explorer mission (BASiX): A mission concept to explore a binary near Earth asteroid system, 45th Lunar and Planetary Science Conference, The Woodlands, Texas, 17 – 21 March.

Annan, A.P. and Cosway S.W. 1992, Ground penetrating radar survey design, 5th EEGS Symposium on the Application of Geophysics to Engineering and Environmental Problems, European Association of Geoscientists and Engineers, Expanded Abstracts, 329-352.

Arrhenius, G., Asunmaa, S.K. and Fitzgerald, R.W. 1972, Electrostatic properties of lunar regolith, in: C. Watkins (Ed.), Lunar Science III, The Lunar Science Institute, Houston, Texas, pp. 30-32.

Ars, J-M., Tarits, P., Hautot, S., Bellanger, M., Coutant, O. and Maia, M. 2019, Joint inversion of gravity and surface wave data constrained by magnetotelluric: Application to deep geothermal exploration of crustal fault zone in felsic basement, *Geothermics* 80: 56-68.

Asphaug, E. 2014, Asteroid structure, Asteroids, Comets, Meteors Conference Proceedings, Helsinki, Finland, 30 June – 4 July.

Ata, S., Bournival, G. and Manefield, M. 2015, Resource recovery in space, Third International Future Mining Conference, Sydney, NSW, 4-6 November, 275-279.

Badescu, V. 2013, Asteroids: Prospective energy and material resources. Springer Science & Business Media.

Bagaini, C., Bunting, T., El-Emam, A., Laake, A. and Strobbia, C. 2010, Land seismic techniques for high-quality data, *Oilfield Review* 2: 28-39.

Ball, A.J., Lognonné, P., Seiferlin, K. Pätzol, M. and Spohn, T. 2004, Lander and penetrator science for near-Earth object mitigation studies, in: M.J.S. Belton, T.H. Morgan, N. Samarasinha, D.K. Yeomans (Eds.), Mitigation of Hazardous Comets and Asteroids, Cambridge University Press, Cambridge, pp. 266-291.

Ballou, E.V., Wood, P.C., Wydeven, T., Lehwalt, M.E. and Mack, R.E. 1978, Chemical interpretation of Viking Lander 1 life detection experiment. *Nature* 271: 644-645.

Banerdt, W., Kaiser, W. and Vanzandt, T. 1993, A microseismometer for terrestrial and extraterrestrial applications, Workshop on Advanced Technologies for Planetary Instruments, Fairfax, VA.

Banerdt, W.B., Smrekar, S.E., Banfield, D., Giardini, D., Golombek, M., Johnson, C.L., Lognonné, P., Spiga, A., Spohn, T., Perrin, C., Stähler, S.C., Antonangeli, D., Asmar, S., Beghein, C., Bowles, N., Bozdag, E., Chi P., Christensen, U., Clinton, J., Collins, G.S., Daubar, I., Dehant, V., Drilleau, M., Fillingim, M., Folkner, W., Garcia, R.F., Garvin, J., Grant, J., Grott, M., Grygorczuk, J., Hudson, T., Irving, J.C.E., Kargl, G., Kawamura, T., Kedar, S., King, S., Knapmeyer-Endrun, B., Knapmeyer, M., Lemmon, M., Lorenz, R., Maki, J.N., Margerin, L., McLennan, S.C., Michaut, C., Mimoun, D., Mittelholz, A., Mocquet, A., Morgan, P., Mueller, N.T., Murdoch, N., Nagihara, S., Newman, C., Nimmo, F., Panning, M., Pike, W.T., Plesa, A.C., Rodriguez, S., Rodriguez-Manfredi, J.A., Russell, C.T., Schmerr, N., Siegler, M., Stanley, S., Stutzmann, E., Teanby, N., Tromp, J., van Driel, M., Warner, N., Weber, R. and Wieczorek, M. 2020, Initial results from the InSight mission on Mars, *Nature Geoscience* 13: 183-189.

Barak, S., Bahroudi, A. and Jozanikohan, G. 2018, Exploration of Kahang porphyry copper deposit using advanced integration of geological, remote sensing, geochemical, and magnetics data, *Journal of Mining and Engineering* 9: 19-39.

Beckstead, N. 2013, On the overwhelming importance of shaping the far future, PhD dissertation, Rutgers University-Graduate School-New Brunswick.

Bell, D.W. and Shirley, D.J. 1980, Temperature variation of the acoustical properties of laboratory sediments, *Journal of the Acoustical Society of America* 68: 227-231.

Belton, M.J.S., Morgan, T.H., Samarasinha, N. and Yeomans, D.K. (Eds.) 2004, Mitigation of Hazardous Comets and Asteroids, Cambridge University Press, Cambridge.

Ben-Menahem, A. and Singh, S.J. 2012, Seismic Waves and Sources, Springer Science & Business Media.

Benner, L.A.M. 2018, *Near-Earth asteroid delta-V for spacecraft rendezvous*, Jet Propulsion Laboratory, California Institute of Technology, (accessed 20/04/2020) <https://echo.jpl.nasa.gov/~lance/delta_v/delta_v.rendezvous.html>.

Beres, M. Jr. and Haeni, F.P. 1991, Application of ground-penetrating-radar methods in hydrogeologic studies, *Ground Water* 29: 375-386.

Bernold, L.E. 2013, An Australian lunar soil simulant to study lunar mining and construction, Off-Earth Mining Forum, UNSW Sydney, Australia, 19-21 February.

Bhattacharya, A., Porwal, A., Dhingra, S., De, S. and Venkataraman, G. 2015, Remote estimation of dielectric permittivity of lunar surface regolith using compact polarimetric synthetic aperture radar data, Advances in Space Research 56: 2439-2448.

Biele, J., Ulamec, S., Maibaum, M., Roll, R., Witte, L., Jurado, E., Muñoz, P., Arnold, W., Auster, H-U., Casas, C., Faber, C., Fantinati, C., Finke, F., Fischer, H-H., Geurts, K., G*üttler, C., Heinisch, P., Herique, A., Hviid, S., Kargl, G., Knapmeyer, M., Knollenberg, J., Kofman, W., K*ömle, N., K*ührt, E., Lommatsch, V., Mottola, S., de Santayana, R.P., Remetean, E., Scholten, F., Seidensticker, K.J., Sierks, H. and Spohn, T.* 2015, The landing(s) of Philae and inferences about comet surface mechanical properties, *Science* 349: aaa9816.

Binley, A. and Kemna, A. 2005, DC resistivity and induced polarization methods, In: S.S. Hubbard, Y. Rubin (Eds.), Hydrogeophysics, Springer, Dordrecht, pp. 129-156.

Blair, B.R. 2000, The role of near-Earth asteroids in long-term platinum supply, Space Resources Roundtable II, 1-15.

Boehnhardt, H., Bibring, J-P., Apathy, I., Auster, H.U., Finzi, A.E., Goesmann, F., Klingelhöfer, G., Knapmeyer, M., Kofman, W., Krüger, H., Mottola, S., Schmidt, W., Seidensticker, K., Spohn, T. and Wright, I. 2017, The Philae lander mission and science overview, *Philosophical Transactions of the Royal Society A: Mathematical, Physical and Engineering Sciences* 375: 20160248.

Bonanno, A. and Bernold, L.E. 2015, Exploratory review of sintered lunar soil based on the results of the thermal analysis of a lunar soil simulant, *Journal of Aerospace Engineering* 28: DOI:10.1051/(ASCE)AS.1943-5525.0000428.

Bosch, M., Mukerji, T. and Gonzalez, E.F. 2010, Seismic inversion for reservoir properties combining statistical rock physics and geostatistics: A review, *Geophysics* 75: 165-176.

Boschetti, F., Dentith, M.D. and List, R.D. 1996, A fractal-based algorithm for detecting first arrivals on seismic traces, *Geophysics* 61: 1095-1102.

Bostrom, N. 2001, Existential risks: Analyzing human extinction scenarios and related hazards, *Journal of Evolution and Technology* 9.

Bostrom, N. 2003, Astronomical waste: The opportunity cost of delayed technological development, *Utilitas* 15: 308-314.

Bottke Jr, W.F., Morbidelli, A. and Jedicke, R., Recent progress in interpreting the nature of the near-Earth object population, in: M.J.S., Belton, T.H. Morgan, N. Samarasinha, D.K. Yeomans (Eds.), Mitigation of Hazardous Comets and Asteroids, Cambridge University Press, Cambridge, 2004, pp. 1–21.

Bourbié, T., Coussy, O., Zinszner, B. and Junger, M.C. 1987, Acoustics of porous media: Editions Technip.

Bowles, J.E. 1988, Foundation analysis and design, McGraw-Hill.

Brandt, O., Langley, K., Kohler, J. and Hamran, S-E. 2007, Detection of buried ice and sediment layers in permafrost using multi-frequency ground penetrating radar: A case examination on Svalbard, *Remote Sensing of Environment* 111: 212-227.

Bras, A.L. and Erard, S. 2003, Reflectance spectra of regolith analogs in the mid-infrared: effects of grain size, Planetary and Space Science 51: 281-294.

Brown, A. 2003, Improved interpretation of wireline pressure data, *AAPG Bulletin* 87: 295-311.

Buddensiek, M-L. 2009, Seismic imaging of sandbox models, PhD. Thesis, Free University of Berlin, Berlin, Germany.

Budynas, R.G. and Nisbett, J.K. 2011, Shigley's mechanical engineering design, New York: McGraw-Hill.

Butel, N., Hossack, A. & Kizil, M.S. 2014, Prediction of in situ rock strength using sonic velocity, *14th Coal Operators Conference*, University of Wollongong, The Australasian Institute of Mining and Metallurgy & Mine Managers Association of Australia, 2014, 89-102.

Byrne, S., Dundas, C.M., Kennedy, M.R., Mellon, M.T., McEwen, A.S., Cull, S.C., Daubar, I.J., Shean, D.E., Seelos, K.D., Murchie, S.L., Cantor, B.A., Arvidson, R.E., Edgett, K.S., Reufer, A., Thomas, N., Harrison, T.N., Posiolova, L.V. and Seelo, F.P. 2009, Distribution of mid-latitude ground ice on Mars from new impact craters, *Science* 325: 1674-1676.

Cai, Z. and Bathurst, R.J. 1995, Seismic response analysis of geosynthetic reinforced soil segmental retaining walls by finite element method, *Computers and Geotechnics* 17: 523-546.

Calió, I., Marletta, M. and Pantó, B. 2012, A new discrete element model for the evaluation of the seismic behaviour of unreinforced masonry buildings, *Engineering Structures* 40: 327-338.

Caltech 2007, Delta-V in the solar system, (accessed 14/05/2020) <https://web.archive.org/web/20070701211813/http:/www.pma.caltech.edu:80/~chirata/deltav.html>.

Campbell, W.C. 1997, Introduction to geomagnetic fields, Cambridge University Press.

Carcione, J.M. and Seriani, G. 1998, Seismic and ultrasonic velocities in permafrost, *Geophysical Prospecting* 46: 441-454.

Carmen, G., Werner, S.C., Saltus, R. and Maus, S. 2011, Circum-Arctic mapping project: new magnetic and gravity anomaly maps of the Arctic, *Geological Society, London, Memoirs* 35: 39-48.

Carrier, W.D. 1973, Lunar soil grain size distribution, *The Moon* 6: 250-263.

Casanova, S., Espejel, C., Dempster, A.G., Anderson, R.C., Caprarelli, G. and Saydam, S. 2020, Lunar polar water resource exploration – Examination of the lunar cold trap reservoir system model and introduction of play-based exploration (PBE) techniques, *Planetary and Space Science* 180: 104742.

Cavcar, M. 2000, The international standard atmosphere (ISA). Anadolu University, Turkey.

Chambers, J.E., Kuras, O., Meldrum, P.I., Ogilvy, R.D. and Hollands, J. 2006, Electrical resistivity tomography applied to geologic, hydrogeologic, and engineering investigations at a former waste-disposal site, *Geophysics* 71: 231-239.

Chang, P.Y., Chen, C.C., Chang, S.K., Wang, T.B., Wang, C.Y. and Hsu, S.K. 2012, An investigation into the debris flow induced by Typhoon Morakot in the Siaolin Area, Southern Taiwan, using the electrical resistivity imaging method, *Geophysics Journal International* 188: 1012-1024.

Chatterjee, K., Choudhury, D. and Poulos, H.G. 2015, Seismic analysis of laterally loaded pile under influence of vertical loading using finite element method, *Computers and Geotechnics* 67: 172-186.

Chave, A.D. and Jones, A.G. 2012, The Magnetotelluric Method: Theory and Practice, Cambridge University Press.

Cheng, A.F., Rivkin, A.S. Reed, C., Barnouin, O., Fletcher, Z. and Ernst, C. 2013, AIDA: Asteroid impact & deflection assessment, IAC-13-A3.4.8, 64th International Astronautical Congress, Beijing, China, 23 – 27 September.

Cheng, A.F., Rivkin, A.S., Michel, P., Atchison, J., Barnouin, O., Benner, L., Chabot, N.L., Ernst, C., Fahnestock, E.G., Kueppers, M., Pravec, P., Rainey, E., Richardson, D.C., Stickle, A.M. and Thomas, C. 2018, AIDA DART asteroid deflection test: Planetary defense and science objectives, *Planetary and Space Science* 157: 104-115.

Chesley, S.R. and Spahr, T.B. 2004, Earth impactors: orbital characteristics and warning times, in: M.J.S., Belton, T.H. Morgan, N. Samarasinha, D.K. Yeomans (Eds.), Mitigation of Hazardous Comets and Asteroids, Cambridge University Press, Cambridge, pp. 22–37.

Chodas, P., Chesley, S., Giorgini, J. and Yeomans, D. 2005, Radar Observations Refine the Future Motion of Asteroid 2004 MN4, (accessed 15/06/2016) <http://neo.jpl.nasa.gov/news/news149.html/>.

Christensen, P.R. and Moore, H.J. 1992, The martian surface layer. In: Kiefer, H.H., Jakovsky, B.M., Snyder, C.W., Matthews, M.S. (Eds.), Mars. University of Arizona Press, Tucson, pp. 686-729.

Ciarletti, V., Corbel, C., Plettemeier, D., Cais, P., Clifford, S.M. and Hamran, S-E. 2011, *IEEE Proceedings*, 99: 824-836.

Clark, B.E., Hapke, B., Pieters, C. and Britt, D. 2002, Asteroid space weathering and regolith evolution, *Asteroids III* 585: 90086-2.

Clark, S. 2020, European Space Agency awards Hera asteroid mission to German firm, (accessed 16/10/2020) <https://www.theguardian.com/science/2020/sep/17/european-space-agency-awards-asteroid-mission-german-firm>.

Cockell, C. and Horneck, G. 2004, A planetary park system for Mars, *Space Policy* 20: 291-295.

Cockell, C. and Horneck, G. 2006, Planetary parks: Formulating a wilderness policy for planetary bodies, *Space Policy* 16: 205-211.

Cockell, C.S. 2006, The ethical relevance of earth-like extrasolar planets, *Environmental Ethics* 28: 303-314.

Conyers, L.B. 2013, Ground-penetrating radar for archaeology, Altamira Press.

Cooper, M.R., Kovach, R.L. and Watkins, J.S. 1974, Lunar near-surface structure. *Reviews of Geophysics and Space Physics* 12: 291-308.

Cox, M.M. and Battista, J.R. 2005, *Deinococcus radiodurans* – the consummate survivor, *Microbiology* 3: 882-892.

Craig, G.A., Saydam, S. and Dempster, A.G. 2014, Mining off-Earth minerals: a long-term play?, 2014 SOMP Annual Meeting, The Southern African Institute of Mining and Metallurgy, pp. 167-182.

Crawford, I.A. 2015, Lunar resources: A review, *Progress in Physical Geography* 39: 137-167.

Cumming, W. and Mackie, R. 2010, Resistivity imaging of geothermal resources using 1D, 2D and 3D MT inversion and TDEM static shift correction illustrated by a Glass Mountain case history, Proceedings World Geothermal Congress, Indonesia, Bali, 25-29.

Dahlman, O. and Israelson, H. 2016, Monitoring underground nuclear explosions, Elsevier.

Dainty, A.M., Toksöz, M.N., Anderson, K.R., Pines, P.J., Nakamura, Y. and Latham, G. 1974, Seismic scattering and shallow structure of the Moon in Oceanus Procellarum, *Moon* 9: 11-29.

Dallas, J.A., Raval, S., Alvarez Gaitan, J.P., Saydam, S. and Dempster, A.G. 2020, The environmental impact of emissions from space launches: A comprehensive review, *Journal of Cleaner Production* 255: 120209.

Daniels, D.J. 2005, Ground penetrating radar, Encyclopedia of RF and Microwave Engineering, John Wiley & Sons.

Daubar, I., Lognonné, P., Teanby, N.A., Miljkovic, K., Stevanović, J., Vaubaillon, J., Kenda, B., Kawamura, T., Clinton, J., Lucas, A., Drilleau, M., Yana, C., Collins, G.S., Banfield, D., Golombek, M., Kedar, S., Schmerr, N., Garcia, R., Rodriguez, S., Gudkova, T., May, S., Banks, M., Maki, J., Sansom, E., Karakostas, F., Panning, M., Fuji, N., Wookey, J., van Driel, M., Lemmon, M., Ansan, V., Böse, M., Stähler, S., Kanamori, H., Richardson, J., Smrekar, S. and Banerdt, W.B. 2018, Impact-seismic investigations of the InSight mission, *Space Science Reviews* 214: 1-68.

De Basabe, J.D. and Sen, M.K. 2009, New Developments in the finite-element method for seismic modeling, *The Leading Edge* 28: 562-567.

De Pascale, G.P., Pollard, W.H. and Williams, K.K. 2008, Geophysical mapping of ground ice using a combination of capacitive coupled resistivity and ground-penetrating radar, Northwest Territories, Canada, *Journal of Geophysical Research* 113: (F2).

DellaGiustina, D.N., Kaplan, H.H., Simon, A.A., Bottke, W.F., Avdellidou, C., Delbo, M., Ballouz, R-L., Golish, D.R., Walsh, K.J., Popescu, M., Campins, H., Barucci, M.A., Poggiali, G., Daly, R.T., Le Corre, L., Hamilton, V.E., Porter,

N., Jawin, E.R., McCoy, T.J., Connolly Jr, H.C., Rizos Garcia, J.L., Tatsumi, E., de Leon, J., Licandro, J., Fornasier, S., Daly, M.G., Al Asad, M.M., Philpott, L., Seabrook, J., Barnouin, O.S., Clark, B.E., Nolan, M.C., Howell, E.S., Binzel, R.P., Rizk, B., Reuter, D.C. and Lauretta, D.S. 2020, Exogenic basalt on asteroid (101955) Bennu, *Nature Astronomy*: 1-8.

Dewart, G. 1968, Seismic investigation of ice properties and bedrock topography at the confluence of two glaciers, Kaskawulsh Glacier, Yukon Territory, Canada, Dissertation, The Ohio State University.

Dreyer, C.B., Sercel, J., Gertsch, L. and Lampe, A. 2016, Optical mining subscale testing, *Earth and Space 2016: Engineering for Extreme Environments*, Reston, VA: American Society of Civil Engineers: 493-506.

DSI 2013, Commercial asteroid hunters announce plans for new robotic exploration fleet, [Press release], 22 January.

Dubinin, E.M., Pissarenko, N., Barabash, S.V., Zacharov, A.V., Lundin, R., Koskinen, H., Schwingenshuh, K. and Yeroshenko, Y.G. 1991, Tails of Phobos and Deimos in the solar wind and in the martian magnetosphere, *Planetary Space Science* 39: 123-130.

Duennebier, F. and Sutton, G.H. 1974, Thermal moonquakes, *Journal of Geophysical Research* 79: 4351-4363.

Duennebier, F., Dorman, J., Lammlein, D., Latham, G. and Nakamura, Y. 1975, Meteoroid flux from passive seismic experiment data, *Proceedings of the 6th Lunar Science Conference*, 2417-2426.

Durand-Manterola, H.J. and Cordero-Tercero, G. 2014, Assessments of the energy, mass and size of the Chicxulub Impactor, *arXiv preprint arXiv* 1403.6391.

Eaton, S.R. 2004, Exploration Technology Goes to Mars: Mini-Seismic for the 'Rosetta Stone', AAPG Explorer, (accessed 24/06/2016) <https://archives.aapg.org/explorer/2004/05may/mars_expl.cfm/>.

Eberhart-Phillips, D., Han, D-H. and Zoback, M.D. 1989, Empirical relationships among seismic velocity, effective pressure, porosity, and clay content in sandstone, *Geophysics* 54: 82-89.

Eckhardt, E.A. 1940, A brief history of the gravity method of prospecting for oil, *Geophysics* 5: 231-242.

Ehlmann, B.L., Edgett, K.S., Sutter, B., Achilles, C.N., Litvak, M.L., Lapotre, M.G.A., Sullivan, R., Fraeman, A.A., Arvidson, R.E., Blake, D.F., Bridges, N.T., Conrad, P.G., Cousin, A., Downs, R.T., Gabriel, T.S.J., Gellert, R., Hamilton, V.E., Hardgrove, C., Johnson, J.R., Kuhn, S., Mahaffy, P.R., Maurice, S., McHenry, M., Meslin, P-Y., Ming, D.W., Minitti, M.E., Morookian, J.M., Morris, R.V., O'Connell-Cooper, C.D., Pinet, P.C., Rowland, S.K., Schröder, S., Siebach, K.L., Stein, N.T., Thompson, L.M., Vaniman, D.T., Vasavada, A.R., Wellington, D.F., Wiens, R.C. and Yen, A.S. 2017, Chemistry, mineralogy, and grain properties at Namib and High dunes, Bagnold dune field, Gale Crater, Mars: A synthesis of Curiosity rover observations, *Journal of Geophysical Research: Planets* 122: 2510-2543.

El Shamy, U. and Zamani, N. 2012, Discrete element method simulations of the seismic response of shallow foundations including soil-foundation-structure interaction, *International Journal for Numerical and Analytical Methods in Geomechanics* 36: 1303-1329.

Emery, J.P., Fernández, Y.R., Kelley, M.S.P., Warden, K.T., Hergenrother, C., Lauretta, D.S., Drake, M.J., Campins, H. and Ziffer, J. 2014, Thermal infrared observations and thermophysical characterization of OSIRIS-REx target asteroid (101955) Bennu, *Icarus* 234: 17-35.

Enos, B. 2020, OSIRIS-REx TAGs surface of asteroid Bennu, NASA, (accessed 23/10/2020) <https://www.nasa.gov/feature/goddard/2020/osiris-rex-tags-surface-of-asteroid-bennu/>.

Ernst, C.M. and Schultz, P.H. 2007, Evolution of the Deep Impact flash: Implications for the nucleus surface based on laboratory experiments, *Icarus* 190: 334-344.

Fa, W. and Jin, Y-Q. 2007, Quantitative estimation of helium-3 spatial distribution in the lunar regolith layer, *Icarus* 190: 15-23.

Fa, W. and Jin, Y-Q. 2010, Global inventory of Helium-3 in lunar regoliths estimated by a multi-channel microwave radiometer on the Chang-E 1 lunar satellite, *Chinese Science Bulletin* 55: 4005-4009.

Fa, W-Z., Zhu, M-H., Liu, T-T and Plescia, J-B. 2015, Regolith stratigraphy at the Chang'E-3 landing site as seen by lunar penetrating radar, *Geophysical Research Letters* 42: 10,179-10,187.

Fanale, F.P. and Salvail, J. 1990, Evolution of the water regime of Phobos, *Icarus* 120: 140-157.

Feldman, W.C., Maurice, S., Lawrence, D.J., Little, R.C., Lawson, S.L., Gasnault, O., Wiens, R.C., Barraclough, B.L., Elphic, R.C., Prettyman, T.H., Steinberg, J.T. and Binder, A.B. 2001, Evidence for water ice near the lunar poles, Journal of Geophysical Research: Planets 106: 23231-23251.

Feng, Z-Y., Lo, C-M. and Lin, Q-F. 2017, The characteristics of the seismic signals induced by landslides using a coupling of discrete element and finite difference methods, Landslides 14: 661-674.

Finzi, A.E., Zazzera, F.B., Dainese, C., Malnati, F., Magnani, P.G., Re, E., Bologna, P., Espinasse, S. and Olivieri, A. 2007, SD2 – How to sample a comet, Space Science Reviews 128: 281-299.

Fogg, M.J. 2011, Terraforming Mars: A review of concepts, Advances in Space Research 22: 2217-2225.

Franqui, A., Seufert, S. and Okutsu, M. 2019, Seismic investigation of icy crust covering subsurface oceans of Europa and Ganymede: Preliminary assessment of hypothetical experiment using impactor, *Acta Astronautica* 155: 170-178.

Frohlich, C. and Nakamura, Y. 2006, Possible extra-solar-system cause for certain lunar seismic events, *Icarus* 185: 21-28.

Garnock, B. and Bernold, L. 2012, Experimental study of hollow-core beams made with waterless concrete, *13th ASCE Aerospace Division Conference on Engineering, Science, Construction, and Operations in Challenging Environments,* Pasadena, California, United States.

Gat, N., Subramanian, S., Bargen, J. and Toomarian, N. 1996, Spectral imaging application: Remote sensing, environmental monitoring, medicine, military operations, factory automation and manufacturing, 25th AIPR Workshop: Emerging Applications of Computer Vision proceedings, 63-77.

Gazoty, A., Fiandaca, G., Pedersen, J., Auken, E. and Christiansen, A.V. 2012, Mapping of landfills using time-domain spectral induced polarization data: the Eskelund case study, *Near Surface Geophysics* 10: 575-586.

Gehrels, T., Matthews, M.S. and Schumann, A.M. (Eds.) 1994, Hazards due to Comets and Asteroids, Vol. 24, University of Arizona Press.

Gertsch, L., Gustafson, R. and Gertsch, R. 2006, Effect of water ice content on excavatability of lunar regolith, *AIP Conference Proceedings* 813: 1093-1100.

Gertsch, L.S. and Gertsch, R.E. 2003, Surface mine design and planning for lunar regolith production, *AIP Conference Proceedings* 654: 1108-1115.

Gertsch, R.E. 1992, Asteroid Mining.

Giardini, D., Lognonné, P., Banerdt, W.B., Pike, W.T., Christensen, U., Ceylan, S., Clinton, J.F., van Driel, M., Stähler, S.C., Böse, M., Garcia, R.F., Khan, A., Panning, M., Perrin, C., Banfield, D., Beucler, E., Charalambous, C., Euchner, F., Horleston, A., Jacob, A., Kawamura, T., Kedar, S., Mainsant, G., Scholz, J-R., Smrekar, S.E., Spiga, A., Agard, C., Antonangeli, D., Barkaoui, S., Barrett, E., Combes, P., Conejero, V., Daubar, I., Drilleau, M., Ferrier, C., Gabsi, T., Gudkova, T., Hurst, K., Karakostas, F., King, S., Knapmeyer, M., Knapmeyer-Endrun, B., Llorca-Cejudo, R., Lucas, A., Luno, L., Margerin, L., McClean, J.B., Mimoun, D., Murdoch, N., Nimmo, F., Nonon, M., Pardo, C., Rivoldini, A., Rodriguez-Manfredi, J.A., Samuel, H., Schimmel, M., Stott, A.E., Stutzmann, E., Teanby, N., Warren, T., Weber, R.C., Wieczorek, M. and Yana, C. 2020, The seismicity of Mars, *Nature Geoscience* 13: 205-212.

Gibbings, A. 2011, A smart cloud approach to asteroid deflection, IAC-11.A3.4, 62nd International Aeronautical Congress, Cape Town, South Africa.

Goins, N.R. and Lazarewicz, A.R. 1979, Martian seismicity, *Geophysical Research Letters* 6: 368-370.

Golombek, M., Grant, J., Kipp, D., Vasavada, A., Kirk, R., Fergason, R., Bellutta, P., Calef, F., Larsen, K., Katayama, Y., Huertas, A., Beyer, R., Chen, A., Parker, T., Pollard, B., Lee, S., Sun, Y., Hoover, R., Sladek, H., Grotzinger, J., Welch, R., Noe Dobrea, E., Michalski, J., Watkins, M. 2012, Selection of the Mars Science Laboratory landing site, *Space Science Reviews* 170: 641-737.

Golombek, M.P. Grott, M., Kargl, G., Andrade, J., Marshall, J., Warner, N., Teanby, N.A., Ansan, V., Hauber, E., Voigt, J., Lichtenheldt, R., Knapmeyer-Endrun, B., Daubar, I.J., Kipp, D., Muller, N., Lognonné, P., Schmelzbach, C., Banfield, D., Trebi-Ollennu, A., Maki, J., Kedar, S., Mimoun, D., Murdoch, N., Piqueux, S., Delage, P., Pike, W.T., Charalambous, C., Lorenz, R., Fayon, L., Lucas, A., Rodriguez, S., Morgan, P., Spiga, A., Panning, M., Spohn, T., Smrekar, S., Gudkova, T., Garcia, R., Giardini, D., Christensen, U., Nicollier, T., Sollberger, D., Robertsson, J., Ali, K., Kenda, B. and Banerdt, W.B. 2018, Geology and physical properties investigations by the InSight lander, *Space Science Reviews* 214: 1-52.

Golombek, M.P. Kipp, D., Warner, N., Daubar, I.J., Fergason, R., Kirk, R.L., Beyer, R., Huertas, A., Piqueux, S., Putzig, N.E., Campbell, B.A., Morgan, G.A., Charalambous, C., Pike, W.T., Gwinner, K., Calef, F., Kass, D., Mischna, M., Ashley, J., Bloom, C., Wigton, N., Hare, T., Schwartz, C., Gengl, H., Redmond, L., Trautman, M., Sweeney, J., Grima, C., Smith, I.B., Sklyanskiy, E., Lisano, M., Benardini, J., Smrekar, S., Lognonné, P. and Banerdt, W.B. 2017, Selection of the InSight landing site, *Space Science Reviews* 211: 5-95.

Golombek, M.P., Banerdt, W.B., Tanaka, K.L. and Tralli, D.M. 1992, A prediction of Mars seismicity from surface faulting, *Science* 258: 979-981.

Graham, J.M. 2004, The biological terraforming of Mars: Planetary ecosynthesis as ecological succession on a global scale, Astrobiology 4: 168-195.

Graves, P.R., The risks of nuclear powered space probes, in: J.S.J. Schwartz, T. Milligan (Eds.), The Ethics of Space Exploration, Springer International Publishing, 2016, pp. 239-249.

Greenberg, J.M. and Huebner, W.F. 2002, Summary of the Workshop on Geophysical and Geological Properties of NEOs: 'Know Your Enemy,' in *International Seminars on Nuclear War and Planetary Emergencies* 26: 419-432.

Gritzner, C. and Kahle, R. 2004, Mitigation technologies and their requirements, in: M.J.S. Belton, T.H. Morgan, N. Samarasinha, D.K. Yeomans (Eds.), Mitigation of Hazardous Comets and Asteroids, Cambridge University Press, Cambridge, pp. 167-200.

Gritzner, C., Dürfeld, K., Kasper, J. and Fasoulas, S. 2006, The asteroid and comet impact hazard: risk assessment and mitigation options, Naturwissenschaften 93: 361-373.

Gudmandsen, P., Nilsson, E., Pallisgaard, M., Dkou, N. and Søndergaard, F. 1975, New equipment for radio echo sounding, *Antarctic Journal of the US* 10: 234-236.

Guérin, R., Baltassat, J.M., Boucher, M., Chalikakis, K., Galibert, P.Y., Girard, J.F., Plagnes, V. and Valois, R. 2009, Geophysical characterisation of karst networks – application to the Ouysse system (Poumeyssen, France), *Comptes Rendus Geoscience* 341: 810-817.

Guerra, V., Silva, T., Ogloblina, P., Grofulović, M., Terraz, L., da Silva, M.L., Pintassilgo, C.D., Alves, L.L. and Guaitella, O. 2017, The case for *in situ* resource utilisation for oxygen production on Mars by non-equilibrium plasmas, *Plasma Sources Science and Technology* 26: 11LT01.

Gundlach, B. and Blum, J. 2013, A new method to determine the grain size of planetary regolith, *Icarus* 223, 479-492.

Haines, S.S. 2006, Design and application of an electromagnetic vibrator seismic source, *Journal of Environmental and Engineering Geophysics*, 11: 9–15.

Hamilton, V.E., Simon, A.A., Christensen, P.R., Reuter, D.C., Clark, B.E., Barucci, M.A., Bowles, N.E., Boynton, W.V., Brucato, J.R., Cloutis, E.A., Connolly, H.C., Donaldson Hanna, K.L., Emery, J.P., Enos, H.L., Fornasier, S., Haberle, C.W., Hanna, R.D., Howell, E.S., Kaplan, H.H., Keller, L.P., Lantz, C., Li, J-Y., Lim, L.F., McCoy, T.J., Merlin, F., Nolan, M.C., Praet, A., Rozitis, B., Sandford, S.A., Schrader, D.L., Thomas, C.A., Zou, X-D. and Lauretta, D.S. 2019, Evidence for widespread hydrated minerals on asteroid (101955) Bennu, *Nature Astronomy* 3: 332-340.

Han, D.H., Nur, A. & Morgan, D. 1986, Effects of porosity and clay content on wave velocities in sandstones, *Geophysics*, 51:2093-2109.

Harker, D.E., Woodward, C.E. and Wooden, D.H. 2005, The dust grains from 9P/Tempel 1 before and after the encounter with Deep Impact, *Science* 310: 278-280.

Harold, J. 1926, The rigidity of the Earth's central core, *Geophysical Supplements to the Monthly Notices of the Royal Astronomical Society* 1: 371-383.

Harper, J., Hubbard, A., Ruskeeniemi, T., Claesson Liljedahl, L., Lehtinen, A., Booth, A., Brinkerhoff, D., Drake, H., Dow, C., Doyle, S., Engström, J., Fitzpatrick, A., Frape, S., Henkemans, E., Humphrey, N., Johnson, J., Jones, G., Joughin, I., Klint, K.E., Kukkonen, I., Kulessa, B., Landowski, C., Lindbäck, K., Makahnouk, M., Meierbachtol, T., Pere, T., Pedersen, K., Pettersson, R., Pimentel, S., Quincey, D., Tullborg, E-L. and van As, D. 2012, The Greenland analogue project, yearly report 2010, Posiva Oy.

Harris, A.W. and D'Abramo, G. 2015, The population of near-Earth asteroids, Icarus 257: 302-312.

Hautot, S., Whaler, K., Gebru, W. and Desissa, M. 2006, The structure of a Mesozoic basin beneath the Lake Tana area, Ethiopia, revealed by magnetotelluric imaging, *Journal of African Earth Sciences* 44: 331-338.

Haynes, R.H., Ecce Ecopoiesis: Playing god on Mars, In: D. MacNiven (Ed.), Moral Expertise, Routledge, London and New York, 1990, pp. 161-183.

He, L., Hu, X., Xu, L., He, Z. and Li, W. 2012, Feasibility of monitoring hydraulic fracturing using time-lapse audio-magnetotellurics, *Geophysics* 77: 119-126.

Heiken, G.H., Vaniman, D.T. and French, B.M. 1991, Lunar sourcebook, Cambridge University Press, Cambridge, UK.

Herique, A., Agnus, B., Asphaug, E., Barucci, A., Beck, P., Bellerose, J., Biele, J., Bonal, L., Bousquet, P., Bruzzone, L., Buck, C., Carnelli, I., Cheng, A., Ciarletti, V., Delbo, M., Du, J., Du, X., Eyraud, C., Fa, W., Fernandez, J.G., Gassot, O., Granados-Alfaro, R., Green, S.F., Grieger, B., Grundmann, J.T., Grygorczuk, J., Hahnel, R., Heggy, E., Ho, T-M.,

Karatekin, O., Kasaba, Y., Kobayashi, T., Kofman, W., Krause, C., Kumamoto, A., K*üppers, M., Laabs, M., Lange, C., Lasue, J., Levasseur-Regourd, A.C., Mallet, A., Michel, P., Mottola, S., Murdoch, N., Mütze, M., Oberst, J., Orosei, R., Plettemeier, D., Rochat, S., RodriguezSuqet, R., Rogez, Y., Schaffer, P., Snodgrass, C., Souyris, J-C., Tokarz, M., Ulamec, S., Wahlund, J-E. and Zine, S.* 2018, Direct observations of asteroid interior and regolith structure: Science measurement requirements, *Advances in Space Research* 62: 2141-2162.

Hertrich, M., Braun, M., Gunther, T., Green, A.G. and Yaramanci, U. 2007, Surface nuclear magnetic resonance tomography, *IEEE Transactions on Geoscience and Remote Sensing* 45: 3752-3759.

Hess, S.L., Henry, R.M. and Tillman, J.E. 1979, The seasonal variation of atmospheric pressure on Mars as affected by the South Polar Cap, *Journal of Geophysical Research* 84: 2923-2927.

Hinkel, K.M., Doolittle, J.A., Bockheim, J.G., Nelson, F.E., Paetzold, R., Kimble, J.M. and Travis, R. 2001, Detection of subsurface permafrost features with ground-penetrating radar, Barrow, Alaska, *Permafrost and Periglacial Processes* 12: 179-190.

Hinners, N.W. 1972, Apollo 16 site selection, Apollo 16: Preliminary Science Report, NASA.

Hinners, N.W. 1973, Apollo 17 site selection, Apollo 17: Preliminary Science Report, NASA.

Hinze, W.J., Von Frese, R.R.B. and Saad, A.H. 2013, Gravity and magnetic exploration: Principles, practices, and applications, Cambridge University Press.

Hodgson, M.E. and Bresnahan, P. 2004, Accuracy of airborne Lidar-derived elevation: Empirical assessment and error budget, *Photogrammetric Engineering & Remote Sensing* 70: 331-339.

Holsapple, K.A. 2004, About deflecting asteroids and comets, in: M.J.S., Belton, T.H. Morgan, N. Samarasinha, D.K. Yeomans (Eds.), Mitigation of Hazardous Comets and Asteroids, Cambridge University Press, Cambridge, pp. 113–140.

Holsapple, K.A. 2010, On YORP-induced spin deformations of asteroids, *Icarus* 205: 430-442.

Hori, S., Inoue, H., Fukao, Y. and Ukawa, M. 1985, Seismic detection of the untransformed 'basaltic' oceanic crust subducting into the mantle, *Geophysical Journal International* 83: 169-197.

Hörig, B., Kühn, F., Oschütz, F. and Lehmann, F. 2001, HyMap hyperspectral remote sensing to detect hydrocarbons, *International Journal of Remote Sensing* 22: 1413-1422.

Hudyma, M.R., Heal, D. and Mikula, P.A. 2003, Seismic monitoring in mines-old technology, new applications, *Proceedings 1st Australasian Ground Control in Mining Conference*, UNSW Sydney, pp. 201-218.

Huebner, W.F. and Bradley, P.A. 2016, Asteroid and comet nucleus impact risk assessment, International Seminars on Nuclear War and Planetary Emergencies, 48th session, 513-536.

Huebner, W.F., Cellino, A., Cheng, A.F. and Greenberg, J.M. 2001, NEOs: Physical properties, in *International Seminars on Nuclear War and Planetary Emergencies* 25: 309-340.

Huebner, W.F., Johnson, L.N., Boice, D.C., Bradley, P., Chocron, S., Ghosh, A., Giguere, P.T., Goldstein, R., Guzik, J.A., Mukerherjee, J., Patrick, W., Plesko, C., Walker, J.D. and Wohletz, K. 2009, A comprehensive program for countermeasures against potentially hazardous objects (PHOs), *Solar System Research* 43: 334-342.

Hurst, A., Griffiths, C.M. and Worthington, P.F. 1992, Geological applications of wireline logs, Geological Society, London.

Ip, W.H., Jun, Y., Li, C-L. and Li, Z-Y. 2014, Preface: The Chang'e-3 lander and rover mission to the Moon, *Research in Astronomy and Astrophysics* 14: 1511-1513.

Itasca Consulting Group 2011, Fast Lagrangian Analysis of Continua, Manual, version 7.0, Itasca, Minneapolis.

Jahn, F., Cook, M. and Graham, M. 2008, Hydrocarbon exploration and production, Elsevier.

Jakosky, B.M. and Edwards, C.S. 2018, Inventory of CO_2 available for terraforming Mars, *Nature Astronomy* 2: 634-639.

Jallouli, C., Chikhaoui, M., Braham, A., Turki, M.M., Mickus, K. and Benassi, R. 2005, Evidence for Triassic salt domes in the Tunisian Atlas from gravity and geological data, *Tectonophysics* 396: 209-225.

JAXA 2020, Joint statement for cooperation in the Hayabusa2 sample return mission by the Australian Space Agency and the Japan Aerospace Exploration Agency, (accessed 23/10/2020) <https://www.jaxa.jp/press/2020/07/20200714-1_j.html>.

Jefferson, R.D., Steeples, D.W., Black, R.A. and Carr, T. 1998, Effects of soil-moisture content on shallow-seismic data, *Geophysics* 63: 1357-1362.

Jenniskens, P., Popova, O.P., Glazachev, D.O., Podobnaya, E.D. and Kartashova, A.P. 2019, Tunguska eyewitness accounts, injuries, and casualties, Icarus 327: 4-18.

Jewitt, D., Ishiguro, M. and Agarwal, J. 2013a, Large particles in active asteroid P/2010 A2, *The Astrophysical Journal Letters* 764: L5.

Jewitt, D., Li, J. and Agarwal, J. 2013b, The dust tail of asteroid (3200) Phaethon, *The Astrophysical Journal Letters* 771: L36.

Johnson, D.B., Grail, B.M. and Hallberg, K.B. 2013, A new direction for biomining: extraction of metals by reductive dissolution of oxidized ores, *Minerals* 3: 49-58.

Johnson, J.R., Swindle, T.D. and Lucey, P.G. 1999, Estimated solar wind-implanted helium-3 distribution on the Moon, *Geophysical Research Letters* 26: 385-388.

Johnson, T.V. and Fanale, F.P. 1973, Optical properties of carbonaceous chondrites and their relationship to asteroids, *Journal of Geophysical Research* 78: 8507-8518.

Jol, H.M. (Ed.) 2009, Ground Penetrating Radar: Theory and Applications, Elsevier.

Jones, H. 2018, The recent large reduction in space launch cost, 48th International Conference on Environmental Systems, Albuquerue, New Mexico, ICES-2018-81.

Kargel, J.S. 1994, Metalliferous asteroids as potential sources of precious metals, *Journal of Geophysical Research* 99: 21,129-21,141.

Karr, L.J., Paley, M.S., Marone, M.J., Kaukler, W.F. and Curreri, P.A. 2012, Metals and oxygen mining from meteorites, asteroids and planets using reusable ionic liquids, 2012 PISCES Conference, Pioneering Planetary Surface Systems Technologies and Capabilities, Waikoloa, 11-15 November.

Kawamura, T., Tanaka, S., Kobayashi, N. and Lognonné, P. 2010, The Lunar Surface Gravimeter as a lunar seismometer, in: Ground-Based Geophysics on the Moon, January 21-22, 2010, Tempe, Arizona. LPI Conbtribution No. 1530.

Keating, P. 1995, A simple technique to identify magnetic anomalies due to kimberlite pipes, *Exploration Mining Geology* 4: 121-125.

Knapmeyer, M. and Weber, R.C., 2015, Seismicity and interior structure of the Moon, in: V.C.H. Tong, R.A. Garcia (Eds.), Extraterrestrial Seismology, Cambridge University Press, Cambridge, pp. 203–224.

Knopoff, L. 1964, Q, *Reviews of Geophysics*: 0096-1043.

Kofman, W. and Safaeinili, A. 2004, Peering inside near-Earth objects with radio tomography, in: M.J.S., Belton, T.H. Morgan, N. Samarasinha, D.K. Yeomans (Eds.), Mitigation of Hazardous Comets and Asteroids, Cambridge University Press, Cambridge, pp. 201–233.

Kofman, W., Barbin, Y., Klinger, J., Levasseur-Regourd, A-C., Barriot, J-P., Hérique, A., Hagfors, T., Nielsen, E., Gr*ün, E., Edenhofer, P., Kochan, H., Picardi, G., Seu, R., van Zyl, J., Elachi, C., Melosh, J., Veverka, J., Weissman, P., Svedhem, L.H., Hamran, S.E. and Williams, I.P.* 1998, Comet nucleus sounding experiment by radiowave transmission, *Advances in Space Research* 21: 1589-1598.

Kovach, R.L. and Chyba, C.F. 2001, Seismic detectability of a subsurface ocean on Europa, *Icarus* 150: 279-287.

Kovach, R.L. and Watkins, J.S. 1973a, The velocity structure of the lunar crust, *The Moon* 7: 63-75.

Kovach, R.L. and Watkins, J.S. 1973b, Apollo 17 seismic profiling: Probing the Lunar crust, *Science* 180: 1063-1064.

Kovach, R.L., Watkins, J.S. and Talwani, P. 1973, Lunar Seismic Profiling Experiment, In: Apollo 17 Preliminary Science Report NASA-SP-330, Johnson Space Center, NASA, Washington D.C., US Government Printing Office 1-10–1-12.

Kruse, F.A., Kierein-Young, K.S. and Boardman, J.W. 1990, Mineral mapping a Cuprite, Nevada with a 63-channel imaging spectrometer, *Photogrammetric Engineering and Remote Sensing* 56: 83-92.

Ksanfomaliti, L.V., Zubkova, V.M., Morozov, N.A. and Petrova, E.V. 1982, Microseisms at the Venera-13 and Venera-14 landing sites, Soviet Astronomy Letters 8: 241-242.

Lachaal, F., Gabtni, H., Bédir, M. and Jamila, T. 2012, Seismic, gravity, and wire line logging characterization of the Zéramdine fault corridor and its influence in the deep Miocene aquifers distribution (east-central Tunisia), *Arabian Journal of Geoscience* 5: 1391-1398.

LaFehr, T.R. 1980, History of geophysical exploration – Gravity method, *Geophysics* 45: 1634-1639.

Landis, G.A. and Perino, M.A. 1989, Lunar production of solar cells: a near-term product for a lunar industrial facility, in: Space Manufacturing, AIAA, New York, pp 144-151.

Landon, M.M., DeGroot, D.J. and Sheahan, T.C. 2007, Nondestructive sample quality assessment of a soft clay using shear wave velocity, *Journal of Geotechnical and Geoenvironmental Engineering*, V. 133, 424-432.

Lang, M.W. and McCarty, G.W. 2009, Lidar intensity for improved detection of inundation below the forest canopy, *Wetlands* 29: 1166-1178.

Latham, G.V., Ewing, M., Press, F. and Sutton, G. 1969, The Apollo Passive seismic experiment, *Science*, 165: 241-250.

Latham, J.P., Munjiza, A. and Lu, Y. 2002, On the prediction of void porosity and packing of rock particulates, *Powder Technology* 125: 10-27, https://doi.org/10.1016/S0032-5910(01)00493-4.

Lau, I.C., Heinson, G., James, P.R. and Mauger, A.J. 2003, Hyperspectral mapping of regolith materials and landforms for mineral exploration, Olary Domain, South Australia, Geoscience and Remote Sensing Symposium, IGARSS'03, *Proceedings 2003 IEEE International* 5, 3329-3331.

Lauretta, D.S., DellaGiustina, D.N., Bennett, C.A., Golish, D.R., Becker, K.J., Balram-Knutson, S.S., Barnouin, O.S., Becker, T.L., Bottke, W.F., Boynton, W.V., Campins, H., Clark, B.E., Connolly Jr, H.C., Drouet d'Aubigny, C.Y., Dworkin, J.P., Emery, J.P., Enos, H.L.., Hamilton, E., Hergenrother, C.W., Howell, E.S., Izawa, M.R.M., Kaplan, H.H., Nolan, M.C., Rizk, B., Roper, H.L., Scheeres, D.J., Smith, P.H., Walsh, K.J., Wolner, C.W.V. and The OSIRIS-REx Team 2019, The unexpected surface of asteroid (101955) Bennu, *Nature* 568: 55-60.

Lee, J.-S. and Santamarina, J.C. 2005, Bender elements: Performance and signal interpretation, *Journal of Geotechnical and Geoenvironmental Engineering* 131: 1063-1070.

Lee, T.J., Han, N. and Song, Y. 2010, Magnetotelluric survey applied to geothermal exploration: An example at Seokmo Island, Korea, *Exploration Geophysics* 41: 61-68.

Legchenko, A. and Valla, P. 2002, A review of the basic principles for proton magnetic resonance sounding experiments, *Journal of Applied Geophysics* 50: 3-19.

Legchenko, A., Baltassat, J-M., Beauce, A. and Bernard, J. 2002, Nuclear magnetic resonance as a geophysical tool for hydrogeologists, *Journal of Applied Geophysics* 50: 21-46.

Lehmann, I. 1936, Publications du Bureau Central Seismologique International, *Serie A, Travaux Scientifiques* 14.

Lehner, F.E., Witt, E.O., Miller, W.F. and Gurney, R.D. 1962, A seismometer for lunar experiments, *Journal of Geophysical Research* 67: 4779-4786.

Lemos, J.V. 2019, Discrete element modeling of the seismic behaviour of masonry construction, *Buildings* 9: DOI:10.3390/buildings9020043.

Leong, E.C., Cahyadi, J. and Rahardjo, H. 2009, Measuring shear and compression wave velocities of soil using bender-extender elements, *Canadian Geotechnical Journal* 13: 430-441.

Leuschen, C., Kanagaratnam, P., Yoshikawa, K., Arcone, S. and Gogineni, P. 2003, Design and field experiments of a ground-penetrating radar for Mars exploration, *Journal of Geophysical Research* 108: 1-12.

Lewis, J.S. 1997, Mining the Sky: Untold Riches from the Asteroids, Comets and Planets, Perseus Publishing, New York.

Lewis, J.S., Asteroid Mining 101: Wealth for the new space economy, Deep Space Industries, California 2015.

Li, C., Su, Y., Pettinelli, E., Xing, S., Ding, C., Liu, J., Ren, X., Lauro, S.E., Soldovieri, F., Zeng, X., Gao, X., Chen, W., Dai, S., Liu, D., Zhang, G., Zuo, W., Wen, W., Zhang, Z., Zhang, X. and Zhang, H. 2020, The Moon's farside shallow subsurface structure unveiled by Chang'E-4 Lunar Penetrating Radar, *Science Advances* 6: eaay6898.

Li, J., Pang, Z., Kong, Y., Lin, F., Wang, Y., Wang, G. and Lv, L. 2017, An integrated magnetotelluric and gamma exploration of groundwater in fractured granite for small-scale freshwater supply: a case study from the Boshan region, Shandong Province, China, *Environmental Earth Science* 76: https://doi.org/10.1007/s12665-017-6486-z.

Lieblich, D.A., Legchenko, A., Haeni, F.P. and Portselan, A.A. 1994, Surface nuclear magnetic resonance experiments to detect subsurface water at Haddam Meadows, Connecticut, In: R.S. Bell and C.M. Lepper (Eds.), Symposium on the Application of Geophysics to Engineering and Environmental Problems, Boston Massachusetts, March 27-31, Environmental and Engineering Geophysical Society, 717-736.

Lin, P-C., Chang, C-C., and Chang, T-S. 2004, The use of MASW method in the assessment of soil liquefaction potential, *Soil Dynamics and Earthquake Engineering* 24: 689-698.

Litvak, M.L., Mitrofanov, I.G., Y.N. Barmakov, Behar, A., Bitulev, A., Bobrovnitsky, Y., Bogolubov, E.P., Boynton, W.V., Bragin, S.I., Churin, S., Grebennikov, A.S., Konovalov, A., Kozyrev, A.S., Kurdumov, I.G., Krylov, A., Kuznetsov, Y.P., Malakhov, A.V., Mokrousov, M.I., Ryzhkov, V.I., Sanin, A.B., Shvetsov, V.N., Smirnov, G.A., Sholeninov, S., Timoshenko, G.N., Tomilina, T.M., Tuvakin, D.V., Tretyakov, V.I., Troshin, V.S., Uvarov, V.N., Varenikov, A. and Vostrukhin, A. 2008, The Dynamic Albedo of Neutrons (DAN) experiment for NASA's 2009 Mars Science Laboratory, *Astrobiology* 8: 605-612.

Liu, Q., Liu, J., Pan, Y., Zhang, X., Peng, X., Gong, Q. and Du, L. 2017, A wear rule and cutter life prediction model of a 20-in. TBM cutter for granite: A case study of a water conveyance tunnel in China, *Rock Mechanics and Rock Engineering* 50: 1303-1320.

Liu, X. and Nur, A. 1996, A new experimental method for studying velocity dispersion in rocks (abs.), *Society of Exploration Geophysicists 66th International Meeting*, Expanded Abstracts. 2: 1683-1686.

Liu, Z.N. and Koyi, H.A. 2013, Kinematics and internal deformation of granular slopes: insights from discrete element modeling, *Landslide* 10: 139-160.

Lo, C.M., Lin, M.L., Tang, C.L. and Hu, J.C. 2011, A kinematic model of the Hsiaolin landslide calibrated to the morphology of the landslide deposit, *Engineering Geology* 123: 22-39.

Lognonné, P. 2005, Planetary seismology, *Annu. Rev. Earth Planet. Sci.*, V. 33, 571-604.

Lognonné, P. and Pike, W.T. 2015, Planetary seismometry, in: V.C.H. Tong, R.A. Garcia (Eds.), Extraterrestrial Seismology, Cambridge University Press, Cambridge, pp. 36–48.

Lognonné, P., Zharkov, V.N., Karczewski, J.K., Romanowicz, B., Menvielle, M., Poupinet, G., Brient, B., Cavoit, C., Desautez, A., Dole, B. and Franqueville, D. 1998, The seismic OPTIMISM experiment, *Planetary and Space Science* 46: 739-747.

Lorenz, R.D., Moersch, J.E., Stone J.A. Morgan Jr, A.R. and Smrekar, S.E. 2000, Penetration tests on the DS-2 Mars microprobes: Penetration depth and impact accelerometry, *Planetary Space Science* 48: 419–436.

Lucas, M.T. and Hagan, P.C. 2014, Comparison of two excavations systems for the mining of Lunar regolith, *Mining Education Australia Journal of Research Projects Review* 3: 39-44.

Luxembourg Space Agency 2018, Opportunities for space resources utilization: Future markets & value chains, Space Resources.

Lyne, J.E. and Tauber, M. 1995, Origin of the Tunguska event, Nature 375: 638-639.

MacGregor, F., Fell, R., Mostyn, G.R. Hocking, G. and McNally, G. 1994, The estimation of rock rippability, *Quarterly Journal of Engineering Geology and Hydrogeology* 27: 123-144.

Macnae, J.C. 1979, Kimberlites and exploration geophysics, *Geophysics* 44: 1395-1416.

Magri, C., Consolmagno, G.J., Ostro, S.J., Benner, L.A.M. and Beeney, B.R. 2001, Radar constraints on asteroid regolith properties using 433 Eros as ground truth, *Meteoritics and Planetary Science* 36: 1697-1709.

Manolakis, D.G., Lockwood, R.B. and Cooley, T.W. 2016, Hyperspectral imaging remote sensing: physics, sensors, and algorithms, Cambridge University Press.

Marcus, R., Melosh, H.J. and Collins, G. 2010, Imperial College London, (accessed 21/04/2020) <https://impact.ese.ic.ac.uk/ImpactEarth/ImpactEffects/>.

Marinova, M.M., McKay, C.P. and Hashimoto, H. 2005, Radiative-convective model of warming Mars with artificial greenhouse gases, Journal of Geophysical Research: Planets 110: E3.

Matheny, J.G. 2007, Reducing the risk of human extinction, Risk Analysis 27: 1335-1344.

McCann, C., Sothcott, J. and Assefa, S.B. 1997, Prediction of petrophysical properties from seismic quality factor measurements, *Geological Society, London, Special Publications* 122: 121-130.

McCann, D.M. and Fenning, P.J. 1995, Estimation of rippability and excavation conditions from seismic velocity measurements, Geological Society, London, Engineering Geology Special Publications, 1;10: 335-343.

McGarr, A., Latham, G.V., and Gault, D.E. 1969, Meteoroid impacts as sources of seismicity on the Moon, *Journal of Geophysical Research* 74: 5981-5994.

McKay, C.P. 1990, Does Mars have rights? An approach to the environmental ethics of planetary engineering, in: D. MacNiven (Ed.), Moral Expertise, Routledge.

McKay, C.P. 2007, Planetary ecosynthesis on Mars: Restoration ecology and environmental ethics, NASA Ames Research Center.

McKay, C.P., Toon, O.B. and Kasting, J.F. 1991a, Making Mars habitable, Nature 352: 489-496.

McKay, D.S., Heiken, G., Basu, A., Blanford, G., Simon, S., Reedy, R., French, B.M. and Papike, J. 1991b, The Lunar regolith. *Lunar sourcebook*. 285-356.

McNally, G.H. 1987, Estimation of coal measures rock strength using sonic and neutron logs, *Geoexploration* 24: 381-395.

McNally, G.H. 1990, The prediction of geotechnical rock properties from sonic and neutron logs, *Exploration Geophysics*, 21:65-71.

McNutt, S.R. 2005, Volcanic seismology, *Annual Review of Earth and Planetary Sciences* 32: 461-491.

Medina, R., Losada, M.A., Losada, I.J. and Vidal, C. 1994, Temporal and spatial relationship between sediment grain size and beach profile, *Marine Geology* 118: 195-206.

Mendes, N., Zanotti, S. and Lemos, J.V. 2020, Seismic performance of historical buildings based on discrete element method: An adobe church, *Journal of Earthquake Engineering*, 24: 1270-1289.

Michel, P. Kuepper, M., Sierks, H., Carnelli, I., Cheng, A.F., Mellab, K., Granvik, M., Kestilä, A., Kohout, T., Muinonen, K., Näsilä, A., Penttila, A., Tikka, T., Tortora, P., Ciarletti, V., Hérique, A., Murdoch, N., Asphaug, E., Rivkin, A., Barnouin, O., Bagatin, A.C., PRavec, P., Richardson, D.C., Schwartz, S.R., Tsiganis, K., Ulamec, S. and Karatekin O. 2018, European component of the AIDA mission to a binary asteroid: Characterization and interpretation of the impact of the DART mission, *Advances in Space Research* 62: 2261-2272.

Michel, R., Ampuero, J.-P., Avouac, J.-P., Lapusta, N., Leprince, S., Redding, D.C. and Somala, S.N. 2012, A geostationary optical seismometer, proof of concept, *IEEE Transactions on Geoscience and Remote Sensing* 51: 695-703.

Mitchell, J.K. and Soga, K. 2005, Fundamentals of soil behaviour, New York: John Wiley & Sons.

Mohamed, A.K., Meju, M.A. and Fontes, S.L. 2002, Deep structure of the northeastern margin of the Parnaiba Basin, Brazil, from magnetotelluric imaging, *Geophysical Prospecting* 50: 589-602.

Moheimani, S.O.R. and Fleming, A.J. 2006, Piezoelectric transducers for vibration control and damping, Springer Science & Business Media.

Mordanova, A. and de Felice, G. 2020, Seismic assessment of archaeological heritage using discrete element method, *International Journal of Architectural Heritage* 14: 345-357.

Morgan, J., Raval, S., Macdonald, B., Falorni, G. and Iannacone, J. 2013, Application of advanced InSAR techniques to detect vertical and horizontal displacements, *Proceedings of the 2013 International Symposium on Slope Stability in Open Pit Mining and Civil Engineering*, Australian Centre for Geomechanics.

Mottola, S. Arnold, G., Grothues, H-G., Jaumann, R., Michaelis, H., Neukum, G., Bibring, J-P., Schröder, S.E., Hamm, M., Otto, K.A., Pelivan, I., Proffe, G., Scholten, F., Tirsch, D., Kreslavsky, M., Remetean, E., Souvannavong, F. and Dolives, B. 2015, The structure of the regolith on 67P/Churyumov-Gerasimenko from ROLIS descent imaging, *Science* 349: aab0232.

Mudd, G.M. 2001, Critical review of acid in situ leach uranium mining: 1. USA and Australia, *Environmental Geology* 41: 390-403.

Muff, T., Johnson, L., King, R. and Duke, M.B. 2004, A prototype bucket wheel excavator for the Moon, Mars and Phobos, *AIP Conference Proceedings* 699: 967-974.

Mullins, O.C., Hashem, M., Elshahawi, H., Fujisawa, G., Dong, C., Betancourt, S. and Terabayashi, T. 2004, Hydrocarbon compositional analysis in-situ in openhole wireline logging, SPWLA 45th Annual Logging Symposium, June 6-9, 1-14.

Murali, M., Biscontin, G. & Aubeny, C. 2015, Soil strength from geophysical measurements for soft clays, white paper.

Muscatello, A. and Santiago-Maldonado, E. 2012, Mars in situ resource utilization technology evaluation, 50th AIAA Aerospace Sciences Meeting Including the New Horizons Forum and Aerospace Exposition.

Nabighian, M.N., Ander, M.E., Grauch, V.J.S., Hansen, R.O., LaFehr, T.R., Li, Y., Pearson, W.C., Peirce, J.W., Phillips, J.D. and Ruder, M.E. 2005a, Historical development of the gravity method in exploration, *Geophysics* 70: 63-89.

Nabighian, M.N., Grauch, V.J.S., Hansen, R.O., LaFehr, T.R., Li, Y., Peirce, J.W., Phillips, J.D. and Ruder, M.E. 2005b, The historical development of the magnetic method in exploration, Geophysics 70: 33-61.

Nabipour, A., Evans, B., Müller, T. and Sarmadivaleh, M. 2011, Evaluation of PFC 2D for modeling seismic monitoring of hydraulic fracture, 2nd International FLAC/DEM Symposium, Feb 14-16, Melbourne, Australia: ITASCA.

Naeye, R. 2008, NASA scientists pioneer method for making giant lunar telescopes, (accessed 15/10/2020) <https://www.nasa.gov/centers/goddard/news/topstory/2008/lunar_telescopes.html>.

Naidu, S., Benner, L., Brozovic, M., Ostro, S.J., Nolan, M.C., Margot, J.L., Giorgini, J.D., Magri, C., Pravec, P., Scheirich, P., Scheeres, D.J. and Hirabayashi, M. 2016, Observations and characterization of the binary near-earth asteroid 65803 Didymos, the target of the AIDA Mission, AGU Fall Meeting Abstracts.

Nakamura, Y., Latham, G., Lammlein, D., Ewing, M., Duennebier, F. and Dorman, J. 1974, Deep lunar interior inferred from recent seismic data, *Geophysical Research Letters* 1: 137-140.

Nakamura, Y. 1977, Seismic energy transmission in an intensely scattering environment, *Journal of Geophysical Research* 43: 389-399.

Nakamura, Y., Latham, G.V., Dorman, H.J. and Harris, J.E. 1981, Passive Seismic Experiment Long-Period Event Catalog, Final version, 1969 day 202 – 1977 day 273, Galveston Geophysics Laboratory, Galveston, UTIG Technical Report No. 18.

Nakamura, Y. 1983, Seismic velocity structure of the lunar mantle, *Journal of Geophysical Research*, 88: 677-686.

Nakamura, Y. 2005, Farside deep moonquakes and deep interior of the Moon, *Journal of Geophysical Research* 110: E01001.

Nakamura, Y. 2011, Timing problem with the Lunar Module impact data as recorded by the LPSE and corrected near-surface structure at the Apollo 17 landing site, *Journal of Geophysical Research* 116: E12005.

Nakamura, T., Noguchi, T., Tanaka, M., Zolensky, M.E., Kimura, M., Tsuchiyama, A., Nakato, A., Ogami, T., Ishida, H., Uesugi, M., Yada, T., Shirai, K., Fujimura, A., Okazaki, R., Sandford, S.A., Ishibashi, Y., Abe, M., Okada, T., Ueno, M., Mukai, T., Yoshikawa, M and Kawaguchi, J. 2011, Itokawa dust particles: A direct link between S-type asteroids and ordinary chondrites, *Science* 333: 1113-1116.

Nakamura, Y. 2015, Planetary seismology: Early observational results, in: V.C.H. Tong, R.A. Garcia (Eds.), Extraterrestrial Seismology, Cambridge University Press, Cambridge, pp. 91-106.

NASA 2010, Image sensors enhance camera technologies, (accessed 20/01/2022) <https://spinoff.nasa.gov/Spinoff2010/cg_3.html>.

NASA 2011a, OSIRIS-Rex factsheet, (accessed 23/10/2020) <https://ehpd.gsfc.nasa.gov/documents/552572main_OSIRIS_REx_Factsheet.pdf>.

NASA 2011b, NASA Space Telescope Finds Fewer Asteroids Near Earth, (accessed 26/6/2016) <http://www.jpl.nasa.gov/news/news.php?feature=3154/>.

NASA 2013, Home air purifiers eradicate harmful pathogens, (accessed 20/01/2022) <https://spinoff.nasa.gov/Spinoff2013/cg_4.html>.

NASA 2016a, OSIRIS-REx: Asteroid sample return mission, (accessed 23/10/2020) <https://www.nasa.gov/sites/default/files/atoms/files/osiris-rex_press_kit.pdf>.

NASA 2016b, NEO Earth Close-Approaches, (accessed 26/06/2016) <http://neo.jpl.nasa.gov/cgi-bin/neo_ca/>.

NASA 2016c, 99942 Apophis (2004 MN4) Earth Impact Risk Summary, (accessed 27/06/2016) <http://neo.jpl.nasa.gov/risk/a99942.html/>.

NASA 2018, Did you know that's a NASA technology?, (accessed 23/09/2020) <https://www.nasa.gov/offices/oct/feature/did-you-know-thats-a-nasa-technology>.

Naville, C., Serbutoviez, S., Throo, A., Vincké, O. 2004, Seismic while drilling (SWD) techniques with downhole measurements, introduced by IFP and its partners in 1990-2000, *Oil & Gas Science and Technology* 59: 371-403.

Neal, A. 2004, Ground-penetrating radar and its use in sedimentology: principles, problems and progress, *Earth-Science Reviews* 66: 361-330.

Nickerson, C.A., Ott, C.M., Mister, S.J., Morrow, B.J., Burns-Keliher, L. and Pierson, D.L. 2000, Microgravity as a novel environmental signal affecting Salmonella enterica serovar Typhimurium virulence, *Infection and Immunity* 68: 3147-3152.

Nickerson, C.A., Ott, C.W., Wilson, J.W., Ramamurthy, R. and Pierson, D.L. 2004, Microbial responses to microgravity and other low-shear environments, *Microbiology and Molecular Biology Reviews* 68: 345-361.

Nolan, M.C., Magri, C., Howell, E.S., Benner, L.A.M., Giorgini, J.D., Hergenrother, C.W., Hudson, R.S., Lauretta, D.S., Margot, J-L., Ostro, S.J., Scheeres, D.J. 2013, Shape model and surface properties of the OSIRIS-REx target Asteroid (101955) Bennu from radar and lightcurve observations, *Icarus* 226: 629-640.

O'Neill, G.K. 1975, Space colonies and energy supply to the Earth, *Science* 190: 943-947.

Okal, E. and Anderson, D.J. 1978, Theoretical models for Mars and their seismic properties, *Icarus* 33: 514-528.

Olympus 2008, Material sound velocities, (accessed 15/10/2020) <https://www.olympus-ims.com/en/ndt-tutorials/thickness-gage/appendices-velocities/>.

Öpik, E.J. 1951, Collisional probabilities with the planets and the distribution of interplanetary matter, *Proceedings of the Royal Irish Academy* 54A: 165-199.

OPP, Detection of Near-Earth Asteroids, (accessed 05/06/2016) <http://www.openphilanthropy.org/research/cause-reports/asteroid-detection/>.

Ostro S.J. and Giorgini, J.D. 2004, The role of radar in predicting and preventing asteroid and comet collisions with Earth, in: M.J.S., Belton, T.H. Morgan, N. Samarasinha, D.K. Yeomans (Eds.), Mitigation of Hazardous Comets and Asteroids, Cambridge University Press, Cambridge, pp. 38–65.

Ostro, S.J. 1985, Radar observations of asteroids and comets, *Publications of the Astronomical Society of the Pacific* 97: 877-884.

Ostro, S.J. and Sagan, C. 1998, Cosmic collisions and the longevity of non-spacefaring galactic civilisations, Jet Propulsion Laboratory.

Oyler, D.C., Mark, C. and Molinda, G.M. 2010, In situ estimation of roof rock strength using sonic logging, *International Journal of Coal Geology* 83: 484-490.

Padovani, E. Priolo, E. and Seriani, G. 1994, Low and high order finite element method: Experience in seismic modelling, *Journal of Computational Acoustics* 2: 371-422.

Panning, M.P., Lognonné, P., Banerdt, W.B., Garcia, R., Golombek, M., Kedar, S., Knapmeyer-Endrun, B., Mocquet, A., Teanby, N.A., Tromp, J. and Weber, R. 2017, Planned products of the Mars structure service for the InSight mission to Mars. *Space Science Reviews* 211: 611-650.

Papike, J.J. and Simon, S.B. 1982, The Lunar regolith: Chemistry, mineralogy, and petrology, *Reviews of Geophysics and Space Physics* 20: 761-826.

Parfit, D. 1984, Reasons and Persons, OUP Oxford.

Parsekian, A.D., Grosse, G., Walbrecker, J.O., Müller-Petke, M., Keating, K., Liu, L., Jones, B.M. and Knight, R. 2013, Detecting unfrozen sediments below thermokarst lakes with surface nuclear magnetic resonance, *Geophysical Research Letters* 40: 535-540.

Pelech, T.P., Roesler, G. and Saydam, S. 2019, Technical evaluation of off-Earth ice mining scenarios through an opportunity cost approach, *Acta Astronautica* 162: 388-404.

Peters, G.H., Abbey, W., Bearman, G.H., Mungas, G.S., Smith, J.A., Anderson, R.C., Douglas, S. and Beegle, L.W. 2008, Mojave Mars Simulant – Characterization of a new geologic Mars analog, *Icarus* 197: 470-479.

Phillips, R.J. 1991, Expected rate of marsquakes, *Scientific Rationale and Requirements for a Global Seismic Network on Mars* :35-38.

Philpotts, A. and Ague, J. 2009, Principles of igneous and metamorphic petrology, Cambridge University Press.

Picardi, G., Biccari, D., Seu, R., Plaut, J., Johnson, W.T.K., Jordan, R.L., Safaeinili, A., Gurnett, D.A., Huff, R., Orosei, R., Bombaci, O., Calabrese, D. and Zampolini, E. 2004, MARSIS: Mars Advanced Radar for Subsurface and Ionosphere Sounding, *Mars Express: The Scientific Payload* 1240: 51-69.

Pletser, V., Lognonné, P., Diament, M. and Dehant, V. 2009, Subsurface water detection on Mars by astronauts using a seismic refraction method: Tests during a manned Mars mission simulation, *Acta Astronautica* 64: 457-466.

Poletto, F., Magnani, P., Gelmi, R., Corubolo, P., Re, E., Schleifer, A., Perrone, A., Salonico, A and Coste, P. 2015, Seismic while drilling (SWD) methodology in support to Moon subsurface stratigraphy investigations, *Acta Astronautica* 110: 99-114.

Pollack, J.B. and Sagan, C., Planetary engineering, In: Resources of Near-Earth Space: Abstracts, Arizona University, 1991, pp. 38.

Porcello, L.J., Jordan, R.L., Zelenka, J.S., Adams, G.F., Phillips, R.J., Brown, W.E., Ward, S.H. and Jackson, P.L. 1974, The Apollo Lunar Sounder Radar System, *IEEE Proceedings*, 62: 769-783.

Power. M., Belcourt, G. and Rockel, E. 2004, Geophysical methods for kimberlite exploration in northern Canada, *The Leading Edge* 23: 1124.

Press, F. 1966, Section 9: Seismic velocities, Geological Society of America Memoirs, 97: 195-218.

Price, S.D. 2004, The surface properties of asteroids, *Advances in Space Research* 33: 1548-1557.

Purnell, G.W. 1986, Observations of wave velocity and attenuation in two phase media, *Geophysics* 51: 2193-2199.

Pursiainen, S. and Kaasalainen, M. 2013, Iterative alternating sequential (IAS) method for radio tomography of asteroids in 3D, *Planetary and Space Science* 82-83: 84-98.

Pursiainen, S. and Kaasalainen, M. 2014, Detection of anomalies in radio tomography of asteroids: Source count and forward errors, *Planetary and Space Science* 99: 36-47.

Putzig, N.E. and Mellon, M.T. 2007, Apparent thermal inertia and the surface heterogeneity of Mars, *Icarus* 191: 68-94.

Rees, M. 2003, Our Final Hour, Basic Books, New York.

Rees, N., Carter, S., Heinson, G. and Krieger, L. 2016b, Monitoring shale gas resources in the Cooper Basin using magnetotellurics, *Geophysics* 81: 13-16.

Rees, N., Carter, S., Heinson, G., Krieger, L., Conway, K., Boren, G. and Matthews, C. 2016a, Magnetotelluric monitoring of coal-seam gas and shale-gas resource development in Australia, *The Leading Edge* 35: 64-70.

Renne, P.R., Deino, A.L., Hilgen, F.J., Kuiper, K.F., Mark, D.F., Mitchell III, W.S., Morgan, L.E., Mundil, R. and Smit, J. 2013, Time scales of critical events around the Cretaceous-Paleogene boundary, Science 339: 684-687.

Reynolds, W.T. 2015, Architecture analysis of wireless power transmission for lunar outposts, Naval Postgraduate School Monterey, CA.

Roach, I.C., Blewett, R.S., Czarnota, K., de Caritat, P., McPherson, A.A., Meixner, A.J., Neumann, N., Schofield, A., Thomas, M. and Wilford, J. 2016, Regolith studies and the UNCOVER Initiative at Geoscience Australia, *Fourth Australia Regolith Geoscientists Association Conference*, 7-10.

Roux, A.T. 1970, The application of geophysics to gold exploration in South Africa, In: L.W. Morley (ed.), Mining and groundwater geophysics, 1967: Geological Survey of Canada, Economic Geology Report No. 26, pp. 425-438.

Rutherford, S.R. and Williams, R.H. 1989, Amplitude-versus-offset variations in gas sands, *Geophysics* 54: 680-688.

Saarenketo, T. and Scullion, T. 2000, Road evaluation with ground penetrating radar, *Journal of Applied Geophysics* 43: 119-138.

Sabins, F.F. 1999, Remote sensing for mineral exploration, *Ore Geology Reviews* 14: 157-183.

Sagan, C. and Ostro, S.J. 1994, Dangers of asteroid deflection, *Nature*, 368: 501.

Salvador, E. and Conyers, L. 2006, The use of ground-penetrating radar to map the buried structures and landscape of the Ceren site, *Geoarchaeology* 10: 275-299.

Sanchez, J.P. and McInnes, C.R. 2012, Assessment on the feasibility of future shepherding of asteroid resources, *Acta Astronautica* 73: 49-66.

Sánchez, P. and Scheeres, D.J. 2014, The strength of regolith and rubble pile asteroids, *Meteoritics and Planetary Science* 49: 788-811.

Santos, A.C.L., Padilha, A.L., Fuck, R.A., Pires, A.C.B., Vitorello, I. and Pádua, M.B. 2014, Deep structure of a stretched lithosphere: Magnetotelluric imaging of the southeastern Borborema province, NE Brazil, *Tectonophysics* 610: 39-50.

Sarangi, A.K. and Beri, K.K. 2000, Uranium mining by in-situ leaching, Technology management for mining processing and environment conference, Kharagpur, December 1-3.

Scheer, J. and Holm, W.A. 2010, Principles of modern radar, M.A. Richards & W.L. Melvin (Eds.), SciTech Pub.

Scheeres, D.J. and Sánchez, P. 2018, Implications of cohesive strength in asteroid interiors and surfaces and its measurement, *Progress in Earth and Planetary Science* 5 DOI:10.1186//s40645-018-0182-9.

Schetselaar, E.M., Tiainen, M. and Woldai, T. 2008, Integrated geological interpretation of remotely sensed data to support geological mapping in Mozambique, *Geological Survey of Finland Special Paper* 48: 35-63.

Schoenberg, M. and Sayers, C.M. 1995, Seismic anisotropy of fractured rock, *Geophysics*, 60: 204-211.

Schubert, S., Caviola, L. and Faber, N.S. 2019, The psychology of existential risk: Moral judgements about human extinction, Scientific Reports 9: 15100.

Schwartz, J.S.J. 2013, On the moral permissibility of terraforming, Ethics and the Environment 18: 1-31.

Sercel, J.C., Dreyer, C.B., Abbud-Madrid, A. and Britt, D. 2016, A coordinated research program to develop the technology to optical mine asteroids, *Earth and Space 2016: Engineering for Extreme Environments*, Reston, VA: American Society of Civil Engineers: 507-522.

Sharafzadeh, A., Esmaeily, A. and Dehghani, M. 2018, 3D modelling of urban area using synthetic aperture radar (SAR), *Journal of the Indian Society of Remote Sensing* 46: 1785-1793.

Shea, D.A. and Morgan, D.L. 2010, The helium-3 shortage: Supply, demand, and options for congress.

Shean, D.E., Head, J.W. and Marchant, D.R. 2007, Shallow seismic surveys and ice thickness estimates of the Mullins Valley debris-covered glacier, McMurdo Dry Valleys, Antarctica, *Antarctic Science* 19: 485-496.

Sherlock, D.H. and Evans, B.J. 2001, The development of seismic reflection sandbox modelling, *AAPH Bulletin* 85: 1645-1659.

Sherrif, R.E. and Geldart, L.P. 1995, Exploration Seismology, Cambridge University Press.

Shirgiri, N. 2012, Correlation between geotechnical and geophysical properties of soil, PhD. thesis, University of Birmingham, Birmingham, UK.

Shirley, J.H. 1985, Shallow moonquakes and large shallow earthquakes: A temporal correlation, *Earth and Planetary Science Letters* 76: 241-253.

Shishko, R., Fradet, R., Do, S., Saydam, S., Tapia-Cortez, C., Dempster, A.G. and Coulton, J. 2017a, Mars Colony *in situ* resource utilization: An integrated architecture and economics model, *Acta Astronautica* 138: 53-67.

Shishko, R., Fradet, R., Saydam, S., Tapia-Cortez, C., Dempster, A.G., Coulton, J. and Do, S. 2017b, An integrated economics model for ISRU in support of a Mars colony – Initial results report, 10th Symposium on Space Resource Utilization, AIAA SciTech Forum.

Shokobayev. N.M., Bouffier, C. and Dauletbakov, T.S. 2015, Rare earth metals sorption recovery from uranium in situ leaching process solutions, *Rare Metals* 34: 195-201.

Siddiqi, A.A. 2018, Beyond Earth: A Chronicle of Deep Space Exploration, 1958-2016, National Aeronautics and Space Administration, Office of Communications, NASA History Division.

Sinclair, L. and Thompson, J. 2015, In situ leaching of copper: Challenges and future prospects, *Hydrometallurgy* 157: 306-324.

Sincraian, G.E. 2011, Seismic behaviour of blocky mason structure. A discrete element method approach, PhD dissertation.

Singer, P. ed. 2013, A companion to ethics, John Wiley & Sons.

Singer, R.B. and Roush, T.L. 1985, Effects of temperature on remotely sensed mineral absorption features, *Journal of Geophysical Research: Solid Earth* 90: 12,434-12,444.

Smith, A., Crawford, I.A., Gowen, R.A., Ambrosi, R., Anand, M., Banerdt, B., Bannister, N., Bowles, N., Braithwaite, C., Brown, P., Chela-Flores, J., Cholinser, T., Church, P., Coates, A.J., Colaprete, T., Collins, G., Collinson, G., Cook, T., Elphic, R., Fraser, G., Gao, Y., Gibson, E., Glotch, T., Grande, M., Griffiths, A., Grygorczuk, J., Gudipati, M., Hagermann, A., Heldmann, J., Hood, L.L., Jones, A.P., Joy, K.H., Khavroshkin, O.B., Klingelhoefer, G., Knapmeyer, M., Kramer, G., Lawrence, D., Marczewski, W., McKenna-Lawlor, S., Miljkovic, K., Narendranath, S., Palomba, E., Phipps, A., Pike, W.T., Pullan, D., Rask, J., Richard, D.T., Seweryn, K., Sheridan, S., Sims, M., Sweeting, M., Swindle, T., Talboys, D., Taylor, L., Teanby, N., Tong, V., Ulamec, S., Wawrzaszek, R., Wieczorek, M., Wilson, L. and Wright,

I. 2012, Lunar Net – a proposal in response to an ESA M3 call in 2010 for a medium sized mission, *Experimental Astronomy* 33: 587-644.

Smith, D.E., Lemoine, F.G. and Zuber, M.T. 1995, Simultaneous estimate of the masses of Mars, Phobos and Deimos using spacecraft encounters, *Geophysical Research Letters* 22: 2171-2174.

Smith, D.E., Zuber, M.T., Jackson, G.B., Cavanaugh, J.F., Neumann, G.A., Riris, H., Sun, X., Zellar, R.S., Coltharp, C., Connelly, J., Katz, R.B., Kleyner, I., Liiva, P., Matuszeski, A., Mazarico, E.M., McGarry, J.F., Novo-Gradac, A-M., Ott, M.N., Peters, C., Ramos-Izquierdo, L.A., Ramsey, L., Rowlands, D.D., Schmidt, S., Scott III, V.S., Shaw, G.B., Smith, J.C., Swinski, J-P., Torrence, M.H., Unger, G., Yu, A.W. and Zagwodzki, T.W. 2009, The Lunar Orbiter altimeter investigation on the Lunar Reconnaissance Orbiter Mission, *Space Science Reviews* 150: 209-241.

Smith, D.E., Zuber, M.T., Neumann, G.A. and Lemoine, F.G. 1997, Topography of the Moon from the Clementine Lidar, *Journal of Geophysical Research* 102: 1591-1611.

Smith, K.C. 2014, Manifest complexity: A foundational ethic for astrobiology?, *Space Policy* 30: 209-214.

Smrekar, S., Catling, D., Lorenz, R., Magalhães, J., Moersch, J., Morgan, P., Murray, B., Presley, M., Yen, A., Zent, A. and Blaney, D. 1999, Deep Space 2: The Mars Microprobe Mission, *Journal of Geophysical Research* 104: 27,013-27,030.

Snodgrass, C., Jones, G.H., Boehnhardt, H., Gibbings, A., Homeister, M., Andre, N., Beck, P., Bentley, M.S., Bertini, I., Bowles, N., Capria, M. T., Carr, C., Ceriotti, M., Coates, A.J., Della Corte, V., Donaldson Hanna, K.L., Fitzsimmons, A., Gutierrez, P.J., Hainaut, O.R., Herique, A., Hilchenbach, M., Hsieh, H.H., Jehin, E., Karatekin, O., Kofman, W., Lara, L.M., Laudan, K., Licandro, J., Lowry, S.C., Marzari, F., Masters, A., Meech, K.J., Moreno, F., Morse, A., Orosei, R., Pack, A., Plettemeier, D., Prialnik, D., Rotundi, A., Rubin, M., Sanchez, J.P., Sheridan, S., Trieloff, M. and Winterboer, A. 2018, The Castalia mission to Main Belt Comet 133P/Elst-Pizarro, *Advances in Space Research* 62: 1947–1976.

Soengkono, S. 2011, Deep interpretation of gravity and airborne magnetic data of the central Taupo Volcanic Zone, Proceedings of the 33rd New Zealand Geothermal Workshop, Auckland, New Zealand, 1-6.

Solem, J.C. and Snell, C.M. 1994, Terminal intercept for less than one orbital period warning, in: T. Gehrels, M.S. Matthews, and A.M. Schumann, (Eds.), Hazards due to Comets and Asteroids, Vol. 24, University of Arizona Press, pp. 1013-1033.

Sorenson, A.C. 2000, Asteroids: More than just chunks of rock, *Space 2000*: 1007-1010.

Sowers, G.F. and Dreyer, C.B. 2019, Ice mining in lunar permanently shadowed regions, *New Space* 7: 235-244.

Sparrow, R. 2015, Terraforming, vandalism and virtue ethics, in: J. Galliott (Ed.), Commercial Space Exploration: Ethics, Policy and Governance, Routledge, pp. 161-178.

Sridhar, K.R., Finn, J.E. and Kliss, M.H. 2000, In-situ resource utilization technologies for Mars life support systems, Advances if Space Research 25:249-255.

Stofan, E.R., Saunders, R.S., Senske, D., Nock, K., Tralli, D., Lundgren, P., Smrekar, S., Banerdt, B., Kaiser, W., Dudenhoefer, J., Goldwater, B., Schock, A. and Neuman, J. 1993, Venus interior structure mission (VISM): Establishing a seismic network on Venus, *LPI Technical Report* 93-02: 23-24.

Strobbia, C.L., Laake, A., Vermeer, P.L. and Glushchenko, A. 2009, Surface waves, use them then lose them, *71st EAGE Conference and Exhibition incorporating SPE EUROPEC 2009*, European Association of Geoscientists & Engineers.

StructX 2021, Typical Poisson's ratio values for common soil types, StructX, (accessed 15/03/2021) <https://https://structx.com/Soil_Properties_004.html>.

Su, H., Xu, F., Lu, S., Jin, Y-Q. 2016, Iterative ADMM for inverse FE-BI problem: A potential solution to radio tomography of asteroids, *IEEE Transactions on Geoscience and Remote Sensing* 54: 5226-5238.

Sudha, K., Israil, M., Mittal, S. and Rai, J. 2009, Soil characterisation using electrical resistivity tomography and geotechnical investigations, *Journal of Applied Geophysics* 67: 74-79.

Šumanovac, F. and Weisser, M. 2001, Evaluation of resistivity and seismic methods for hydrogeological mapping in karsts terrains, *Journal of Applied Geophysics* 47: 13-28.

Sumner, J.S. 2012, Principles of induced polarization for geophysical exploration, Elsevier.

Sunshine, J.M., A'Hearn, M.F., Groussin, O., Li, J-Y., Belton, M.J.S., Delamere, W.A., Kissel, J., Klaasen, K.P., McFadden, L.A., Meech, K.J., Melosh, H.J., Schultz, P.H., Thomas, P.C., Veverka, J., Yeomans, D.K., Busko, I.C., Desnoyer, M., Farnham, T.L., Feaga, L.M., Hampton, D.L., Lindler, D.J., Lisse, C.M. and Wellnitz, D.D. 2006, Exposed water ice deposits on the surface of comet 9P/Tempel 1, *Science* 311: 1453-1455.

Surkov, Y. 1989, Exploration of Terrestrial Planets from Spacecraft, New York: Ellis Horwood.

Sutton, G.H. and Latham, G.V. 1964, Analysis of a feedback controlled seismometer, *Journal of Geophysical Research* 69: 3865-3882.

Sviatoslavsky, I.N. and Jacobs, M. 1988, Mobile helium-3 mining and extraction system and its benefits toward lunar base self-sufficiency, Space '88 Conference, Albuquerque, August 29-31, New York, American Society of Civil Engineers, 310-321.

Swint, D. and Schmidt, S. 1991, Optimizing lunar concrete, *Lunar Concrete*, *American Concrete Institute* 125: 41-56.

Tahmasebinia, F. 2008, Numerical modelling of reinforced concrete slabs subject to impact loading, PhD. Thesis, University of Wollongong, NSW, Australia.

Talwani, P., Nur, A. and Kovach, R.L. 1973, Compressional and shear wave velocities in granular materials to 2.5 kilobars, *Journal of Geophysical Research* 78: 6899-6909.

Tan, K., Li, C., Liu, J., Qu, H., Xia, L., Hu, Y. and Li, Y. 2014, A novel method using a complex surfactant for in-situ leaching of low permeable sandstone uranium deposits, *Hydrometallurgy* 150: 99-106.

Tancredi, G. 2014, A criterion to classify asteroids and comets based on the orbital parameters, *Icarus* 234: 66-80.

Tang, C.L., Hu, J.C., Lin, M.L., Angelier, J., Lu, C.Y., Chan, Y.C. and Chu, H.T. 2009, The Tsaoling landslide triggered by the Chi-Chi earthquake, Taiwan: insights from a discrete element simulation, *Engineering Geology* 106: 1-19.

Tariq, Z., Elkatatny, S., Mahmoud, M., Ali, A.Z. and Abdulraheem, A. 2017, A new technique to develop rock strength correlation using artificial intelligence tools, *World Well Logging Technology* 1: 10-14.

Taylor, L. and Meek, T. 2005, Microwave sintering of lunar soil: Properties theory and practice, *Journal of Aerospace Engineering*, 18: 188-197.

Taylor, L.A. and Kulcinski, G.L. 1999, Helium-3 on the Moon for fusion energy: the Persian Gulf of the 21st Century, *Solar System Research* 33: 338.

The Planetary Society 2020, DART: Testing asteroid redirection technology, (accessed 16/10/2020) <https://www.planetary.org/space-missions/dart>.

Thomas, N., Sierks, H., Barbieri, C., Lamy, P.L., Rodrigo, R., Rickman, H., Koschny, D., Keller, H.U., Agarwal, J., Bertini, I., Besse, S., Bodewits, D., Cremonese, G., Da Deppo, V., Davidsson, B., De Cecco, M., Debei, S., El-Maarry, M.R., Ferri, F., Fornasier, S., Fulle, M., Giacomini, L., Groussin, O., Gutierrez, P.J., G*üttler, C., Hviid, S.F., Ip, W-H., Jorda, L., Knollenberg, J., Kramm, J-R., Kührt, E., Küppers, M., La Forgia, F., Lara, L.M., Lazzarin, M., Moreno, J.J.L., Magrin, S., Marchi, S., Marzari, F., Massironi, M., Michalik, H., Moissl, R., Mottola, S., Naletto, G., Oklay, N., Pajola, M., Pommerol, A., Preusker, F., Sabau, L., Scholten, F., Snodgrass, C., Tubiana, C., Vincent, J-B. and Wenzel, K-P.* 2015, The morphological diversity of comet 67P/Churyumov-Gerasimenko, *Science* 347: aaa0440.

Timur, A. 1968, Velocity of compressional waves in porous media at permafrost temperatures, *Geophysics* 33: 584-595.

Toksöz, M.N., Dainty, A.M., Solomon, S.C. and Anderson, K.R. 1974, Structure of the Moon, *Reviews of Geophysics and Space Physics* 17: 1641-1655.

Tommasi, P., Campedel, P., Cosorti, C. and Ribacchi, R. 2008, A discontinuous approach to the numerical modelling of rock avalanches, *Rock Mechanics and Rock Engineering* 41: 37-58.

Tong, V.C.H. and García, R.A., Extraterrestrial Seismology, Cambridge University Press, Cambridge, 2015.

Toutanj, H., Evans, S. and Grugel, R. 2005, Performance of "waterless concrete", *International Congress on Polymers in Concrete*: 1-8.

Tuncer, E.R. and Lohnes, R.A. 1977, An engineering classification for certain basalt-derived lateritic soils, *Engineering Geology* 11: 319-339.

Trilling, D.E., Mommert, M., Hora, J.L., Farnocchia, D., Chodas, P., Giorgini, J., Smith, H.A., Carey, S., Lisse, C.M., Werner, M., McNeill, A., Chesley, S.R., Emery, J.P., Fazio, G., Fernandez, Y.R., Harris, A., Marengo, M., Mueller, M., Roegge, A., Smith, N., Weaver, H.A., Meech, K. and Micheli, M. 2018, Spitzer observations of interstellar object 1I/'Oumuamua, The Astronomical Journal 156: 261.

Valle-Molina, C. and Stokoe, K.H. 2012, Seismic measurements in sand specimens with varying degrees of saturation using piezoelectric transducers, *Canadian Geotechnical Journal* 49: 671-685.

Valois, R., Bermejo, L., Guérin, R., Hinguant, S., Pigeaud, R. and Rodet, J. 2010, Karstic morphologies identified with geophysics around Saulges caves (Mayenne, France), *Archaeological Prospection* 17: 151-160.

Van Schoor, M. 2002, Detection of sinkholes using 2D electrical resistivity imaging, *Journal of Applied Geophysics* 50: 393-399.

Veeken, P.C.H. and Da Silva, M. 2004, Seismic inversion methods and some of their constraints, *First Break* 22: 47-70.

Veeken, P.C.H., Legeydo, P.J., Davidenko, Y.A., Kudryavceva, E.O., Ivanov, S.A. and Chuvaev, A. 2009, Benefits of the induced polarization geoelectric method to hydrocarbon exploration, *Geophysics* 74: 47-59.

Veldanov, V.A., Smirnov, V.E., Khavroshkin, O.B. 1999, Lunar penetrator: reducing overload and penetration control, *Astronomich. Vestnik* 33: 432-436.

Vukanti, R., Model, M.A. and Leff, L.G. 2012, Effect of modeled reduced gravity conditions on bacterial morphology and physiology, *BMC Microbiology* 12: 4-14.

Walker, J.D. and Huebner, W.F. 2004, Seismological investigation of asteroid and comet interiors, in: M.J.S. Belton, T.H. Morgan, N. Samarasinha, D.K. Yeomans (Eds.), Mitigation of Hazardous Comets and Asteroids, Cambridge University Press, Cambridge, pp. 234-265.

Walker, J.D., Huebner, W.F., Chocron, S., Bigger, R.P. and Kirchdoerfer, T. 2015, Seismic waves in small bodies: Sources and propagation, In: V.C.H. Tong, R.A. Garcia (Eds.), Extraterrestrial Seismology, Cambridge University Press, Cambridge, pp. 323–338.

Walker, J.D., Huebner, W.F., Chocron, S., Gray, W., & Boice, D., 2009, Active seismology of asteroids through impact and/or blast loading, White Paper for Primitive Bodies Decadal Survey.

Walker, J.D., Sagebiel, E.J. and Huebner, W.F. 2006, A preliminary analysis of seismological techniques to study Eros and other asteroids, *Advances In Space Research* 37: 142-152.

Walsh, K.J. 2018, Rubble pile asteroids, *Annual Review of Astronomy and Astrophysics* 56: 593-624.

Ward, S.N. and Asphaug, E. 1999, Asteroid impact tsunami: A probabilistic hazard assessment, Icarus 145: 64-78.

Watanabe, S., Hirabayahi, M., Hirata, N., Hirata, Na., Noguchi, R., Shimaki, Y., Ikeda, H., Tatsumi, E., Yoshikawa, M., Kikuchi, S., Yabuta, H., Nakamura, T., Tachibana, S., Ishihara, Y., Morota, T., Kitazato, K., Sakatani, N., Matsumoto, K., Wada, K., Senshu, H., Honda, C., Michikami, T., Takeuchi, H., Kouyama, T., Honda, R., Kameda, S., Fuse, T., Miyamoto, H., Komatsu, G., Sugita, S., Okada, T., Namiki, N., Arakawa, M., Ishiguro, M., Abe, M., Gaskell, R., Palmer, E., Barnouin, O.S., Michel, P., French, A.S., McMahon, J.W., Scheeres, D.J., Abell, P.A., Yamamoto, Y., Tanaka, S., Shirai, K., Matsuoka, M., Yamada, M., Yokota, Y., Suzuki, H., Yoshioka, K., Cho, Y., Tanaka, S., Nishikawa, N., Sugiyama, T., Kikuchi, H., Hemmi, R., Yamaguchi, T., Ogawa, N., Ono, G., Mimasu, Y., Yoshikawa, K., Takahashi, T., Takei, Y., Fujii, A., Hirose, C., Iwata, T., Hayakawa, M., Hosoda, S., Mori, O., Sawada, H., Shimada, T., Soldini, S., Yano, H., Tsukizaki, R., Ozaki, M., Lijima, Y., Ogawa, K., Fujimoto, M., Ho, T-M., Moussi, A., Jaumann, R., Bibring, J-P., Krause, C., Terui, F., Saiki, T., Nakazawa, S. and Tsuda, Y. 2019, Hayabusa2 arrives at the carbonaceous asteroid 162173 Ryugu – A spinning top-shaped rubble pile, *Science* 364: 268-272.

Watanabe, S-I., Tsuda, Y., Yoshikawa, M., Tanaka, S., Saiki, T. and Nakazawa, S. 2017, Hayabusa 2 mission overview, *Space Science Reviews* 208: 3-16.

Watters, T.R., Leuschen, C.J., Plaut, J.J., Picardi, G., Safaeinili, A., Clifford, S.M., Farrell, W.M., Ivanov, A.B., Phillips, R.J. and Stofan, E.R. 2006, MARSIS radar sounder evidence of buried basins in the northern lowlands of Mars, *Nature* 444: 905-908.

Weber, R.C., Knapmeyer, M., Panning, M. and Schmerr, N. 2015, Modeling approaches in planetary seismology, in: V.C.H. Tong, R.A. Garcia (Eds.), Extraterrestrial Seismology, Cambridge University Press, Cambridge, pp. 140-155.

Weber, R.C., Lin, P-Y., Garnero, E.J., Williams, Q. and Lognonné, P. 2011, Seismic detection of the lunar core, *Science* 331: 309-312.

Whitely, R.J., Tholen, D.J., Bell, J.F. and Hergenrother, C.W. 2000, Sample return from small asteroids: mission impossible?, In: Near-Earth Asteroid Sample Return Workshop (abstracts), Lunar and Planetary Institute, Houston, TX, LPI Contribution no. 1073.

Wichtmann, T. and Triantafyllidis, T. 2009, On the influence of the grain size distribution curve on P-wave velocity, constrained elastic modulus M_{max} and Poisson's ratio of quartz sands, *Soil Dynamics and Earthquake Engineering* 30: 757-766.

Wilhelms, D.E. 1986, Selection of the Apollo 15 landing site, In: P.D. Spudis and G. Ryder (Eds.), Geology and Petrology of the Apollo 15 Landing Site, LPI Technical Report 86-03, Lunar and Planetary Institute, pp. 116-118.

Williams, B.G., Duxbury, T.C. and Hildebrand, C.E. 1988, Improved determination of Phobos and Deimos masses from Viking fly-bys, *Lunar and Planetary Science Conference* 19: 1274.

Williford, K.H., Farley, K.A., Stack, K.M., Allwood, A.C., Beaty, D., Beegle, L.W., Bhartia, R., Brown, A.J., Juarez, M.T., Hamran, S-E., Hecht, M.H., Hurowitz, J.A., Rodriguez-Manfredi, J.A., Maurice, S., Milkovich, S. and Wiens, R.C. 2018, Chapter 11 – The NASA Mars 2020 rover mission and the search for extraterrestrial life, in: N.A. Cabrol, E.A. Grin (Eds.), From Habitability to Life on Mars, Elsevier, pp. 275-308.

Wilson, L., Keil, K. and Love, S.J. 1999, The internal structures and densities of asteroids, *Meteoritics and Planetary Science* 34: 479-483.

Worland, R.S. and Wilson, D.D. 1999, The speed of sound in air as a function of temperature. *The Physics Teacher*. 37: 53-57.

World Platinum Investment Council 2019, Where does platinum come from?, (accessed 29/06/2020) <https://platinuminvestment.com/about/60-seconds-in-platinum/2019/03/20>.

Worsey, P.N. 1985, In situ measurement of blast damage underground by seismic refraction surveys, *Proceedings – Symposium on Rock Mechanics*, CRC Press.

Wyllie, M. R., Gregory, A.R. and Gardner, L.W. 1956, Elastic wave velocities in heterogeneous and porous media, *Geophysics* 21: 41–79.

Xiao, W. and Unsworth, M. 2006, Structural imaging in the Rocky Mountain Foothills (Alberta) using magnetotelluric exploration, *AAPG Bulletin* 90: 321-333.

Yamashita, M., Hashimoto, H. and Wada, H. 2009, On-site resources availability for space agriculture on Mars, in: Mars: Prospective energy and material resources, Springer Science & Business Media.

Yang, S-R., Lin, H-D, Kung, J.H.S. and Liao, J-Y. 2008, Shear wave velocity and suction of unsaturation soil using bender element and filter paper method, *Journal of Geoengineering* 3: 67-74.

Yano, H., Kubota, T., Miyamoto, H., Okada, T., Scheeres, D., Takagi, Y., Yoshida, K., Abe, M., Abe, S., Barnouin-Jha, O., Fujiwara, A., Hasegawa, S., Hashimoto, T., Ishiguro, M., Kato, M., Kawaguchi, J., Mukai, T., Saito, J., Sasaki, S. and Yoshikawa, M. 2006, Touchdown of the Hayabusa spacecraft at the Muses Sea on Itokawa, *Science* 312: 1350-1353.

Yeomans, D.K., Barriot, J.P., Dunham, D.W., Farquhar, R.W., Giorgini, J.D., Helfrich, C.E., Konopliv, A.S., McAdams, J.V., Miller, J.K., Owen, W.M., Scheeres, D.J. and Synnott, S.P. 1997, Estimating the mass of asteroid 253 Mathilde from tracking data during the Near flyby, *Science* 278: 2106-2109.

Yilmaz, Ö. 2001, Seismic data analysis: Processing, inversion, and interpretation of seismic data, Society of Exploration Geophysicists.

Yoder, C.F., Konopliv, A.S., Yuan, D.N., Standish, E.M. and Folkner, W.M. 2003, Fluid core size of Mars from detection of the solar tide, *Science* 300: 299-303.

Youn, J.U. and Kim, D.S. 2008, Measurement of small strain shear modulus gmax of dry and saturated sands by bender element, resonant column, and torsional shear tests, *Canadian Geotechnical Journal*, V. 45, 1426-1438.

Zacny, K. Chu, P., Craft, J., Cohen, M.M., James, W.W. and Hilscher, B. 2013, Asteroid mining, *AIAA SPACE 2013 Conference and Exposition*, AIAA 2013-5304.

Zemanek, J. and Rudnick, I. 1961, Attenuation and dispersion of elastic waves in a cylindrical bar, *The Journal of the Acoustical Society of America* 33: 1283-1288.

Zerriffi, H. 1996, Tritium production: DOE moves ahead where non-proliferationists fear to tread, *Science for Democratic Action* 5: 1-16.

Zhang, K., Wei, W., Lu, Q., Dong, H. and Li, Y. 2014, Theoretical assessment of 3-D magnetotelluric method for oil and gas exploration: Synthetic examples, *Journal of Applied Geophysics* 106: 23-36.

Zhou, B. 2018, Electrical resistivity tomography: A subsurface-imaging technique, In: Applied Geophysics with Case Studies on Environmental, Exploration and Engineering Geophysics, IntechOpen.

Zhou, B., Fraser, S., Borsaru, M., Aizawa, T., Sliwa, R. and Hashimoto, T. 2005, New approaches for rock strength estimation from geophysical logs, *Proceedings of Bowen Basin Symposium*, pp. 151-164.

Zhou, B., Fullagar, P.K. and Fallon, G.N. 1998, Radio frequency tomography trial at Mt Isa Mine, *Exploration Geophysics* 29: 675-679.

Zhou, H-W. 2014, Practical Seismic Data Analysis, Cambridge University Press.

Zhou, W., Beck, B.F. and Adams, A.L. 2002, Effective electrode array in mapping karst hazards in electrical resistivity tomography, *Environmental Geology* 42: 922-928.

Zhu, J., Currens, J-C. and Dinger, J-S. 2011, Challenges of using electrical resistivity method to locate karst conduits – a field case in the Inner Bluegrass Region, Kentucky, *Journal of Applied Geophysics* 75: 523-530.

Zimmer, M.A., Prasad, M., Mavko, G. and Nur, A. 2007, Seismic velocities of unconsolidated sands: Part 1 – Pressure trends from 0.1 to 20 MPa, *Geophysics* 72: E1-E13.

Zuber, M.T., Smith, D.E., Solomon, S.C., Muhleman, D.O., Head, J.W., Garvin, J.B., Abshire, J.B. and Bufton, J.L. 1992, The Mars Observer laser altimeter investigation, *Journal of Geophysical Research* 97: 7781-7797.

Zubrin, R. 2011, The case for Mars: The plan to settle the red planet and why we must, Simon and Schuster.